Importance-Truncated No-Core Shell Model for Fermionic Many-Body Systems

***Importance*-trunkiertes *No-Core*-Schalenmodell für fermionische Vielteilchensysteme**

Zur Erlangung des Grades eines Doktors der Naturwissenschaften (Dr. rer. nat.)
genehmigte Dissertation von Dipl.-Phys. Helena Spies aus Frunse
Tag der Einreichung: 22. November 2016, Tag der Prüfung: 30. Januar 2017
März 2017— Darmstadt — D 17

1. Gutachten: Prof. Dr. Robert Roth
2. Gutachten: Prof. Dr. Jens Braun

TECHNISCHE UNIVERSITÄT DARMSTADT

Fachbereich Physik
Institut für Kernphysik

Importance-Truncated No-Core Shell Model for Fermionic Many-Body Systems
Importance-trunkiertes *No-Core*-Schalenmodell für fermionische Vielteilchensysteme

Genehmigte Dissertation von Dipl.-Phys. Helena Spies aus Frunse

1. Gutachten: Prof. Dr. Robert Roth
2. Gutachten: Prof. Dr. Jens Braun

Tag der Einreichung: 22. November 2016
Tag der Prüfung: 30. Januar 2017

Darmstadt — D 17

Дорогу осилит идущей!

Erklärung zur Dissertation

Hiermit versichere ich, die vorliegende Dissertation ohne Hilfe Dritter nur mit den angegebenen Quellen und Hilfsmitteln angefertigt zu haben. Alle Stellen, die aus Quellen entnommen wurden, sind als solche kenntlich gemacht. Diese Arbeit hat in gleicher oder ähnlicher Form noch keiner Prüfungsbehörde vorgelegen.

Darmstadt, den 14. November 2016

(Helena Spies)

Abstract

The exact solution of quantum mechanical many-body problems is only possible for few particles. Therefore, numerical methods were developed in the fields of quantum physics and quantum chemistry for larger particle numbers. Configuration Interaction (CI) methods or the No-Core Shell Model (NCSM) allow *ab initio* calculations for light and intermediate-mass nuclei, without resorting to phenomenology. An extension of the NCSM is the Importance-Truncated No-Core Shell Model, which uses an *a priori* selection of the most important basis states. The importance truncation was first developed and applied in quantum chemistry in the 1970s and latter successfully applied to models of light and intermediate-mass nuclei. Other numerical methods for calculations for ultra-cold fermionic many-body systems are the Fixed-Node Diffusion Monte Carlo method (FN-DMC) and the stochastic variational approach with Correlated Gaussian basis functions (CG). There are also such method as the Coupled-Cluster method, Green's Function Monte Carlo (GFMC) method, *et cetera*, used for calculation of many-body systems.

In this thesis, we adopt the IT-NCSM for the calculation of ultra-cold Fermi gases at unitarity. Ultra-cold gases are dilute, strongly correlated systems, in which the average interparticle distance is much larger than the range of the interaction. Therefore, the detailed radial dependence of the potential is not resolved, and the potential can be replaced by an effective contact interaction. At low energy, s-wave scattering dominates and the interaction can be described by the s-wave scattering length. If the scattering length is small and negative, Cooper-pairs are formed in the Bardeen-Cooper-Schrieffer (BCS) regime. If the scattering length is small and positive, these Cooper-pairs become strongly bound molecules in a Bose-Einstein-Condensate (BEC). In between (for large scattering lengths) is the unitary limit with universal properties.

Calculations of the energy spectra (ground-state and first excited-state) have so far only been performed for up to five particles using CI or NCSM methods or for up to six particles using the CG method. Calculations with larger particle numbers have only been performed with Monte Carlo methods and only for the ground state of up to 30 particles. We extend *ab initio* calculations of the energy spectra of ultra-cold Fermi gases at unitarity for up to 20 particle using the IT-NCSM.

For our calculations we use different interactions: an effective interaction introduced by Alhassid, Bertsch and Fang and an interaction constructed using an effective field theory (EFT) approach. Furthermore, we use a Gauss-shaped potential as it is also used for the calculations of ultra-cold Fermi gases at unitarity using CG or FN-DMC methods. Although more effort must be invested to make the Gauss-shaped potential suitable for IT-NCSM calculations of ultra-cold Fermi gases, calculations with the other two interactions yield ground-state energies which agree excellently with the results obtained using the FN-DMC method. The IT-NCSM extends the range of the NCSM and permits the calculation of energy spectra (ground-state and excited-state energies) of fermionic systems with large particle numbers for which previously only the ground states could be calculated using Monte Carlo methods.

Zusammenfassung

Im Allgemeinen ist eine exakte Lösung für quantenmechanische Vielteilchensysteme nur für sehr wenige Teilchen möglich. Deshalb wurden sowohl in der Quantenchemie als auch Quantenphysik numerische Verfahren zur Lösung von Vielteilchensystemen entwickelt. *Ab initio* Methoden wie *Configuration Interaction* (CI) oder das *No-Core*-Schalenmodell (NCSM) werden für leichte sowie mittelschwere Kerne angewandt und ermöglichen eine *ab initio*-Beschreibung ohne Zurückgreifen auf phänomenologische Ansätze. Eine Optimierung des NCSM stellt das *Importance*-trunkierte *No-Core*-Schalenmodel (IT-NCSM) dar, das eine *a priori*-Selektion der wichtigen Zustände beinhaltet. Die *Importance*-Trunkierung wurde zuerst in der physikalischen Chemie in den 1970er Jahren entwickelt und angewandt und später erfolgreich auch für leichte und mittelschwere Kerne angewandt. Weitere Methoden zur Berechnung von ultrakalten fermionischen Vielteilchensystemen sind die *Fixed-Node-Diffusion*-Monte-Carlo-Methode (FN-DMC) und stochastische Variationsrechnungen mit *Correlated-Gaussian*-Basisfunktionen (CG). Es gibt noch weitere Methoden wie zum Beispiel die *Coupled-Cluster*-Methode, die *Green's-Function*-Monte-Carlo-Methode (GFMC) und andere, die für Berechnungen von Vielteilchensysteme verwendet werden.

In dieser Arbeit wird das IT-NCSM zur Berechnung ultrakalter Fermigase im unitären Limit verwendet. Ultrakalte Gase sind verdünnte, stark korrelierte Systeme, in denen der mittlere Teilchenabstand viel größer ist als die Reichweite der Wechselwirkung. Dies hat zur Folge, dass die detaillierte Radialabhängigkeit des Potentials nicht aufgelöst wird. Somit kann das Potential durch eine effektive Kontaktwechselwirkung ersetzt werden. Bei niedrigen Energien dominieren die Streuprozesse der *s*-Welle die Streuung. So kann die Wechselwirkung durch die *s*-Wellen-Streulänge beschrieben werden. Bei kleinen negativen Streulängen bilden sich Cooper-Paare im Bardeen-Cooper-Schrieffer-Regime (BCS), bei kleinen positiven Streulängen stark gebundene Moleküle eines Bose-Einstein-Kondensats (BEC). Dazwischen (bei sehr großen Streulängen) befindet sich das unitäre Regime mit universellen Eigenschaften.

Berechnungen des Energiespektrums (Grundzustand und erster angeregter Zustand) wurden bisher nur für höchstens fünf Teilchen mit CI- oder NCSM-Methoden und für bis zu sechs Teilchen mit der CG-Methode durchgeführt. Höhere Teilchenzahlen konnte man bislang nur mit Monte-Carlo-Methoden erreichen und auch nur den Grundzustand von bis zu 30 Teilchen berechnen. Diese Arbeit erweitert *ab initio*-Berechnungen des Energiespektrums auf bis zu 20 Teichen unter Verwendung des IT-NCSM.

In dieser Arbeit kommen für die IT-NCSM Rechnungen eine Wechselwirkung auf Basis effektiver Feldtheorien sowie eine effektive Wechselwirkung nach Alhassid, Bertsch und Fang zum Einsatz. Diese Wechselwirkungen werden erfolgreich zur Berechnung des Energiespektrums im unitären Limit angewandt und ihre Ergebnisse mit denen von anderen Methoden (CI und FN-DMC) verglichen. Weiterhin wird auch eine einfache Gauss-förmige Wechselwirkung betrachtet, wie sie zur Berechnung der Energie im unitären Limit mit CI- oder FN-DMC- Methoden zum Einsatz kommt. Während für die Gauss-förmige Wechselwirkung noch weitere Forschung notwendig ist, um sie für IT-NCSM Berechnungen nutzbar zu machen, liefern Berechnungen mit den beiden anderen Wechselwirkungen Grundzustandsenergien, die hervorragend mit den Ergebnissen der FN-DMC-Methode übereinstimmen. Das IT-NCSM erweitert somit den Anwendungsbereich des NCSM auf deutlich größere Teilchenzahlen und erlaubt die Berechnung von Energiespektren (Grundzustand und angeregte Zustände) von fermionischen Systemen, für die bislang nur die Grundzustandsenergie mit Monte-Carlo-Methoden numerisch berechnet werden konnte.

Contents

1 Introduction

Ultra-cold atomic gases are dilute systems at extremely low temperatures of the order of nano-Kelvin, in which quantum statistical effects become significant and can be observed. Experimentally, such systems can be prepared for example by trapping atoms with laser light or with magnetic fields, precooling them using laser beams and finally cooling them using evaporative cooling [49, 50, 93]. Such temperatures and densities can only be reached if the sample does not come into contact with other matter; hence, magnetic and laser traps must be employed. These systems are pure and controllable, and only contain impurities if they are intended to. With optical lattices, cold Bose or Fermi gases or mixtures of them can be trapped in one-, two- or three-dimensional periodic structures. One-dimensional structures with a periodic potential can be created by using two counter-propagating laser beams. With more laser beams, two- or three-dimensional lattices can be formed [9]. The depth and geometry of the trapping potentials can be controlled. Experimentally the interparticle interaction between the fermions in the optical or magnetic trap can be controlled by means of Feshbach resonances (see chapter 2.4); the strength of the interaction can be varied and the interaction can be chosen to be either attractive or repulsive.

Theoretical methods have been developed to describe these systems; for an overview of such methods for Bose gases, see the publications by Dalvovo *et al.* [26], and Stoof [93], and for an overview of such methods for Fermi gases, see the publications by Ketterle and Zwierlein [50], Blume [10], and Stoof [93]. A summary of the current status in experimental and theoretical research on cold Bose and Fermi gases can be found in the publications by Blume *et al.* [11], by Giorgini *et al.* [34], by Krems *et al.* [54] and in [43].

Bose gases, which consist of particles with integer spin and hence obey Bose-Einstein statistics, form Bose-Einstein condensates (BEC) at low temperature, in which particles occupy the same single-particle state with minimal energy. This behavior has been predicted theoretically by Bose [13] and Einstein [29]. Cold gases received great interest in recent years after the first BEC were successfully produced in 1995 by Anderson *et al.* [4] and by Davis *et al.* [28]. In the former experiment, a system of bosonic ^{87}Rb atoms was confined in a magnetic field and cooled evaporatively. The system was cooled to a temperature of around 170 nK and had a density of $2.5 \cdot 10^{12}\,\mathrm{cm}^{-3}$. Since then, many experimental and theoretical studies of Bose gases and BECs have been carried out. Experiments using Fermi gases followed later [34].

The Pauli principle states that two identical fermions cannot occupy the same quantum state. Therefore, an ideal Fermi gas, which obeys the Fermi-Dirac statistics, does not undergo Bose-Einstein condensation. According to Bardeen-Cooper-Schrieffer (BCS) theory, Fermi gases with weak attractive interactions enter a superfluid phase at sufficiently low temperature T by forming so-called Cooper pairs (fermionic superfluidity) that can occupy the same state [34, 45, 103]. Superfluids are irrotational gases with zero viscosity. For charged particles like electrons the formation of Cooper pairs leads to superconductivity at low temperatures [7]. Since the attractive interaction between the fermions is much smaller than the Fermi energy, the size of Cooper pairs is larger than the average interparticle spacing by a factor of the order 10^3 in conventional superconductors.

The interaction in the BCS limit is too weak to support a bound state, hence the s-wave scattering length is negative. For a stronger interparticle interaction, the scattering length is positive and the fermions form strongly bound diatomic molecules (dimers), which form a BEC whose ground state is superfluid. The transition between the fermionic system described by BCS theory and the system of molecular bosons described by the BEC is the so-called BCS–BEC crossover, in which the scattering length diverges — as the interparticle interaction in the BCS regime grows stronger, the scattering length

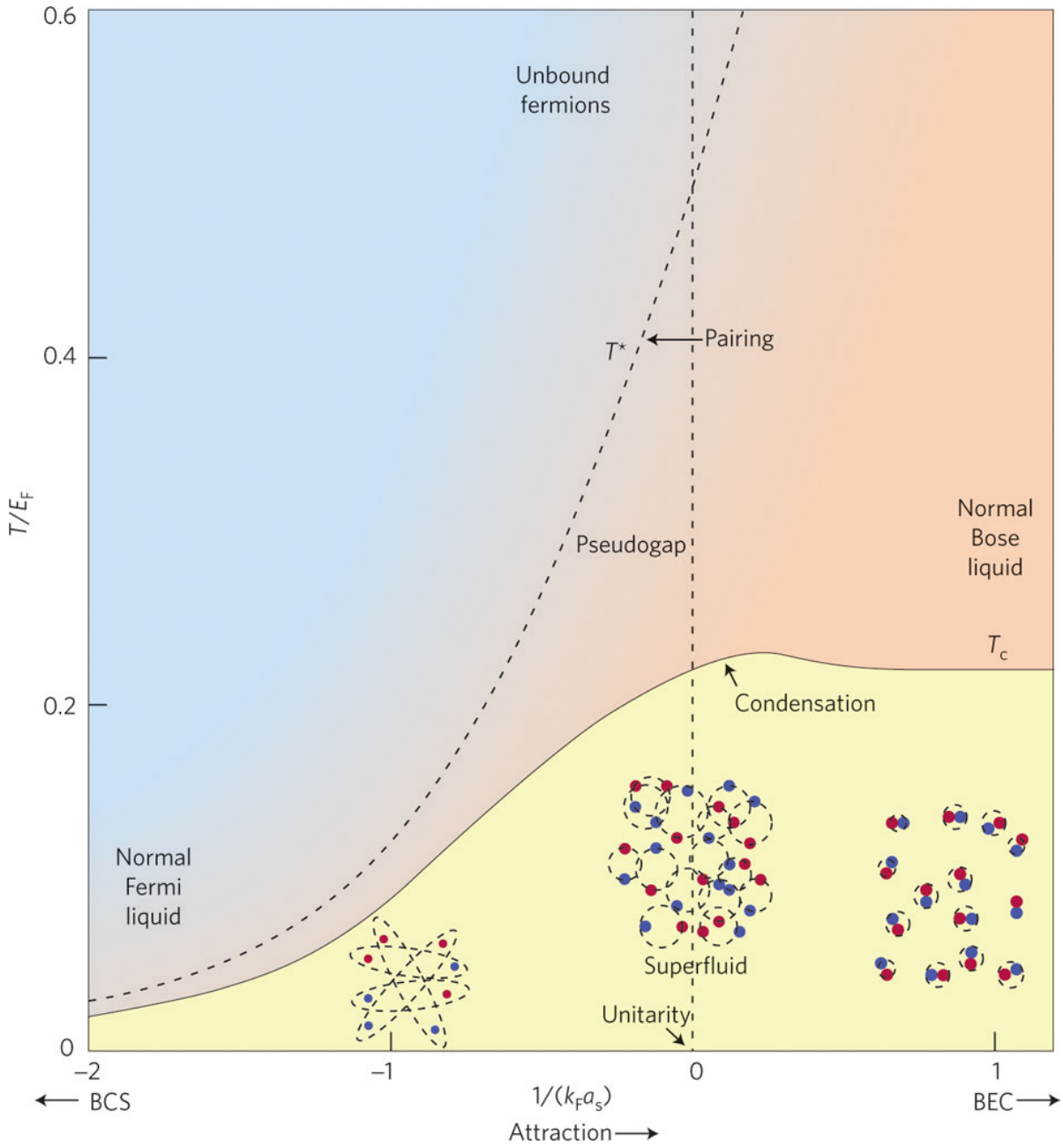

Figure 1.1.: Phase diagram of the BCS–BEC crossover as a function of $(k_F a_0)^{-1}$, where k_F is the Fermi momentum, a_0 (a_s in the figure) the s-wave scattering length, and the temperature T is in units of the Fermi energy E_F. The figure shows schematically the evolution from the BCS limit with Cooper pairs to the BEC limit with tightly bound molecules. In between is the BCS–BEC crossover with the unitary limit ($(k_F a)^{-1} = 0$) where the scattering length diverges. Away from the transition temperature T_c, the pair-formation crossover scale T^* diverges (figure taken from [66]).

becomes more negative and approaches $-\infty$, and as the interparticle interaction in the BEC grows weaker, the scattering length becomes more positive and approaches $+\infty$.

Figure 1.1 shows the phase diagram of the BCS–BEC crossover in a dilute Fermi gas as a function of $(k_F a_0)^{-1}$, where k_F is the Fermi momentum and a_0 the s-wave scattering length and the temperature T in units of the Fermi energy E_F. This figure also shows the dependence of behavior of the Fermi gas on the temperature T and the strength of the interaction. At temperatures below T^*, pairing starts [50]. For $T < T_c$, superfluidity can be observed for positive $(k_F a_0)^{-1}$ in BECs of tightly bound molecules and for negative $(k_F a_0)^{-1}$ in the BCS limit of fermions forming Cooper pairs.

The weak attractive interaction between the fermions forming the Cooper pairs can be tuned using Feshbach resonances, which allows precise control of the sign and magnitude of the scattering length a_0. The resonant limit with infinite scattering length is the so-called unitary limit. More details on Feshbach resonances can be found in the literature [11, 22, 54, 34, 93, 103] and in chapter 2.4.

Experiments with ultra-cold Fermi gases were motivated by the search for superfluidity, which BCS theory predicted for low temperatures. The experiments showed that superfluidity can be achieved using Feshbach resonances [104]. O'Hara *et al.* [39] and Bourdel *et al.* [14] arrived at the strongly interacting regime in an optically trapped fermionic ^{6}Li using Feshbach resonances. Later, condensation of fermionic atom pairs in the BCS-BEC crossover regime was observed by Regal *et al.* [67] and the observation of BEC of fermionic molecules were reported in [35, 105]. The first convincing proof of superfluidity was obtained by Zwierlein *et al.* [104], where quantized vortices in a rotating gas were observed; which are a direct consequence of the existence of a macroscopic wave function that describes the superfluid.

Systems in the unitary limit have been studied experimentally by confining atoms in traps or optical lattices (see, for instance, [103, 11, 54, 34, 93] and the references given therein, as well as [51, 92]). For example, Serwane *et al.* [83] confined between one and ten two-component equal-mass fermionic atoms in precisely defined quantum states in an optical dipole trap by focussing a single laser beam. They used a mixture of ^{6}Li in two different hyperfine states. In optical lattices at extremely low temperatures, the lattice sites can be considered as independent harmonic oscillator (HO) traps, containing only a few atoms each.

Theoretical calculations of thermodynamical properties for trapped many-body fermionic systems were performed in [16, 21] using a Monte Carlo method and density-functional theory for up to about 30 fermions. Many-body calculations of the ground-state energy of trapped two-component equal-mass fermionic systems in the unitary limit have been performed using Monte Carlo methods [5, 12, 18, 21, 85, 87, 88] (up to about 30 fermions). *Ab initio* calculations can also describe the excited states, but have been successfully used with at most about 6 fermions so far. Furthermore, *ab initio* calculations are exact methods without any approximation applied to the many-body system, with controlled truncation applied to the many-body system. Calculations of ground-state energy and excited-state energies were performed using the correlated Gaussian basis set expansion [25, 86, 87, 88] (up to 6 fermions), the Configuration Interaction (CI) method (for three and four fermions) [1] and No-Core Shell Model (NCSM) calculations (for up to five fermions) at unitarity [76, 77]. The complete analytical solution for the ground-state energy was obtained only for $A = 3$ fermions at unitarity by Werner *et al.* [102].

CI approaches are widely used for the description of quantum many-body systems in atomic and molecular physics, quantum chemistry, condensed matter, and nuclear physics and have also been used for the description two-component fermionic systems at unitarity using contact interactions and an effective interaction introduced by Alhassid, Bertsch and Fang [1, 33]. We refer to it as the Alhassid-Bertsch-Fang (ABF) interaction. NCSM calculations were performed for fermions at unitarity using an interaction constructed with an effective field theory (EFT) approach [91]. The NCSM is a CI method successfully used in nuclear many-body problems. In the NCSM, the many-body Hamiltonian is expanded on a basis of harmonic-oscillator Slater determinants up to a certain excitation energy $N_{\max}\hbar\omega$ and diagonalized to get energies and wave functions of its eigenstates.

The basis states of the many-body basis in the CI approach are often Slater determinants constructed from single-particle HO wave functions in the laboratory frame. In contrast to the NCSM, where the excitation energy is used as a truncation, in general CI method one uses only the single-particle energy of the HO as a truncation. Basis states depending only on internal (Jacobi) coordinates are also used (for instance in [76, 77]), where the radial part is described by HO wave functions. While in the Jacobi coordinate basis the antisymmetrization becomes increasingly difficult with growing number of particles, the dimension of the full space grows factorially with the number of particles and single-particle orbitals when using Slater determinants. Using the Jacobi coordinate basis is more computationally efficient than using Slater determinants only for up to five particles [77]. The basis required to obtain converged results for large particle numbers becomes extremely large and hence difficult to treat with existing computer technology.

However, since we search for the ground state and few excited states, the model space contains many states which are irrelevant for the calculation. Introducing an importance measure that allows to identify and omit these irrelevant basis states changes the results very little but reduces the model space dimension greatly, enabling the calculation of previously intractable model spaces or particle numbers. The importance truncation scheme was first developed in quantum chemistry in the 1970s. Roth *et al.* [71, 75] derived an importance truncation scheme for nuclear structure calculations using the NCSM, the so-called Importance-Truncated No-Core Shell Model (IT-NCSM). Using an *a priori* measure for the importance of a basis state one can reduce the dimension of the model space, allowing converged *ab initio* calculations for ^{16}O and beyond [71, 75]. For example, *ab initio* IT-NCSM calculation of oxygen isotopes with even mass number up to ^{26}O were performed with chiral two- plus three-nucleon interaction [40]. To that end, an importance measure is constructed using many-body perturbation theory. We use the importance truncation for the calculation of the energy of a two-component Fermi gas in the unitary limit. As in the nuclear structure calculation, the importance truncation allows converged calculation of larger systems compared to the full NCSM method.

In this thesis, we focus on ultra-cold two-component equal-mass Fermi gases in a trap in the unitary limit, and extend the previously described *ab initio* calculations to higher particle numbers and model spaces. We consider two-component fermion systems with $A = 4, \ldots, 20$ consisting of A_1 and A_2 particles with either $A_1 = A_2$ or $A_1 = A_2 - 1$, where A_1 are the number of atoms of the one species and A_2 of the other and $A_1 + A_2 = A$. We calculate the energies of the trapped fermion systems in the unitary limit using the IT-NCSM.

The remainder of this thesis is structured as follows: In chapter 2 we briefly summarize the scattering theory for particles at low temperature, introduce in more detail the BCS–BEC crossover and the unitary limit in particular. Also, we briefly discuss the Feshbach resonances used to tune the strength of the interaction.

Chapter 3 covers the interactions used in this thesis, that is, the EFT approach by Stetcu *et al.* [91], the ABF interaction [1], and a Gaussian-shaped potential as used in Monte Carlo calculations [12]. For our many-body calculations we need the interaction matrix elements. The interaction matrix elements are calculated in relative coordinates. The relative matrix elements have to be transformed into laboratory-frame coordinates, which is done using Talmi-Moshinsky transformation. This transformation is described in chapter 3.2.1.

Chapter 4 explains the *ab initio* many-body methods used for our calculations, the NCSM and the IT-NCSM, in more detail. We perform our many-body calculations in the m-scheme; the Jacobi coordinates and the m-scheme are described in section 4.2. Furthermore, we discuss the uncertainties of the results calculated using NCSM in that chapter. We use results calculated by other groups with other methods like the Fixed-Node Diffusion Monte Carlo (FN-DMC) method and variational approaches using a correlated Gaussian basis set expansion as a benchmark for our calculations of two-component fermion systems at unitarity. We discuss these methods in sections 4.5 and 4.6.

We present our results for the energy spectra of systems in the unitary limit in chapter 5. The extrapolation to the infinite model space is also described in chapter 5. For these calculations, we used the

EFT and the ABF interaction. We compare our results with benchmark calculations obtained by [12]. Chapter 5 contains also the results of our calculations using a Gaussian interaction.

2 Ultra-Cold Gases

We consider ultra-cold two-component fermionic systems in a harmonic oscillator (HO) trap. The fermions are not self-bound. The systems are dilute and the interaction can be characterized using only the s-wave scattering length, which can be tuned via a Feshbach resonance. In the following, we discuss briefly the collision physics at low temperatures in order to understand the properties of ultra-cold gases. We define the scattering length and analyze its behavior for a simple potential. We briefly discuss the BCS-BEC crossover and, in particular, the unitary limit in section 2.2. At low temperature only different components of the Fermi gas can interact (see section 2.1), these components we describe in the section 2.3. The strength of the potential between the interacting particles can be modified by Feshbach resonances that we describe briefly in section 2.4.

2.1 Scattering Properties of Ultra-Cold Gases

We consider dilute, ultra-cold systems. Because of their diluteness, the two-body collisions dominates over the three-body or multi-body collisions. As a consequence, the scattering properties of the ultra-cold atoms can be understood by considering two-body collisions in which the interparticle interaction is described by a central potential $V(r)$ and the weak magnetic dipole interaction between the spins is neglected[50].

The exact description of the interparticle potential is complicated [50]. At short distances on the order of few Bohr radii a_B, mutual repulsion of the two electron clouds becomes significant. At large distances, atoms interact with the van-der-Waals potential $\propto r^{-6}$. Hence, when the gases are ultra-cold and ultra-dilute, the range of the interparticle potential R_{int} (for ^{6}Li, for example, $R_{\text{int}} \propto 50a_B$) is much smaller than the interparticle distance $n^{-1/3} \sim 5000a_B$ to $10000a_B$, as well as the de Broglie wavelength $\lambda^2 = {}^{2\pi\hbar^2}/_{mk_BT}$ and the inverse Fermi wave number k_{F}^{-1}: $R_{\text{int}} \ll \lambda$, $R_{\text{int}} \ll k_F^{-1}$ [34, 50, 70]. As a result the relative wave function of two interacting atoms of the system is so broad and its derivatives so small in comparison to the range of the interaction that the details of the short-range potential cannot be resolved [50, 70]. At large distances, different many-body systems may show the same behavior although their short-distance behavior can be quite different. Their constituents and, consequently, the potentials may be different, but if the scattering length is the same, their macroscopic behavior is the same as well [15]. Therefore, the details of the interaction can be neglected and the interaction can be approximated by the delta function (δ for short), whose effect on the system behavior is no different from that of the actual potential [15]. Such many-particle systems, whose properties can be described by the s-wave scattering length only, are called universal.

Due to the short range of the interaction and the diluteness of the ultra-cold Fermi gas, the length of the HO trap

$$a_{\text{HO}} = \sqrt{\frac{\hbar}{m\omega}} \tag{2.1}$$

with HO frequency ω and mass m has to be large compared to the range of the interparticle potential: $R_{int} \ll a_{\text{HO}}$ [103].

We consider the scattering properties (collision process) of two particles with equal mass m interacting through a central potential $V(r)$. The eigenstates of the relative Hamiltonian H_{rel} can be determined by a Schrödinger equation of the form

$$\left[-\frac{\hbar^2}{2\mu}\vec{\nabla}^2 + V(r)\right]\Psi_{\vec{k}}(\vec{r}) = E_{\vec{k}}\Psi_{\vec{k}}(\vec{r}) \tag{2.2}$$

with reduced mass μ and wave vector $\vec{k}$. The asymptotic behaviour as $\vec{r} \to \infty$ can be described as the sum of the plane wave and an outgoing spherical wave:

$$\psi_k(\vec{r}) \overset{r\to\infty}{\propto} e^{i\vec{k}\vec{r}} + f_k(\theta,\varphi)\frac{e^{ikr}}{r}, \tag{2.3}$$

where $f_k(\theta,\varphi)$ is the scattering amplitude. We can now determine the differential cross section

$$\frac{d\sigma}{d\Omega} = \left|f_k(\theta,\varphi)\right|^2 \tag{2.4}$$

and the total cross section

$$\sigma_{\text{tot}} = \int \frac{d\sigma}{d\Omega} d\Omega \tag{2.5}$$

for distinguishable particles for this potential, where the total cross section is obtained by integrating over the solid angle $d\Omega$, the azimuthal angle φ, and the scattering angle θ.

For a central potential $V(\vec{r}) = V(r)$, the Schrödinger equation has spherical symmetry and angular momentum is conserved. The solutions are also eigenfunctions of the angular momentum L and can be expanded on a basis set of eigenfunctions of L^2 and L_z, the so-called partial wave expansion. The z-axis is fixed through the incident wave, which is an eigenstate of L_z with eigenvalue 0 and the expansion is independent of the azimuthal angle around the z-axis. Therefore, we can omit all coefficients with $m_l \neq 0$. Using the partial wave expansion, we can resolve the asymptotical solution (2.3) and the scattering amplitude $f_k(\theta,\varphi)$. The scattering amplitude can then be written as

$$f_k(\theta,\varphi) = \sum_{l=0}^{\infty} \frac{2l+1}{k\cot\delta_l(k) - ik} P_l(\cos\theta) = \sum_{l=0}^{\infty} (2l+1) P_l(\cos\theta) \frac{e^{i\delta_l(k)}}{k} \sin\delta_l(k), \tag{2.6}$$

where l is the relative angular momentum, m_l the projection of the relative angular momentum and $P_l(\cos\theta)$ are the Legendre polynomials and δ_l the phase shifts. The corresponding scattering cross-section for two distinguishable particles is therefore given by

$$\sigma_{\text{tot}}(k) = \frac{4\pi}{k^2} \sum_l (2l+1) \sin^2\delta_l(k). \tag{2.7}$$

Furthermore, using the symmetry of the problem, the wave function can be written as

$$\Psi_{\vec{k}}(\vec{r}) = \sum_{l=0}^{\infty} \sum_{m_l=-l}^{l} Y_{lm_l}(\theta,\varphi) \frac{u_{kl}(r)}{r}, \tag{2.8}$$

where $Y_{lm_l}(\theta,\varphi)$ are the spherical harmonics. The radial functions $u_{kl}(r)$ are unknown.

Using eq. (2.8) and assuming that $u_{kl}(r)/r$ is regular in $r = 0$ and because the interaction has a radial symmetry, eq. (2.2) can be written as:

$$u''_{kl}(r) + \left(k^2 - \frac{l(l+1)}{r^2} - \frac{2\mu V(r)}{\hbar^2}\right) u_{kl}(r) = 0. \tag{2.9}$$

Figure 2.1 shows the interparticle interaction for s-wave scattering (a) and higher partial waves (b). For the partial wave with $l = 0$, the potential is simply given by the interatomic potential $V(r)$. For higher partial waves, the centrifugal barrier has to be added to the potential, which therefore takes the form

$$V_{\text{eff}}(r) = \frac{\hbar^2 l(l+1)}{2\mu r^2} + V(r). \tag{2.10}$$

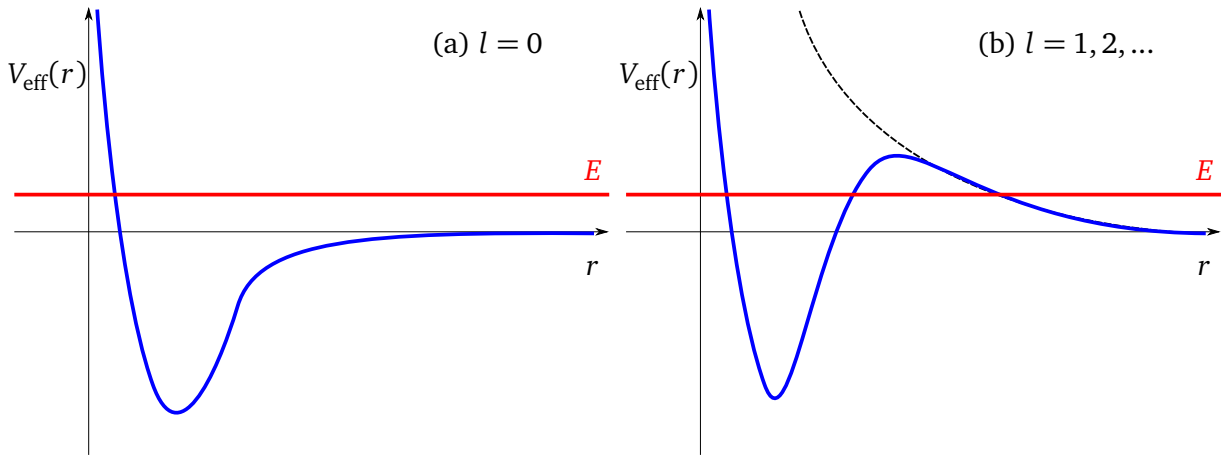

Figure 2.1.: The interparticle potential of two particles with energy E entering into the radial Schrödinger equation (2.9) for the s-wave scattering (a) and higher partial wave (b). The dotted line is the centrifugal barrier $\hbar^2 l(l+1)/(2\mu r^2)$ [27].

We consider ultra-cold gases at very low energies, lower than the height of the centrifugal barrier (see fig. 2.1). Therefore, almost all particles with $l > 0$ are being reflected at the centrifugal barrier. That barrier does not exist for particles with $l = 0$, so that we only need to take s-wave scattering into account. The contributions of the p-, d- and higher-order waves are insignificant and can be neglected.

The above statement only holds for distinguishable particles. The wave function of an identical one-component Fermi gas must be antisymmetric; as a consequence, the only partial waves contributing to the scattering cross-section are those with odd values of l. In a one-component Fermi gas, the particles interact mainly via p-wave scattering because the Pauli principle precludes s-wave scattering. At ultra-low temperatures, p- and higher wave scattering is very weak and, therefore, one-component Fermi gases are practically non-interacting; cooling them is very difficult. For a two-component Fermi system the s-wave interaction between the different components of Fermions becomes important, in addition to the p-wave scattering which is relevant for the so-called p-wave Feshbach resonances [19, p. 15]. For the calculation of ultra-cold two-component Fermi gases away from p-wave Feshbach resonances, the p- and higher wave scattering can be omitted and pure s-wave scattering is a good approximation [19]. According to Roth, the interplay of s- and p-wave scattering causes several important effects, but only for systems with large particle numbers ($> 10^5$ [70, p. 194]). We consider only systems with up to 20 particles. Therefore, we only take s-wave scattering into account in this thesis.

At low energy the phase shift δ_0 is given by the effective range expansion,

$$k \cot \delta_0(k) = -\frac{1}{a_0} + \frac{1}{2} r_0 k^2, \tag{2.11}$$

where r_0 is the effective range of the potential. Therefore the s-wave scattering length can be written as

$$a_0 = -\lim_{k \to 0} \frac{\tan \delta_0(k)}{k}. \tag{2.12}$$

For $k \to 0$ the scattering amplitude $f_0 \to a_0$ and we get for the scattering cross-section (see eq. (2.6) and (2.7)):

$$\lim_{k \to 0} \sigma_{l=0}(k) = 4\pi a_0^2, \tag{2.13}$$

which corresponds to four times the classical scattering cross-section for hard spheres with radius a_0. All scattering properties can now be described by the s-wave scattering length alone; the form of the actual

potential is not important for the description of the scattering process. The properties of the system become independent of the details of the interaction, and the potential can be approximated by a simple contact interaction (δ-function).

The asymptotic scattering solution for the radial function can be given for $l = 0$:

$$u_{kl=0}(r) \overset{r\to\infty}{\propto} k^{-1} \sin(kr + \delta_0(k)). \tag{2.14}$$

As mentioned previously, the interaction potential between two atoms can be described by the van-der-Waals potential, which falls off quickly (it is proportional to r^{-6}) and is therefore a so-called short-range potential. As a consequence, at large distances, eq. (2.9) reduces to the free Schrödinger equation. Since we consider particles with low energy ($k \to 0$) and $l = 0$ holds additionally, eq. (2.9) further reduces to

$$u''_{k\to 0, l=0}(r) = 0 \tag{2.15}$$

with the trivial solution

$$u(r) = u_{k\to 0, l=0}(r) \overset{r\to\infty}{\propto} r - a_0 \tag{2.16}$$

for the asymptotic behavior of the radial wave function, where a_0 is the s-wave scattering length.

We can understand the physical meaning of the scattering length by considering fig. 2.2, which shows the scattering length for different potentials. In fig. 2.2 the blue curves are the potentials and the red curve is the radial wave function $u(r)$. The dashed line shows the extrapolated asymptotic behavior $u^{\text{as}}(r)$ of $u(r)$ for $r \to \infty$ (eq. (2.16)). The extrapolation of $u^{\text{as}}(r)$ intersects the r-axis at $r = a_0$ [82, p. 357].

The s-wave scattering lengths take different values for different potentials. For a repulsive potential, the phase shift is negative and the scattering length is positive, see fig. 2.2 (a). The scattering length is negative for an attractive potential without bound state, see fig. 2.2 (b), and the phase shift $\lim_{k\to 0} \delta_{l=0}(k) < \pi/2$. By increasing the potential to a critical value, the scattering length goes to infinity when the phase shift approaches $\pi/2$. The potential is now strong enough to support a bound state at $E = 0$ (see fig. 2.2(c), dashed green line). The scattering length is positive for an attractive potential with a bound state (dashed green line), see fig. 2.2 (d). The phase shift is negative and takes values from $-\pi$ to $-\pi/2$.

Normally, the scattering length is approximately equal to the range of the interaction [15, 27]. Some atoms have large scattering length, also there are atoms with tuneable scattering length, which can be experimentally tuned to an arbitrary size. By cooling those atoms to sufficiently low temperature, the universal regimes can be reached, with such phenomena like Bose-Einstein condensation for bosonic atoms or superfluidity for fermions [15]. There are also systems in particle and nuclear physics, for example, neutrons, neutron-proton systems or $\alpha\alpha$-systems, where α stands for the ^{4}He nucleus [15].

2.2 BCS-BEC Crossover and Unitary Limit

In dilute ultra-cold Fermi gases in BCS or dilute ultra-cold Bose gases in BEC, the details of finite-range interactions are unimportant [77] and universal behavior of the system is expected (see [34, 50, 77], etc.). The properties of the system are determined by the scattering length. The BCS theory describes an ultra-cold Fermi gas at absolute zero temperature interacting through a weak attractive potential. The potential does not support a two-body bound state. As already mentioned, at sufficiently low temperature, the fermionic atoms form Cooper pairs and enter the superfluid or superconducting phase. Since the attractive interaction between the fermions is very weak, the size of the Cooper pairs is larger than the interparticle distance between the fermions. In the real space, the pairs are highly overlapping as can be seen in fig. 2.3, which shows the BEC and BCS states as well as the BCS–BEC crossover schematically. As the attraction becomes stronger, the size of the Cooper pairs decreases, and

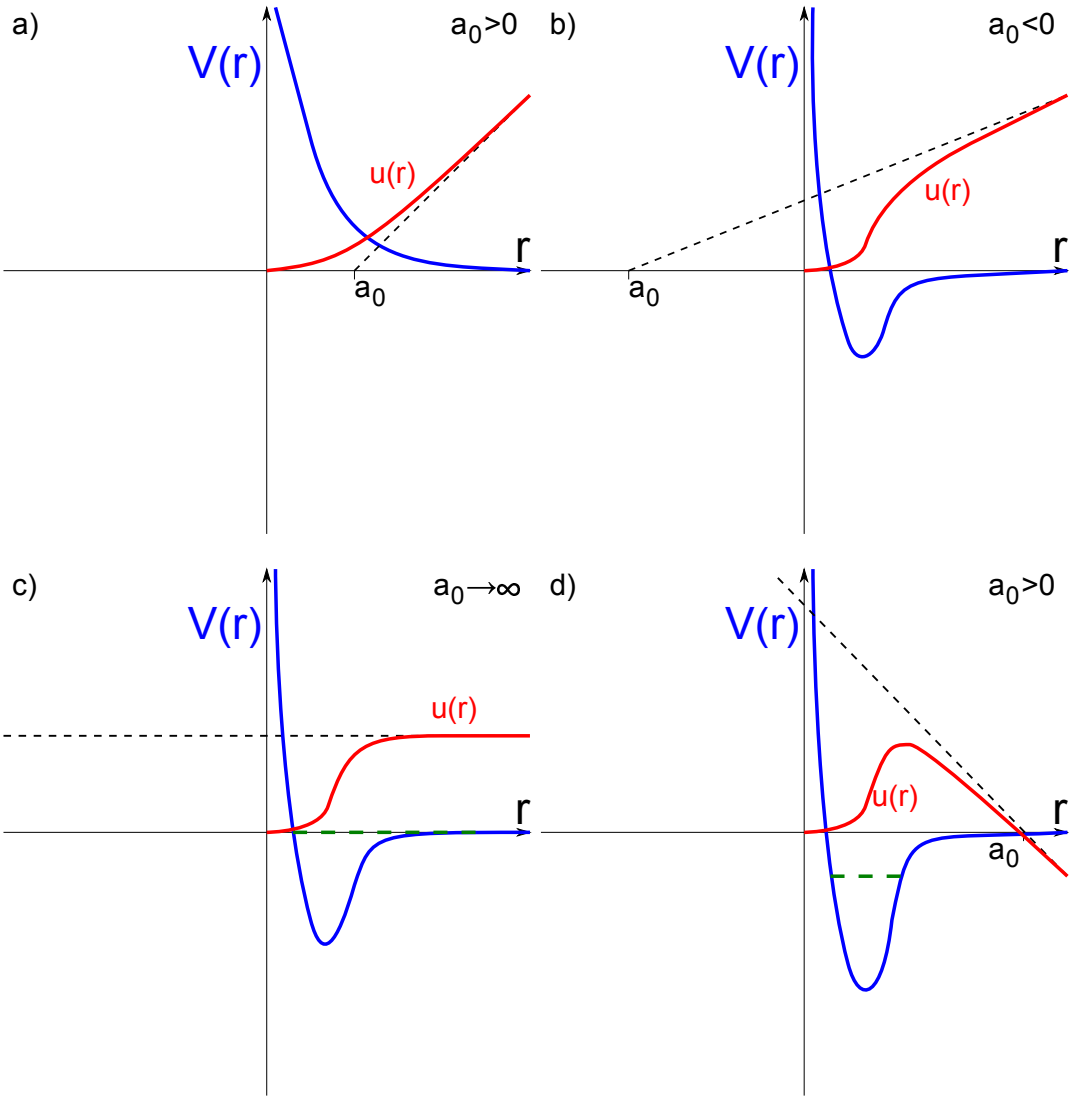

Figure 2.2.: Sketch of the scattering length for a repulsive (a) and an attractive (b),(c),(d) potential. The solid line is the wave function $u(r)$ and the dotted line is its extrapolation. The intersection of the dotted line with the r-axis corresponds to the s-wave scattering length. For a weak potential without a bound state, the scattering length is negative. The scattering length diverges for a potential with a state at $E = 0$ and becomes positive for a potential with a bound state.

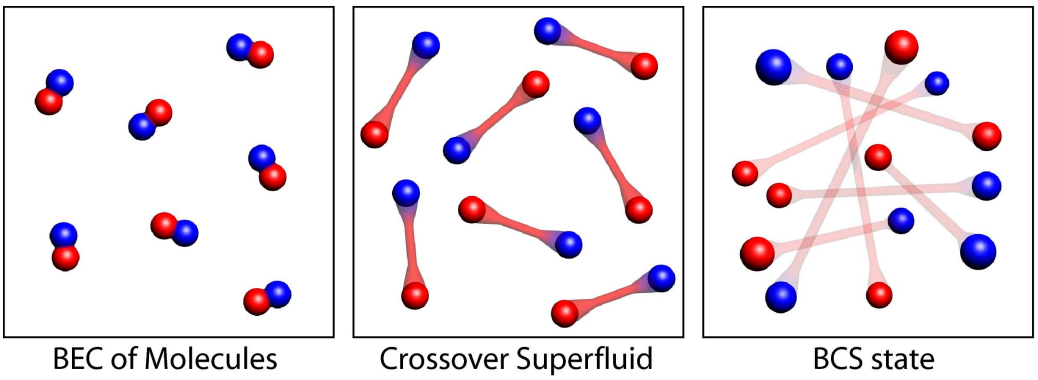

Figure 2.3.: The BCS–BEC crossover. By tuning the interparticle interaction in an ultra-cold Fermi gas in the vicinity of the Feshbach resonance, the Fermions undergo a crossover from long-range Cooper pairs to a BEC of tightly bound molecules. The strongly interacting regime with pair size comparable to interparticle spacing is in between these two limits. Figure taken from [50].

the fermions enter the BEC–BCS crossover; for an even stronger interaction, the fermionic atoms form tightly bound diatomic molecules. The size of these diatomic molecules is much smaller than the average interparticle distance.

In the BCS–BEC crossover, the point where the s-wave scattering length diverges defines the unitary limit with universal properties. As the two-body scattering length a_0 approaches infinity, the scattering cross-section reaches the maximal value with eq. (2.13). The only relevant scale for the ground state is the interparticle spacing $n^{-1/3}$, where n is the particle density of the system, and the only relevant energy scale is the Fermi energy E_F for fermionic systems [41]. Quantities such as the average energy of the gas, the binding energy of a pair and the critical temperature are proportional to E_F [50]. In the BCS–BEC crossover, the interparticle potential is just strong enough to bind two particles in free space; the scattering length tends to infinity and is larger than the range of interatomic potential. The fermions are strongly interacting, with the pair size being of the order of the spacing between fermions [45]. At the same time, the gas is dilute, since the range of the interatomic potential is much smaller than the interparticle distance. The system is dilute and strongly interacting at the same time [34]. The unitary limit is characterised by $a_0 \gg a_{\mathrm{HO}}$ and $R_{\mathrm{int}} \ll a_{\mathrm{HO}}$.

The behavior of the scattering length as a function of the magnetic field B in the vicinity of the Feshbach resonance is shown in fig. 2.4. Region I is the BCS, region III the BEC and in the middle, region II is the unitary regime with diverging scattering length. At the critical field B, the sign of the scattering length changes from negative to positive. For a bound state near the threshold ($E = 0$), the scattering length is large, see fig. 2.2 (c). As the strength of the interaction increases, the scattering length diverges and goes to infinity for a particular critical strength of B. Experiments [39, 44] have shown that the scattering length a_0 can be tuned using Feshbach resonances (see section 2.4).

2.3 The Two Components of the Fermi Gas

We consider in this section the electronic structure of the atoms used in the ultra-cold collisions experiments. The atoms have the electronic orbital angular momentum L and electronic spin S. The spin-orbit couples L with S to the total electronic angular momentum J. For ultra-cold collision experiments, alkali atoms in the ground state are used. In the ground state, their total electronic orbital momentum is zero ($L = 0$), since all electrons in the core occupy closed shells, and the outer electron is in the s orbital. Therefore the total electronic angular momentum J is equal to the spin of the valence electron $s = 1/2$,

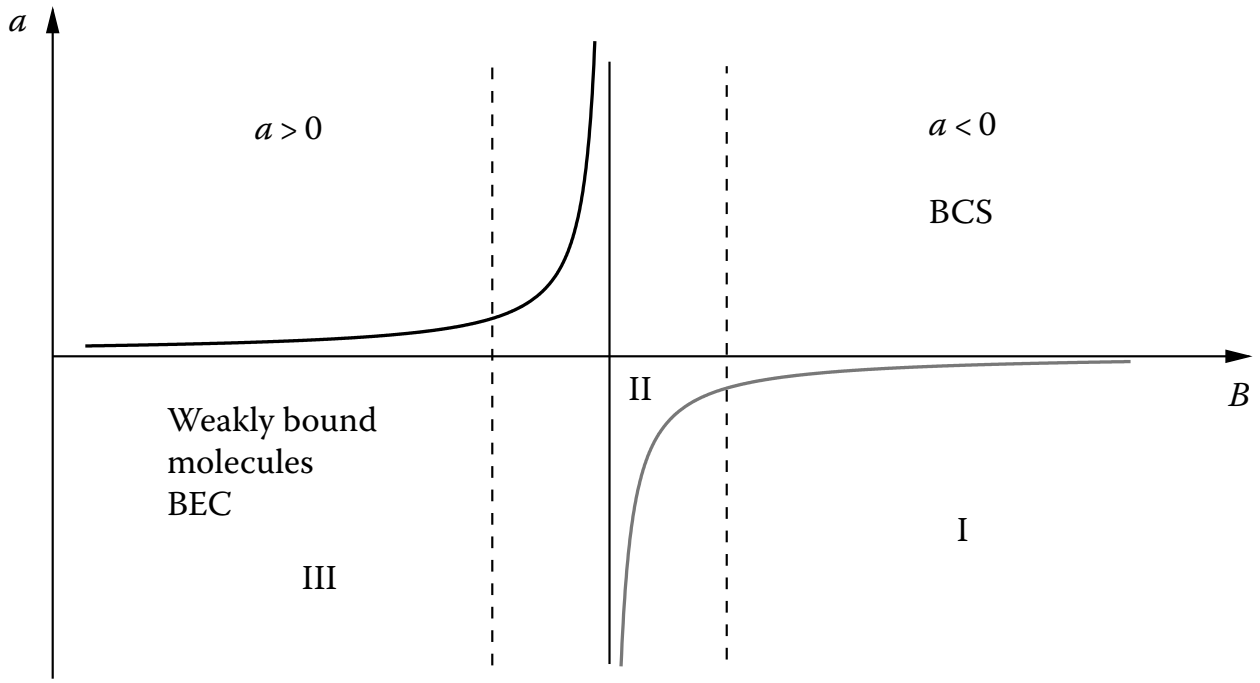

Figure 2.4.: Feshbach resonance. The scattering length can be tuned using a magnetic field from a regime with weakly bound molecules, with positive scattering length (regime III) to the weakly-interacting Fermi gas regime, with negative scattering length, or the other way around. In the strongly interacting regime of the BCS–BEC crossover, the scattering length changes from a very large negative to very large positive value [54, ch. 10]

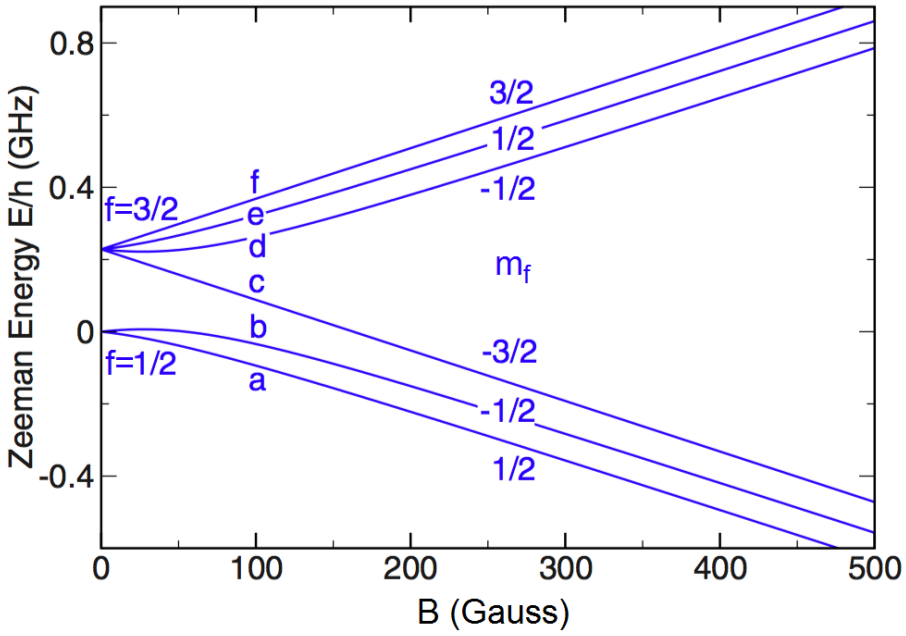

Figure 2.5.: Atomic energy levels of the fermionic ^{6}Li atom, with $s = 1/2$, $I = 1$, and $f = 1/2$ and $3/2$. The figure shows the projection m_f of f. The different hyperfine states are labeled by the alphabetical shorthand notation q_i = a,b,c,d,e and f in order of increasing energy. The figure was taken from [22, p. 6].

and fine-structure splitting due to spin-orbit coupling does not occur. The nuclear spin I of the atom couples with the electron spin due to the magnetic dipole–dipole interaction and the ground state of the alkali atoms splits into the hyperfine structure. This splitting is described by the hyperfine interaction

$$\mathrm{H}_{hf} = \frac{\alpha_{hf}}{\hbar^2}\vec{\mathrm{I}}\cdot\vec{\mathrm{S}}, \tag{2.17}$$

where α_{hf} is the hyperfine constant which connects the spin S and the nuclear spin I [93, p. 217]. Therefore, only the total angular momentum operator $\vec{\mathrm{F}} = \vec{\mathrm{I}} + \vec{\mathrm{S}}$ commutes with the Hamiltonian and is conserved.

The hyperfine eigenstates of the alkali atoms in the ground state with $l = 0$ are completely determined by the quantum number f, its projection m_f as well as I and s and can be written as $\left|nl;(Is)f\,m_f\right\rangle = \left|00;(Is)f\,m_f\right\rangle$. Since, for alkali atoms, $s = 1/2$, the allowed number for f is $I \pm 1/2$, with $m_f = -(I + 1/2), \cdots, (I + 1/2)$ and $m_f = -(I - 1/2), \cdots, (I - 1/2)$. The states with different m_f are degenerate in the absence of a magnetic field (see for example fig. 2.5).

In an external magnetic field, the hyperfine coupling causes an energy shift (called the Zeeman shift) of the hyperfine states, which lifts the degeneracy in m_f of the hyperfine states. For a weak magnetic field, the Zeeman splitting is dominated by the hyperfine states $\left|(Is),f\,m_f\right\rangle$ [93], the hyperfine state splits into $(2s+1)(2I+1) = 4I+2$ sub-levels. Good quantum number are f and its z-projection m_f. At high magnetic fields strength $B \gg {}^{\alpha_{\mathrm{hf}}}/_{(\mu_B\hbar)}$ the electronic and the nuclear spin z-projection m_s and m_I are good quantum numbers [50, 97].

By controlling the external field, the hyperfine states can be manipulated. This is used in experiments. Fig 2.5 shows the Zeeman energy levels as a function of the magnetic field B for an alkali fermion ^{6}Li. ^{6}Li is often used in ultra-cold experiments, because it has an experimentally easily accessible Feshbach resonance, which allows accurate tuning of the interaction. ^{6}Li has nuclear spin $I = 1$ and hence the ground state splits into two hyperfine levels with $f = 3/2$ or $f = 1/2$. In a magnetic field, the $f = 3/2$

state splits into four Zeeman sub-levels and the $f = 1/2$ state splits into two sub-levels. These sub levels are labeled in the figure by the standard notation of atomic Zeeman levels for any species and any field strength. The q_i refer symbolically to the $(f_i m_{f_i})$.

The ultra-cold atoms are prepared in two different hyperfine states, q_1 and q_2. For magnetic trapping one uses a stable pair of magnetically trappable hyperfine states; hence the collisions can be considered to be elastic and the two final states are the same as the initial ones, $(q_1, q_2) = (q_1', q_2')$. A consequence is that, in a two-component system with A particles, the sum over m_{f_i} is conserved. Since each particle stays in its hyperfine state and particles do not change state, we can treat the hyperfine state as a particle property like, for instance, the isospin, and introduce an additional two-valued quantum number q_i, which distinguishes the two hyperfine states. Mixtures of the lowest hyperfine states are, for example, stable against spin relaxation, where an inelastic collision becomes possible by an exchange of angular momentum between electrons and nuclei. Furthermore, for fermions, the states are also stable against dipolar relaxation, where angular momentum is transferred from the electrons and/or nuclei to the relative motion of the atom. When dipolar relaxation occurs, the only allowed state has both atoms in the same state and the wave function becomes symmetric. Since the wave function of the fermions has to be antisymmetric, dipolar relaxation cannot occur. The situation changes near a Feshbach resonances, where all inelastic processes are usually strongly enhanced. For the ultra-cold experiments at unitarity the Fermi gases are prepared in two hyperfine states near a Feshbach resonance that is used to control the interaction. Therefore, we can still consider the mixture of the two hyperfine states as stable. More about the collision properties in ultra-cold gases can be found, for example, in [50].

2.4 Feshbach Resonances

Feshbach resonances play an important role in the physics of ultra-cold atomic gases. They allow the scattering length to be tuned to any values, also to the so-called unitary limit with large scattering length. Feshbach resonances were first investigated in bosonic systems (for instance, by Inouye *et al.* [44] and Courteille *et al.* [24]) and later in fermionic systems (first in ^{6}Li by O'Hara *et al.* [39] and Bourdel *et al.* [14]). With magnetically tunable Feshbach resonances it is possible to modify the interaction of two colliding atoms by simply changing a magnetic field [54, 103].

In section 2.1 we did not consider the internal states of the atoms. For Feshbach resonances, more realistic interactions have to be considered, where the atoms have internal states (see section 2.3). For the description of magnetically tunable Feshbach resonances, a two-channel model is used, the channels are the possible internal states of the colliding atoms. For alkali atoms, the spin of the valence electron is $s = 1/2$. The valence electrons of the collision partners are either in the singlet state $\left|\mathrm{S}\right\rangle$ with $S = 0$ or in the triplet $S = 1$ state $\left|\mathrm{T}\right\rangle$, where the state (triplet or singlet) refers to the total electronic spin of the interacting atoms. Feshbach resonances occur if the potential of the singlet state is just deep enough to contain a bound state near the dissociation threshold. In an ultra-cold atomic gas we have for the energy of the colliding atoms $E \approx k_\mathrm{B} T \ll \Delta\mu B$, where k_B is Boltzmann's constant, T the temperature. B is the magnetic field, $\Delta\mu$ the difference between the magnetic moments of the colliding atoms and the product $\Delta\mu B$ is the difference in Zeeman energy between them due to the interaction with the magnetic field. Therefore, the atoms collide in the triplet $S = 1$ configuration, since the singlet $S = 0$ is energetically forbidden [93, p. 432] because of the energy conservation. Without the hyperfine coupling, two atoms scattering in the triplet state cannot move into the singlet state, thus the singlet state is called the closed channel and the triplet state the open channel. The different states have different Zeeman shifts in the presence of a magnetic field, and the energy difference between these states can be experimentally changed. Figure 2.6 shows the potential of the both channels schematically, as well as the energy of both channels without the hyperfine coupling as a function of magnetic field. The open channel is a scattering channel with the interaction potential $V_\mathrm{T}(r)$ (red line in fig. 2.6). In the closed channel, the atoms are bound in a molecule with energy E_c and interact via the interaction potential $V_\mathrm{S}(r)$ (blue line in fig. 2.6).

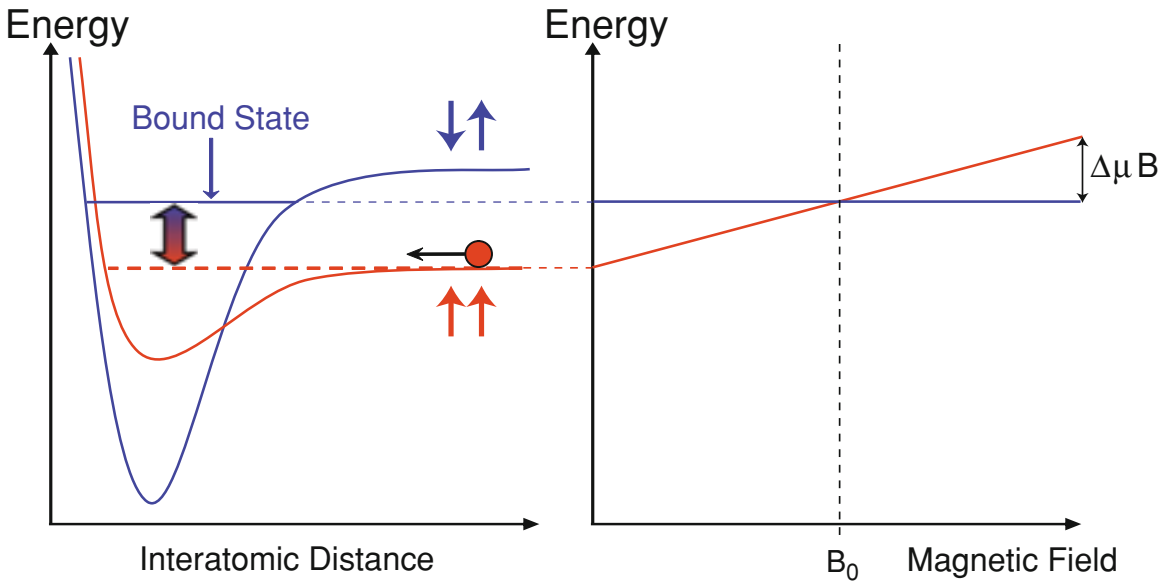

Figure 2.6.: Feshbach Resonance two-channel model [103, ch. 1]. The open channel with interaction potential (in red) is coupled to the bound state of the closed channel (in blue) with energy E_c. The two particles collide in the entrance (open) channel with energy E. A Feshbach resonance occurs when the energy of the bound state is close to the dissociation energy in the open channel. The energy of the closed channel can be tuned with respect to the open channel. The figure was taken from [103, p. 8].

The hyperfine interaction eq. (2.17) does not commute with S^2, and provides the coupling between the singlet and triplet potentials [50, 97]. The electronic spin of the triplet state can be flipped to a singlet configuration by the hyperfine interaction [97]. Therefore the two-channel Schrödinger equation can be written as

$$\begin{bmatrix} -\frac{\hbar^2\vec{\nabla}^2}{m} + V_{\mathrm{T}}(\vec{r}) - E & V_{\mathrm{hf}} \\ V_{\mathrm{hf}} & -\frac{\hbar^2\vec{\nabla}^2}{m} + \Delta\mu B + V_{\mathrm{S}}(\vec{r}) - E \end{bmatrix} \begin{bmatrix} \Phi_{\mathrm{T}}(\vec{r}) \\ \Phi_{\mathrm{S}}(\vec{r}) \end{bmatrix} = 0 \tag{2.18}$$

where V_{T} and V_{S} are the interaction potentials of the atoms in the triplet and singlet internal state, respectively. The $V_{\mathrm{hf}} = \langle \mathrm{T} | \mathrm{H_{hf}} | \mathrm{S} \rangle$ are the matrix elements of the hyperfine coupling [93] which couples the two channels. One assumes that $0 < V_{\mathrm{hf}} \ll V_{\mathrm{T}}, V_{\mathrm{S}}, \Delta\mu B$ [93].

Figure 2.7 shows the energy of the bound state calculated using Schrödinger equation (2.18) for the two coupled square-well interaction potentials, with $V = 0$. The dashed line shows the bound-state energy with $V_{\mathrm{hf}} = 0$. For non-zero hyperfine coupling, the calculated binding energy of the singlet state is shifted and depends quadratically on the magnetic field near Feshbach resonances (instead of linearly). For magnetic fields larger than B_0, where B_0 is the magnetic field at which the scattering length diverges, a bound state no longer exists. The molecule now decays due to the hyperfine coupling into two free atoms, because its energy is above the two-atom continuum threshold. This was also observed in experiments [93].

The magnetic field dependence of the s-wave scattering length near a Feshbach resonances can be described as [22, 93]

$$a_0(B) = a_{bg}\left[1 - \frac{\Delta B}{B - B_0}\right] \tag{2.19}$$

with the width ΔB of the resonance. a_{bg} denotes the off-resonant background scattering length. In a two-body scattering process, magnetically tunable Feshbach resonances occur if the closed channel

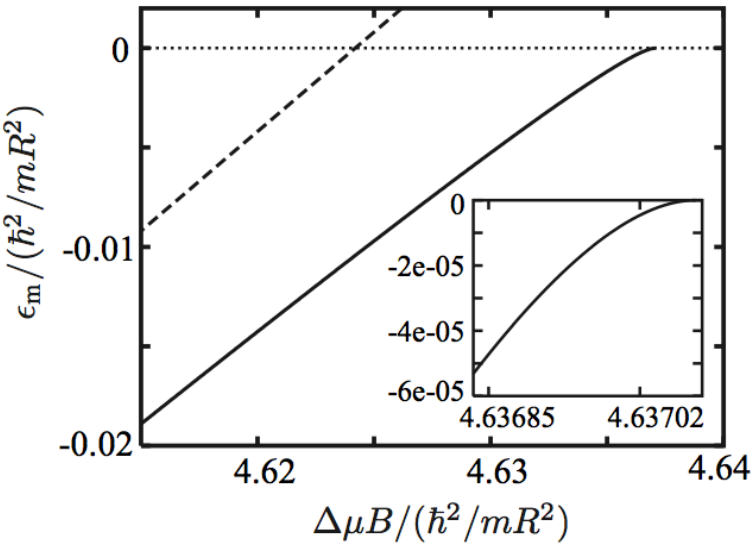

Figure 2.7.: Bound-state energy of the closed channel near a Feshbach resonance for the two coupled square-well interaction potentials with $V = 0$. The dashed line corresponds to $V_{\text{hf}} = 0$ and the solid line to $V_{\text{hf}} = 0.1\hbar^2/mR$. The figure was taken from [93, p. 438].

supports a bound state near continuum and is hence close to zero. The energy E of colliding atoms is, as already mentioned, very low $E \approx k_B T$. The two channels are resonantly coupled and the energy difference of the two channels can be modified by varying the magnetic field. The Feshbach resonance, therefore, allows to tune the scattering length and, consequently, the collision properties of the particles, thereby tuning the properties of the interparticle interaction in ultra-cold gases.

In the fermionic case, the gas near the Feshbach resonance is stable and long-lived, with a lifetime between about 100 ms for ^{40}K and 10 s for ^{6}Li, in contrast to the bosonic case ($\approx 100\,\mu$s). The interacting atoms can form molecules near a Feshbach resonance. These so-called Feshbach molecules are extremely weakly bound and become halo dimers. Further relaxation into a more deeply bound state is possible [50]. Another possibility to achieve resonant coupling is using optical methods, the optical Feshbach resonances [22].

As already mentioned, for extremely large scattering length gases experience universal properties. This regime is also called the unitary limit which we consider in this thesis.

3 Interactions

We use *ab initio* many-body techniques, e.g. the no-core shell model, for the calculation of the energy spectra of two-component ultra-cold Fermi gases at unitarity. To perform the many-body calculations we first need to compute the matrix elements of the interaction between the fermions. In chapter 2 we discussed the scattering properties of the ultra-cold Fermi gas, introduced the scattering length and the unitary limit. In this chapter, we give a brief summary of the interactions we apply to calculate the ground-state and excited-state energies of the trapped two-component fermion systems at unitarity.

In the unitary limit, the s-wave scattering length a_0 diverges. The details of the interparticle interaction at short distances cannot be resolved (see section 2.1). Therefore, the details of the interparticle interaction are irrelevant and the interaction can be approximated by a simple contact interaction (a δ-function). The contact interaction is singular and must be regularized [33, 91]. In order to perform this regularization, a momentum or energy cutoff in relative coordinates is introduced and the strength V_0 of the interaction is renormalized. Calculations with different interparticle potentials provide the same results for the ground-state energy. The only requirement on the potential is that the s-wave scattering length must be very large.

For our IT-NCSM calculations we need matrix elements of the interparticle interaction in single-particle coordinates. However, the two-body matrix elements of the interparticle interaction are initially computed in relative coordinates. Hence we have to transform the matrix elements of the interaction calculated in relative coordinates to the single-particle coordinates, which is done by a Talmi-Moshinsky transformation [60, 96]. We briefly introduce different two-body bases as well as the Talmi-Moshinsky transformation and our implementation in section 3.2. The Hamiltonian and the wave-function of a two-particle two-component ultra-cold Fermi system in a trap is introduced in section 3.3. Furthermore, we consider the energy spectrum for two cold atoms in a HO trap interacting through a contact interaction (a regularized δ-function) for different scattering lengths in section 3.4. We use the energy in the unitary limit for calculation of various interactions. The cutoff used to regularize the δ-potential is described in section 3.5.

We use for our calculations an interparticle interaction derived using an effective field theory (EFT) approach (see section 3.6 and [77]), where the interaction is approximated by a δ function and its derivatives, the ABF interaction (see section 3.7 and [1]), and a Gaussian-shaped interaction (see section 3.8).

3.1 Two-Component Fermions in a Trap: Formalism

We consider a two-component gas of identical fermions in a trap, such as ^{6}Li or ^{40}K atoms in two different hyperfine states. The system is trapped in a HO potential with HO length a_{HO}. The details of the interaction are irrelevant as long as the density is small (that is, the interparticle distance is much larger than R_{int}).

The non-relativistic Schrödinger equation for an A fermion system

$$\mathrm{H}_A \left|\psi_A\right\rangle = E \left|\psi_A\right\rangle \tag{3.1}$$

is solved by numerical diagonalization by using Slater determinants constructed from a discrete single-particle basis. We choose the eigenstates of the three-dimensional harmonic oscillator as the single-particle basis and this introduces the HO length a_{HO} as a length scale.

The Hamiltonian for a non-relativistic cold trapped two-component atomic system with A fermions of mass m has the form:

$$\mathrm{H}_A = \sum_{i=1}^{A} \frac{\vec{\mathrm{p}}_\mathrm{i}^{\,2}}{2m} + \sum_{i=1}^{A} \frac{m\omega^2}{2} \vec{\mathrm{r}}_\mathrm{i}^{\,2} + \sum_{i<j}^{A} \mathrm{V}_{ij} + \ldots, \tag{3.2}$$

where ω is the trap frequency, $\vec{\mathrm{p}}_i$ and $\vec{\mathrm{r}}_i$ corresponds to the single-particle momenta and coordinates of i-th particle, V_{ij} is the two-body interaction and the dots denote the contributions of possible three- and higher-body interactions. The dominant interactions are two-body interactions (see section 2.1). In the available literature, only two-body interactions are being taken into account; to our best knowledge, three-body interactions have not been used so far. In this thesis, we consider a set of different two-body interactions:

- an effective field theory approach at next-to-leading order [91] (see chapter 3.6)
- the ABF interaction used by Alhassid *et al.* [1] (see chapter 3.7), and
- a Gaussian-shaped potential (see chapter 3.8).

The two-body matrix elements of the interaction are calculated in the relative coordinates. In the next section we describe the different two-body basis states as well as the transformation between them.

3.2 Two-Body Basis State and Talmi Transformation

For calculations of the energy spectra of two-component fermionic systems, we use the Hamiltonian (3.2) with any of the two-particle interactions discussed in this chapter. Since the matrix elements of the interaction are in relative coordinates, they first have to be transformed to the single-particle coordinates. To this end, we use the Talmi-Moshinsky transformation. The matrix elements are stored in an L-coupled scheme. We describe in this section the different schemes to store the two-body matrix elements as well the transformation between them.

3.2.1 Two-Body Basis State

In the following we introduce the two-body basis states in relative and center-of-mass coordinates as well as the antisymmetrized L-coupled states in single-particle coordinates and define the notation we use later on. We only consider a two-particle interaction, because of the diluteness of the system (see section 2.1). The antisymmetrized two-body L-coupled states are given by

$$\Big|\big[n_1 l_1, n_2 l_2\big]\, L M_L \Big\rangle \otimes \Big| f_1 m_{f_1}, f_2 m_{f_2} \Big\rangle, \tag{3.3}$$

where either the space part or the hyperfine part is antisymmetric. In the above equation n_i are the single-particle harmonic-oscillator quantum numbers, l_i the single-particle orbital angular momenta and m_{l_i} their projection in single-particle coordinates $\vec{r}_i$, $i = 1, 2$. The l_i are coupled to the total orbital angular momentum L and the quantum number M_L is the corresponding projection. The $\Big| f_i m_{f_i} \Big\rangle$ denote the two different hyperfine states of the atomic Fermi gas (see section 2.3). We store the computed matrix elements of the interaction in the L-coupled scheme and transform them on-the-fly into the m-scheme used for our IT-NCSM calculations (see section 4.2). The transformation into the two-body basis state in the m-scheme from the L-coupled scheme can be easily performed using the Clebsch-Gordan coefficients.

The interparticle interaction is translationally invariant and hence must depend on relative coordinates only and not on center-of-mass coordinates. Therefore, matrix elements of the interaction are calculated in relative coordinates. In this representation, the size of the matrix becomes minimal. The two particles

with single-particle coordinates $\vec{r}_1, \vec{r}_2$ have the relative coordinate $\vec{r} = {}^1/\sqrt{2}\left(\vec{r}_1 - \vec{r}_2\right)$ and the center-of-mass coordinate $\vec{r}_{\mathrm{cm}} = {}^1/\sqrt{2}\left(\vec{r}_1 + \vec{r}_2\right)$. The two-body HO states in relative and center-of-mass coordinates are

$$\left|\left[n_{\mathrm{cm}} l_{\mathrm{cm}}, nl\right] LM_L\right\rangle \otimes \left|f_1 m_{f_1}, f_2 m_{f_2}\right\rangle, \tag{3.4}$$

where n_{cm}, l_{cm} and m_{cm} denote the radial quantum number, the orbital angular momentum and the projection of the orbital angular momentum of the center of mass of the two-body HO basis state, respectively. The radial quantum number, the orbital angular momentum and the projection of the orbital angular momentum in the relative frame are denoted by n, l and m_l.

The center-of-mass part is symmetric under particle exchange by definition, hence the relative part or the part with additional quantum number defining the hyperfine state must be antisymmetric, because the complete state has to be antisymmetric. Furthermore, the two-particle interaction does not affect the center-of-mass part, hence we can omit the center-of-mass part and only consider the matrix elements in the relative basis and the part with the hyperfine states $\left|f_i m_{f_i}\right\rangle$.

As already mentioned (see section 2.1) we consider particles at low energy and the scattering occurs in the s-wave and hence $l = 0$. Therefore, the spatial part of the wave function

$$\left\langle \vec{r}\middle| nlm_l \right\rangle = \left\langle \vec{r}\middle| n00 \right\rangle = \phi_n(\vec{r}). \tag{3.5}$$

is also symmetric. Since for fermions the total wave function must be antisymmetric the part with the hyperfine states $\left|f_i m_{f_i}\right\rangle$ (see section 2.3) has to be antisymmetric

$$\left|n00\right\rangle \otimes \left|f_1 m_{f_1}, f_2 m_{f_2}\right\rangle_a. \tag{3.6}$$

The subscript a shows that the state is antisymmetric with respect to particle exchange. States where both interacting atoms belong to the same hyperfine state $\left|f_i m_{f_i}\right\rangle$ are symmetric, hence the corresponding matrix elements are zero. Therefore the only states with non-zero martix elements are those with

$$\left|f_1 m_{f_1}, f_2 m_{f_2}\right\rangle_a = \frac{1}{\sqrt{2}}\left|f_1 m_{f_1}, f_2 m_{f_2}\right\rangle - \left|f_2 m_{f_2}, f_1 m_{f_1}\right\rangle \tag{3.7}$$

as hyperfine part, where $f_1 m_1 \neq f_2 m_2$. In the following we have to transform the symmetric spatial wave function via a Talmi-Moshinsky transformation from the relative and center-of-mass coordinates into the L-coupled scheme. For this reason we consider first the Harmonic Oscillator Brackets (HOBs).

3.2.2 Harmonic Oscillator Brackets

In the following we use HOBs which are defined by [47]

$$\left|\left[n_1 l_1, n_2 l_2\right] LM_L\right\rangle = \sum_{n_{\mathrm{cm}} l_{\mathrm{cm}}, nl} \left|\left[n_{\mathrm{cm}} l_{\mathrm{cm}}, nl\right] LM_L\right\rangle \left\langle\left\langle n_{\mathrm{cm}} l_{\mathrm{cm}}, nl\middle| n_1 l_1, n_2 l_2; L\right\rangle\right\rangle_d. \tag{3.8}$$

This equation describes an orthogonal transformation in general (for arbitrary values of d), with the HOB $\left\langle\left\langle n_{\mathrm{cm}} l_{\mathrm{cm}}, nl\middle| n_1 l_1, n_2 l_2; L\right\rangle\right\rangle_d$, where d is a nonnegative real number. The transformation of the coordinates is written as follows:

$$\begin{pmatrix} \vec{r}_{\mathrm{cm}} \\ \vec{r} \end{pmatrix} = \begin{pmatrix} \sqrt{\frac{d}{1+d}} & \sqrt{\frac{1}{1+d}} \\ \sqrt{\frac{1}{1+d}} & -\sqrt{\frac{d}{1+d}} \end{pmatrix} \begin{pmatrix} \vec{r}_1 \\ \vec{r}_2 \end{pmatrix}. \tag{3.9}$$

We have to transform from relative and center-of-mass coordinates to single-particle coordinates. $d = {}^{m_1}/_{m_2}$ is the ratio of the masses of the two interacting particles and we consider only particles with equal masses, that is, $d = 1$.

The HOB conserve total energy on both sides of the bracket, i. e.,

$$e_1 + e_2 = e_{\mathrm{cm}} + e_{\mathrm{rel}} \tag{3.10}$$

with $e_i = 2n_i + l_i$, $e_{\mathrm{cm}} = 2n_{\mathrm{cm}} + l_{\mathrm{cm}}$ and $e_{\mathrm{rel}} = 2n + l$ the principal oscillator quantum numbers of the relative, center-of-mass or single-particle frame, respectively, so that only those HOBs that satisfy

$$2n_1 + l_1 + 2n_2 + l_2 = 2n_{\mathrm{cm}} + l_{\mathrm{cm}} + 2n + l \tag{3.11}$$

can be nonzero. The sum in eq. (3.8) is finite because of this conservation property since $n_{\mathrm{cm}}, l_{\mathrm{cm}}$ and n, l are nonnegative integers. Furthermore, the conservation of energy also implies the conservation of parity in the wave function, i. e.,

$$(-1)^{l_1+l_2} = (-1)^{l_{\mathrm{cm}}+l} \tag{3.12}$$

The HOBs defined this way are real. Furthermore,

$$\left\langle\!\left\langle\, n_1 l_1, n_2 l_2 \middle| nl, n_{\mathrm{cm}} l_{\mathrm{cm}}; L \,\right\rangle\!\right\rangle_d = \left\langle\!\left\langle\, nl, n_{\mathrm{cm}} l_{\mathrm{cm}} \middle| n_1 l_1, n_2 l_2; L \,\right\rangle\!\right\rangle_d . \tag{3.13}$$

In the remainder of this thesis the subscript d is omitted since $d = 1$.

3.2.3 Talmi-Moshinsky Transformation

Now we perform the transformation of relative two-body matrix elements of the interaction V into L-coupled two-body matrix elements; the operator V represents an arbitrary two-body interaction. As already mentioned (see section 3.2.1) the spatial part of the wave function in relative and center-of-mass frame is symmetric and hence the part with hyperfine states $\left| f_1 m_{f_1}, f_2 m_{f_2} \right\rangle$ has to be antisymmetric. We can also omit the hyperfine part (see section 2.3) for brevity without loss of universality, since the interaction only acts on the spatial part of the wave function. Therefore, we only have to transform the matrix elements

$$\left\langle \left[n_1 l_1, n_2 l_2 \right] L M_L \middle| \mathrm{V} \middle| \left[n_1' l_1', n_2' l_2' \right] L' M_L' \right\rangle . \tag{3.14}$$

First we consider the bra state. Inserting the HOBs, we obtain:

$$\left\langle \left[n_1 l_1, n_2 l_2 \right] L M_L \right| = \sum_{n_{\mathrm{cm}} l_{\mathrm{cm}}, nl} \left\langle\!\left\langle\, n_1 l_1, n_2 l_2 \middle| n_{\mathrm{cm}} l_{\mathrm{cm}}, nl; L \,\right\rangle\!\right\rangle \left\langle \left[n_{\mathrm{cm}} l_{\mathrm{cm}}, nl \right] L M_L \right| \tag{3.15}$$

Now we decouple the center-of-mass momentum from the relative momentum

$$\left\langle \left[n_{\mathrm{cm}} l_{\mathrm{cm}}, nl \right] L M_L \right| = \sum_{m_{l_{\mathrm{cm}}} m_l} \left\langle\, l_{\mathrm{cm}} m_{\mathrm{cm}} l m_l \middle| L M_L \,\right\rangle \left\langle\, n_{\mathrm{cm}} l_{\mathrm{cm}} m_{\mathrm{cm}}, nl m_l \right| , \tag{3.16}$$

using the Clebsch-Gordan coefficients $\left\langle\, l_{\mathrm{cm}} m_{\mathrm{cm}} l m_l \middle| L M_L \,\right\rangle$.

The ket state of the matrix element (3.14) can be transformed in an analogous way; we first decouple the center-of-mass momentum from the relative momentum of the matrix elements (3.14) and obtain

$$\begin{aligned} &\left\langle \left[n_{\mathrm{cm}} l_{\mathrm{cm}}, nl \right] L M_L \middle| \mathrm{V} \middle| \left[n_{\mathrm{cm}}' l_{\mathrm{cm}}', n' l' \right] L' M_L' \right\rangle = \\ &\sum_{m_{l_{\mathrm{cm}}} m_l} \sum_{m_{l_{\mathrm{cm}}}' m_l'} \left\langle\, l_{\mathrm{cm}} m_{l_{\mathrm{cm}}} l m_l \middle| L M_L \,\right\rangle \left\langle\, l_{\mathrm{cm}}' m_{\mathrm{cm}}' l' m_l' \middle| L' M_L' \,\right\rangle \left\langle\, n_{\mathrm{cm}} l_{\mathrm{cm}} m_{l_{\mathrm{cm}}}, nl m_l \middle| \mathrm{V} \middle| n_{\mathrm{cm}}' l_{\mathrm{cm}}' m_{l_{\mathrm{cm}}}', n' l' m_l' \,\right\rangle . \end{aligned} \tag{3.17}$$

As already mentioned, the interaction between the particles does not act on the center-of-mass part; therefore, only matrix elements with equal n_{cm}, l_{cm} and $m_{l_{\mathrm{cm}}}$ are nonzero. Also, using the rotational symmetry of the interaction we get:

$$\left\langle n_{\mathrm{cm}} l_{\mathrm{cm}} m_{l_{\mathrm{cm}}}, nlm_l \middle| \mathrm{V}_{nn'} \middle| n'_{\mathrm{cm}} l'_{\mathrm{cm}} m'_{l_{\mathrm{cm}}}, n'l'm'_l \right\rangle = \delta_{n_{\mathrm{cm}},n'_{\mathrm{cm}}} \delta_{l,l'_{\mathrm{cm}}} \delta_{m_{l_{\mathrm{cm}}},m'_{l_{\mathrm{cm}}}} \delta_{l,l'} \delta_{m_l,m'_l} \left\langle nlm_l \middle| \mathrm{V} \middle| n'l'm'_l \right\rangle; \tag{3.18}$$

only the matrix elements satisfying this relation are nonzero. Therefore we can eliminate the sum over $n'_{\mathrm{cm}}, l'_{\mathrm{cm}}, m'_{l_{\mathrm{cm}}}$ as well as l', m'_l in eq. (3.17) and, because we consider only s-waves, we can also eliminate the sum over l and m_l.

Using the orthogonality relation

$$\sum_{m_{l_{\mathrm{cm}}} m_l} \left\langle l_{\mathrm{cm}} m_{l_{\mathrm{cm}}} l m_l \middle| LM_L \right\rangle \left\langle l_{\mathrm{cm}} m_{l_{\mathrm{cm}}} l m_l \middle| L'M'_L \right\rangle = \delta_{LL'} \delta_{M_L M'_L} \tag{3.19}$$

of the Clebsch-Gordan coefficients, we therefore obtain

$$\begin{aligned} &\left\langle \left[n_1 l_1, n_2 l_2\right] LM_L \middle| \mathrm{V} \middle| \left[n'_1 l'_1, n'_2 l'_2\right] LM_L \right\rangle = \\ &\sum_{n_{\mathrm{cm}} l_{\mathrm{cm}}, nl} \sum_{n'} \left\langle \left\langle n_1 l_1, n_2 l_2 \middle| n_{\mathrm{cm}} l_{\mathrm{cm}}, nl; L \right\rangle \right\rangle \left\langle \left\langle n_{\mathrm{cm}} l_{\mathrm{cm}}, n'l \middle| n'_1 l'_1, n'_2 l'_2; L \right\rangle \right\rangle \left\langle nlm_l \middle| \mathrm{V} \middle| n'lm_l \right\rangle . \end{aligned} \tag{3.20}$$

As already mentioned we only consider the s-wave (i. e. $l = l' = 0$, $m_l = m'_l = 0$, see section 2.1) and hence we only need to transform matrix elements with

$$V_{n,n'} = \left\langle nlm_l \middle| V \middle| n'lm_l \right\rangle = \left\langle n00 \middle| V \middle| n'00 \right\rangle \tag{3.21}$$

Using eq. (3.20), we can transform the matrix elements of the three different interactions, which have been calculated in relative coordinates, into the L-coupled matrix elements that we need for our many-body calculations (see chapter 4).

3.2.4 Implementation, Computational Strategy

We use the m-scheme as the basis for the many-body calculations because the calculation of many-body matrix elements and antisymmetrization are trivial (see section 4.2). The simplicity of the m-scheme is counterbalanced by the large dimension of the Hamilton matrix. For the many-body calculation in the m-scheme, the two-body L-coupled matrix elements are decoupled during the calculation. Using the coupled scheme for the storage of the Hamilton matrix reduces the amount of memory required compared to storing m-scheme two-body matrix elements by up to three orders of magnitude, since we can use rotational invariance ($L = L'$, see also section 3.2.3) in the L-coupled scheme. In the m-scheme many matrix elements are redundant: a single coupled matrix element is combined with different Clebsch-Gordan coefficients, yielding different m-scheme matrix elements. The m-scheme stores them independently, but the physics is in the coupled matrix elements only; the rest is angular momentum algebra. Some properties of the Hamiltonian can also be accommodated in the m-scheme: The Hamilton operator does not change the parity of the many-body state, so that we can restrict the calculation to the positive- or negative-parity part of the Hilbert space. Furthermore, we can take into account that the hyperfine states of the interacting fermions do not change (see chapter 2.3) as a consequence the sum over all m_{f_i} is conserved and that only particles with different m_{f_i} interact.

We use a cache-optimized storage scheme for the L-coupled matrix elements to facilitate a fast on-the-fly decoupling, in which the matrix elements' values are stored in an one-dimensional array. The position of each L-coupled matrix element in that array is uniquely defined by all its quantum numbers. For this reason we introduce an index $a = \{n_a, l_a\}$ that collects the harmonic-oscillator radial quantum number and orbital angular momentum of the single-particle. We do not use the hyperfine state for the index, since we take into account that only those matrix elements are nonzero for which the hyperfine state of the two particles are different.

- Matrix elements are ordered by the indices a, b, a', b' of the single-particle orbitals in that order of evaluation, that is, elements with a smaller value of a are located at a lower index than those with a larger value of a, and the order of elements with identical a is determined by their value of b, then a', then b'.
- Matrix elements with identical indices a, b, a', b' are ordered by the coupled quantum number $L = L'$.

We do not exploit antisymmetry constraints for matrix elements with identical single-particle orbitals in order to keep a fixed stride. To evaluate a specific m-scheme matrix element, we compute the position in the array defined by the orbital quantum numbers stored in a, b, a', b' go there and then iterate over the contiguous segment of the array containing the matrix elements for different values of L and the hyperfine state. This way the decoupling operation is very simple and highly cache-efficient because matrix elements over which we loop are located close to each other in memory. A similar approach, the so-called JT-coupled scheme, has been adopted in nuclear physics [73].

3.3 Two-Component Two-Particle Fermi System in a Trap

As already mentioned the gas is very dilute and we only need to consider a two-particle interaction; hence we need to calculate only two-particle matrix elements with the Hamiltonian of a two-particle system

$$\mathrm{H}_2 = \sum_{i=1}^{2} \frac{\vec{\mathrm{p}}_\mathrm{i}^2}{2m} + \sum_{i=1}^{2} \frac{m\omega^2}{2} \vec{\mathrm{r}}_\mathrm{i}^2 + \mathrm{V}_{12}. \tag{3.22}$$

In field-free space or in the presence of a homogeneous field, the motion of particles is independent of the center-of-mass position [54, ch. 1]. We consider particles in a trap, but as long as we use either the Jacobi basis or the m-scheme with N_max truncation, the center-of-mass system factorises exactly from the relative system (see [77] and section 4.2). Therefore, we can separate the Hamiltonian into a center-of-mass part H_cm and a relative part H_rel. The solution of the eigenvalue problem of the center-of-mass Hamiltonian,

$$\mathrm{H}_\mathrm{cm} = \frac{\vec{\mathrm{p}}_\mathrm{cm}^2}{2M} + \frac{M\omega^2 \vec{\mathrm{r}}_\mathrm{cm}^2}{2}, \tag{3.23}$$

for a two-particle system, where $\vec{\mathrm{p}}_\mathrm{cm}$ and $\vec{\mathrm{r}}_\mathrm{cm}$ corresponds to the center-of-mass momenta and coordinate and $M = 2m$, is given by

$$E_\mathrm{cm} = \left(2n_\mathrm{cm} + l_\mathrm{cm} + {}^3/_2\right) \hbar\omega, \tag{3.24}$$

Therefore, we only have to solve the Schrödinger equation for the relative motion:

$$\mathrm{H}_\mathrm{rel} \left|\psi\right\rangle = E \left|\psi\right\rangle \tag{3.25}$$

with the relative Hamiltonian

$$\mathrm{H}_\mathrm{rel} = \frac{\vec{\mathrm{p}}_\mathrm{r}^2}{2\mu} + \frac{\mu\omega^2 \vec{\mathrm{r}}^2}{2} + \mathrm{V}_{12}, \tag{3.26}$$

the relative momentum $\vec{\mathrm{p}}_\mathrm{r} = {}^1/\sqrt{2}\left(\vec{\mathrm{p}}_1 - \vec{\mathrm{p}}_2\right)$ and coordinate $\vec{\mathrm{r}} = {}^1/\sqrt{2}\left(\vec{\mathrm{r}}_2 - \vec{\mathrm{r}}_1\right)$ and reduced mass $\mu = {}^m/_2$. V_{12} represents the two-body interparticle interaction.

Now we switch to coordinate representation. The relative two-body wavefunction $\psi(\vec{r})$ can be expressed as a superposition of HO wave functions $\phi_{nlm_l}(\vec{r})$:

$$\psi_{nlm_l}(\vec{r}) = \sum_{n,l=0}^{\infty} \sum_{m_l=-l}^{l} c_{nlm_l} \phi_{nlm_l}(\vec{r}), \tag{3.27}$$

where the c_{nlm_l} are the unknown expansion coefficients, which we determine in the following. The HO wave function $\phi_{nlm_l}(\vec{r})$ is the solution of the three-dimensional non-interacting Schrödinger equation:

$$H_0\phi_{nlm_l}(\vec{r}) = E_{nl}\phi_{nlm_l}(\vec{r}) \tag{3.28}$$

with energy eigenvalues $E_{nl} = (2n + l + 3/2)\hbar\omega$ of the non-interacting Hamiltonian in coordinate representation

$$H_0 = -\frac{\hbar^2}{2\mu}\vec{\nabla}_r^2 + \frac{\mu\omega^2\vec{r}^2}{2}. \tag{3.29}$$

Due to the rotational symmetry, the three-dimensional Schrödinger equation (3.28) can be separated into a radial part $R_{nl}(r)$ depending only on the radial distance and the spherical harmonics $Y_{lm_l}(\Theta, \varphi)$. Accordingly, the HO wave function is given as

$$\left\langle \vec{r}\middle| nlm_l \right\rangle = \phi_{nlm_l}(\vec{r}) = R_{nl}(r)Y_{lm_l}(\Theta, \varphi). \tag{3.30}$$

The radial part $R_{nl}(r)$ can be written as [91]

$$R_{nl}(r) = \left(\frac{2}{a_{\mathrm{HO},\mu}^3\Gamma(l+3/2)}\right)^{1/2}\left[L_n^{(l+1/2)}(0)\right]^{-1/2}\left(\frac{r}{a_{\mathrm{HO},\mu}}\right)^l e^{-r^2/2a_{\mathrm{HO},\mu}^2}\left[L_n^{(l+1/2)}(\frac{r^2}{a_{\mathrm{HO},\mu}^2})\right], \tag{3.31}$$

where the $L_n^{(\alpha)}(x)$ are the generalized Laguerre polynomials and $a_{\mathrm{HO},\mu} = \sqrt{\hbar/\mu\omega}$ is the relative coordinate harmonic oscillator length with reduced mass μ.

In the present thesis, only the s-wave contributions to the two-body potential are taken into account. Therefore, the states with angular momentum $l \neq 0$ are not influenced by the interaction and the eigenfunctions for $l > 0$ correspond to the HO wave functions $\phi_{nlm_l}(\vec{r})$ with the eigenvalues E_{nl}. For calculation of the matrix elements of the interparticle interaction, we only need to consider the terms with $l = 0$ and, consequently, $m_l = 0$, and the wave function for $l = 0$ can be written as

$$\psi(r) = \sum_n c_n\phi_n(r), \tag{3.32}$$

where $\phi_n(r) \equiv \phi_{n00}(\vec{r}) = R_{n0}(r)Y_{00}(\Theta, \varphi)$, and

$$\phi_n(r) = \pi^{-3/4}a_{\mathrm{HO},\mu}^{-3/2}\left[L_n^{(1/2)}(0)\right]^{-1/2}e^{-r^2/2a_{\mathrm{HO},\mu}^2}L_n^{(1/2)}(\frac{r^2}{a_{\mathrm{HO},\mu}^2}). \tag{3.33}$$

Furthermore, by setting $r = 0$ in eq. (3.33), we obtain at the origin [91]:

$$\phi_n(0) = \pi^{-3/4}a_{\mathrm{HO},\mu}^{-3/2}\left[L_n^{(1/2)}(0)\right]^{1/2}. \tag{3.34}$$

We use from now on the notation $\phi_n(r) = \phi_{n00}(\vec{r}) = \left\langle \vec{r}\middle| n00 \right\rangle = \left\langle \vec{r}\middle| n \right\rangle$.

We use these wave functions (eq. (3.33) and eq. (3.34)) for the calculation of the matrix elements of the interaction.

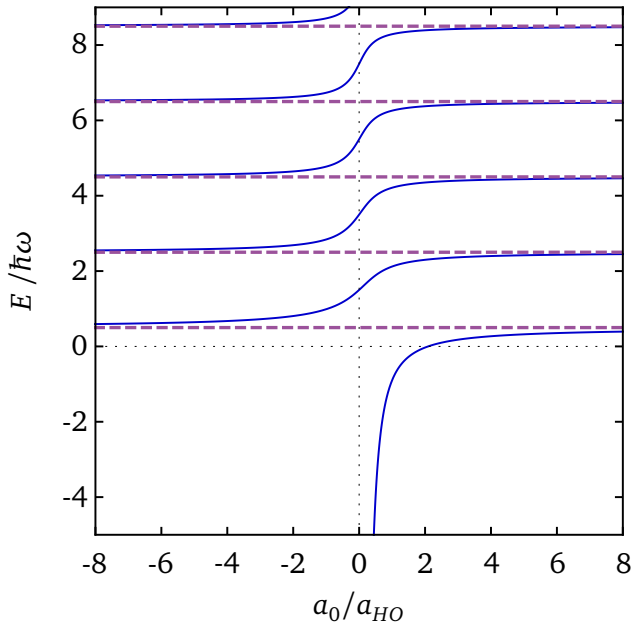

Figure 3.1.: Energy spectrum of two fermions in a trap for the $l = 0$ state calculated using a regularized contact interaction in three dimensions as a function of the s-wave scattering length a_0 in units of a_{HO}. Solid lines represent the energy as a function of a_0. The dashed lines represent the solution for the unitary limit where the s-wave scattering length goes to infinity.

3.4 Spectrum of a Two-Particle System in a Trap

We consider now a two-particle two-component fermion system in a trap. An analytical solution for a two-particle system with a zero-range interaction in a HO trap is given by Busch *et al.* [17]. This solution also gives the exact energy of the two-particle system in a trap in the unitary limit. Alhassid *et al.* [1] and Stetcu *et al.* [91] used this two-particle energy for the calculation of the matrix elements of the interaction. For the calculation of the energy of a two-particle systems, a δ-function can be used as an parametrisation for a zero-range potential [17].

Using the regularized δ-function as potential, Busch *et al.* [17] obtained the following equation for the ground-state energy of a two-particle system in a trap:

$$\frac{\Gamma\left(-\frac{E}{2\hbar\omega}+\frac{3}{4}\right)}{\Gamma\left(-\frac{E}{2\hbar\omega}+\frac{1}{4}\right)} = \frac{a_{\mathrm{HO}}}{\sqrt{2}a_0} \tag{3.35}$$

where $a_{\mathrm{HO}} = \sqrt{\hbar/m\omega} = \sqrt{2}a_{\mathrm{HO},\mu}$ is the HO length and a_0 is the scattering length. Γ represents the Gamma function. For a detailed derivation, see [17]. This transcendental equation links the energy to the scattering length.

Figure 3.1 shows the spectrum of the two-particle system according to eq. (3.35). The left-hand side of eq. (3.35) has poles at

$$E_i(0) = \left(2i+\frac{3}{2}\right)\hbar\omega \tag{3.36}$$

and zeros at

$$E_i(\infty) = \left(2i+\frac{1}{2}\right)\hbar\omega. \tag{3.37}$$

The right hand side vanishes if $a_0 \to \infty$ and diverges for $a_0 \to 0$. Thus the zeros and poles of the left-hand side are the energies for $a_0 \to \infty$ and $a_0 \to 0$, respectively. The former are shown in fig. 3.1. We use eq. (3.34) in order to determine the interaction parameters for the EFT and ABF interactions in the unitary limit. In the following we call the energy calculated using eq. (3.34) E_i^{ex}, the exact energy of the i-th state of the two-particle system. Both interactions are used for calculations of the ground-state ($i = 0$) and excited-state energies of fermionic systems.

3.5 Contact Interaction and Cutoff Regularisation

The short-range interaction between two particles in a two-component Fermi gas is often approximated by a contact interaction [1, 17, 33] modeled as a δ potential. This interaction, however, is singular and must be regularized [33, 91] to be used in a many-body method.

The δ potential can be regularized by limiting the relative HO energy and introducing a relative cutoff as a maximum number of $e_{\text{rel,max}}$, which can be translated into a momentum scale [77]

$$\Lambda_{2;\text{UV}} = \sqrt{m_n \left(e_{\text{rel,max}} + \frac{3}{2} \right) \hbar\omega} = \frac{\hbar}{a_{\text{HO},\mu}} \sqrt{2e_{\text{rel,max}} + 3}. \tag{3.38}$$

With $e_{\text{rel,max}}$, the number of quanta of the highest energy of the two-body relative coordinate wave function, we can introduce a natural cutoff in the HO basis. Since only particles with $l = 0$ are affected by the interaction, $e_{\text{rel,max}} = 2n_{\text{max}}$ holds (see section 2.1 for more details). Therefore, the wavefunctions (3.32) can be written as

$$\psi_n(r) = \sum_n^{n_{\text{max}}} c_n \phi_n(r), \tag{3.39}$$

where n_{max} is the maximum radial quantum number. We omit in eq. (3.39) the labels l and m_l, since we have only the s-wave interaction with $l = 0$ and $m_l = 0$. Only the lowest $e_{\text{rel,max}} + 1$ shells of the HO basis with $l = 0$ are being included in the calculation of the matrix elements, all other interaction matrix elements with $e_{\text{rel}} > e_{\text{rel,max}}$ are set to zero.

To show the need for the renormalization of the δ potential $V(\vec{r}) = V_0 \delta^{(3)}(\vec{r})$, we start with the Schrödinger equation (3.25) for the wave function of the two-particle system $\psi(\vec{r})$ and the relative coordinate Hamiltonian (3.26). We write from here on $\delta^{(3)}(\vec{r}) = \delta(\vec{r})$ for the δ-function in three dimensions and $\delta(r)$ in one dimension. After projecting onto the state $\phi_{n'}(r)$ eq. (3.34), we arrive at

$$(E - E_{n'}) c_{n'} = V_0 \sum_{n=0}^{\infty} c_n \int \mathrm{d}^3 r \, \phi_{n'}^*(r) \delta(\vec{r}) \phi_n(r) = V_0 \phi_{n'}(0) \sum_{n=0}^{\infty} c_n \phi_n(0). \tag{3.40}$$

We use here and in the following that the eigenvalue functions of the HO are real and, therefore, $\phi_{n'}^*(r) = \phi_{n'}(r)$. After rearranging eq. (3.40), we get for the expansion coefficients:

$$c_{n'} = \frac{\phi_{n'}(0) A}{E - E_{n'}} \tag{3.41}$$

$A = V_0 \sum_n c_n \phi_n(0)$ is a constant for all n', depending only on the energy and V_0 because it basically is the solution of the Schrödinger equation. Inserting this into eq. (3.40), we arrive at:

$$\frac{1}{V_0} = \sum_{n=0}^{\infty} \frac{\phi_n^2(0)}{E - E_n} = \pi^{-3/4} a_{\text{HO},\mu}^{-3} \sum_{n=0}^{\infty} \frac{L_n^{(1/2)}(0)}{E - E_n} \tag{3.42}$$

We used here eq. (3.34) for $\phi_n^2(0)$.

The strength of the interaction can be renormalized so that the ground-state energy of the truncated Hamiltonian equals the energy of the two-body system in the unitary limit $E_0^{\text{ex}} = \frac{1}{2}$ given by eq. (3.37) and therefore

$$\frac{1}{V_0} = \pi^{-3/4} a_{\text{HO},\mu}^{-3} (-2\hbar\omega)^{-1} \sum_{n=0}^{\infty} \frac{L_n^{(1/2)}(0)}{n+1} \tag{3.43}$$

We now truncate the sum at finite n_{max} to obtain a meaningful expression and then consider the behavior for $n_{\text{max}} \to \infty$. Using identities for sums involving the generalized Laguerre polynomials at the origin (see eq. (B.21) also used in appendix B) we arrive for a given n_{max} at:

$$\frac{1}{V_0^{(n_{\text{max}})}} = \frac{2}{\pi^2 a_{\text{HO},\mu}^3 \hbar\omega} \frac{\Gamma\left[n_{\text{max}} + \frac{3}{2}\right]}{\Gamma[n_{\text{max}} + 1]} \tag{3.44}$$

Using Stirling's formula:

$$\frac{\Gamma[j+h]}{j^h \Gamma[j]} = 1 + \frac{h(h-1)}{2j} + \mathcal{O}\left(j^{-2}\right) \tag{3.45}$$

we can see that for large n_{max} the expression (3.44) diverges with $n_{\text{max}}^{1/2}$. Therefore, for $n_{\text{max}} \to \infty$, the strength V_0 of the δ potential goes to zero, showing the need for renormalisation.

Because of the renormalization, the calculated energy depends not only on the harmonic oscillator frequency ω but also on n_{max}. In the limit where n_{max} goes to infinity, the results no longer depend on n_{max} and converge to the exact values. For sufficiently large values of n_{max}, the truncation error of the calculation becomes small. For $A = 3$ particles it was shown [1, 77, 89] that the ground-state energy converges to the exact value calculated by Werner *et al.* [102] when n_{max} goes to infinity.

However, convergence of calculated results with a increasing n_{max} is slow [1, 89]. To improve the convergence, higher orders (next-to-leading order (NLO) and next-to-next-to leading order (N^2LO)) of the interaction were included perturbatively in the framework of the effective field theory [77, 91]. Furthermore, the ABF interaction was introduced by Alhassid, Bertsch, and Fang [1]. The latter is no longer a contact interaction, but this interaction also is truncated by a regularization parameter in relative frame.

3.6 Effective Field Theory Approach

As already mentioned in section 2.1, in the unitary limit the particle energy is close to the scattering threshold of zero energy [15]. The behavior of the interaction for large distances $r \gg R_{\text{int}}$ is known, but the behavior at short distances is not known sufficiently well to calculate the low-energy observables [15]. Effective field theory (EFT) is an approach to describe the low-energy behavior of a physical system even in cases where the underlying fundamental theory is unknown or not explicitly solvable. It is a general approach to fundamental theories which summarizes existing phenomenological knowledge [8].

The relevant physics at the considered energy scale can be approximated by a set of appropriate parameters relevant for the energy scale of interest only. Using a single description of the physics in the entire parameter space may not be appropriate: The low-energy dynamics are independent of the details of the high-energy interaction, and consequently the latter is irrelevant for describing the former; it is not necessary to know every high-energy detail in order to obtain a useful description of the physical phenomena of interest. This is called scale separation and greatly reduces the number of parameters involved, as the effects coming from the other scales can be parametrized into the theory with parameters calculated from an underlying theory or fitted to experiment [32, 64]. This approximation can be improved through corrections, which take the influence of the neglected parameters into account as small perturbations [64].

EFTs yields good approximations in cases where calculations using the fundamental theory would be too time-consuming or if the underlying theory is not even known. EFTs can be used to describe the low energy physics using an effective Lagrangian which contains only a few relevant degrees of freedom and ignores additional degrees of freedom which are only important at higher energies. EFTs have been used for calculations on weakly-interacting Bose [2, 15] and Fermi gases [77, 91]. EFTs are also used, for instance, in quantum electrodynamics (QED) and quantum chromodynamics (QCD) and also were applied in nuclear structure physics [57], first by Weinberg [101]. Further applications of EFTs exist in elementary particle physics (Standard Model calculations) as well as in condensed matter physics (for example, Landau theory of Fermi liquids, phonons, and spin waves, see [15] and the references therein). We use an EFT to construct an interaction for the calculation of the ground-state and excited-state energy of a two-component Fermi system in a trap at unitarity.

When calculating binding energies between nucleons, isospin has to be considered, unlike in ultra-cold unitary gases. Other than that, an EFT for describing atomic systems [15] is formally indistinguishable from pionless EFT describing nucleon systems [8], even though the underlying theories are very different [91]. For trapped Fermi gases, the effective field theory approach to two-particle short-range interactions was introduced by Stetcu *et al.* [91] for a two-particle system. They added higher-order terms (NLO and $\mathrm{N^2LO}$) on top of the contact interaction, at LO, which improved convergence of the energy with the many-body cutoff $N_{\max}$ (see chapter 4) and the momentum cutoff Λ of the interaction (see section 3.5). The higher orders (NLO, $\mathrm{N^2LO}$) of an EFT lead to corrections of the LO results and are treated in perturbation theory. The corrections become smaller as Λ increases (see chapter 5 and [1, 77]).

The ground-state and excited-state energies for a three- and four-particle system were calculated by Rotureau *et al.* [77] using EFT interaction introduced in [91] up to $\mathrm{N^2LO}$. For a three-particle system they reached a better convergence with increasing $N_{\max}$ to the exact value calculated by Werner *et al.* [102] by adding NLO and $\mathrm{N^2LO}$ terms. We use this approach for our benchmark calculations of up to 10 fermions (see section 5). In the following, we describe the approach introduced by Stetcu *et al.* [91].

As already mentioned in section 2.1, the fermions have low energy, all interactions are short-ranged, and can be approximated by a contact interaction [38, p. 5]. The idea behind an EFT for particles at low energy is to replace the two-particle potential $V(r)$ by an effective potential $V_{\mathrm{eff}}(r, C_0)$, which is identical to $V(r)$ at large distances for $r > R_{\mathrm{int}}$, where R_{int} is the range of the interaction. In order to describe the interaction at short distances, one introduces an additional tuning parameter C_0, which is chosen such that a given observable is reproduced. The contact interaction is ill-defined and, therefore, has to be regularized by introducing an interaction cutoff in relative space (see section 3.5). This cutoff introduces an error that can be corrected either by letting the cutoff go to infinity, or by taking higher orders into account. For three particles, the ground-state energy of the systems goes to the exact value [102] for very large cutoffs [77]. For large particle numbers, the calculations become very involved and the corrections can be performed by introducing higher-order terms (NLO, $\mathrm{N^2LO}$; see also [77] for three and four particles). Furthermore, the potential is only exact in the unitary limit for $a_0 \to \infty$; away from unitarity, at finite scattering length, the effective range of the interaction has to be considered as well [77]. However, in this thesis, we are only interested in the results at unitarity.

Observables calculated with the effective potential $V_{\mathrm{eff}}(\vec{r}, C_0)$ contain scale-dependent errors. In order to reduce these errors and improve convergence, additional information can be introduced in the form of an additional parameter C_2. The effective potential $V_{\mathrm{eff}}(r, C_0, C_2)$ now depends on two parameters, C_0 and C_2, both of which can be tuned to reproduce given observables. The use of further parameters C_i improves the accuracy without any information about the short-distance potential. Therefore, the effective short-range two-body potential depends on a set of short-distance tuning parameters $C = (C_0, C_2, \ldots)$, which are called low energy constants (LEC). In our case, the observable is the ground-state energy of the trapped two-body system in the unitary limit. To reproduce this expansion with an EFT, one considers a general Lagrangian for a non-relativistic fermion field that is invariant under Galilean, parity and time reversal transformations [15, 52].

The short-range two-body interaction V can be expanded as a Taylor series in momentum space:

$$V\left(\vec{p}',\vec{p}\right) = C_0 + C_2\left(\vec{p}'^2+\vec{p}^2\right) + C_4\left(\vec{p}'^2+\vec{p}^2\right)^2 + \cdots, \tag{3.46}$$

where $\vec{p}$ and $\vec{p}'$ are the initial and final relative momenta, respectively, and C_0, C_2 and C_4 are parameters [52, 63, 91]. Due to the Galilean invariance, only even powers of the momenta appear on the right-hand side of eq. (3.46). Higher powers of the momenta are being neglected. This approach is valid for low momenta only; in these cases, the details of the interaction cannot be resolved. Only s-wave scattering is taken into account.

The Fourier transformation of the effective potential in momentum space, eq. (3.46), into coordinate space is given in appendix B.1 and yields the two-body potential in coordinate space

$$\begin{aligned} \mathrm{V}\left(\vec{r},\vec{r}'\right) &= C_0\delta(\vec{r}')\delta(\vec{r}) - C_2\{[\vec{\nabla}'^2\delta(\vec{r}')]\delta(\vec{r}) + \delta(\vec{r}')[\vec{\nabla}^2\delta(\vec{r})]\} \\ &+ C_4\{[\vec{\nabla}'^4\delta(\vec{r}')]\delta(\vec{r}) + [\vec{\nabla}'^2\delta(\vec{r}')][\vec{\nabla}^2\delta(\vec{r})] + \delta(\vec{r}')[\vec{\nabla}^4\delta(\vec{r})]\} + \ldots \end{aligned} \tag{3.47}$$

Therefore, the interaction can be approximated by δ-functions and their derivatives [52, 63].

Furthermore, the interparticle potential is local and finite and, therefore, only depends on the momentum transfer $\vec{p}-\vec{p}'$ or also $V\left(\vec{r},\vec{r}'\right) = V(\vec{r})\delta\left(\vec{r}-\vec{r}'\right)$. Using this we get the potential

$$V\left(\vec{r},\vec{r}'\right) = V(\vec{r})\delta\left(\vec{r}-\vec{r}'\right) = \left(C_0\delta(\vec{r}) + C_2^{(1)}\left\{\left[\vec{\nabla}^2\delta(\vec{r})\right] + 2\left[\vec{\nabla}\delta(\vec{r})\right]\vec{\nabla} + \delta(\vec{r})\vec{\nabla}^2\right\}\right)\delta(\vec{r}-\vec{r}') \tag{3.48}$$

The derivation is given in the appendix B.1. From now we use the coordinate representation for the EFT section.

The leading order (LO), the NLO and N^{2}LO support only the s-wave [91]. In this thesis, we use the LO and NLO and hence only need to consider the contribution of s-waves to the two-body potential. As previously explained (see section 3.1), we use a HO basis with relative wave functions $\psi_{nlm_l}(\vec{r})$ and energies $E_{nl} = \left(2n+l+\frac{3}{2}\right)\hbar\omega$. For the calculation of matrix elements we use again the interaction cutoff (3.38) by taking into account only the shells (in relative coordinates) up to a given $e_{\mathrm{rel,max}} = 2n_{\max}$ and dropping all other shells from the calculation.

The parameters C_i will be derived in the following using the perturbation theory approach (see appendix A for details). The Hamiltonian in relative coordinates, H_{rel}, for two particles trapped in a harmonic oscillator potential of frequency ω is given by eq. (3.26).

The relative Hamiltonian can be decomposed into an unperturbed component $\mathrm{H}^{(0)}$, which can be solved exactly, and the perturbation W. The Hamiltonian then takes the form

$$\mathrm{H}_{\mathrm{rel}} = \mathrm{H}^{(0)} + W. \tag{3.49}$$

The leading-order (LO) part is the unperturbed part and the eigenvalue problem at LO is calculated exactly. The LO or the unperturbed Hamiltonian reads:

$$\mathrm{H}^{(0)} = -\frac{\hbar^2}{2\mu}\nabla_r^2 + \frac{1}{2}\mu\omega^2 r^2 + C_0^{(0)}\delta\left(\vec{r}\right) \tag{3.50}$$

The LO wave function is, therefore, the solution of the Schrödingier equation:

$$H^{(0)}\psi^{(0)}\left(\vec{r}\right) = E^{(0)}\psi^{(0)}\left(\vec{r}\right) \tag{3.51}$$

The higher-order terms — containing derivatives of the contact interaction — are treated using perturbation theory. The perturbation W contains the corrections

$$\mathrm{W} = \mathrm{V}^{(1)} + \mathrm{V}^{(2)} + \cdots \tag{3.52}$$

where $V^{(1)}$ are the NLO correction, the $V^{(2)}$ the N^{2}LO and $\cdots$ denotes higher orders. We only use the NLO correction to the potential. The corresponding relative wave function can be expressed via a perturbation series:

$$\langle \vec{r} | \psi \rangle = \psi(\vec{r}) = \psi^{(0)}(\vec{r}) + \psi^{(1)}(\vec{r}) + \psi^{(2)}(\vec{r}) + \cdots \tag{3.53}$$

This is also true for the energy

$$E = E^{(0)} + E^{(1)} + E^{(2)} + \cdots, \tag{3.54}$$

where the superscript $^{(n)}$ denotes the order of the different terms in perturbation theory. The first-order corrections for the wave function $\psi^{(1)}(\vec{r})$ and to the energy $E^{(1)}$ can be calculated using first-order perturbation theory. For the corrections for $\psi^{(2)}(\vec{r})$ and $E^{(2)}$, we also need second-order corrections, and so on [77, 91]. In the following, the superscripts $^{(n)}$ are also added to the parameters C in eq. (3.48), which are split among different orders, for example $C_0 = C_0^{(0)} + C_0^{(1)} + C_0^{(2)} + \cdots$ and $C_2 = C_2^{(1)} + C_2^{(2)} + \cdots$ etc. $C_0^{(1)}$ is the correction to the $C_0^{(0)}$ at NLO. We explain this in more detail in section 3.6.2.

For the calculation we need to determine the matrix elements of the interaction potential $V(\vec{r}', \vec{r}) = V(r)\,\delta(\vec{r} - \vec{r}')$, eq. (3.48):

$$\begin{aligned} V_{n,n'} &= \langle n | \vec{r}' \rangle \langle \vec{r}' | V | \vec{r} \rangle \langle \vec{r} | n' \rangle \\ &= \iint d^3r' d^3r \phi_n(r') V(\vec{r}', \vec{r}) \phi_{n'}(r) \\ &= \int d^3r \phi_n(r) V(r) \phi_{n'}(r). \end{aligned} \tag{3.55}$$

with $l = m_l = 0$ since we have only s-wave scattering.

We derive each term separately (LO and NLO). The ground-state and excited-state energies are being obtained by diagonalizing the Hamiltonian (see chapter 4). Therefore we calculate the matrix element of the relative Hamiltonian by using an interaction cutoff $n_{\max}$ (see section 3.5). We transform the Hamiltonian from relative and center-of-mass coordinates into the laboratory frame using the Talmi-Moshinsky transformation (see section 3.2.3). The relative matrix elements are being calculated for the interaction as follows:

$$V^{(0)}_{n,n'} = \langle n | \vec{r'} \rangle \langle \vec{r'} | V^{(0)} | \vec{r} \rangle \langle \vec{r} | n' \rangle = \int d^3r\, \phi_n(r) C_0^{(0)} \delta(\vec{r}) \phi_{n'}(r) = C_0^{(0)} \phi_n(0) \phi_{n'}(0) \tag{3.56}$$

We show the derivation of the LO constant $C_0^{(0)}$ in the next section.

The interaction cutoff in relative space $n_{\max}$ leads to a dependence of the calculated many-particle energy on the cutoff (see section 3.5). In the limit $n_{\max} \to \infty$, the error in the calculation vanishes as shown in [77] for a three-particle system for large value of $n_{\max}$. For larger systems, the calculation becomes very involved. The truncation leads to energy-dependent errors, since a part of the model space (with $e_{\text{rel}} = 2n + l > e_{\text{rel,max}}$) is being neglected. This error we try to correct using higher-order Hamiltonians (NLO, N^{2}LO, ...) [91].

The NLO corrections are considered as first-order perturbations of the LO wave function $\langle \vec{r} | \psi^{(0)} \rangle = \psi^{(0)}(\vec{r})$ [91]. They introduce additional parameters, which we denote as $C_0^{(1)}$ and $C_2^{(1)}$. The NLO correction to the potential reads:

$$V^{(1)} = C_0^{(1)} \delta(\vec{r}) - C_2^{(1)} \left\{ [\nabla^2 \delta(\vec{r})] + 2[\vec{\nabla} \delta(\vec{r})] \vec{\nabla} + 2\delta(\vec{r}) \nabla^2 \right\}, \tag{3.57}$$

where $C_0^{(1)}$ is the correction to the $C_0^{(0)}$ at NLO.

The matrix elements of the NLO of the two-particle interaction for two-component Fermi gases can be written as:

$$V^{(1)}_{n,n'} = \langle n|\vec{r'}\rangle \langle \vec{r'}| V^{(1)} |\vec{r}\rangle \langle \vec{r}|n'\rangle = \int d^3r \phi_n(r) V^{(1)}(\vec{r}) \phi_{n'}(r)$$
$$= \int d^3r \phi_n(r) \left(C_0^{(1)} \delta(\vec{r}) - C_2^{(1)} \left\{ [\nabla^2 \delta(\vec{r})] + 2[\vec{\nabla}\delta(\vec{r})]\vec{\nabla} + 2\delta(\vec{r})\nabla^2 \right\} \right) \phi_{n'}(r) \tag{3.58}$$

Now we can use the integration by parts (see appendix B.1 eq. (B.16)) and get for the matrix elements at NLO:

$$\begin{aligned} V^{(1)}_{n,n'} &= C_0^{(1)} \int d^3r \phi_n(r) \delta(\vec{r}) \phi_{n'}(r) \\ &\quad - C_2^{(1)} \int d^3r \delta(\vec{r}) \left\{ \vec{\nabla}^2 \left[\phi_n(r) \phi_{n'}(r) \right] - 2\vec{\nabla} \left[\phi_n(r) \vec{\nabla} \phi_{n'}(r) \right] + 2\phi_n(r) \vec{\nabla}^2 \phi_{n'}(r) \right\} \\ &= C_0^{(1)} \phi_n(0) \phi_{n'}(0) \\ &\quad - C_2^{(1)} \int d^3r \delta(\vec{r}) \left\{ \left[\vec{\nabla}^2 \phi_n(r) \right] \phi_{n'}(r) + \phi_n(r) \left[\vec{\nabla}^2 \phi_{n'}(r) \right] \right\} \\ &= C_0^{(1)} \phi_n(0) \phi_{n'}(0) - C_2^{(1)} \left\{ \left[\vec{\nabla}^2 \phi_n(r) \right]_{r=0} \phi_{n'}(0) + \phi_n(0) \left[\vec{\nabla}^2 \phi_{n'}(r) \right]_{r=0} \right\}. \end{aligned} \tag{3.59}$$

The detailed derivation of $V^{(1)}_{n,n'}$ is similar to the derivation of the NLO contribution to the energy (see appendix B.3 for more details). For the calculation of the matrix elements we have to determine the coupling constants. Reference [91] shows this for LO, NLO and NNLO. We show the calculation of the coupling constants in the LO, $C_0^{(0)}$, and the NLO corrections $C_0^{(1)}$ and $C_2^{(1)}$, in the next sections.

3.6.1 The Leading-Order Constant

In this section we derive the $C_0^{(0)}$ constant for the LO for a two-component Fermi gas. We start with the Schrödinger equation (3.51) and insert the wave function $\psi(\vec{r})$ in relative coordinates, eq. (3.33) into it. Since the interaction is a pure contact interaction it acts only on the s-wave (the matrix elements for $l = 0$). The Schrödinger equation (3.51) is solved by projection onto the HO basis state $\langle n|$:

$$\begin{aligned} \langle n| \left(H^{(0)} - E^{(0)} \right) |\psi^{(0)}\rangle &= \int d^3r \langle n|\vec{r}\rangle \sum_{n'=0}^{n_{\max}} \left(E_{n'} + C_0^{(0)} \delta(\vec{r}) - E^{(0)} \right) c_{n'} \langle \vec{r}|n'\rangle \\ &= \sum_{n'=0}^{n_{\max}} \left(E_{n'} - E^{(0)} \right) c^{(0)}_{n'} \langle n|n'\rangle + C_0^{(0)} \phi_n(0) \psi^{(0)}(0) \\ &= - \sum_{n'=0}^{n_{\max}} \left(E^{(0)} - E_{n'} \right) c^{(0)}_{n'} \delta_{n,n'} + \kappa^{(0)} \phi^{(0)}_n(0) \\ &= - \left(E^{(0)} - E_n \right) c^{(0)}_n + \kappa^{(0)} \phi^{(0)}_n(0) \\ &= 0. \end{aligned} \tag{3.60}$$

In the third step, we set $\kappa^{(0)} = C_0^{(0)} \psi^{(0)}(0)$. $\kappa^{(0)}$ is a combination of unknown coefficients. This leads to the expansion coefficient in LO:

$$c^{(0)}_n = \kappa^{(0)} \frac{\phi_n(0)}{E^{(0)} - E_n} \tag{3.61}$$

with $E_n = \hbar\omega(2n + 3/2)$. Inserting the expansion coefficient from eq. (3.61) into eq. (3.39) yields the LO eigenfunction of the relative Hamiltonian, eq. (3.26):

$$\begin{aligned}\psi^{(0)}(r) &= \sum_{n=0}^{n_{\max}} c_n^{(0)} \phi_n(r) \\ &= \sum_{n=0}^{n_{\max}} \kappa^{(0)} \frac{\phi_n(0)}{E^{(0)} - E_n} \phi_n(r) \\ &= \frac{\kappa^{(0)}}{2\pi^{3/2} a_{\mathrm{HO},\mu}^3 \hbar\omega} e^{-r^2/2a_{\mathrm{HO},\mu}^2} \sum_{n=0}^{n_{\max}} \frac{L_n^{(1/2)}(\frac{r^2}{a_{\mathrm{HO},\mu}^2})}{\frac{E^{(0)}}{(2\hbar\omega)} - (n + 3/4)}.\end{aligned} \tag{3.62}$$

This equation must hold for any r, even $r = 0$; this is the so-called consistency condition. In eq. (3.62), we set $r = 0$ and simultaneously insert the expression for $\kappa^{(0)}$, and obtain

$$\psi_0^{(0)}(r = 0) = \frac{C_0^{(0)} \psi^{(0)}(0)}{2\pi^{3/2} a_{\mathrm{HO},\mu}^3 \hbar\omega} \sum_{n=0}^{n_{\max}} \frac{L_n^{(1/2)}(0)}{\frac{E^{(0)}}{(2\hbar\omega)} - (n + 3/4)}. \tag{3.63}$$

Solving this equation yields the LO coefficient $C_0^{(0)}$ [91], where identities for sums involving the generalized Laguerre polynomials at the origin can be used. We show a detailed deduction of the transformation steps in appendix B.2. For LO coefficient $C_0^{(0)}$ can be written as

$$\frac{1}{C_0^{(0)}} = -\frac{2}{\pi^2 a_{\mathrm{HO},\mu}^3 \hbar\omega} \left\{ \frac{\Gamma\left(n_{\max} + \frac{3}{2}\right)}{\Gamma(n_{\max} + 1)} \left[1 + R\left(n_{\max}, \frac{E^{(0)}}{2\hbar\omega} \right) \right] - \frac{\pi}{2} \frac{\Gamma\left(\frac{3}{4} - \frac{E^{(0)}}{2\hbar\omega}\right)}{\Gamma\left(\frac{1}{4} - \frac{E^{(0)}}{2\hbar\omega}\right)} \right\} \tag{3.64}$$

with

$$\begin{aligned}R\left(m, \frac{E^{(0)}}{2}\right) =& \frac{1 - 2E^{(0)}}{8(m+1)\left(m + \frac{7}{4} - \frac{E^{(0)}}{2}\right)} \cdot \\ & {}_3F_2\left(1, m + \frac{3}{2}, m + \frac{7}{4} - \frac{E^{(0)}}{2}; m + 2, m + \frac{11}{4} - \frac{E^{(0)}}{2}; 1\right),\end{aligned} \tag{3.65}$$

where ${}_3F_2$ is the generalized hypergeometric function.

Equation (3.64) implies that the coupling constant $C_0^{(0)}$ depends on ω as well as on $n_{\max}$. The LO coupling constant $C_0^{(0)}$ can be calculated by fixing it to reproduce, for example, one of the energies of the spectrum from the two-particle system, in our case it is fixed to reproduce the ground-state energy of the two-body system system calculated using the equation (3.35) [91]

$$E_0^{(0)} = E_0^{\mathrm{ex}}. \tag{3.66}$$

In the unitary limit we choose the coupling constant such that the overall calculation reproduces the exact relative two-body energy calculated by Busch in the unitary limit (see chapter 3.4) in the chosen model space [91]

$$E_0^{(0)} = E_0^{\mathrm{ex}}(\infty) = \frac{\hbar\omega}{2} \tag{3.67}$$

(see equations (3.35) and (3.37)). We can further simplify the relation for the coefficient $C_0^{(0)}$. Therefore, $C_0^{(0)}\left(n_{\max},\omega\right)$ is defined by

$$C_0^{(0)}(n_{\max},\omega) = -\frac{\pi^2 a_{\mathrm{HO},\mu}^3 \hbar\omega}{2} \frac{\Gamma\left(n_{\max}+1\right)}{\Gamma\left(n_{\max}+\frac{3}{2}\right)}, \tag{3.68}$$

taking into account that

$$\Gamma\left(\frac{1}{4}-\frac{E_0^{\mathrm{ex}}}{2\hbar\omega}\right) = \Gamma\left(\frac{1}{4}-\frac{1}{4}-n\right) = \Gamma(-n)\to\infty \;\text{ for }\; n=0,1,2\ldots \tag{3.69}$$

Equation (3.69) can be used as long as the range of the interaction R_{int} is small compared to the scattering length a_0. Whereas the ground-state energy for a trapped two-body system in the unitary limit is fixed to $E_0(\omega) = E_0^{\mathrm{ex}}$, the excited states in LO for a two particle system have to be calculated using eq. (3.68) like in [77]. Inserting eq. (3.69) into eq. (3.56) yields the matrix elements of the two-particle interaction in the unitary limit of two-component Fermi gas at the LO:

$$V_{n,n'} = -\frac{\pi^2 a_{\mathrm{HO},\mu}^3 \hbar\omega}{2} \frac{\Gamma\left(n_{\max}+1\right)}{\Gamma\left(n_{\max}+\frac{3}{2}\right)} \phi_n(0)\,\phi_{n'}(0) \tag{3.70}$$

We calculate these matrix elements up to a cutoff $n_{\max} = {}^{e_{\mathrm{rel,max}}}/_2$ and transform them into the coupled scheme (see section 3.2). With these matrix elements we calculate the ground-state and excited-state energies using the importance-truncated NCSM (see section 4.4.1 for more details).

The ground-state energy in LO for a two particle system $E_0^{(0)}$ is fixed; the energies of the excited states in LO in the spectrum $E_{i\geq 1}^{(0)}$ depend on ω as well as on the two-body cutoff $n_{\max}$ and must satisfy equation (3.64). For $n_{\max}\to\infty$, we expect the energies of the excited states to converge to finite values $E_{i\geq 1}(\infty,\omega)$ (see section 3.5). The calculated energy contains errors because of the cutoff. To reduce these errors, we use the NLO and need to determine again the next coupling constants $C_2^{(1)}$ and $C_0^{(1)}$. The calculation of the observables at LO is performed exactly, that is, the observables are obtained by diagonalisation of the Hamiltonian using the IT-NCSM. By contrast, the NLO and higher-order corrections are treated in many-body perturbation theory.

3.6.2 The Next-to-Leading Order Constants

We determine in this section the coupling constants $C_0^{(1)}$ and $C_2^{(1)}$ of the NLO, which can be chosen such that a second energy level is fixed, in the same way as $C_0^{(0)}$. We fixed the ground-state energy in LO to calculate $C_0^{(0)}$. Since the NLO term also corrects the ground state energy, the leading-order coupling constant must be corrected as well. Hence not one, but two new variables are being introduced by taking the NLO corrections into account. In order to separate the corrections, the corrected leading-order coupling constant can be separated into the unchanged parameter $C_0^{(0)}$ and its NLO correction $C_0^{(1)}$. The first (LO) part $C_0^{(0)}$ remains unchanged, while the NLO part $C_0^{(1)}$ is considered as the perturbation. We denote the new parameters as $C_0^{(1)}$ and $C_2^{(1)}$. For higher orders ($\mathrm{N^2LO}$ etc.), additional correction terms must be added.

Additionally to fixing the $C_0^{(0)}$ so that the ground-state energy of the two-body spectrum E_0^{ex} in LO is reproduced we fix at NLO the two NLO coupling constants so that the calculation reproduce also the first-excited state energy E_1^{ex} of the spectrum of the two-body system. Fixing two energy levels in the two-body spectrum yields two equations, which can be solved for the unknown coupling constants $C_0^{(1)}$ and $C_2^{(1)}$ in each model space:

$$E_i^{(1)}(n_{\max},\omega) = E_i^{\mathrm{ex}}(\omega) - E_i^{(0)}(n_{\max},\omega),\; i=0,1. \tag{3.71}$$

where E_0^{ex} and E_1^{ex} are the exact ground and first excited state energies of the two-body system calculated using the eq. (3.35). $E_0^{(0)}$ and $E_1^{(0)}$ are the ground and first excited state energies of the two-body system calculated using the $C_0^{(0)}$ constant at LO, and $E_0^{(1)}$ and $E_1^{(1)}$ their corrections at NLO calculated using the NLO constants.

In the present thesis, the energy $E_0^{(0)}$ is always set to the exact ground-state energy $E_0^{\text{ex}}(\omega)$ calculated using eq. (3.35), and therefore the correction term $E_0^{(1)}$ vanishes. Away from the unitary limit one has also to account for the effective range of the interaction and, therefore, the correction to the ground state energy is in general nonzero [91]. The interaction cutoff leads to errors that will be corrected in NLO. Therefore, the correction to the first excited state energy of the two-particle system $E_1^{(1)}$ is non zero [91].

The first-order energy correction can be calculated by using first-order perturbation theory. For this reason we insert the NLO potential equation (3.57) into the first-order correction eq. (A.9) and project it onto the state $\left|\psi^{(0)}\right\rangle$ [91]. We show the detailed derivation of the first-order energy correction in appendix B.3:

$$E^{(1)} = \left\langle \psi^{(0)} \right| V^{(1)} \left| \psi^{(0)} \right\rangle = \frac{\left(\kappa^{(0)}\right)^2}{\left(C_0^{(0)}\right)^2} \left\{ C_0^{(1)} + \frac{4\mu C_2^{(1)}}{\hbar^2} \left[E^{(0)} - \frac{4C_0^{(0)}}{3\pi^2 a_{\text{HO},\mu}^3} \frac{\Gamma\left(n_{\max} + \frac{5}{2}\right)}{\Gamma\left(n_{\max}+1\right)} \right] \right\} \tag{3.72}$$

with $\kappa^{(0)} = C_0^{(0)} \psi^{(0)}(0)$.

For the calculation of both parameters we need also to determine the parameter $\kappa^{(0)}$. $\kappa^{(0)}$ can be derived by using the orthogonality of the wave function $\psi^{(0)}$, and is given by:

$$\left[\kappa^{(0)}\left(E_i^{(0)}\right)\right]^{-2} = \sum_n^{n_{\max}} \frac{\phi_n^2(0)}{(E_i^{(0)} - E_n)^2}, \tag{3.73}$$

(see appendix B.4). We use the notation $\kappa^{(0)}\left(E_i^{(0)}\right)$ since the parameter $\kappa^{(0)}$ depends on the energy.

We can get the NLO coefficients $C_0^{(1)}$ and $C_2^{(1)}$ by inserting the first-order energy correction into eq. (3.71) [91]. The equations for the NLO coefficients read (see appendix B.4)

$$\frac{4\mu C_2^{(1)}}{\left(\hbar C_0^{(0)}\right)^2} = \frac{E_1^{(1)}/\left[\kappa^{(0)}\left(E_1^{(0)}\right)\right]^2 - E_0^{(1)}/\left[\kappa^{(0)}\left(E_0^{(0)}\right)\right]^2}{E_1^{(0)} - E_0^{(0)}} \tag{3.74}$$

and

$$\frac{C_0^{(1)}\hbar^2}{4\mu C_2^{(1)}} = \frac{4C_0^{(0)}}{3\pi^2 a_{\text{HO},\mu}^3} \frac{\Gamma\left(n_{\max} + \frac{5}{2}\right)}{\Gamma\left(n_{\max}+1\right)} - \frac{E_0^{(0)} E_1^{(1)}/\left[\kappa^{(0)}\left(E_1^{(0)}\right)\right]^2 - E_1^{(0)} E_0^{(1)}/\left[\kappa^{(0)}\left(E_0^{(0)}\right)\right]^2}{E_1^{(1)}/\left[\kappa^{(0)}\left(E_1^{(0)}\right)\right]^2 - E_0^{(1)}/\left[\kappa^{(0)}\left(E_0^{(0)}\right)\right]^2}. \tag{3.75}$$

Taking into account that $E_0^{(1)} = 0$, one obtains the relation for the coupling constant $C_2^{(1)}$ and $C_0^{(1)}$ in the unitary limit

$$\frac{4\mu C_2^{(1)}}{\left(\hbar C_0^{(0)}\right)^2} = \frac{E_1^{(1)}/\left[\kappa^{(0)}\left(E_1^{(0)}\right)\right]^2}{E_1^{(0)} - E_0^{(0)}}. \tag{3.76}$$

and

$$\frac{C_0^{(1)}\hbar^2}{4\mu C_2^{(1)}} = \frac{4C_0^{(0)}}{3\pi^2 a_{\text{HO},\mu}^3} \frac{\Gamma\left(n_{\max} + \frac{5}{2}\right)}{\Gamma\left(n_{\max}+1\right)} - E_0^{(0)} \tag{3.77}$$

With these two equations we obtain the constants $C_0^{(1)}$ and $C_2^{(1)}$ in order to solve the NLO correction.

The calculated energies E depend on $n_{\max}$ because of the truncation (see section 3.5). $n_{\max}$ is an arbitrarily chosen parameter and therefore this dependence should be as weak as possible. It is not possible to ensure that the dependence on $n_{\max}$ is weak in general. By taking the limit as $n_{\max}$ goes to infinity, one recovers results corresponding to the original potential [63].

3.7 The Alhassid-Bertsch-Fang Interaction

Alhassid *et al.*[1] introduced an effective interaction, the ABF interaction for trapped fermions in the unitary limit and compared it to a renormalized contact interaction. The ABF interaction was generalized by Gilbreth and Alhassid [33] for arbitrary scattering lengths. The ABF interaction is separable and no longer a contact interaction. For three-particle Fermi systems in a trap at unitarity, the ABF interaction shows faster convergence (with increasing maximum number of shells $e_{\mathrm{rel,max}} = 2n_{\mathrm{max}}$) towards the exact energy calculated by Werner *et al.* [102] than a regularized contact interaction [1]. The latter can be considered as leading-order EFT, while the former is not a contact interaction and has some connection with Suzuki's unitary regularization [1].

We use the ABF interaction for our benchmark calculation of the ground-state and excited-state energies for systems comprising $A \geq 4$ particles. Results of calculations of the energy of three- and four-particle systems are given by Alhassid *et al.* [1]. Alhassid *et al.* constructed an effective interaction, in order to improve a renormalized contact interaction with a regularization parameter $q = n_{\mathrm{max}}$ with the only requirement on the model space Hamiltonian that it converges for $n_{\mathrm{max}} \to \infty$ to the unitary limit [1]. It is important to keep the separable form of the interaction, since this form permits an algebraic diagonalization of the Hamiltonian in two-body space [1].

The ABF interaction also affects only the s-wave [1]. A general separable s-wave interaction has the form

$$\left\langle nlm_l \right| V_{\mathrm{eff}}^{(q)} \left| n'lm_l \right\rangle = -\hbar\omega f_n^{*(q)} f_{n'}^{(q)} \delta_{l,0} \delta_{m,0} \tag{3.78}$$

for $n, n' \leq q$ [33]. The matrix element of the relative Hamiltonian with the ABF interaction reads

$$\mathrm{H}_{n,n'} = \left\langle n00 \right| \mathrm{H}_{\mathrm{rel}}^{(q)} \left| n'00 \right\rangle = \delta_{n,n'} E_n^{\mathrm{HO}} - \hbar\omega f_n^{*(q)} f_{n'}^{(q)}, \tag{3.79}$$

since the particles interact only in the s-wave with $l = l' = 0$ and $m_l = m_l' = 0$. The coefficient $f_n^{(q)}$ has been determined by Gilbreth and Alhassid [33]. Their derivation is the following: For $E_0^{\mathrm{ex}} < E_1^{\mathrm{ex}} < \cdots < E_q^{\mathrm{ex}} \in \mathbb{R}$ and $E_0^{\mathrm{HO}} < E_1^{\mathrm{HO}} < \cdots < E_q^{\mathrm{HO}} \in \mathbb{R}$ with $E_i^{\mathrm{ex}} \neq E_j^{\mathrm{HO}} \forall i, j$ and $f_0^{(q)}, f_1^{(q)}, \ldots, f_q^{(q)} \in \mathbb{C}$, the $(q+1)$-dimensional matrix $H_{n,n'}$ has the E_i^{ex} as its eigenvalues if

$$\left| f_n^{(q)} \right| = \sqrt{\frac{\prod_k \left(E_n^{\mathrm{HO}} - E_k^{\mathrm{ex}} \right)}{\prod_{k \neq n} \left(E_n^{\mathrm{HO}} - E_k^{\mathrm{HO}} \right)}}, \tag{3.80}$$

in which case the i-th eigenvector $b^{(i)}$ has components

$$b_n^{(i)} = C_i \frac{f_n^{(q)*}}{E_n^{\mathrm{HO}} - E_i^{\mathrm{ex}}} \tag{3.81}$$

with

$$C_i = \sqrt{\frac{\prod_k \left(E_k^{\mathrm{HO}} - E_i^{\mathrm{ex}} \right)}{\prod_{k \neq i} \left(E_k^{\mathrm{ex}} - E_i^{\mathrm{ex}} \right)}}. \tag{3.82}$$

A solution for those equations which satisfies eq. (3.80) exists if and only if $E_0^{\mathrm{ex}} < E_0^{\mathrm{HO}} < E_1^{\mathrm{ex}} < \cdots < E_q^{\mathrm{HO}}$. A detailed proof is given in the paper by Gilbreth and Alhassid [33].

For the $l = 0$ partial wave the eigenvalue problem of relative Hamiltonian is given by the solution of the transcendental equation (3.35) (see section 3.4 and [17]). In the unitary limit, the exact energy for the trapped two-body system E_i^{ex} is given by eq. (3.37). Inserting this into eq. (3.80) leads to

$$\left(f_n^{(q)} \right)^2 = \frac{\prod_k (2(n-k)+1)}{\prod_{k \neq n} 2(n-k)}. \tag{3.83}$$

This can be rewritten as

$$f_n^{(q)} = \sqrt{\frac{(2n+1)!!}{(2n)!!}\frac{\left(2\left(q-n\right)-1\right)!!}{\left(2\left(q-n\right)\right)!!}} \tag{3.84}$$

Alhassid *et al.* used this interaction to calculate three- and four-particle two-component fermion systems in a trap in the unitary limit [1]. In order to obtain the exact many-body energy, Bertsch *et al.* first calculated the energy in the laboratory frame for a fixed cutoff q and then estimated the energy for $q \to \infty$. For a three-particle system, they showed that the ABF interaction leads to a better convergence to the exact energy [102] than a conventional contact interaction.

We calculate the relative matrix elements for a given $q = n_{\max}$ and then transform them into the laboratory frame using the Talmi-Moshinsky transformation (see section 3.2.3). In chapter 5 we compare the resulting ground-state and excited-state energy of two-component fermion systems at unitarity ($A \geq 4$) with the results obtained with the interaction derived using the EFT approach by Stetcu *et al.* [91] introduced in section 3.6. The benchmark calculations with both interactions are compared with results from Monte Carlo calculations obtained by other groups.

3.8 Gaussian-shaped Potential

In addition to an EFT and ABF interactions, we also study a purely attractive potential of a simple form, a Gaussian-shaped potential, in the present thesis. A purely attracting Gaussian two-body potential has the form

$$V\left(\vec{r}\right) = -V_0 \exp\left(-\frac{\vec{r}^2}{2r_0^2}\right), \tag{3.85}$$

where $V_0 > 0$ is the depth and r_0 the width of the Gaussian. r_0 is fixed and is chosen much smaller than the harmonic oscillator length a_{HO}, since we consider dilute systems at low energy (see section 2.1). V_0 is tuned to produce the desired two-body s-wave scattering length a_0; in our case, we tune V_0 such that a_0 becomes very large. Calculations for different small values of r_0 have been performed by Blume *et al.* [12] and von Stecher *et al.* [88] and extrapolated for $r_0 \to 0$ in order to estimate the dependence of the results on r_0.

We can determine V_0 from eq. (2.9); ignoring the HO potential and considering only $l = 0$, eq. (2.9) becomes

$$\left(-\frac{\hbar^2}{2\mu}\frac{d^2}{dr^2} + V(r)\right)\frac{u_{n0}(r)}{r} = E\frac{u_{n0}(r)}{r}. \tag{3.86}$$

Thereby, we use the $E = 0$ solution, to extract the scattering length. As described in section 2.1, the scattering length is the point of the r-axis intersected by the wave function (as shown in fig. 2.2). We determine V_0 such that the wave function $u_{n0}(r)$ intersects the r-axis at the largest possible value of r or not at all, with $E = 0$. With this value of V_0, we then calculate the matrix element in the relative basis, transform them into single-particle coordinates using the Talmi-Moshinsky transformation (see section 3.2.3), and calculate the energies using the NCSM or IT-NCSM (see chapter 4).

3.9 Summary

We use the interactions introduced in this chapter for the calculation of the matrix elements in the relative frame for a ultra-cold two-component fermion system at unitarity. The contact interaction (usually, a δ function) is ill-defined and has to be regularized. This can be done by using an interaction cutoff (see section 3.5) in the relative frame of the interaction. We use the HO basis, which implies a natural cutoff by using only shells with $e_{\mathrm{rel}} \leq e_{\mathrm{rel,max}} = 2n_{\max}$. The cutoff introduces errors which can be

computationally eliminated by extrapolating the results for $n_{\max} \to \infty$. However, the regularized contact interactions show slow convergence with the regularization parameter. To improve convergence, the ABF interaction (see section 3.7) as well as higher orders (NLO and N^{2}LO) in the framework of an EFT (see section 3.6) were introduced. The advantage of these approaches compared to the contact interaction is that the convergence of the energy with regularization parameter $n_{\max}$ as well as with many-body cutoff is improved even for smaller values of $N_{\max}$ [1], that is, identical results can be obtained by evaluating smaller model spaces or more precise results can be obtained with a given computational effort. We also use a purely attractive potential of a simple form, a Gaussian-shaped potential (see section 3.8), for our calculation, used to model the interaction for a many-body calculation using correlated Gaussians and a Fixed-Node Diffusion Monte Carlo method [11, 12, 88]. We perform benchmark calculations and compare our results to those published by other groups.

4 Many-Body Methods

In this chapter we present the numerical methods used for the calculation of the energy spectra of ultra-cold fermionic gases. Configuration Interaction methods in general and the No-Core Shell Model (NCSM) as a special case of the CI are used in molecular [81], atomic [46] and nuclear physics [20, 61]. However, CI and NCSM calculations become computationally intractable with larger model spaces. The dimension of the model space increases exponentially; for example, the dimension of the full NCSM calculation in nuclear physics for ^{6}Li increases from $1.5 \cdot 10^6$ at $N_{\max} = 8$ to $2.8 \cdot 10^8$ at $N_{\max} = 14$ ([55, Table 3.1, p. 54]). We also show in the present thesis the exponential increase of the model space dimension for the full NCSM calculation for an ultra-cold Fermi gas in section 5.6. The Importance-Truncated No-Core Shell Model (IT-NCSM) identifies and discards the less important basis states for the solution of the eigenvalue problem, reducing the dimension of the model space, which gives access to larger values of the maximum oscillator excitation quantum number $N_{\max}$ and larger particle numbers [71].

First, we briefly discuss the Configuration Interaction approach and the NCSM, the most successful CI-type method at present [71] in section 4.1. The many-body model space is spanned by many-body basis states that are often Slater determinants constructed from single-particle states; we also use this approach for our calculations. In this chapter, we briefly introduce this approach, as well as the Jacobi basis (the other possible way to form the many-body model space) and discuss advantages and disadvantages of both in section 4.2. We use the Lanczos algorithm described in section 4.3 in order to solve the large-scale eigenvalue problem of the Hamiltonian. Furthermore, we introduce the importance truncation in the context of NCSM in section 4.4.1 as well as implementation of the IT-NCSM in section 4.4.2. We discuss the theoretical uncertainties of the results of IT-NCSM calculations in section 4.4.3. We compare the results for the ground-state energy for two-component fermion system at unitarity with $A_1 = A_2 = 3$ and $A_1 = A_2 = 4$ calculated using the IT-NCSM to those of the full NCSM. The results calculated using IT-NCSM show good agreement to those calculated using full NCSM, where the latter is feasible. These calculations demonstrate that the IT-NCSM allows to extend the applicability of the NCSM while preserving the desirable properties of the full NCSM calculation.

Besides the NCSM, the two methods most commonly found in the available literature on calculating energies of Fermi systems are the Fixed-Node Diffusion Monte Carlo method (FN-DMC) [5, 12, 85, 88] and the stochastic variational approach using Correlated Gaussian (CG) basis functions [12, 65, 84]. We introduce these methods (FN-DMC in section 4.5 and CG in section 4.6) and compare them to the IT-NCSM.

4.1 CI and NCSM

The CI method (and, therefore, the NCSM) is a conceptually simple and very flexible *ab initio* method. In the CI approach the model space is typically spanned by Slater determinants constructed from a set of single-particle states. The eigenvalue problem

$$\mathrm{H} \left| \psi \right\rangle = E \left| \psi \right\rangle \tag{4.1}$$

of the many-body Hamiltonian is solved numerically. In order to make the numerical calculation feasible, the many-body space has to be truncated in some way. One possibility is the truncation with respect to the single-particle basis: one uses all possible Slater determinants constructed with all single-particle states in the oscillator shells $e = 0, \ldots, e_{\max}$ in order to span the model space. Figure 4.1 (a) illustrates

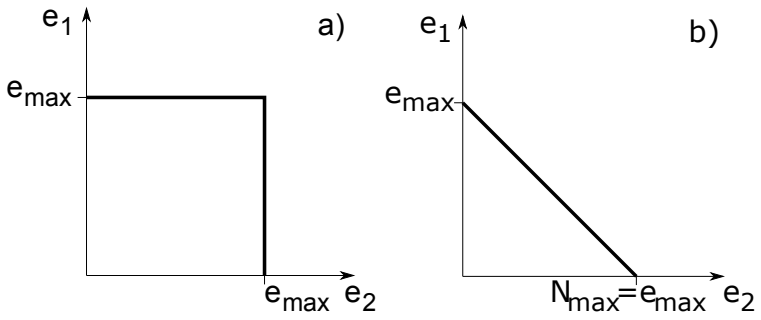

Figure 4.1.: Illustration of the $e_{\max}$ (a) and the $N_{\max}$ (b) truncation. The area in the square or triangle contains all possible configuration allowed in the basis with the certain $e_{\max}$ or $N_{\max}$, respectively. The e_1 or e_2 represents the oscillator quantum number of the respectve particle.

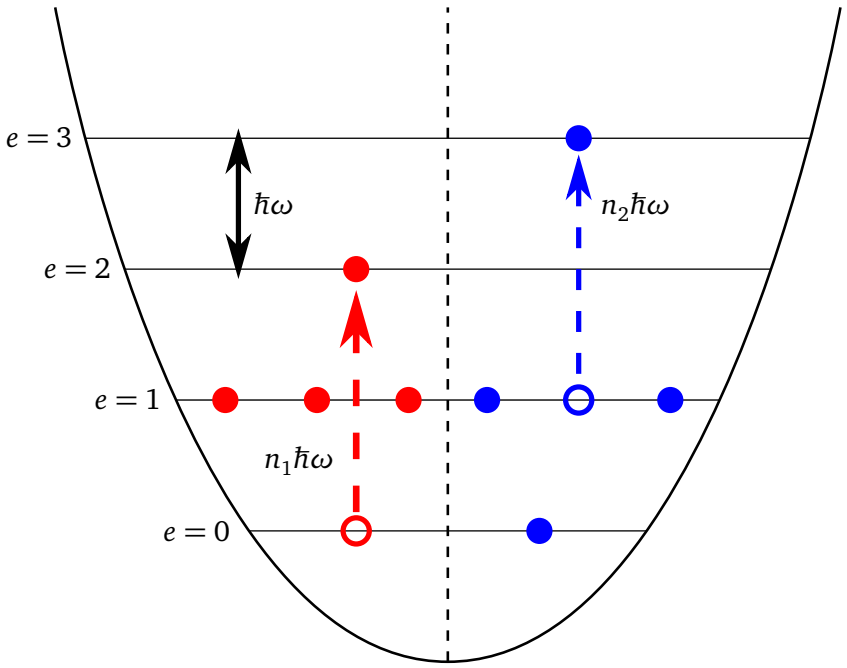

Figure 4.2.: Truncation Scheme in NCSM: $4\hbar\omega$ excitation of the configuration of $A_1 = A_2 = 4$ two-component particles in HO potential.

the $e_{\max}$-truncation for a two-particle system. The square contains all possible configurations of the basis allowed for the maximal $e_{\max}$ for the two interacting particles.

The NCSM is a special case of the CI method and is one of the standard *ab initio* methods in nuclear theory. The model space is spanned by spherical harmonic-oscillator eigenstates that are formulated either in the form of A-body Slater-determinants of single-particle HO states — the so-called m-scheme — or in the form of relative HO states with respect to the A-body Jacobi coordinates (see section 4.2). The model space is truncated in such a way that only eigenstates with a total excitation energy of the many-body basis states up to $N_{\max}\hbar\omega$ are used (see figure 4.2). For example, for three two-component fermions with $A_1 = 2$ and $A_2 = 1$ the total energy quantum number is $e_1 + e_2 + e_3 = 1$. There are two particles, one of each kind, in the s-shell, and one particle in the p-shell. For a two-particle system we have only particles in the s-shell in the $0\hbar\omega$ space, hence the total energy quantum number is $e_1 + e_2 = 0$. Next we take this unperturbed Slater determinant and add HO excitations, moving one of the particles to the upper shells. For the calculation of the HO excitation energy we use the difference between the final and the initial energy quantum numbers of the particle, since the shells differ by $\hbar\omega$. For example, for a four-particle system, the basis Slater determinant with the lowest possible HO-energy contains two particles with $e_i = 1$, hence for the p-shell $e_{\max} = N_{\max} + 1$. Figure 4.1 (b) illustrates the $N_{\max}$-truncation in a two-particle system; here all possible states allowed for a certain $N_{\max}$ are in the triangle. The truncation with respect to the unperturbed excitation energy $N_{\max}$ is computationally more efficient than the truncation with respect to the single-particle basis [73].

The NCSM is employed successfully in nuclear physics, and calculations with two- and three-body interactions are performed for light nuclei. Important quantities such as the energy, form factor, and density, of the ground state and low-lying excited states as well as electromagnetic observables such as multipole moment and transition strengths can be determined using the NCSM. For ultra cold Fermi gases, the CI method was used by Alhassid *et al.* [1] and the NCSM in particular by Rotureau *et al.* [77] for the calculations for up to five-particle systems. CI or NCSM calculations for larger trapped fermionic systems at unitarity were not considered yet since the dimension of the model space grows factorially with the particle number A and $N_{\max}$ or $e_{\max}$ [71, p. 7].

We additionally use the importance truncation (see section 4.4), which has been successfully applied in nuclear physics, for the calculation of the energy spectra of trapped ultra-cold fermionic gases at unitarity for 4 to 20 particles and compare the results with published results [12] calculated using the FN-DMC method and the stochastic variational approach using CG basis functions.

4.2 Many-Body Basis States

There are two ways to choose a basis for the NCSM calculations: An antisymmetrized basis formulated in terms of Jacobi coordinates, the Jacobi basis and an antisymmetrized basis in single-particle coordinates, the so-called m-scheme.

4.2.1 Jacobi Basis

In a Jacobi basis, the many-body basis states depend on the internal (Jacobi) coordinates. One possibility to choose the set of Jacobi coordinates for an A-body system is:

$$\vec{\xi}_0 = \sqrt{\frac{1}{A}} \left(\vec{r}_1 + \vec{r}_2 + \cdots + \vec{r}_A\right), \tag{4.2}$$

$$\vec{\xi}_1 = \frac{1}{2} \left(\vec{r}_1 - \vec{r}_2\right), \tag{4.3}$$

$$\vec{\xi}_2 = \sqrt{\frac{2}{3}} \left[\frac{1}{2} \left(\vec{r}_1 + \vec{r}_2\right) - \vec{r}_3\right], \tag{4.4}$$

$$\vec{\xi}_{A-1} = \sqrt{\frac{A-1}{A}} \left[\frac{1}{A-1} \left(\vec{r}_1 + \vec{r}_2 + \cdots + \vec{r}_{A-1}\right) - \vec{r}_A\right], \tag{4.5}$$

where $\vec{\xi}_0$ corresponds to the center-of-mass coordinate for A particles and $\vec{\xi}_1$ to $\vec{\xi}_{A-1}$ to the relative coordinates of A particles. These coordinates are used to construct the HO basis in Jacobi coordinates, the Jacobi basis. The antisymmetrized two-body state in Jacobi coordinates was already described in eq. (3.4) in section 3.2.1, which also explains the antisymmetrisation of the state. For three particles the basis state can be written as

$$\left|N_{\mathrm{cm}(3)} L_{\mathrm{cm}(3)}\right\rangle \otimes_{\mathscr{A}} \left|N_1 N_2; \left(L_1 L_2\right) L_{12}; f_1 m_{f_1}, f_2 m_{f_2}, f_3 m_{f_3}\right\rangle. \tag{4.6}$$

As already mentioned, the many-body states have to be antisymmetric since we consider fermionic systems. The operator $\mathscr{A}$ antisymmetrizes the three-particle relative wave function and does not act on the center-of-mass state, since it is symmetric by construction. The subscript cm(A) corresponds to the center-of-mass coordinate $\vec{\xi}_0$ and denotes the corresponding quantum numbers in the A-body HO basis state. N_i and L_i are the radial and orbital angular momentum quantum numbers, respectively, defined with respect to the Jacobi coordinate $\vec{\xi}_i$. The relative orbital angular momenta L_1 and L_2 couple to the total orbital angular momentum L_{12}. The total energy quantum number of the HO Jacobi basis state is given by $E_3 = E_{\mathrm{cm}(3)} + E_{12}$ with the relative energy quantum number $E_{12} = 2N_1 + L_1 + 2N_2 + L_2$ and center-of-mass part $E_{\mathrm{cm}(3)} = 2N_{\mathrm{cm}(3)} + L_{\mathrm{cm}(3)}$. E_3 can be used for the truncation of the three-body basis. Jacobi bases have been used by Rotureau and Stetcu [77] for the calculation of the energy spectra of three-particle, four-particle and five-particle systems at unitarity.

One advantage of an antisymmetrized basis depending on Jacobi coordinates is that larger $N_{\max}$ can be used. Since the center-of-mass degrees of freedom factorize exactly from the internal ones, one can omit the center-of-mass degrees of freedom, reducing the dimension of the model space. The dimension is also reduced since coupled bases are used in which L is a good quantum number. Furthermore, since the interacting atoms do not change their hyperfine state (see section 2.3) also the sum over all m_{f_i} is conserved. This is also the case in the m-scheme. A major disadvantage of the Jacobi basis is that the antisymmetrization of the basis states becomes computationally involved with increasing particle number.

4.2.2 m-Scheme

In the m-scheme, the basis states are (antisymmetrized) Slater determinants of harmonic oscillator single-particle states $\left|n_i l_i m_{l_i}; f_i m_{f_i}\right\rangle$ defined with respect to the absolute coordinates of the A particles; the antisymmetrized A-body state can be written as

$$\left|\alpha_1, \alpha_2 \cdots, \alpha_A\right\rangle_a = \sqrt{A!}\mathscr{A} \left|n_1 l_1 m_{l_1}; f_1 m_{f_1}\right\rangle \otimes \left|n_2 l_2 m_{l_2}; f_2 m_{f_2}\right\rangle \cdots \left|n_A l_A m_{l_A}; f_A m_{f_A}\right\rangle. \tag{4.7}$$

The number of basis states is limited by the $N_{\max}\hbar\omega$ energy truncation.

In the m-scheme, the antisymmetrization of the basis states is trivial; the many-body space in that scheme is easy to construct. Since the basis states are Slater determinants constructed from single-particle HO wave functions in the laboratory frame, the wave function factorizes exactly in the relative and the center-of-mass coordinates as long as one uses an energy truncation of the basis states, such that all states up to a given $N_{\max}\hbar\omega$ are included [77]. For up to five particles, the antisymmetrized basis in Jacobi coordinates is typically more efficient than the m-scheme [77]. Since we consider systems with more than five particles, we use the m-scheme as the basis for the many-body calculation.

The calculated results for intrinsic states of any system are the same, independent of whether one uses the m-scheme or the Jacobi basis, as long as one uses the same truncation [77].

The simplicity of the m-scheme is counterbalanced by the dimension of the matrix, since only $M_L = \sum_{i=1}^{A} m_{l_i}$, the parity, and the sum over m_{f_i} defining the hyperfine states (see section 2.3) are conserved. Another disadvantage of the m-scheme is that the total orbital angular momentum and center-of-mass quantum numbers are not included (unlike in the Jacobi basis [77]), hence the corresponding symmetries cannot be used to reduce the storage space.

4.2.3 Center-of-Mass Contamination

In NCSM calculations for untrapped few-nucleon system in nuclear physics, the Hamiltonian is translationally invariant. The eigenstates of the Hamiltonian factorize exactly into a center-of-mass and a relative component:

$$\left|\psi\right\rangle = \left|\psi_{\text{rel}}\right\rangle \otimes \left|\psi_{\text{cm}}\right\rangle . \tag{4.8}$$

This factorization of the many-body state guarantees the transitional invariance of the solution, and as a result, all observables are free of spurious center-of-mass contamination. The center-of-mass problem arises because the coordinates of the shell-model wave function are defined with respect to a fixed reference point. In nuclear many-body calculations, one usually chooses a spherical single-particle basis depending on A coordinates and momenta. Only $A-1$ of them are linearly independent, since the solution only depends on intrinsic coordinates. The Hamiltonian of the atomic nucleus is invariant under translation and rotation, thus any intrinsic operator commutes with the center-of-mass coordinate and momentum operator. A shell-model wave function is a linear combination of the function in relative and center-of-mass coordinates and, since the solution only depends on relative coordinates, the same wave function in relative coordinates can have different center-of-mass motion [20, 58, 100]. As long as one uses all basis states up to a given energy $N_{\max}$, the factorization of the center-of-mass and intrinsic coordinates stays exact.

In contrary to the nuclear case we consider a trapped Fermi gas. For the description of the trap, we use a HO potential, which is a part of the physics of the system, and therefore the solution depends explicitly on the trap. The Hamiltonian is not translationally invariant. Therefore, center-of-mass contamination, which plays an important role in the calculations for nuclei, is not relevant in the case of trapped fermions.

4.3 The Lanczos Method

In order to solve the eigenvalue problem, we have to construct and diagonalize the many-body matrix representation of the Hamiltonian including the effective interaction (see chapter 3). The underlying model space has a very large dimension. In dense diagonalization algorithms, such as the Wilkinson algorithm, the required computational effort increases cubically ($\mathcal{O}(D^3)$) with the matrix dimension D [20]. Hence these standard diagonalization methods are not suited for large-scale calculations. Iterative methods, such as the Lanczos method, are of general use in many-body calculations for the diagonalization, since only a few of the lowest eigenstates are needed and the Hamilton matrices are very sparse.

The Lanczos method converges towards the extremal eigenvalues (the largest and the smallest one) first and, therefore, allows calculating the ground state at comparatively low computational cost. The number of nonzero matrix elements in many-body calculations increases linearly (and not quadratically) with the matrix dimension [20].

The Hermitian Lanczos algorithm is an orthogonal projection method on a Krylov subspace [79] for Hermitian matrices. The algorithm applied to a Hermitian matrix H iteratively constructs an orthogonal basis in which the resulting matrix T_m is tridiagonal [78, 79]

$$T_m = \begin{pmatrix} \alpha_1 & \beta_2 & & & \\ \beta_2 & \alpha_2 & \beta_3 & & \\ & \cdot & \cdot & \cdot & \\ & & \beta_{m-1} & \alpha_{m-1} & \beta_m \\ & & & \beta_m & \alpha_m \end{pmatrix}, \tag{4.9}$$

where $\alpha_j := T_{j,j}$, $\beta_j := T_{j-1,j}$, and m is the dimension of the orthogonal basis [79]. We introduce the Hermitian Lanczos algorithm in the following.

The Lanczos algorithm starts with an initial, normalized, arbitrarily chosen starting vector $\left|v_1\right\rangle$, which is called the *pivot state*. One sets $\beta_1 \equiv 0$ and $\left|v_0\right\rangle \equiv 0$ and iterates for $j = 1, 2, \ldots m$. The next vector $\left|v_2\right\rangle$ is calculated by applying the matrix H to the starting vector $\left|v_1\right\rangle$:

$$H\left|v_1\right\rangle = \alpha_1 \left|v_1\right\rangle + \left|w_1\right\rangle \tag{4.10}$$

where $\alpha_1 = \left\langle v_1\right| H \left|v_1\right\rangle$ and $\left|w_1\right\rangle$ a vector orthogonal to $\left|v_1\right\rangle$. One gets the next vector $\left|v_2\right\rangle$ by normalizing $\left|w_1\right\rangle$:

$$\left|v_2\right\rangle = \frac{\left|w_1\right\rangle}{\beta_2} \tag{4.11}$$

with

$$\beta_2 = \left\langle v_1\right| H \left|v_2\right\rangle = \left\langle w_1 | w_1\right\rangle^{1/2}. \tag{4.12}$$

Now one iterates from $j = 2$ to m by using

$$H\left|v_j\right\rangle = \beta_j \left|v_{j-1}\right\rangle + \alpha_j \left|v_j\right\rangle + \left|w_j\right\rangle \tag{4.13}$$

where

$$\alpha_j = \left\langle v_j\right| H \left|v_j\right\rangle \quad \text{and} \quad \beta_{j+1} = \left\langle v_j\right| H \left|v_{j+1}\right\rangle = \left\langle v_{j+1}\right| H \left|v_j\right\rangle = \left\langle w_j | w_j\right\rangle^{1/2} \tag{4.14}$$

By normalizing $\left|w_j\right\rangle$ one gets the vector $\left|v_{j+1}\right\rangle = \left|w_j\right\rangle / \beta_{j+1}$. The matrix T_m being tridiagonal has the consequence that only the two preceding basis vectors need to be saved during the computation, if we do not use any form of reorthogonalization [79]. Therefore, the Lanczos method is very memory efficient and fast. After performing $k < m$ steps of the Lanczos process the matrix T_k, $k \times k$ sub matrix of T_m, can be diagonalized using standard diagonalization methods. The eigenvalues of T_k provide already after a few iteration a good approximation to the extreme eigenvalues of H. In principle the matrix can be diagonalized at each iteration and the process is stopped if a given criterion for the convergence of the eigenvalues is satisfied, that is, if an additional iteration step does not affect the target eigenvalue. The required computation time is proportional to the number of matrix elements and increases linearly with the matrix dimension [20, p. 16].

In exact arithmetic, the above simple algorithm guarantees that the vectors $\left|v_i\right\rangle$, $i = 1, 2, \ldots$, are orthogonal. In practice the exact othogonality of these vectors is only given at the beginning of the

process and vectors lose orthogonality due to numerical errors and the vectors $\left|v_j\right\rangle$ have to be reorthogonalized to all previous vectors. The relative magnitude of those numerical errors depends a lot on the Hamiltonian.

In large eigenvalue problems, one cannot know in advance how many steps are required to achieve convergence. In order to recover the eigenvectors, all Lanczos vectors $\left|v_i\right\rangle$ have to be stored or recomputed [56], leading to extensive memory requirements. The reorthogonalization procedure also requires more computation time as the number of vectors increases. As a consequence, both the computation time and the required storage space increase with the number of Lanczos steps m [78, p. 167].

Implicit restarting is an efficient way to overcome the often intractable storage and computational requirements in the original Lanczos method by extracting interesting information from the Krylov subspace and compressing it into a k-dimensional subspace. To this end, the implicitly shifted QR mechanism is used [79, 78].

We use the implicitly restarted Arnoldi algorithm of the ARPACK library [56]. Arnoldi's method is an orthogonal projection method for general non-Hermitian matrices onto Krylov subspaces $\mathscr{K}_m$ and was first introduced in 1951 as a means of reducing a dense matrix into Hessenberg form with unitary transformations [78]. The resulting matrix

$$M_m = \begin{pmatrix} * & * & * & * & * & * \\ * & * & * & * & * & * \\ & * & * & * & * & * \\ & & * & * & * & * \\ & & & * & * & * \\ & & & & * & * \end{pmatrix},$$

is an upper Hessenberg matrix, with zero matrix elements below its sub diagonal. In the case that Arnoldi's method is applied to a Hermitian matrix, such as the Hamiltonian H, the resulting matrix is real, tridiagonal and symmetric. The symmetric Lanczos algorithm can be viewed as a simplification of Arnoldi's method for Hermitian matrices [78].

As implemented in the ARPACK library [56], the implicitly restarted Arnoldi method proceeds as follows: First it executes m steps of the Arnoldi (or Lanczos) algorithm, and computes m eigenvalues of H. The algorithm sorts these eigenvalues according to the users selection criterion into a wanted and unwanted set, then performs $m-k$ implicitly shifted QR steps on M_m. In each step of the shifted QR algorithm, the equation $(M_m - \theta_j I) = QR$ is solved, where Q is a unitary matrix, R upper tridiagonal matrix and θ_j the selected shifts, which are the unwanted eigenvalues. Because

$$Q\tilde{H}_m Q^H = Q(RQ + \theta_j I)Q_m^M = QR + \theta_j I = M_m, \tag{4.15}$$

the resulting matrix $\tilde{H}_m$ is similar to the original matrix M_m, and, therefore, has the same eigenvalues. As already mentioned the Hessenberg matrix M_m reduces in our case to a tridiagonal and symmetric matrix T_m since the Hamiltonian is Hermitian. We are looking for the smallest eigenvalues, which are, therefore, 'wanted' in our case. The θ_i are selected from the 'unwanted' eigenvalues [79], that is, we use the $m-k$ largest eigenvalue estimates as shifts. The irrelevant information is thereby removed from the starting vector and the Arnoldi factorization, and the relevant information is compressed into $p = m-k$ basis states. The Arnoldi algorithm is then restarted whereby the wanted components are enhanced by the procedure while the unwanted ones are suppressed. The procedure is repeated until the eigenvalues converge [56, 79].

4.4 The Importance-Truncated No-Core Shell Model (IT-NCSM)

We introduce in this section the general concepts of the importance-truncation scheme, where we follow the detailed review of reference [71].

4.4.1 Importance Truncation Scheme

In CI methods, global truncation schemes are used to construct the many-body model space (see section 4.1). For instance, the NCSM uses the $N_{\max}$-truncated model space. As the particle number A and the truncation parameters $N_{\max}$ or $e_{\max}$ grow, the dimension of the model space grows as well and calculations become more time-consuming. On the other hand, the contributions of some many-body states to the eigenstates of the system are very small. Since the specific properties of the Hamiltonian or physical properties of the state one is interested in are not considered, the model space contains many states that are of no consequence for the later calculations, but which increase the problem dimension. We, therefore, introduce an *a priori* importance measure derived from multiconfigurational perturbation theory (MCPT) in order to identify and remove theses states from the computation, so that the problem dimension is limited to a tractable value. To this end, information obtained from the Hamiltonian is used and an importance threshold $\kappa_{\min}$ is introduced. Note that in the limit $\kappa_{\min} \to 0$ the results of the IT-NCSM calculation are the same as for the full NCSM calculation. A variant of the importance truncation was first used in the area of quantum chemistry [71].

4.4.1.1 The Importance Measure

In order to introduce the *a priori* measure for the importance of an individual basis state we consider the full model space $\mathscr{M}_{\text{full}}$ in a NCSM calculation for a given value of $N_{\max}$ spanned by a set of the Slater determinants $\left|\phi_\nu\right\rangle$. The full NCSM calculation yields eigenstates $\left|\psi_{\text{ref}}\right\rangle$ (i. e. ground state and few low-lying excited states) of the Hamiltonian we are interested in. The eigenstates can be expanded in terms of the many-body basis states $\left|\phi_\nu\right\rangle$ with amplitudes C_ν:

$$\left|\psi_{\text{full}}\right\rangle = \sum_{\nu \in \mathscr{M}_{\text{full}}} C_\nu^{(\text{full})} \left|\phi_\nu\right\rangle . \tag{4.16}$$

The contribution of many of the basis state is insignificant, since the corresponding amplitudes C_ν have very small values. Therefore, the dimension of the basis can be reduced significantly by discarding the states with sufficiently small amplitude. We use the initial approximation of the target state, the so-called reference state,

$$\left|\psi_{\text{ref}}\right\rangle = \sum_{\nu \in \mathscr{M}_{\text{ref}}} C_\nu^{(\text{ref})} \left|\phi_\nu\right\rangle . \tag{4.17}$$

to estimate these amplitudes. The reference state is typically determined from a previous NCSM calculation in smaller $N_{\max}$.

The next step is to calculate the first order correction $\left|\psi^{(1)}\right\rangle$ to the target state $\left|\psi_{\text{ref}}\right\rangle$ resulting from states outside of the reference space. For this purpose, multiconfigurational perturbation theory is used, which is widely applied in quantum chemistry [69, 94], in order to estimate the leading correction [71].

The full Hamiltonian H can be divided into the unperturbed part H_0 and the perturbation W, where H_0 is chosen such that

$$\mathrm{H}_0 \left|\psi_{\text{ref}}\right\rangle = \epsilon_{\text{ref}} \left|\psi_{\text{ref}}\right\rangle \tag{4.18}$$

with the eigenstates $\left|\psi_{\text{ref}}\right\rangle$ and the eigenvalue ϵ_{ref}, where the eigenvalue ϵ_{ref} is the expectation value of the full Hamiltonian H [71]:

$$\epsilon_{\text{ref}} = \left\langle \psi_{\text{ref}}\right| \mathrm{H} \left|\psi_{\text{ref}}\right\rangle . \tag{4.19}$$

The unperturbed Hamiltonian can be defined as [69, 71, 94]

$$\mathrm{H}_0 = \epsilon_{\text{ref}} \left|\psi_{\text{ref}}\right\rangle \left\langle \psi_{\text{ref}}\right| + \sum_{\nu \notin \mathscr{M}_{\text{ref}}} \epsilon_\nu \left|\phi_\nu\right\rangle \left\langle \phi_\nu\right| . \tag{4.20}$$

The states $\left|\phi_\nu\right\rangle$, $\nu \in \mathscr{M}_{\text{ref}}$, orthogonal to $\left|\psi_{\text{ref}}\right\rangle$ can be omitted, since they will not contribute later on [71].

There are different possibilities to choose the unperturbed energies ϵ_ν for basis states $\left|\phi_\nu\right\rangle \notin \mathscr{M}_{\text{ref}}$ [71, 94] and their choice affects the convergence as well as some other properties [71]. We use the Møller-Plesset form [71]

$$\epsilon_\nu = \epsilon_{\text{ref}} + \Delta\epsilon_\nu, \tag{4.21}$$

where $\Delta\epsilon_\nu$ is the excitation energy of the basis state $\left|\phi_\nu\right\rangle$ and can be computed using the single-particle energies of the underlying basis. Since we use a harmonic-oscillator basis, those single-particle energies are just the HO energies.

Based on the unperturbed Hamiltonian H_0, which has been fixed previously, one defines the perturbation W:

$$\mathrm{W} = \mathrm{H} - \mathrm{H}_0 \tag{4.22}$$

Using the lowest-order terms of the Rayleigh-Schrödinger perturbation series and taking advantage of the property that all matrix elements of H_0 between $\left|\psi_{\text{ref}}\right\rangle$ and the basis states $\left|\phi_\nu\right\rangle \notin \mathscr{M}_{\text{ref}}$ outside the reference space vanish by construction, we obtain the zeroth-, first- and second-order contributions to the energy [71, 69, 94] (see also appendix A for more details):

$$E^{(0)} = \left\langle \psi_{\text{ref}}\right| \mathrm{H}_0 \left|\psi_{\text{ref}}\right\rangle = \epsilon_{\text{ref}}, \tag{4.23}$$

$$E^{(1)} = \left\langle \psi_{\text{ref}}\right| \mathrm{W} \left|\psi_{\text{ref}}\right\rangle = 0, \tag{4.24}$$

$$E^{(2)} = -\sum_{\nu\notin\mathscr{M}_{\text{ref}}} \frac{\left|\left\langle \phi_\nu\right| \mathrm{W} \left|\psi_{\text{ref}}\right\rangle\right|^2}{\epsilon_\nu - \epsilon_{\text{ref}}} = -\sum_{\nu\notin\mathscr{M}_{\text{ref}}} \frac{\left|\left\langle \phi_\nu\right| \mathrm{H} \left|\psi_{\text{ref}}\right\rangle\right|^2}{\epsilon_\nu - \epsilon_{\text{ref}}} \tag{4.25}$$

The first-order correction to the unperturbed state $\left|\psi^{(0)}\right\rangle = \left|\psi_{\text{ref}}\right\rangle$ is given by [71, 69, 94] (see also appendix A for more details):

$$\left|\psi^{(1)}\right\rangle = -\sum_{\nu\notin\mathscr{M}_{\text{ref}}} \frac{\left\langle \phi_\nu\right| \mathrm{W} \left|\psi_{\text{ref}}\right\rangle}{\epsilon_\nu - \epsilon_{\text{ref}}} \left|\phi_\nu\right\rangle = -\sum_{\nu\notin\mathscr{M}_{\text{ref}}} \frac{\left\langle \phi_\nu\right| \mathrm{H} \left|\psi_{\text{ref}}\right\rangle}{\epsilon_\nu - \epsilon_{\text{ref}}} \left|\phi_\nu\right\rangle. \tag{4.26}$$

The multi-configurational perturbation theory provides an efficient way to estimate the importance of the basis states outside of the reference space $\mathscr{M}_{\text{ref}}$. Equation (4.26) provides a dimensionless measure for the relevance of the basis states $\left|\phi_\nu\right\rangle \notin \mathscr{M}_{\text{ref}}$. The amplitude of the basis state can be chosen as an *a priori* importance measure:

$$\kappa_\nu = -\frac{\left\langle \phi_\nu\right| \mathrm{H} \left|\psi_{\text{ref}}\right\rangle}{\epsilon_\nu - \epsilon_{\text{ref}}} = -\sum_{\mu\in\mathscr{M}_{\text{ref}}} C_\mu^{(\text{ref})} \frac{\left\langle \phi_\nu\right| \mathrm{H} \left|\phi_\mu\right\rangle}{\epsilon_\nu - \epsilon_{\text{ref}}} \tag{4.27}$$

States whose importance measure $|\kappa_\nu|$ is smaller than a threshold $\kappa_{\min}$ are not taken into account for further calculations.

An alternative way to derive the importance measure is to use the second-order energy correction (see eq. (4.23)) in order to approximate the basis states' relevance for the computation of the energy. The energy-based importance measure can be defined as:

$$\xi_\nu = \frac{|\left\langle \phi_\nu\right| H \left|\psi_{\text{ref}}\right\rangle|^2}{\epsilon_\nu - \epsilon_{\text{ref}}} \tag{4.28}$$

We use for our calculations the dimensionless state-based importance measure, since both measures provide very similar results and the state-based importance measure is easier to handle [71].

The importance-truncated model space, in which the eigenvalue problem is being solved, is smaller than the full space $\mathscr{M}_{\text{full}}$ and the calculation is simplified. The size of the model space can be controlled using the importance threshold. For a two-body Hamiltonian, the importance measure κ_ν vanishes if there is no state in the reference space that differs from the basis state $\left|\phi_\nu\right\rangle$ by two or less single-particle states.

4.4.1.2 Characteristics of the Importance-Truncated CI

The most important property of the approach described so far is that it is a strictly variational approach [71], that is, the calculated eigenvalue for a given $\kappa_{\min}$ always provides an upper bound for the exact ground-state energy. We use this property for the extrapolation of $\kappa_{\min} \to 0$. According to the Hylleraas-Undheim theorem [42], the n^{th} energy eigenvalues E_n of the Hamiltonian in a given space are lower bounds on the eigenvalues of the projection of that Hamiltonian on any subspace. Consequently, the eigenvalues $E_n^{(\text{full})}$ in the full space are lower bounds on the eigenvalues $E_n(\kappa_{\min})$ in a truncated space $\mathscr{M}(\kappa_{\min})$, and these eigenvalues in turn are lower bounds on the eigenvalues $E_n(\kappa'_{\min})$ for $\kappa_{\min} < \kappa'_{\min}$:

$$E_n^{(\text{full})} \leq E_n(\kappa_{\min}) \leq E_n(\kappa'_{\min}) \text{ for } \kappa_{\min} < \kappa'_{\min}, \tag{4.29}$$

that is, the calculated eigenvalues decrease monotonically as $\kappa_{\min}$ decreases and are an upper bound for the exact eigenvalues. Other observables, for example, transition matrix elements, form factors, and densities do not necessarily decrease monotonically. Furthermore, all observables approach the values obtained through full NCSM calculation in the limit $\kappa_{\min} \to 0$, hence the *a posteriori* extrapolation of the observables is possible [71, 73].

4.4.1.3 *A posteriori* Energy Corrections

In addition to the definition of an importance measure, we can use perturbation theory for *a posteriori* corrections to the calculated energies $E_n(\kappa_{\min})$. To estimate the contribution of the discarded states with $|\kappa_\nu| < \kappa_{\min}$, which are not included in the importance-truncated space $\mathscr{M}(\kappa_{\min})$, we can use the second-order perturbative contribution to the energy (4.23) and sum the energy corrections of each discarded state:

$$\Delta^{\text{excl}}(\kappa_{\min}) = -\sum_{\nu \notin \mathscr{M}(\kappa_{\min})} \frac{\left|\langle \phi_\nu | \mathrm{H} | \psi_{\text{ref}} \rangle\right|^2}{\epsilon_\nu - \epsilon_{\text{ref}}} \tag{4.30}$$

During the many-body calculations, the second-order contribution of each discarded state is calculated at no additional cost. The energy contribution $\Delta^{\text{excl}}(\kappa_{\min})$ can then be added to the energy obtained through IT-NCSM at the end of the calculation. However, this contribution is not defined for anything but the energy, since other quantities do not show the monotonic decrease with decreasing $\kappa_{\min}$ [73].

4.4.2 Iterative Construction of the IT-NCSM Model Space and Implementation

The implementation of the IT-NCSM for ultra-cold Fermi gases is formally the same as in nuclear physics. The computationally most demanding part is the construction of the importance-truncated space. To this end, we use the iteration method described by Roth [71]. A somewhat different implementation was described by Kruse [55].

For the IT-NCSM, we use a sequential scheme like for the full NCSM, since it is most efficient [73]. We are interested in the convergence behavior with increasing $N_{\max}$ in order to perform the extrapolation to the infinite model space. In every iteration step, we use the many-body state obtained in the $N_{\max}$ model space to construct a reference state for the calculation of the $N_{\max}+2$ space. The next larger space is constructed by creating all $1p1h$ and $2p2h$ excitations. Furthermore, we check for all created states whether that state is already contained in the space in order to avoid duplicates. For $N_{\max} = 2$ and 4, we perform the complete NCSM calculations, that is, we include all states ($\kappa_{\min} = 0$). For all subsequent calculations, that is, for $N_{\max} = 6, 8, 10, \ldots$, we use the IT-NCSM. We only calculate a few eigenstates with the lowest energies.

In order to extrapolate the results to $\kappa_{\min} \to 0$, we calculate the eigenvalues for a set of values of $\kappa_{\min}$. We first construct the importance-truncated model space with the smallest value of $\kappa_{\min}$ for which we want to calculate the eigenvalues, compute the Hamilton matrix and solve the eigenvalue problem. For the construction of the space corresponding to the second smallest $\kappa'_{\min}$ we remove all the states $\left|\phi_\nu\right\rangle$ for which $|\kappa_\nu| < \kappa'_{\min}$ as well as the corresponding matrix elements from the Hamilton matrix. We solve the eigenvalue problem again in the importance-truncated model space spanned by the remaining basis states $\left|\phi_\nu\right\rangle$ that fulfill the condition $|\kappa_\nu| \geq \kappa'_{\min}$. We repeat this procedure for all values of $\kappa_{\min}$. In this way, the most computationally expensive parts of the calculation (the construction of the space and the computation of the Hamilton matrix) only need to be performed once.

We introduce an additional reference threshold to the importance measure, in order to accelerate the calculation and drop basis state from the reference state whose amplitude is less than $C_{\min}$; that is, we do not use all basis states $\left|\phi_\nu\right\rangle \in \mathscr{M}^{(1)}(\kappa_{\min})$ to construct the reference state $\left|\psi^{(1)}_{\text{ref}}\right\rangle$ for the subsequent iteration, but only those whose amplitude $|C_\nu|$ exceeds the threshold $C_{\min}$ ($|C_\nu| \geq C_{\min}$). In the limit $(\kappa_{\min}, C_{\min}) \to 0$ the results of the IT-NCSM calculation approaches the exact results of the full NCSM calculation.

The diagonalization is, of course, performed for each value of $\kappa_{\min}$ individually. We use Lanzcos- or Arnoldi-type algorithms to perform the diagonalization (see section 4.3). The many-body matrix elements of the Hamiltonian are pre-computed and stored in memory or on disk (see section 3.2.4). The construction of the importance-truncated space and computation of the Hamiltonian matrix can be almost perfectly parallelized. Only little information needs to be exchanged between processing instances, therefore, an almost linear speed-up can be achieved. We use a hybrid OpenMP plus MPI parallelization strategy.

4.4.3 Importance Truncation Uncertainties

In the IT-NCSM calculation, we discard the physically unimportant states controlled by the importance threshold $\kappa_{\min}$. Furthermore we use only states with amplitude $|C_\nu| \geq C_{\min}$ for the construction of the reference state (see sections 4.4.1 and 4.4.2). $\kappa_{\min}$ and $C_{\min}$ are the only source of errors in comparison to the full NCSM, since the discarded states might contribute to the many-body observables. Here we discuss possibilities to eliminate these errors and to obtain the energy in the limit $(\kappa_{\min}, C_{\min}) \to 0$, which corresponds to the energy obtained through the full NCSM calculation. For that purpose we use two methods: the extrapolation of the observables as $\kappa_{\min}$ approaches zero and the estimation of the contribution of the discarded states with $|\kappa_\nu| < \kappa_{\min}$ during the many-body calculation. We also calculate the energy for different $C_{\min}$ in order to estimate the influence of this threshold.

In order to estimate the uncertainties, which are introduced by considering only the physically important states $\left|\phi_\nu\right\rangle$ with $|\kappa_\nu| \geq \kappa_{\min}$, we compute the observables through a sequence of IT-NCSM calculations using different values for the threshold $\kappa_{\min}$ as described in section 4.4.2, and we extrapolate the results for a vanishing threshold $\kappa_{\min} \to 0$. We use as extrapolation function a p^{th}-order polynomial (usually p is an integer between 3 and 5 inclusively), since the energy eigenvalues are smooth and monotonically decreasing with $\kappa_{\min}$. In the following figures we chose $C_{\min} = 0.0002, 0.0003, 0.0004$ and 0.0005 in those cases in which we used different $C_{\min}$ and $C_{\min} = 0.0002$ in those cases in which we used only one $C_{\min}$, and we used a sequence of $\kappa_{\min}$ from $3 \cdot 10^{-5}$ to $1 \cdot 10^{-4}$ as importance thresholds. We used $n_{\max} = 4$ as a two-body cutoff (see section 3.5) for all calculations in this section.

Figure 4.3 shows an example for such a calculation. The ground-state energy of eight fermions ($A_1 = A_2 = 4$) in the unitary limit for different $C_{\min}$ and $\kappa_{\min}$ is calculated for $N_{\max} = 8$ and $N_{\max} = 12$. We used the LO of the EFT interaction (see chapter 3.6) for the calculation with $n_{\max} = 4$ as a two-body cutoff (see section 3.5). Until $N_{\max} = 4$, we used the full NCSM calculation and from then on, sequential IT-NCSM with $N_{\max}$ increasing in steps of two ($N_{\max} = 6, 8, \ldots$). The figure also shows the energy calculated with the full NCSM for $N_{\max} = 8$ as a reference. We use for the extrapolation a third-order polynomial.

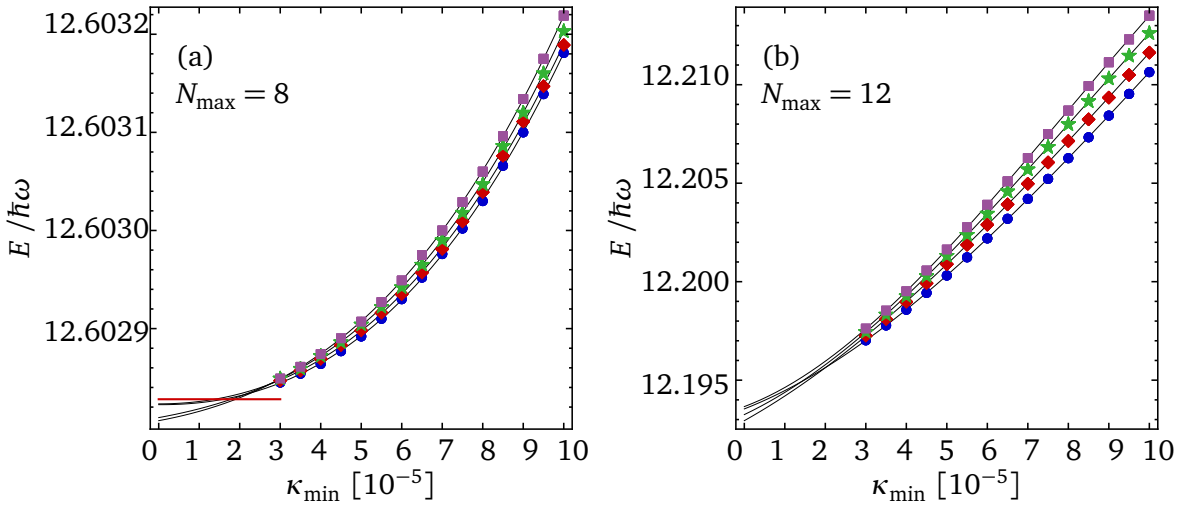

Figure 4.3.: The energy of the ground state with $L^\pi = 0^+$ of a two-component fermion system with $A_1 = A_2 = 4$ in the unitary limit for $N_{\max} = 8$ (a) and $N_{\max} = 12$ (b) for different $C_{\min}$ from 0.0002 to 0.0005 (●, ◆, ★, ■) and a sequence of $\kappa_{\min}$ from $3\cdot10^{-5}$ to $1\cdot10^{-4}$ as importance thresholds. The calculation was done using the LO of the EFT interaction. We used third-order polynomials as extrapolation functions. The horizontal line in panel (a) shows the results of the full NCSM calculation.

The calculated observables show no or very little dependence on the reference threshold $C_{\min}$ for both values of $N_{\max}$. The relative difference between the results for different $C_{\min}$ is of the order 10^{-5}, and hence very small. We use for each particle number a reference threshold $C_{\min}$ that is small enough so it does not affect the results. The ground-state energy obtained with the importance-truncated NCSM for $N_{\max} = 8$ is close to the exact value obtained with the full NCSM calculation.

We also estimate the uncertainty of the energy extrapolation to $\kappa_{\min} \to 0$. To this end, we construct a sequence of fits (like in [71, 73]): As already mentioned we used a p^{th}-order polynomial fit for the extrapolation to $\kappa_{\min} \to 0$ to estimate the extrapolated value of the observable. For the quantification of the extrapolation uncertainty we use $(p-1)^{\text{th}}$- and $(p+1)^{\text{th}}$-order polynomials for all data points. Additionally, we fit p^{th}-order polynomials to the data points where the lowest and the two lowest $\kappa_{\min}$ are discarded. The results obtained from these fits provide an error band for the extrapolated observable. We can apply this error estimation to all observables for different values of $C_{\min}$ and different sequences of $\kappa_{\min}$.

Figure 4.4 shows the estimation of the extrapolation uncertainty. Here we also used the EFT interaction at LO for $N_{\max} = 8$ and 12. The calculation of the ground-state energy for both $N_{\max} = 8$ and 12 were done with the reference threshold $C_{\min} = 2 \cdot 10^{-4}$. The estimation of the uncertainties of the calculation were done with the method explained above. We used a polynomial of 3^{rd} order for the extrapolation function and polynomials of 2^{nd} and 4^{th} order as well as two 3^{th} order polynomials obtained by omitting the data points for the smallest and the two smallest values $\kappa_{\min}$, respectively. The ground-state energy obtained through the importance-truncated NCSM for $N_{\max} = 8$ reproduces the exact value obtained with the full NCSM calculation within the estimated extrapolation uncertainty. For the calculation with $N_{\max} = 12$, where the full NCSM calculation is more computationally expensive, the uncertainties are larger than for $N_{\max} = 8$ but still negligibly small — the relative uncertainty is only about 10^{-4}. The same behavior is observed in nuclear physics with light nuclei for the IT-NCSM calculations [73].

We also performed the same estimation for the energies of the ground state and the first excited state of a six-fermion system with $A_1 = A_2 = 3$ in the unitary limit with $L^\pi = 0^+$ (see fig. 4.5). Again, we

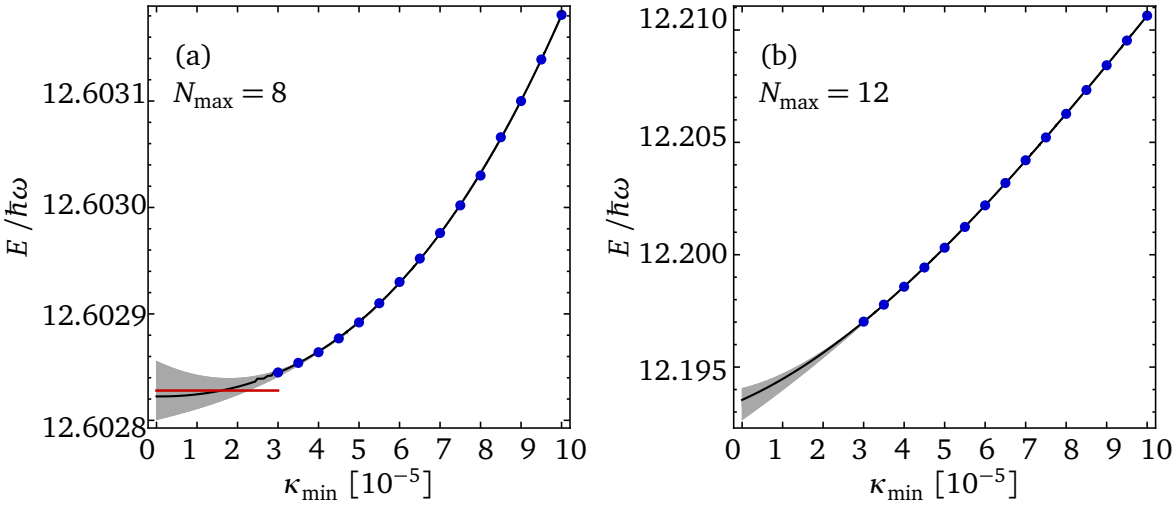

Figure 4.4.: The energy of the ground state with $L^\pi = 0^+$ of a two-component fermion system with $A_1 = A_2 = 4$ in the unitary limit for $N_{\max} = 8$ (a) and $N_{\max} = 12$ (b) for $C_{\min} = 0.0002$ and a sequence of $\kappa_{\min}$ from $3 \cdot 10^{-5}$ to $1 \cdot 10^{-4}$ as importance thresholds. The calculation was done using the LO of the EFT interaction. We used third-order polynomials as extrapolation functions and the extrapolation procedure described in the text for the uncertainty bands. The horizontal line in panel (a) shows the results of the full NCSM calculation.

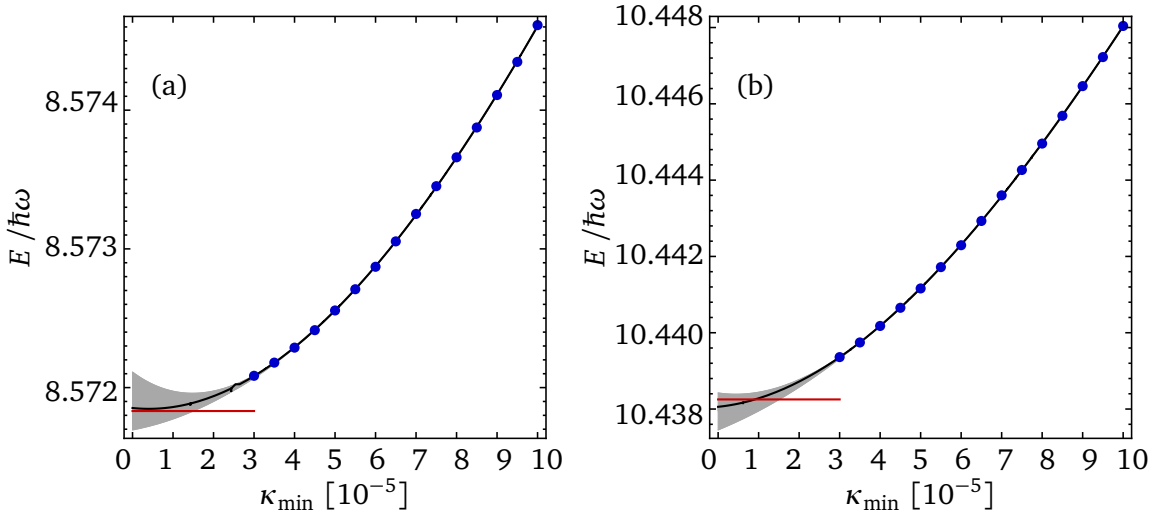

Figure 4.5.: The energy of the ground state (a) and first excited state (b) with $L^\pi = 0^+$ of a two-component fermion system with $A_1 = A_2 = 3$ in the unitary limit for $N_{\max} = 12$ for $C_{\min} = 0.0002$ and a sequence of $\kappa_{\min}$ from $3 \cdot 10^{-5}$ to $1 \cdot 10^{-4}$ as importance thresholds. The calculation was done using the LO of the EFT interaction. We used third-order polynomials as extrapolation functions and the extrapolation procedure described in the text for the uncertainty bands. The horizontal line shows the results of the full NCSM calculation.

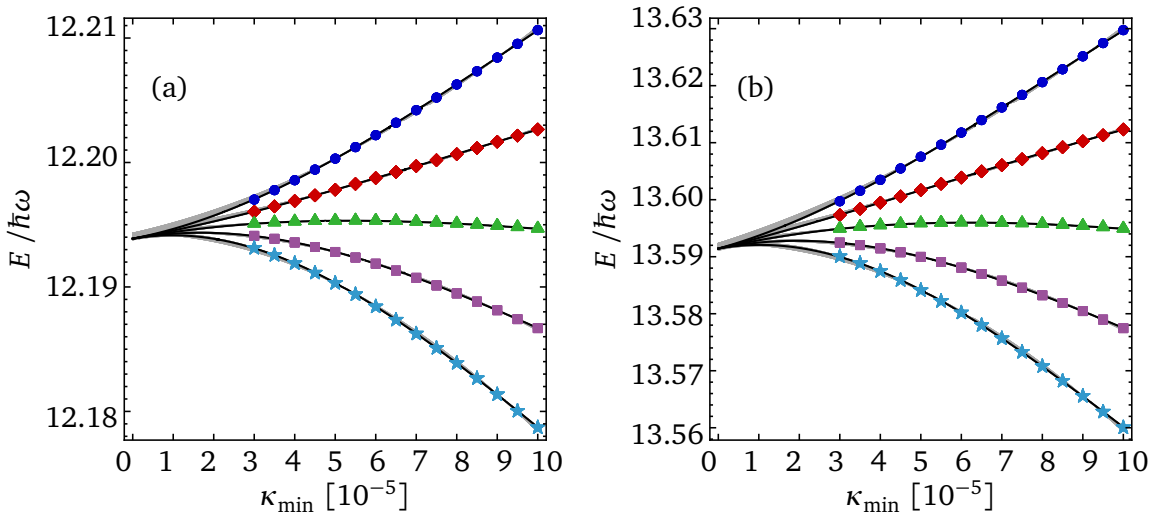

Figure 4.6.: Illustration of the constrained simultaneous extrapolation of the energy of the ground state (a) and the first excited state (b) with $L^\pi = 0^+$ of a two-component fermion system with $A_1 = A_2 = 4$ in the unitary limit for $N_{\max} = 12$ for $C_{\min} = 0.0002$ and a sequence of $\kappa_{\min}$ from $3 \cdot 10^{-5}$ to $1 \cdot 10^{-4}$ as importance thresholds. The calculation was done using the LO of the EFT interaction. We used third-order polynomials as the extrapolation functions and the extrapolation procedure described in the text for the uncertainty bands. We used $\lambda = 0, 0.5, 1, 1.5, 2$ (a) and $\lambda = 0, 0.55, 1.1, 1.65, 2.2$ (b).(●, ◆, ▲, ■, ★)

used the full NCSM calculation up to $N_{\max} = 4$ and used IT-NCSM from there on. Figure 4.5 (a) shows the calculated ground-state energy and fig. 4.5 (b) the excited-state energy for $N_{\max} = 12$. Extrapolation and error estimation have been performed in the same way as for a two-component fermion system with $A_1 = A_2 = 4$ described previously. Furthermore, the result of a full NCSM calculation for $N_{\max} = 12$ is also shown in fig. 4.5 as a reference. The value is well within the error bars of the importance-truncated calculation.

For the estimation of the energy and the uncertainties of the energy we can combine the extrapolation of the importance threshold $\kappa_{\min}$ with the *a posteriori* correction to the IT-NCSM energies (see section 4.4.1.3). In order to estimate the contribution of the discarded states, we introduce an auxiliary control parameter λ such that

$$E_n^\lambda(\kappa_{\min}) = E_n^{\text{eval}}(\kappa_{\min}) + \lambda \Delta_n^{\text{excl}}(\kappa_{\min}), \tag{4.31}$$

where $\lambda\Delta_n^{\text{excl}}(\kappa_{\min})$ is the energy correction (4.30) to the energy eigenvalues $E_n^{\text{eval}}(\kappa_{\min})$ obtained in the importance-truncated space [71, 73]. Here we use the fact that, in the limit $\kappa_{\min} \to 0$, the energy correction vanishes and hence $E_n^\lambda(\kappa_{\min})$ is independent of λ in the limit $\kappa_{\min} \to 0$. One calculates $E_n^\lambda(\kappa_{\min})$ for different values of λ and different values of $\kappa_{\min}$ and then performs the extrapolation as described previously for $\kappa_{\min}$ (using polynomials of different orders and omitting the data points for small $\kappa_{\min}$ as described previously). Furthermore, we ignore both the smallest and the largest value of λ in the extrapolation. This approach makes the extrapolation more robust, since the energies $E_n^\lambda(\kappa_{\min})$ calculated using different values of λ typically approach the energy $E_n^0(\kappa_{\min} = 0)$ calculated using the full NCSM from both sides [71].

Figure 4.6 shows the perturbatively corrected energy of the ground (a) and first excited state (b) of a two-component fermion system with $A_1 = A_2 = 4$ in the unitary limit for an importance-truncated NCSM calculation with $N_{\max} = 12$ and $C_{\min} = 2 \cdot 10^{-4}$. The parameter λ has been chosen such that the fitted curves $E_\lambda(\kappa_{\min})$ are nearly symmetric. Like in nuclear physics [73], we observe that the errors become

smaller by additionally using information obtained for the second-order energy corrections due to the excluded states. Figure 4.6 (b) shows the same extrapolation for the energy of the first excited state. Again, we observe a reduction of the errors. In most cases, we employ the simpler extrapolation using $\kappa_{\min}$ alone; we only introduce the additional parameter λ in particularly difficult cases, that is, in those cases where the IT-NCSM calculation with a lower value of $\kappa_{\min}$ would be too computationally expensive and the errors of the simpler extrapolation would be too large.

4.5 The Fixed Node Diffusion Monte Carlo Method (FN-DMC)

We describe in this section the Diffusion Monte Carlo (DMC) method which uses the concept of imaginary time propagation, then we briefly consider the general aspects of the FN-DMC. The method is based on the similarity between the time-independent Schrödinger equation and a diffusion equation [3]. The solution for the time-dependent Schrödinger equation

$$i\hbar\frac{\partial}{\partial t}\Psi(\vec{R},t) = H\Psi(\vec{R},t), \tag{4.32}$$

where $\vec{R} = \{\vec{r}_1,\ldots,\vec{r}_A\}$ includes the coordinates of all particles, is given by the superposition of stationary states $\phi_n(\vec{R})$ multiplied by a phase factor

$$\Psi(\vec{R},t) = \sum_{n=0}^{\infty} c_n\phi_n(\vec{R})\exp\left(-\frac{i}{\hbar}E_n t\right). \tag{4.33}$$

The eigenvalues E_n and the eigenfunctions $\phi_n(\vec{R})$, $n = 0,1,\ldots$, which are assumed to be real and orthogonal, of the Hamiltonian

$$H = -\sum_{i=1}^{A}\frac{\hbar^2}{2m_i}\vec{\nabla}_i^2 + V(\vec{R}) \tag{4.34}$$

can be obtained from the time-independent Schrödinger equation. When time t is replaced by imaginary time $\tau = it$ (also known as Wick rotation), the solution is given by a sum of transients of the form $\exp(^{-E_n\tau}/_{\hbar})$ where the longest-lasting transient is given by the ground-state energy E_0 [53, 84, 95]. In order to keep the long-time limit finite, it is useful to introduce a shift of the energy scale, which can be performed by replacing $V(\vec{R}) \to V(\vec{R}) - E_T$ and $E_n \to E_n - E_T$ [53], where E_T is a constant shift in the energy [3, 48, 53, 68]. Equation (4.32) then takes the form

$$\hbar\frac{\partial}{\partial\tau}\Psi(\vec{R},\tau) = \left(\sum_{i=1}^{A}\frac{\hbar^2}{2m}\vec{\nabla}^2 - \left[V(\vec{R}) - E_T\right]\right)\Psi(\vec{R},\tau) \tag{4.35}$$

with the solution

$$\Psi(\vec{R},\tau) = \sum_{n=0}^{\infty} c_n\phi_n(\vec{R})\exp\left(-\frac{i}{\hbar}\left(E_n - E_T\right)\tau\right) \tag{4.36}$$

The offset in the energy affects the wave function. If E_T equals the ground state energy, $E_T = E_0$, the wave function converges up to a constant factor c_0 to the ground state wave function if the evolution in the imaginary time is performed long enough. One then gets the ground-state energy and wave function of the quantum system [48, 53]. If $E_T > E_0$, all amplitudes will go to infinity and the wave function diverges exponentially fast. If $E_T < E_0$, the wave function vanishes exponentially fast. The c_0 term dominates in all three cases, given that $\Psi(\vec{R},\tau)$ is not orthogonal to the ground state. In order to determine the ground state energy and the wave function, we therefore have to adjust E_T so that the norm of the state tends to a constant [53, 36].

Equation (4.35) is similar to a diffusion equation with an added first-order reaction term, where $\Psi(\vec{R},\tau)$ represents the density of diffusing particles (or "walkers"). The first term in eq. (4.35) is a common diffusion term and can be simulated by a random walk of particles through configuration space. The second therm is used in order to readjust E_T and renormalize [62, p. 250] the wave function. One possibility to do this is to let the second term describe the branching process (the birth and death process in the "walker" population). The second term serves to increase the number of particles in regions with lower $V(\vec{R})$ and decrease the number in regions with higher $V(\vec{R})$, making the distribution correspond to the ground-state wave function [3, 48, 68]. The changes in the number of walkers as result of death and birth processes are used in order to readjust the energy E_T [53].

The branching term $V(\vec{R}) - E_T$ may diverge, which leads to a very large fluctuation in the particle density [68, 84]. These fluctuations can be reduced by the technique of importance sampling. Here, an initial guess $\phi_T(\vec{R})$ (the trial wave function or guiding function) is used to bias the "walkers" to reproduce the distribution $f(\vec{R},\tau) = \Psi(\vec{R},\tau)\phi_T(\vec{R})$. The imaginary time evolution of $f(\vec{R},\tau)$ describes an equation similar to eq. (4.35). The better the guess, the smaller are the fluctuations.

This technique can also be used to overcome the sign problem. The interpretation of the wave function $\Psi(\vec{R},\tau)$ as probability density implies that it must either be positive everywhere or negative everywhere, since the phase of the wave function is arbitrary. That would restrict the imaginary time propagation to Bose systems in their ground state, since its wave function has no nodes. The wave function of a Fermi system has nodes (it changes sign). The problem can be solved by treating the positive and negative regions separately and not allowing diffusion between them. This method is called fixed-node approximation [68]. Using the FN-DMC, however, one can force the wave function to have the same structure as a guiding wave function $\phi_T(\vec{R})$ and get an upper bound to the exact ground state within statistical uncertainties [84]. Stecher [84] used the variational Monte Carlo method in order to optimize the wave function $\phi_T(\vec{R})$, which is important in FN-DMC since the choice of $\phi_T(\vec{R})$ significantly affects the result (as explained previously).

Table 4.1.: Energy of the ground state E_{00} of 3 to 30 two-component fermionic system at unitary calculated using the FN-DMC method (values taken from [12])

N	E_{00}	N	$E_{00}/(\hbar\omega)$	N	$E_{00}/(\hbar\omega)$
		11	20.11(7)	21	45.47(15)
		12	21.28(5)	22	46.89(9)
3	4.281(4)	13	24.79(9)	23	51.01(18)
4	5.051(9)	14	25.92(5)	24	52.62(20)
5	7.61(1)	15	29.59(10)	25	56.85(22)
6	8.64(3)	16	30.88(6)	26	58.55(18)
7	11.36(2)	17	34.64(12)	27	63.24(22)
8	12.58(2)	18	35.96(7)	28	64.39(31)
9	15.69(1)	19	39.83(15)	29	69.13(31)
10	16.80(4)	20	41.30(8)	30	70.93(30)

In [12], the FN-DMC method was used for the calculation of up to 30 fermions in the unitary limit. Table 4.1 (taken from [12]) shows the ground-state energy from $A = 3$ to $A = 30$ two-component fermionic systems at unitarity, calculated using the FN-DMC method.

4.6 Correlated Gaussian Basis (CG)

Now we briefly describe an alternative method also used for calculation of ultra-cold fermion gases that does not rely on Monte Carlo techniques, the correlated Gaussian (CG) basis state expansion. The combination of a Gaussian basis and the stochastically variational method was extensively used in nuclear

physics by Suzuki and Varga [95, 98]. For the calculation of the energy of fermionic systems at unitarity it was used in Refs. [12, 65, 84]. A detailed description can be found in [84, 95, 98, 99].

In the direct approaches such as CI (NCSM) used in this thesis, the energy and the eigenstates of the Hamiltonian, spanned within a model space by a set of many-body states, are calculated by diagonalization. The range of application of these methods is limited. With growing dimension of the model space and with increasing particle number the calculations become intractable. Basis optimization is one possibility to avoid this problem. One uses only basis states essential to the calculation of the energy and wave function to a certain accuracy. Since some states are essential to the ground state and others to the excited state, this selection is state-dependent. In the Stochastic Variational Method (SVM), the basis functions are selected by a trial-and-error procedure [95, 98]. The accuracy of the variational approach depends essentially on the choice of the basis functions. A correlated Gaussian basis function of the form

$$\begin{aligned}\Phi(\vec{\xi}_1,\vec{\xi}_2\ldots,\vec{\xi}_A) &= \exp\left(-\frac{1}{2}\vec{\xi}^T M\vec{\xi}\right) \equiv \exp\left(-\frac{1}{2}\sum_{i=1}^{A-1}\sum_{j=1}^{A-1} M_{ij}\vec{\xi}_i\vec{\xi}_j\right) \\ &= \exp\left(-\frac{1}{2}\sum_{j>i=1}^{A}\alpha_{ij}\left(\vec{r}_i-\vec{r}_j\right)^2\right)\end{aligned} \tag{4.37}$$

seems to be the best choice for variational approaches [95, 98]. Here M is an $(A-1)\times(A-1)$ positive definite symmetric matrix and M_{ij} or α_{ij} are nonlinear parameters of the basis, $\vec{r}_i-\vec{r}_j$ are interparticle distance vectors and $\vec{\xi}=(\vec{\xi}_1,\ldots,\vec{\xi}_{A-1})$ is a vector with Jacobi coordinates $\vec{\xi}_i$ (see section 4.2.1). Both in the CI methods and in the CG method we transform the single-particle coordinates to center-of-mass and intrinsic coordinates. This allows the complete separation of the center-of-mass motion from the intrinsic motion (see also the discussion to the center-of-mass contamination in section 4.2.2). Therefore, the wave function is translationally invariant and is written in terms of the independent Jacobi coordinates $(\vec{\xi}_1,\ldots,\vec{\xi}_{A-1})$ (see section 4.2.1) [98]. Additional degrees of freedom such as spin etc. have to be multiplied by suitable trial functions in these additional spaces.

The wave function of the A-particle system can be expanded as

$$\Psi(\vec{\xi}_1,\vec{\xi}_2\ldots,\vec{\xi}_A) = \sum_i^K c_i\phi_i(\vec{\xi}_1,\vec{\xi}_2\ldots,\vec{\xi}_A) \tag{4.38}$$

with a selected set of basis functions $\phi_i(\vec{\xi}_1,\vec{\xi}_2\ldots,\vec{\xi}_A)$; $i=1,\ldots,K$, of the form (4.37), that adequately spans the state space and a set of linear variational parameters $\vec{c}^T=\left(c_1,\ldots,c_K\right)$ [98].

Now the time-independent Schrödinger equation can be solved in this basis and the eigenvalue problem is reduced to

$$\mathscr{H}\vec{c} = E\mathscr{N}\vec{c} \tag{4.39}$$

in a subspace $\mathscr{V}_K$, where $\mathscr{H}$ and $\mathscr{N}$ are matrices of the Hamiltonian and of the overlap with matrix elements

$$\mathscr{H}_{ij} = \left\langle \phi_i\middle| H \middle|\phi_j\right\rangle \quad\text{and}\quad \mathscr{N}_{ij} = \left\langle \phi_i\middle|\phi_j\right\rangle \quad (i,j=1,\ldots,K) \tag{4.40}$$

Using, for example, the trial-and-error procedure of SVM, one can now optimize the basis by the following stepwise procedure: One generates a basis function by choosing the nonlinear parameters randomly and solves the eigenvalue problem. The basis functions with parameters that produce the lowest energy are used in the next calculations, all other can be discarded. This procedure is used until convergence [95, 98].

The CG method provides an accurate description of the ground and excited states up to $A=6$ [12, 84]. Table 4.2 shows the energy of the ground state and some excited state of two-component fermions in the unitary limit by using the CG method.

Table 4.2.: The ground-state and excited-state energy of the two-component fermionic system at unitarity calculated using the SVM with CG set as a basis function (table taken from [12])

N	L_{rel}	$E_{00}/(\hbar\omega)$	$E_{01}/(\hbar\omega)$	$E_{02}/(\hbar\omega)$	$E_{10}/(\hbar\omega)$	$E_{20}/(\hbar\omega)$
3	0	4.682	6.685	8.688	7.637	9.628
3	1	4.275	6.276	8.279	6.868	8.229
4	0	5.028	7.032	9.039	7.464	8.051
5	0	8.03	10.04	12.06	8.83	10.38
5	1	7.53			9.13	
6	0	8.48	10.50	12.52	10.44	11.00

4.7 Conclusions

In this chapter, we have presented the IT-NCSM, which allows us to extend NCSM calculations to larger model spaces by introducing an importance threshold $\kappa_{\min}$ derived using multi-configurational perturbation theory (see section 4.4.1). The basis states with $|\kappa_\nu| < \kappa_{\min}$ are neglected, leading to a smaller model space dimension and thus lower computational effort. Furthermore, we introduce a reference threshold $C_{\min}$ and consider for the construction of the next higher model space $N_{\max}+2$ only those basis states of the reference space, which satisfy the condition $|C_\nu| \geq C_{\min}$ (see section 4.4.2). The results are extrapolated to vanishing thresholds $(\kappa_{\min}, C_{\min}) \to 0$. The uncertainties of these extrapolation is the only source of uncertainties in comparison to the results of the full NCSM calculation. In order to obtain an approximation to the NCSM results as well as the uncertainties we use *a posteriori* threshold extrapolation, which can be improved by using the contributions of excluded configurations.

We also introduced in this chapter two additional methods used for the calculation of two-component fermionic systems at unitarity: the FN-DMC and CG method. Whereas the FN-DMC method has been successfully applied to systems comprising up to 30 particles, but only yields the ground-state energy, the CG method can also be used to calculate excited-state energies, but only for smaller systems ($A \leq 6$). We use the results calculated using FN-DMC and CG method for comparison in the chapter 5. The full NCSM (without importance truncation) can only be used for small systems ($A \leq 4$, $A \leq 5$ only for small values of $N_{\max}$).

5 Benchmark Calculations

We present in this chapter the results of our calculations using the IT-NCSM for the ABF and EFT interactions and the NCSM for the Gaussian-shaped potential. More precisely, we compute the energies of two-component fermionic systems ($A \leq 20$) in the unitary limit in a harmonic oscillator (HO) trap. In order to describe the interaction between the fermions we use three different interactions: the EFT interaction (see section 3.6), the ABF interaction (see section 3.7) and the Gaussian-shaped potential (see section 3.8). The matrix elements of the interactions were transformed from relative coordinates into the single-particle basis using the Talmi-Moshinsky transformation explained in section 3.2.3. We computed the energies by solving the eigenvalue problem using the Hamiltonian (3.2) with the NCSM and the IT-NCSM (see chapter 4).

Alhassid, Bertsch *et al.* [1] as well as Rotureau *et al.* [77] calculated few-body systems with $A = 3$ and 4 fermions in a HO trap in the unitary limit. Rotureau *et al.* used the NCSM while Alhassid, Bertsch *et al.* used the CI method (see section 4.1). NCSM calculations for three- and four-fermion systems can be done in large many-body spaces. In larger systems, however, the model space (and, consequently, the required memory and computation time) quickly grows too large. This scaling is mitigated by importance-truncating the many-body space, permitting the computation of larger systems and higher $N_{\max}$ values. For $A = 3$ particles, using the importance-truncated NCSM does not provide any advantage, since the energies of such small systems can be calculated quickly even for higher values of $N_{\max}$.

We consider fermionic systems with particle number $A = A_1 + A_2$, with A_1 being the number of particles of the first component (of the one hyperfine state $\left| f_1 m_{f_1} \right\rangle$) and A_2 of the second component (of the other hyperfine state $\left| f_2 m_{f_2} \right\rangle$) (see chapter 2.3 for more details). We consider only systems with $A_1 = A_2$ or $A_1 = A_2 + 1$ and refer to them in terms of the total particle number $A = A_1 + A_2$. We performed a full calculation for the $N_{\max} = 2$ and $N_{\max} = 4$ spaces and used the results from the latter to build the importance-truncated space for $N_{\max} = 6$; the results obtained in that space were then used to build the $N_{\max} = 8$ space etc. (see section 4.4.2). We calculated the energies of the ground state and the first excited state at unitarity for $A = 4$ through $A = 10$ and for $A = 20$ particles using the ABF and the EFT interaction. For our calculations using the Gaussian-shaped potential we used only the NCSM and performed only calculations for $A = 3$ particles. Besides the energy, we also evaluated the orbital angular momentum of each state in order to select the states with the desired value of L^π.

In the IT-NCSM we discard the physically unimportant states by using the thresholds $\kappa_{\min}$, $C_{\min}$ (see section 4.4.3). For the extrapolations to $\kappa_{\min} \to 0$ as well as quantification of the uncertainties we used the methods introduced in section 4.4.3. For the NLO correction of the EFT interaction, we use a perturbation theory approach. We start with the discussion of the errors of the calculation in section 5.1 and explain the extrapolation method and why we discard the errors of the NLO calculations in the subsequent sections. We analyze the convergence behavior for $3 + 2$ and $2 + 2$ systems with increasing relative cutoff for the EFT interaction and increasing regularization parameter for the ABF interaction. In section 5.2 we consider the consequences for the convergence behavior of the results for $N_{\max} < 2n_{\max}$. We discuss in the next section 5.3 the convergence behavior with $N_{\max}$ in general for different values of the relative cutoff of the EFT interaction or the regularization parameter of the ABF interaction.

Besides the truncation parameters $n_{\max}$ for the ABF and EFT interaction and $N_{\max}$ for the many-body basis, our calculation depends also on the HO frequency. We discuss the dependency of the results on $N_{\max}$ and the HO frequency in section 5.4. With increasing $N_{\max}$, the required computational effort also increases; extrapolations allow us to estimate the results for infinitely large many-body spaces. In

section 5.5 we discuss the convergence with $n_{\max}$ for the ABF and EFT interaction and in the following section 5.5 the optimal choice for the relative cutoff.

We study in section 5.6 the energy spectra for small values of A (4 and 5) using the ABF interaction (see section 3.7) and the EFT interaction (see section 3.6). We performed full NCSM and IT-NCSM calculations and compare the energies, spectra and dimensions of the full and truncated model spaces. Furthermore, we present the convergence behavior of the energies of the ground state and the first excited state for $A \leq 20$ particles. For values of A larger than 4 or 5, full NCSM calculations are no longer feasible, and we compare our results for the EFT and ABF interaction to the results obtained with the fixed node diffusion Monte-Carlo method (FN-DMC) (see section 4.5) or the Correlated Gaussian basis state expansion (CG) (see section 4.6) published by other groups [12] as a benchmark. The Monte-Carlo calculations provide results only for the ground-state energy. For $A \leq 6$ fermions there are also results for the ground state and excited states of the fermionic systems at unitarity using CG method (see section 4.6). Both methods used as interaction a Gaussian-shaped potential. Sections 5.3, 5.5 and 5.7 contain the results of our calculations using the ABF interaction [1] and the EFT interaction [77] for 8 and 20 particles, respectively. Finally, we compare the calculated energies for different particle numbers A with the results of Monte-Carlo calculations [12] in section 5.8. The results of our calculations using a Gaussian-shaped potential are discussed in section 5.9.

5.1 Importance Truncation Uncertainties at NLO

As previously explained, we perform the many-body calculation using the IT-NCSM only for the LO, but calculate the NLO corrections using a perturbation theory approach, treating the corrections as first-order perturbations. In the following, we discuss the errors caused by the importance truncation in those higher-order perturbations. For the calculation of higher orders, we use the energy eigenstates which we obtained in the IT-NCSM calculation at LO. These eigenstates are truncated by an importance measure $\kappa_{\min}$. In order to estimate the NLO energies as $\kappa_{\min} \to 0$, we can calculate the NLO correction for all values of $\kappa_{\min}$, add the correction to the corresponding LO energies and perform the extrapolation like for the LO (see section 4.4.3). Since the calculations for each value of $\kappa_{\min}$ are very time-consuming, we can alternatively calculate only the correction for the smallest value of $\kappa_{\min}$ and add this correction to the LO energy extrapolated to $\kappa_{\min} \to 0$.

Figure 5.1(a) shows the ground-state energy calculated using the LO and the NLO of the EFT interaction for $N_{\max} = 10$ for $4+4$ particles. The energy calculated using the full NCSM is shown in this figure as a red solid line. This figure compares the two different methods described above: In figure 5.1(a) we calculated the NLO correction to the ground-state energy for a sequence of $\kappa_{\min}$ from $1 \cdot 10^{-5}$ to $1 \cdot 10^{-4}$ and added these corrections to the corresponding LO values. We then extrapolated the resulting NLO energy like in the case of the LO (see section 4.4.3 for more details). We used a third-order polynomial for the extrapolation. The calculated energy is plotted in figure 5.1(a) as a dashed line. We additionally extrapolated the LO ground-state energy using a third-order polynomial and then added the NLO correction obtained for the smallest value of $\kappa_{\min}$ (10^{-5}) to all LO results (●). Calculating the NLO correction for each value of $\kappa_{\min}$ does not lead to a significant improvement of the results; the difference is less than 0.001%. Note also that the deviation to the exact value calculated using the full NCSM is less than 0.001% for both methods. As a consequence, in the remainder of this thesis we take the NLO corrections to be independent of $\kappa_{\min}$ and compute it only for the smallest $\kappa_{\min}$ value and add it to the extrapolated LO value. This is more computationally efficient than calculating the corrections for each value of $\kappa_{\min}$ used for the LO calculation.

Due to the importance truncation, we neglect all states $\left|\phi_\nu\right\rangle$ below the importance threshold $|\kappa_\nu| < \kappa_{\min}$ in the LO calculation. The importance threshold, however, is determined based on the LO matrix elements, and no additional information obtained from the NLO calculation is taken into account. The importance threshold is not reevaluated based on the NLO results, that is, no states are being discarded and no new states are being included. For different particle numbers, we calculated the LO energies and

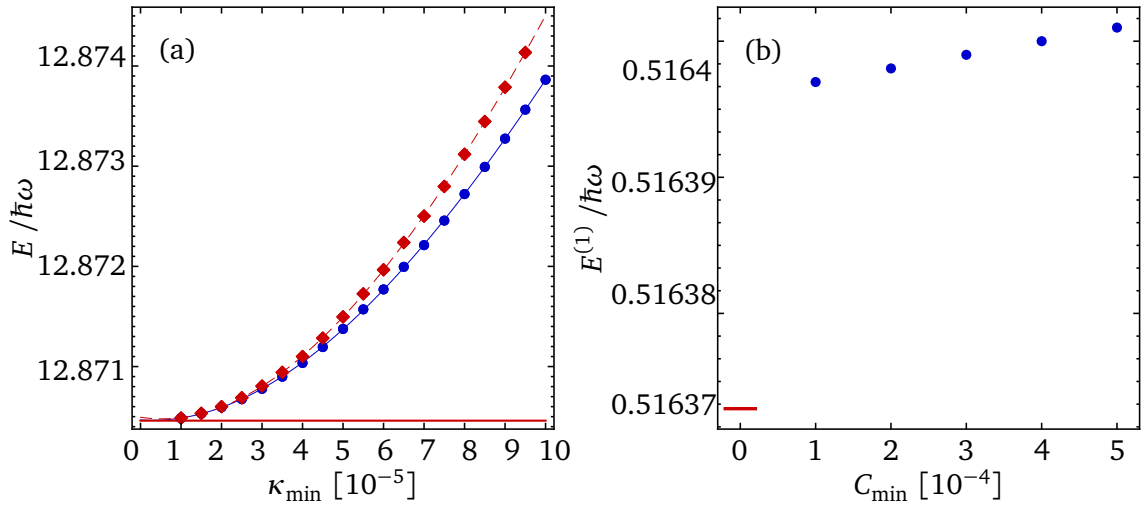

Figure 5.1.: The energy of the ground state (a) as well as the NLO corrections $E^{(1)}$ to the energy of the ground state (b) with $L^\pi = 0^+$ of a two-component $4+4$ fermion system in the unitary limit for $N_{\max} = 10$. The calculation of the ground-state energy (a) was done using the EFT interaction with corrections up to the NLO. We used $n_{\max} = 4$ as a two-body cutoff. For (a) we used $C_{\min} = 0.0001$ and a sequence of $\kappa_{\min}$ from $1 \cdot 10^{-5}$ to $1 \cdot 10^{-4}$ computing the NLO corrections for each value of $\kappa_{\min}$ (◆) or only for the smallest value $1 \cdot 10^{-5}$ (●). For the NLO correction (b) we used $\kappa_{\min} = 3 \cdot 10^{-5}$ (●), and a sequence of $C_{\min}$ from $1 \cdot 10^{-4}$ to $5 \cdot 10^{-4}$. The energy obtained by a full NCSM calculation is shown as a solid horizontal line.

the NLO corrections using both the IT-NCSM and the full NCSM and compared the results. Although we do not consider the NLO corrections in the IT-NCSM, the difference between the two sets of results is significantly less than 1% in all cases, even for larger spaces. For instance, for eight fermions for $N_{\max} = 8$, we obtain $E^{(1)} = 13.221145\hbar\omega$ using the full NCSM and $E^{(1)} = 13.23395\hbar\omega$ using the IT-NCSM; the difference is only about 0.097%.

We also analyzed the influence of the reference threshold $C_{\min}$. For this purpose, we calculated the NLO corrections for different values of $C_{\min}$ ($1 \cdot 10^{-4}$ to $5 \cdot 10^{-4}$) for $\kappa_{\min} = 3 \cdot 10^{-5}$ (●), and plotted the NLO corrections as a function of $C_{\min}$. We did not use the smallest value $\kappa_{\min} = 1 \cdot 10^{-5}$ since for this value we got almost identical results in the error bars for any value of $C_{\min}$. Figure 5.1(b) shows the NLO corrections to the ground-state energy for the $4+4$ system at unitarity for $N_{\max} = 10$. We also calculated the NLO correction using the full NCSM; this value is shown in the figure as a solid line. The calculated energies for different values of $\kappa_{\min}$ show a dependency on $C_{\min}$, but even for the largest $C_{\min}$ the difference to the value calculated with the full NCSM is much smaller than 0.01%. As expected for $C_{\min}, \kappa_{\min} \to 0$ the calculated value approaches the value calculated used the full NCSM. Therefore, like for the LO calculation we can consider the reference threshold $C_{\min}$ small enough not to influence the results.

5.2 Relative Cutoff and the Truncation Parameter $N_{\max}$

The two-body interaction is calculated in relative coordinates with the maximum relative orbital quantum number $n_{\max}$ (see section 3.5 and eq. (3.38)). The ABF interaction uses also a regularization parameter $n_{\max}$. The interaction matrix elements with $e_{\text{rel}} > 2n_{\max}$ are set to zero (see section 3.5), and are not included in the many-body calculation. Hence, each calculation is dependent on the relative cutoff (in

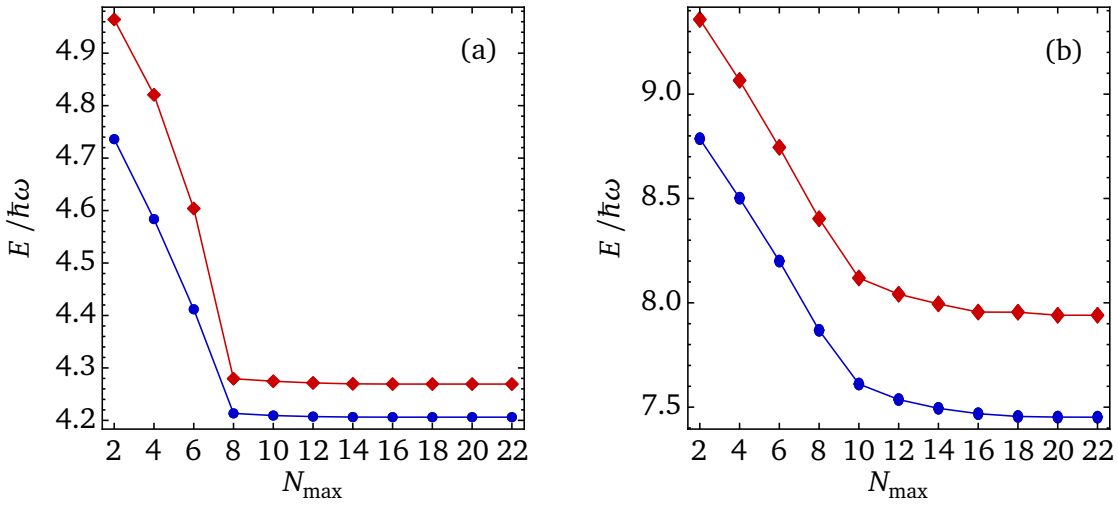

Figure 5.2.: The ground-state energy of a $2+1$ (a) and $3+2$ (b) system in the unitary limit with $L^\pi = 1^-$ with increasing $N_{\max}$. The calculation was done using the EFT interaction. We used $n_{\max} = 4$ (a) and $n_{\max} = 7$ (b) as a two-body cutoff. For IT-NCSM calculations we used $C_{\min} = 0.0001$ (a), and 0.0002 (b) and a sequence of $\kappa_{\min}$ from $1 \cdot 10^{-5}$ to $1 \cdot 10^{-4}$ (a) and $3 \cdot 10^{-5}$ to $1 \cdot 10^{-4}$ (b). We calculated both the LO (●) and NLO (◆) parts of the EFT interaction.

case of the EFT interaction) or the regularization parameter (in case of the ABF interaction) and the truncation parameter $N_{\max}$ of the many-body system.

We consider the convergence with $N_{\max}$ for constant $n_{\max}$. Figure 5.2 shows the energy of the ground state for $2+1$ (a) and $3+2$ (b) particles with increasing many-body cutoff $N_{\max}$ at a constant interaction cutoff $n_{\max} = 4$ (a) and $n_{\max} = 5$ (b). One can see a strong dependence of the calculated energy on $N_{\max}$ for $N_{\max} < 2n_{\max}$ in figure 5.2, especially for the three-particle system. For $N_{\max} \geq 2n_{\max}$, the changes in energy from one value of $N_{\max}$ to the next are drastically reduced and the result converges.

As already mentioned, for the Fermi gas at unitarity we consider only s-wave scattering and only two-body interaction. We also use the regularisation parameter $n_{\max}$ for the calculation of the matrix elements of the interaction in relative coordinates. Therefore, the maximum energy quantum number in relative basis $e_{\max,\mathrm{rel}} = 2n_{\max}$ is always even. We transform the matrix elements of the interaction into single-particle coordinates with maximum energy quantum number $e_{\max}$ in the single-particle basis. For $e_{\max} = e_{\max,\mathrm{rel}}$ all matrix elements from the relative basis should be included in the single-particle basis. We construct for our IT-NCSM calculations the A-body model space using $N_{\max}$-truncation (see section 4.1). The maximum number of HO quanta in the eigenstates of the Hamiltonian H used to construct the many-body basis for A particles is $e_{\mathrm{A},\max} = e_{\mathrm{A},\min} + N_{\max}$, where $e_{\mathrm{A},\min}$ is the energy quantum number of the lowest Pauli-allowed many-body basis state (with $N_{\max} = 0$, for example, $e_{3,\min} = 1$ and $e_{5,\min} = 3$) and $N_{\max}$ is the maximum excitation energy above $N_{\max} = 0$. Since the parity of the state is conserved, we can choose $N_{\max}$ from the set of positive even numbers.

We decouple the interaction cutoff in relative coordinates from those of the many-body system [1, 90]. In an NCSM calculation one chooses $N_{\max}$ of the many-body system such that the many-body space contains the whole relative space with the relative cutoff $e_{\max,\mathrm{rel}}$. Therefore, for the $N_{\max}$ truncation, the maximum energy quantum number of the many-body state should be at least equal or larger than the energy quantum number of the relative system. Hence, for the extrapolation to the limit $N_{\max} \to \infty$, we use only data points with $e_{A,\max} \geq 2n_{\max}$.

For the $e_{\max}$ truncation, all single particle states with single-particle energy $e_i \leq e_{\max}$ are used for the construction of the many-body state, and hence $e_{\mathrm{A};\max} = Ae_{\max}$. The difference to the $e_{\max}$ truncation is

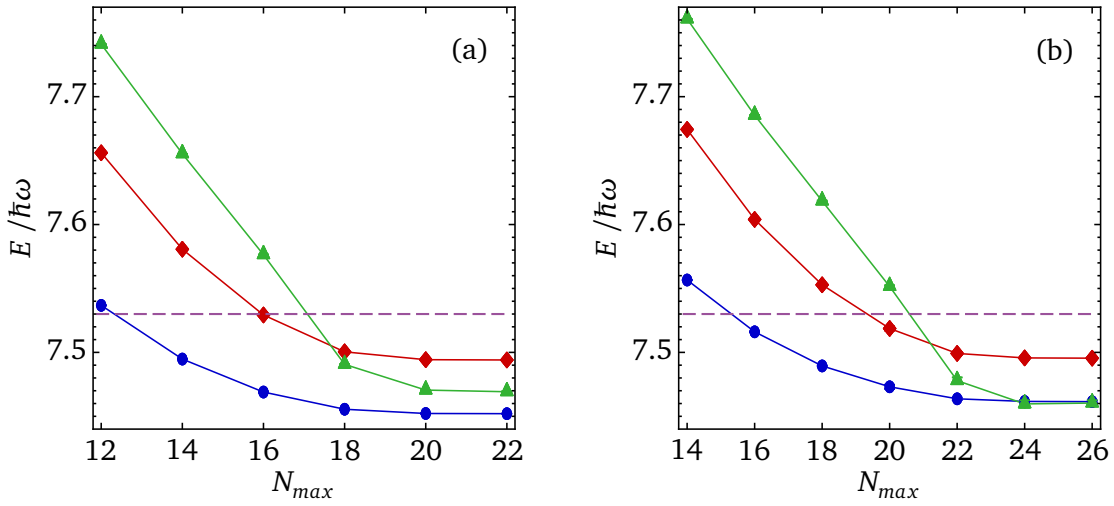

Figure 5.3.: The energy of the ground state with $L^\pi = 1^-$ of an $3+2$ fermion system calculated using the LO and NLO of the EFT interaction and the ABF interaction as a function of $N_{\max}$ for $n_{\max} = 5$ (a) and $n_{\max} = 6$ (b). The blue solid circles (●) correspond to the LO , the red solid diamonds (◆) to the NLO EFT, the green triangles (▲) to the ABF interaction. The violet dashed line is the value of CG method [12].

discussed in section 4.1 and illustrated in figure 4.1, which shows that the many-body space contains the whole relative space at least for $e_{\max} \geq {}^{e_{\max,\mathrm{rel}}}/_2 = n_{\max}$.

5.3 Convergence with $N_{\max}$ for different $n_{\max}$

In this section we analyze the convergence with increasing $N_{\max}$ for five- (3+2) and eight-particle (4+4) systems at unitarity. For this purpose we calculate the ground-state energy for this system for different cutoff values for the EFT interaction as well as for different regularization parameters $n_{\max}$ for the ABF interaction using the IT-NCSM.

For a five-particle system we use $n_{\max} = 5$ and 6 and a sequence of importance thresholds $\kappa_{\min}$ from $3{\cdot}10^{-5}$ to $1{\cdot}10^{-4}$, and extrapolate the results of the eigenvalue problem to the limit $\kappa_{\min} \to 0$ as proposed by Roth [71] (see chapter 4.4.3). Figure 5.3 shows the ground-state energy as a function of $N_{\max}$ for $n_{\max} = 5$ and $n_{\max} = 6$ for EFT and ABF interaction. The ABF interaction converges slower than the EFT interaction as $N_{\max}$ increases. Comparing both figures, one can see that with increasing $n_{\max}$ one needs higher $N_{\max}$ to achieve convergence. The calculated values are in the vicinity of the value from [12] calculated using CG (the dashed line in the figure). Blume *et al.* used a variational approach (FN-DMC / CG) for the calculation, which provides an upper bound for the energies / energy spectra. We use for our calculation *ab initio* methods (NCSM or IT-NCSM). Therefore, we expect our results be more exact than the ones calculated using variational methods.

Next, we consider a system consisting of $4+4$ fermions in the unitary limit in a HO trap. For this particle number, we calculate the energy for the cutoff or regularization parameter $n_{\max} = 2,3,4,5,6,7$. We used a sequence of importance thresholds from $\kappa_{\min} = 5{\cdot}10^{-5}$ to $\kappa_{\min} = 1.5{\cdot}10^{-4}$. Figures 5.4 (a), (c), and (e) and 5.5 (a), (c), and (e) show the ground-state energies as a function of $N_{\max}$ for the relative cutoffs $n_{\max} = 2,3,4,5,6,7$ for a system consisting of $4+4$ two-component fermions. The ground state of the $4+4$-fermions system has $L = 0$ and positive parity.

For the EFT interaction we considered both the LO and NLO terms. Furthermore, figures 5.4 and 5.5 also shows results for the ABF interaction. The energies are only plotted starting from $N_{\max} = 2n_{\max}$

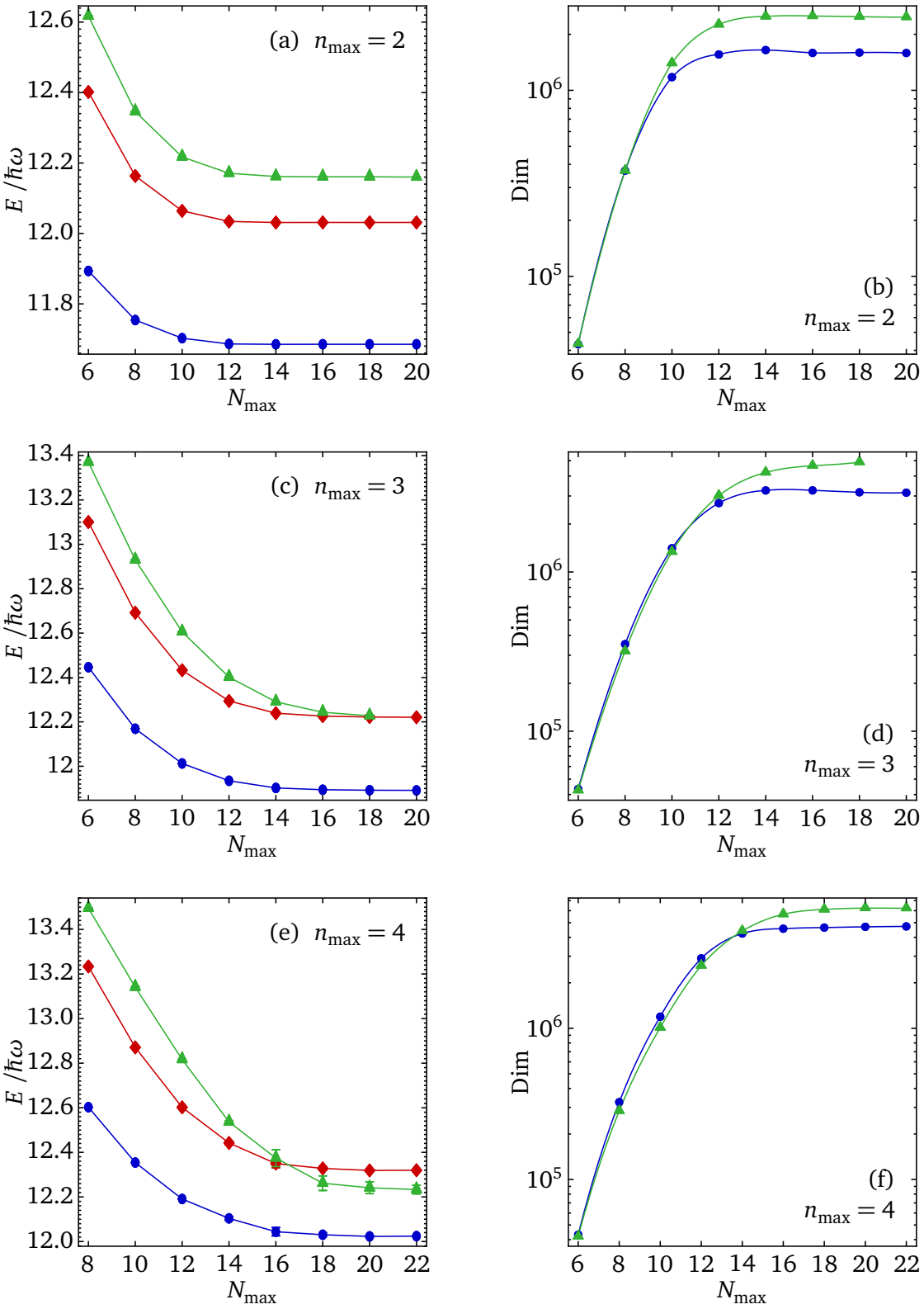

Figure 5.4.: The energy of the ground state and the dimension of the many-body space with $L^\pi = 0^+$ of an $4 + 4$-fermion system calculated using the LO and NLO EFT interaction and the ABF interaction as a function of $N_{\max}$ for different two-body cutoffs $n_{\max} = 2, 3$ and 4. The blue solid circles (●) correspond to the LO and the red solid diamonds (◆) to the NLO EFT, the green triangles (▲) to the ABF interaction.

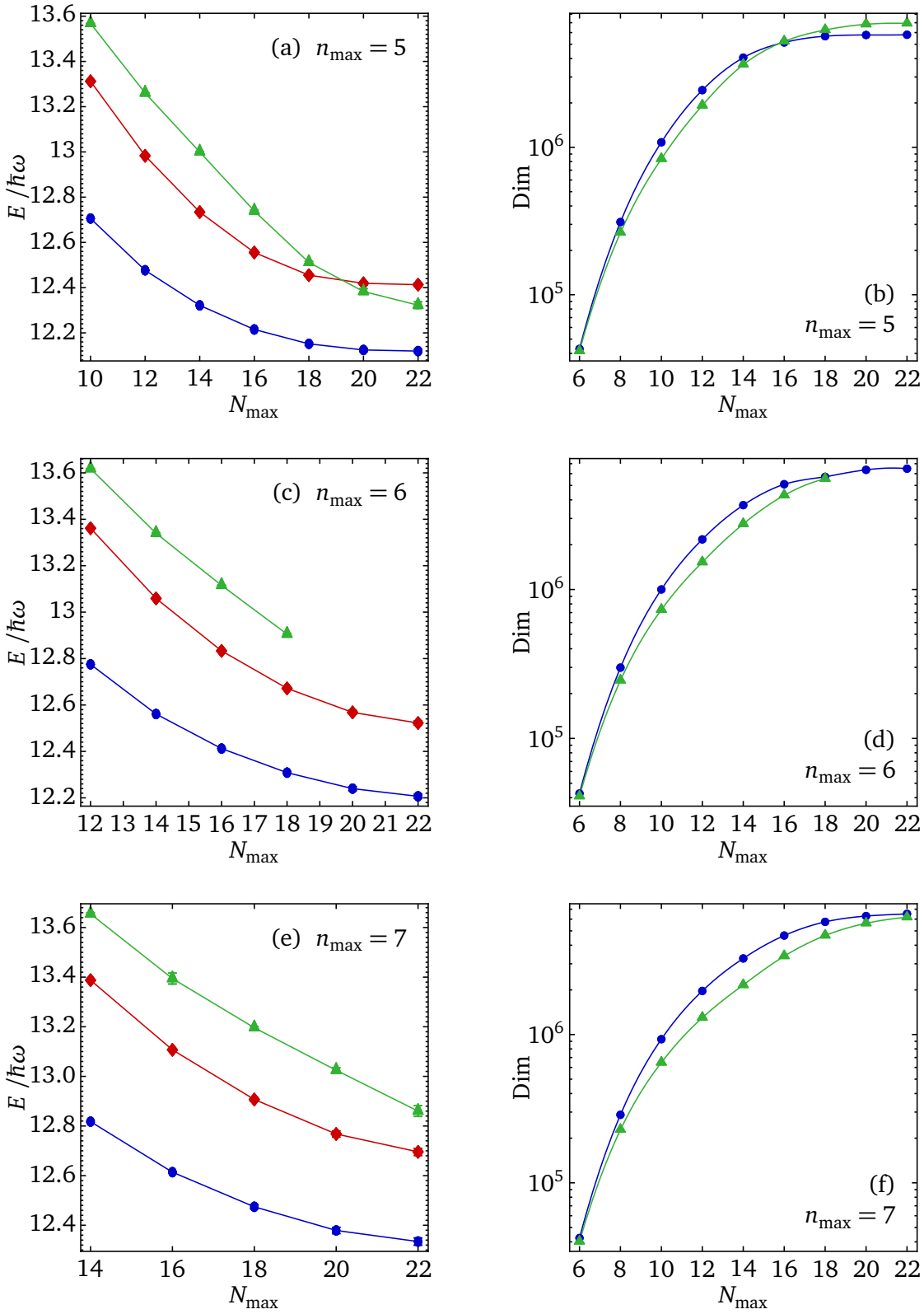

Figure 5.5.: The energy of the ground state and the dimension of the many-body space with $L^\pi = 0^+$ of an $4 + 4$-fermion system calculated using the LO and NLO EFT interaction and the ABF interaction as a function of $N_{\max}$ for different two-body cutoffs $n_{\max} = 5, 6$ and 7. The blue solid circles (●) correspond to the LO and the red solid diamonds (◆) to the NLO EFT, the green triangles (▲) to the ABF interaction.

(see section 5.2 for a justification). The errors introduced by the importance truncation (due to the extrapolation to $\kappa_{\min} \to 0$) are shown as error bars, which can only be seen well for the ABF interaction for $n_{\max} = 4$ because the errors are too small otherwise. For the results in figures 5.4 and 5.5 we only use simple extrapolation methods (see section 4.4.3) without taking into account the second-order contributions of the discarded states.

For $n_{\max} = 2$, the energy is converged for $N_{\max} \geq 14$; for $n_{\max} = 3$, this is the case for $N_{\max} \geq 16$, for $n_{\max} = 3$ for $N_{\max} \geq 18$ and for $n_{\max} = 5$ for $N_{\max} \geq 20$, but only for EFT. Since we did not perform calculations with $N_{\max} > 22$, the energy is not converged for $n_{\max} = 6$ and $n_{\max} = 7$. The error grows larger as $n_{\max}$ increases: While convergence is achieved at $N_{\max} = 18$ for $n_{\max} = 4$, calculations at higher $N_{\max}$ are required to achieve the convergence at $n_{\max} = 7$, see figures 5.4 and 5.5. For the EFT we are in the vicinity of the convergence for $n_{\max} = 7$; for the ABF interaction we would need a larger value of $N_{\max}$. The same is true for the ABF interaction for $n_{\max} = 6$. Therefore, we only extrapolated the energies calculated using the ABF interaction up to $n_{\max} = 5$ to the limit $N_{\max} \to \infty$.

Another observation is that the converged results for the NLO EFT and the ABF interaction are not identical (see $n_{\max} = 2$ or 4). Furthermore, for $n_{\max} = 5$ the result obtained using the ABF interaction is smaller than the one obtained using the NLO of the EFT interaction. This is due to the fact that we only used the NLO, but no higher-order corrections to the EFT. Using higher order would improve the result. Also using larger values of $n_{\max}$ would improve the result both for the EFT and the ABF interaction. Using either interaction should yield the same result as $n_{\max} \to \infty$.

In general the EFT converges faster than the energy calculated with the ABF interaction. Once convergence has been achieved, the importance truncation cannot find any important new state (which would change the energy — but then it would not be converged in the first place), so the model-space dimension saturates (see figures 5.4 and 5.5). To understand this we have to consider the calculation of the matrix elements in relative coordinates for EFT and ABF interaction chapter 3. First we set the matrix elements with $n > n_{\max}$ to zero. We have to transform these matrix elements in relative coordinates into single-particle coordinates. With increasing principal quantum number of the single-particle basis, the contribution of these nonzero matrix elements decreases. For both interactions, the matrix elements are only nonzero for $l = m = 0$ (in relative coordinates). With increasing $n_{\max}$, the ratio of nonzero to zero matrix elements in relative coordinates for $l > 0$ decreases. Also the contribution of these nonzero matrix elements decreases in single particle coordinates.

Figures 5.4 (b), (d), and (f) and 5.5 (b), (d), and (f) show the dimension of the many-body space depending on $N_{\max}$ for the relative cutoffs $n_{\max} = 2, 3, 4, 5, 6, 7$ for a system consisting of $4 + 4$ two-component fermions. The dimension is shown logarithmically. The dimension of the many-body space grows with increasing $n_{\max}$, but for equal $\kappa_{\min}$ and $C_{\min}$, the dimension of the many-body space is larger for the ABF interaction. The ABF interaction also requires a longer computation time on an identical computer configuration. Furthermore, the ABF interaction reaches the point from which on the dimension stays nearly constant at a larger value of $n_{\max}$ than the EFT interaction. This is why calculations using the ABF interaction take longer on the same computer than calculations using the EFT. On the other hand, one needs to take into account higher orders of the EFT interaction in order to achieve the same degree of accuracy as the ABF interaction. Furthermore the NLO corrections to the energy calculated using the EFT interaction introduce additional errors (see chapter 5.1). However, these are negligible in comparison to those introduced by the extrapolation to $N_{\max} \to \infty$.

5.4 The Ultraviolet and Infrared Cutoffs and Extrapolation

We consider systems placed in a trap and use the Harmonic Oscillator (HO) basis as a trapping potential. As a consequence, the solution depends explicitly on the trap frequency. In nuclear physics, where the systems are self bound, the HO basis is widely used for *ab initio* methods. Using the HO basis has several advantages; for instance, it simplifies the implementation of the symmetries of the many-body system. The limitation of the available computational resources requires truncation of the HO basis before the

observables are fully converged, and the results depend on the basis parameters $N_{\max}$ and $\hbar\omega$ and need to be extrapolated to infinite basis size [30]. The NCSM using a HO basis is a variational method using two truncation parameters, $N_{\max}$ and $\hbar\omega$. We want our computed observables to be independent of these two parameters, which is computationally difficult to achieve. Extrapolation from smaller model spaces will extend the reach of any computational method. The parameters $N_{\max}$ and $\hbar\omega$ define the UV and IR momentum scales, respectively, and EFT-based extrapolation methods have been devised for removing them. In recent works [30, 59], a sophisticated and theoretically motivated extrapolation method for the extrapolation to the infrared limit was proposed in a framework inspired by effective field theory for untrapped nucleons [30]. In this section we introduce the UV and IR scale. Since the calculated energies of our systems explicitly depend on the trap frequency, we only have one parameter, $N_{\max}$, for our calculations; hence we only introduce the extrapolation method for infinite basis size.

In the HO basis we can identify a maximum momentum cutoff as an ultraviolet momentum scale

$$\Lambda_{\mathrm{UV}} \equiv \sqrt{2(e_{\max} + 3/2)}\frac{\hbar}{a_{\mathrm{HO}}} \tag{5.1}$$

associated with the energy of the highest HO level, with the maximum single-particle energy quantum number $e_{\max}$ and the oscillator length a_{HO} [30].

Furthermore several infrared (IR) scales have been introduced [23, 30]. One of the definitions for the IR scale results from the fact that the minimum allowed momentum difference between single-particle orbitals is

$$\lambda = \sqrt{m_n \hbar\omega} = \frac{\hbar}{a_{\mathrm{HO}}}. \tag{5.2}$$

In the second definition the radius of the system has to be smaller than the radial extent of the highest HO level [30, 31]

$$L_0 = \sqrt{2(e_{\max} + 3/2)}a_{\mathrm{HO}}. \tag{5.3}$$

This corresponds to the definition of the IR scale as the infrared momentum [23]

$$\Lambda_{\mathrm{IR}} = \sqrt{\frac{m_n \hbar\omega}{(e_{\max} + 3/2)}} = \frac{\hbar}{\sqrt{e_{\max} + 3/2}a_{\mathrm{HO}}} = \frac{\lambda}{\sqrt{e_{\max} + 3/2}}. \tag{5.4}$$

This can be derived from a consideration of the spatial extent of the single-particle one-dimensional HO functions [55]. For the nuclei a very accurate approximation for the radial extent of the highest HO level L was found by [31].

In the case of self-bound nuclei, the dependence of the HO frequency is given through the use of a finite oscillator basis in the NCSM. Examples and the behavior of the calculated energy and other observables of a nuclear system at different HO frequencies and $N_{\max}$ and, therefore, different values of the IR and UV cutoffs are given, for instance, in the works of Roth and Calci [73], Coon and Avetian [23] or Kruse [55]. In the case of untrapped nuclei in nuclear physics, one increases $N_{\max}$ until convergence at an optimal value of the HO frequency ω, which provides the minimum energy in the largest model space.

Ultra-cold fermions in the unitary limit are not self-bound systems; they are placed in a trap, which influences the long-range behavior of the wave functions and thus the energy of the state [90]. The dependence on the trap frequency is physically motivated and hence explicit, contrary to self-bound nuclear systems, where the dependence comes from using the HO basis in an NCSM calculation. Therefore, we cannot use the IR cutoff in the calculations for trapped ultra-cold gases. As already mentioned, the definition of the IR scale, eq. (5.4), is not applicable for ultra-cold systems. Therefore, the IR scale and the theoretically founded formula cannot be directly applied to Fermi gases.

For the extrapolation to $N_{\max} \to \infty$, the empirical formula

$$E(N_{\max}, \hbar\omega) = E_\infty + A_0 e^{-2\left(\frac{\Lambda_{\mathrm{UV}}}{A_1}\right)^2} \tag{5.5}$$

can be used where E_∞, A_0 and A_1 are fit parameters. The ultraviolet momentum scale is given by eq. (5.1), where the single-particle energy quantum number in the basis $e_{\max}$ corresponds for example $e_{\max} = N_{\max} + 1$ for p-schell nuclei and for up to $4+4$ fermions at unitarity. This empirical formula works quite well [30, p. 5] and is used in nuclear physics many body calculation with the NCSM for the extrapolation to the limit $N_{\max} \to \infty$ [23, 55, 73].

In the many-body calculations for ultra-cold Fermi gases at unitarity, also an another empirical method was used. In reference [1, 33] the authors estimated the energy for a certain regularisation parameter of the interaction $n_{\max}$ for infinite basis size using quadratic polynomial by extrapolating logaritmically the energy difference

$$\Delta E_{e_{\max}} \equiv E_{e_{\max}-1} - E_{e_{\max}}, \tag{5.6}$$

where $e_{\max}$ is the maximum energy quantum number of the $e_{\max}$-truncation used in [1, 33]. Alhassid *et al.* found [1] that the convergence of the energy difference for $e_{\max}$ truncation should be faster than exponential. They used extrapolation function of the form

$$\Delta E = 10^{A + B e_{\max} + C e_{\max}^2} \tag{5.7}$$

for the extrapolation in $e_{\max}$. These differences were then summed up in order to calculate the energy for $e_{\max} \to \infty$:

$$\begin{aligned} E_{e_{\max}\to\infty} &= E_{e_{\max}} + \Delta E_{e_{\max}+1} + \Delta E_{e_{\max}+2} + \dots \\ &\approx E_{e_{\max}} + 10^{f(e_{\max}+1)} + 10^{f(e_{\max}+2)} + \dots \end{aligned} \tag{5.8}$$

where f is the interpolating function $f(n_{\max}) = A + B n_{\max} + C n_{\max}^2$ (with $C < 0$).

The extrapolation to the limit $e_{\max} \to \infty$ allows estimating the energy (or other observables) for systems for which it is not possible to achieve convergence due to the size of the model space and the required computational effort. We replaced $e_{\max}$ by $N_{\max}$ since we used NCSM and, therefore, the $N_{\max}$-tunctation. We used this kind of extrapolation for both the EFT and ABF interactions in those cases, where our calculations did not converge but the size of the model space did not permit calculations for larger $N_{\max}$.

For the extrapolation as $N_{\max} \to \infty$, we used the four or five largest values of $N_{\max}$, since they are the closest to convergence. We do not assign different weights to the different data points. Furthermore we only used those $N_{\max}$ with $N_{\max} \geq e_{\max,\mathrm{rel}} = 2n_{\max}$, where $e_{\max}$ is the number of quanta of the highest energy and $n_{\max}$ is the maximum radial quantum number in relative coordinates (the relative cutoff, see chapter 5.2). This is difficult for large values of $n_{\max}$ and large particle numbers A, since the model space and the required computational effort grow with both, $N_{\max}$ and A and the calculations become inrtactable for large model spaces. In order to estimate the extrapolation error, we use the same value of $N_{\max}$ as for the extrapolation itself, and omit the points corresponding to the largest value of $N_{\max}$. When doing so, one must make sure that enough points remain in order to perform the extrapolation since the difference $\Delta E(N) = E(N) - E(N-1)$ of the energy is being extrapolated and, therefore, one point less is available. This is particularly important for the extrapolation method used by Alhassid *et al.* (eq. (5.8)).

We now compare the two extrapolation methods introduced in this section (the empirical formula (5.5) and the extrapolation formula (5.8) used by Alhassid) for an eight-particle $(4+4)$ system. For this purpose we used the NLO of the EFT interaction and the ABF interaction. Figure 5.6 shows the result of extrapolations to $N_{\max} \to \infty$ for the ground-state energy using different relative cutoffs of the EFT interaction and different regularization parameter of the ABF interaction. Figure 5.6 (a) shows the

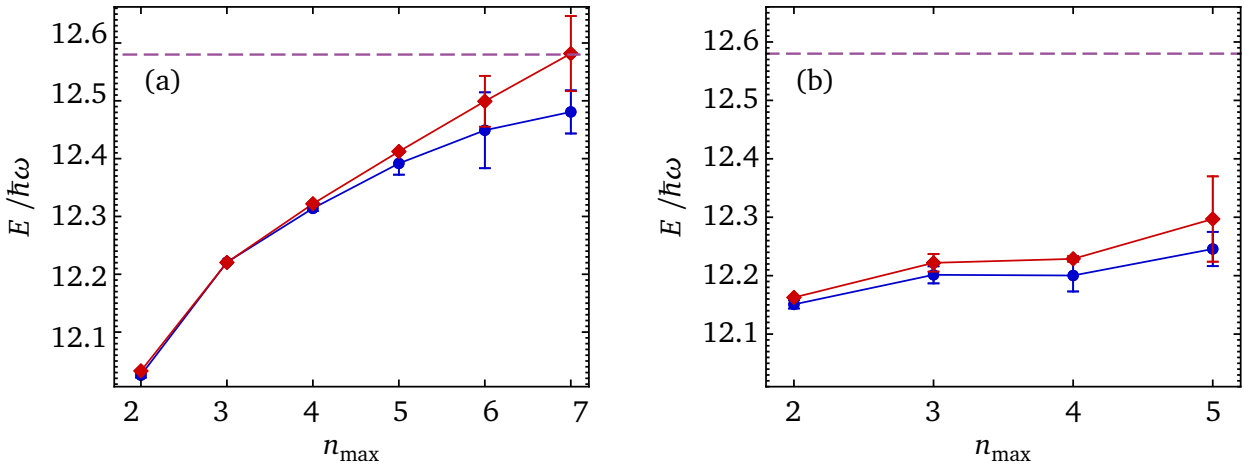

Figure 5.6.: The extrapolated energy of the ground state of a eight-particle fermionic system with $L^\pi = 0^+$ in the unitary limit as a function of $n_{\max}$. The calculation was done using (a) the EFT (with NLO corrections) and (b) the ABF interaction. For IT-NCSM calculations we use $\kappa_{\min} = 0.0005$. The results for the empirical formula or UV cutoff (eq. (5.5)) are shown as (●) and the extrapolation used by Alhassid (eq. (5.8)) as (◆).

energies calculated using the NLO correction of the EFT and figure 5.6 (b) shows the energies calculated using the ABF interaction. The dashed line in 5.6 (a) shows the ground-state energy of 8 particles at unitarity calculated using the FN-DMC. We performed for each value of $n_{\max}$ a sequence of IT-NCSM calculations.

For each calculation with a given value of $n_{\max}$ and $N_{\max}$, we used the threshold extrapolation method described in section 4.4.3 with the *a posteriori* correction to the energies in order to extrapolate the energy to vanishing importance threshold $\kappa_{\min} \to 0$. Furthermore, we extrapolated the energy for each value of $n_{\max}$ to $N_{\max} \to \infty$ as described previously using the two extrapolation methods described above.

For the EFT interaction, we used values of $n_{\max} = 2$ to 7 and for the ABF interaction, we used values of $n_{\max} = 2$ to 5. The calculated energies are shown in figures 5.4 and 5.5 as a function of $N_{\max}$. Even for the largest relative cutoff $n_{\max} = 7$ we calculated only results for $N_{\max} \leq 22$. The values obtained for the ABF interaction for $n_{\max} = 6$ and $n_{\max} = 7$ converged too slowly to perform the extrapolation to $N_{\max} \to \infty$. For $n_{\max} = 2$, the results converge for both interactions and for the EFT interaction $n_{\max} = 3$ also yields converging results. For large values of $N_{\max}$, the differences between the energies calculated for one value of $N_{\max}$ and the next are smaller than the errors of the IT truncation (see section 4.4.3), which itself are very small in magnitude. The extrapolated ground-state energy converges faster for smaller values $n_{\max}$ than for larger values, but the extrapolation errors are also larger in magnitude in the former case. The errors of the extrapolation to $\kappa_{\min} \to 0$ are smaller than those of the extrapolation to $N_{\max} \to \infty$; only the latter are shown in figure 5.6 and grow larger as $n_{\max}$ increases. For the estimation of the errors of the extrapolation to $N_{\max} \to \infty$ we discard the last largest value of $N_{\max}$ and fit the function again to the data points. With increasing $n_{\max}$ the higher-order contributions of the interaction get smaller and, therefore, the calculated energy is closer to the exact energy (see section 3.5). The anomalous behavior shown in figure 5.6 (b) for the ABF interaction is because we performed calculations using $n_{\max} = 3$ only up to $N_{\max} = 18$ due to restrictions on the available computing resources, but performed calculations using $n_{\max} = 4$ up to $N_{\max} = 22$. The second value is obviously closer to the limit of an infinitely large space.

The extrapolated values do not yet converge using Alhassid's extrapolation method, neither for the EFT nor for the ABF interaction. As can be seen in figure 5.6, Alhassid's method yields almost identical

results for small values of $n_{\max}$ for which there are more values for $N_{\max}$ for which calculations are feasible and meaningful (we use only values with $N_{\max} > 2n_{\max}$ and $N_{\max}$ is limited from above by the available computing power; the more values we have, the closer they are to the exact result and the better the extrapolation becomes). For larger values of $n_{\max}$ we have too few data points and the error bars grow large and the energies extrapolated using this method are likely too high. However, Alhassid *et al.* used the CI method to calculate the energy and used the maximum single-particle energy $e_{\max}$ as a cutoff (see chapter 4.1), which may lead to a different convergence behavior with increasing $e_{\max}$ and, consequently, increasing basis dimension. Using Alhassid's extrapolation method, both the extrapolated values and the extrapolation errors actually increase for large values of $n_{\max}$. The same is true for the ABF interaction using the Alhassid's extrapolation method. As seen in figure 5.6 (a) for the EFT interaction, the extrapolation using the empirical exponential function exhibits convergent behavior as $n_{\max}$ increases. We extrapolate the results to $n_{\max} \to \infty$ for EFT interaction using the empirical formula in the next section. Since the errors are still too large, performing calculations for larger values of $n_{\max}$ is notfeasible due to the computational effort that would be required.

The ground-state energy calculated using the FN-DMC method for an eight-particle system $(4+4)$ is $(12.58 \pm 0.03)\hbar\omega$ (see [12] or section 4.5). The value calculated using the EFT interaction for $n_{\max} = 7$ and extrapolated using the empirical formula ($(12.48 \pm 0.04)\hbar\omega$) differs by less than 1%. When using Alhassid's extrapolation, we obtain the same value ($(12.58 \pm 0.06)\hbar\omega$) as calculated by the FN-DMC, which is likely too high. Since we did not achieve convergence using Alhassid's extrapolation at $n_{\max} = 7$, the next value at $n_{\max} = 8$ is higher than calculated using the FN-DMC method. These extrapolated values only contain the NLO corrections and neither take higher-order corrections nor the behavior as $n_{\max} \to \infty$ into account; this may cause additional errors, see section 3.6. Considering this, our results agree well with those published by other groups. In order to achieve a more accurate result, we would need to consider the N^{2}LO terms or move to higher values of $N_{\max}$ and $n_{\max}$. For the ABF interaction, the differences are larger since we have not been able to perform calculations with high values of $N_{\max}$ due to limited computing resources; the difference for $n_{\max} = 5$ is about 2.2% when extrapolating using Alhassid's function ($(12.30 \pm 0.03)\hbar\omega$) and about 2.6% when extrapolating using the empirical function ($(12.24 \pm 0.03)\hbar\omega$). To the best of our knowledge, no results for the energy of the first excited state for $N > 6$ particles have been published yet with which we could compare our results.

In the remainder of this chapter, we use the exponential function (5.5) for the extrapolation for ultracold Fermi gases. The extrapolation function according to Alhassid, Bertsch *et al.* is just as empirical and not physically motivated. The exponential function is the better choice, as it asymptotically approaches the reference value as $n_{\max} \to \infty$. Since we are close to convergence (by virtue of the IT-NCSM), this extrapolation method is sufficient (see section 5.4).

5.5 Convergence with $n_{\max}$

In order to eliminate the dependency of the calculated observables on the relative cutoff $n_{\max}$ and the truncation parameter $N_{\max}$, we consider first the convergence with $N_{\max}$ for constant $n_{\max}$ and extrapolate to $N_{\max} \to \infty$. The calculated observables depend now only on the interaction cutoff $n_{\max}$. To eliminate this dependency, we have to consider convergence of the observable with increasing $n_{\max}$. We calculate the ground-state and first-excited state energies for five $(3+2)$ and eight $(4+4)$ fermions at unitarity for different values of $n_{\max}$ and increasing values of $N_{\max}$ using the IT-NCSM and the EFT and ABF interactions. We extrapolated the results to $N_{\max} \to \infty$ for $2 \leq n_{\max} \leq 7$ for the EFT interaction and for $2 \leq n_{\max} \leq 6$ for the ABF interaction. Figure 5.7 (a) shows the extrapolated ground-state energies of the five-particle system at unitarity for different values of $n_{\max}$ with error bars from the $N_{\max}$ extrapolation. The LO value for the ground-state energy increases strictly monotonically and approaches a certain value but is not fully converged. The energy of the NLO seems to converge faster and is nearly converged at $n_{\max} = 7$.

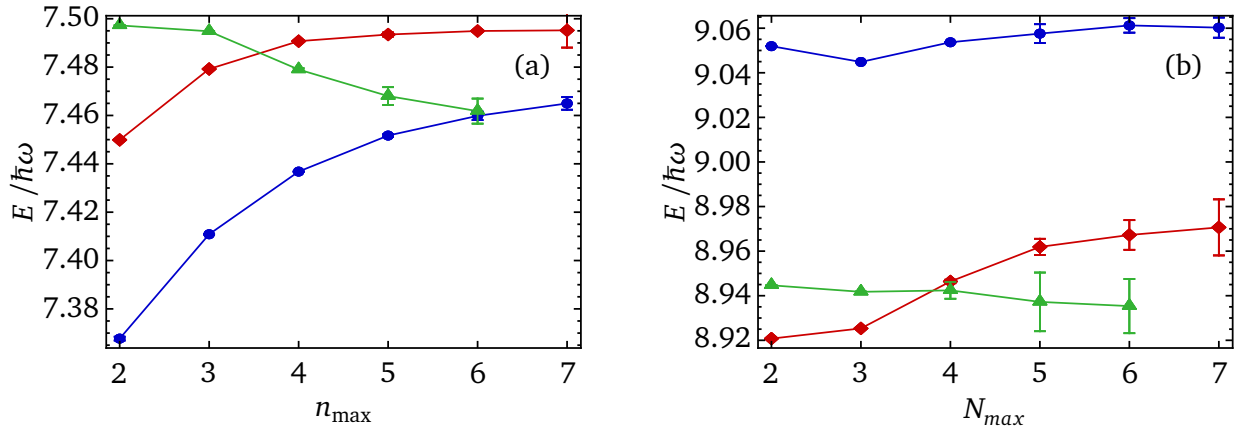

Figure 5.7.: The extrapolated energy of the ground state (a) and first excited state (b) of an $3+2$ fermion system with $L^\pi = 1^-$, calculated using the LO and NLO of the EFT interaction and the ABF interaction as a function of $n_{\max}$. The blue solid circles (●) correspond to the LO and the red solid diamonds (◆) to the NLO EFT, the green triangles (▲) to the ABF interaction.

As already mentioned we would need to perform calculations for the ABF interaction using higher values of $N_{\max}$ than for the EFT interaction to achieve a better extrapolation for any given $n_{\max}$, which would require even more computation time on the same computer equipment. Therefore, we can only calculate the energy for the ABF interaction up to $n_{\max} = 6$; the extrapolation uncertainties are too large for $n_{\max} = 7$. The extrapolation errors for $n_{\max} = 6$ are larger for the ABF interaction than for the EFT interaction (both LO and NLO).

Figure 5.7 (b) shows the extrapolated first excited-state energy. The first excited-state energies for both interactions show slower convergence than for the ground state. We need at least a value of $n_{\max}$ which is higher by 1 than for the ground-state calculations in order to obtain the same degree of convergence. That can be explained by the choice of the LO parameter $C_0^{(0)}$ (see section 3.6.1): We fix the constant $C_0^{(0)}$ so that the ground-state energy of a two-particle system at unitarity is reproduced exactly. The energy of the first-excited state is then only an approximation and is corrected at the NLO. The choice of the constants also affects the energy spectrum of systems with more than two particles.

The energies calculated using the EFT interaction show a "kink" at $n_{\max} = 3$. The ground-state energies show a similar kink at $n_{\max} = 2$ which is not visible in figure 5.7 since the value for $n_{\max} = 1$ is not shown. At such low values of $n_{\max}$, important matrix elements are removed from the calculation which leads to this behavior.

We can use the extrapolation method introduced in [1, 33] to extrapolate the energy to $n_{\max} \to \infty$ (see section 5.4 for more details). This method yields the extrapolated value for the ground-state energy calculated using the EFT interaction up to NLO as $E(n_{\max} \to \infty) = (7.49 \pm 0.01)\hbar\omega$, hence the deviation to the value calculated using CG method ($7.53\hbar\omega$, see section 4.6) is only 0.5%, but also the deviation of the value at $n_{\max} = 4$ is very low (only 0.5%). We can also extrapolate the value for the first excited-state energy for a five-particle system at unitarity with $L^\pi = 1^-$, again using the NLO of the EFT interaction. The value is $E(n_{\max} \to \infty) = (8.97 \pm 0.01)\hbar\omega$, hence the deviation to the value calculated using the CG approach ($9.13\hbar\omega$) is 1.7% and for $n_{\max} = 4$ about 2%. For the first excited state, the difference between the result for $n_{\max} = 4$ and the extrapolated result as $n_{\max} \to \infty$ is about 0.5%. This means that $n_{\max} = 4$ is a relatively good (and not too computationally expensive) choice for the two-body cutoff, at least for the p-shell. We will discuss the selection of $n_{\max}$ further in section 5.5.

Figure 5.8 shows the energy of the ground state and the first excited state of an eight-particle system at unitarity for different relative cutoffs $n_{\max}$ calculated with the EFT and ABF interactions. We calculated

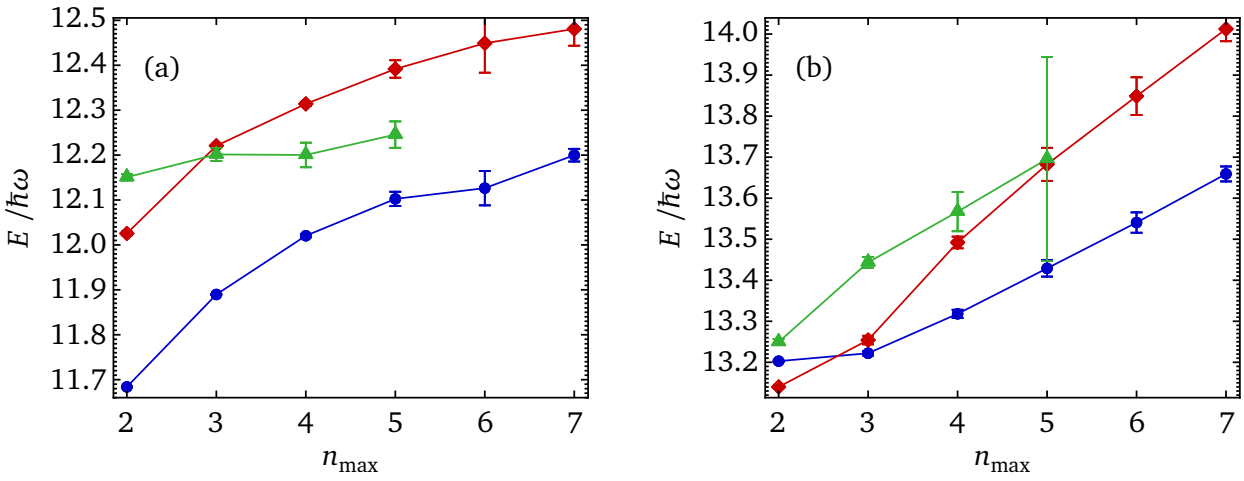

Figure 5.8.: The ground-state energy with $L^\pi = 0^+$ (a) and the first-excited state energy (b) of the $4+4$ fermion system at unitarity calculated using the EFT interaction (up to NLO corrections) as well as the ABF interaction as a function of the two-body cutoff $n_{\max}$. The notation is the same as in figure 5.4: the blue circles (●) correspond to the LO results, the red solid diamonds (◆) to the NLO and the green triangles (▲) to the ABF interaction.

the energy as follows: We performed IT-NCSM calculations for each value of $n_{\max}$, for a sequence of increasing values for $N_{\max}$, with a sequence of values for $\kappa_{\min}$ between $5 \cdot 10^{-5}$ and $15 \cdot 10^{-5}$ and $C_{\min} = 5 \cdot 10^{-4}$. In order to calculate the energies, we extrapolated the results to $\kappa_{\min} \to 0$ and combined them with the information obtained from the second-order corrections of the energy (see chapter 4.4.3). We can now extrapolate the energies to an infinite basis size, that is, $N_{\max} \to \infty$, for each value of $n_{\max}$ (see chapter 5.4 for more details).

While for the EFT interaction and $n_{\max} = 2$ the energy is converged for $N_{\max} \geq 14$, we have not nearly reached convergence for the ABF interaction and $n_{\max} = 7$ (see figures 5.4 5.5). In general, for larger values of $n_{\max}$, convergence is reached at larger values of $N_{\max}$ (see section 5.3). For instance, for the EFT interaction the energy converges for $n_{\max} = 2$ and $n_{\max} = 3$; therefore, the error bars shown in figure 5.8 show the errors caused by the importance truncation ($\kappa_{\min}$ and $C_{\min}$). We used the empirical formula, which is also used in nuclear physics, for the extrapolation to $N_{\max} \to \infty$ (see chapter 5.4).

One can see that the ground-state energy asymptotically approaches some value as $n_{\max}$ increases, but do not yet converge to that value within the range of $n_{\max}$ used in our calculations. The convergence of the first-excited state is even slower (like for the five-particle system). We can explain the slower converge behavior (or better, the absence of the convergence) for the first-excited state (like for the five-particle system above) with the choice of the LO and NLO constants. Note that, as $n_{\max}$ increases, the errors grow larger (the farther from convergence the calculated energy, the larger the errors obviously are). The "kink" in the plotted energy in figure 5.8 for the ABF interaction for $n_{\max} = 3$ is due to the fact that, in order to extrapolate to $N_{\max} \to \infty$, we performed calculations up to $N_{\max} = 18$ for $n_{\max} = 3$, but up to $N_{\max} = 22$ for $n_{\max} = 4$. Therefore, the value for $n_{\max} = 4$ is closer to the exact value. The errors are too large to discuss the convergence behavior as $n_{\max} \to \infty$.

Figure 5.9 shows the difference in the energy $\Delta E^{(n_{\max})} = E^{(n_{\max}-1)} - E^{(n_{\max})}$ with increasing $n_{\max}$ for the EFT interaction for the ground state and first-excited state. Here we used the NLO correction of the EFT and the simple extrapolation scheme (5.5) to extrapolate the energy to $N_{\max} \to \infty$. Our results are not sufficiently converged to yield precise values, but we can extrapolate the energy values for the NLO of the EFT interaction. For $n_{\max} \to \infty$, we use an extrapolation function similar to the one used for the Alhassid method with $\log_{10}(\Delta E) = A + Bn_{\max} + Cn_{\max}^2$. For the extrapolation we do not consider the

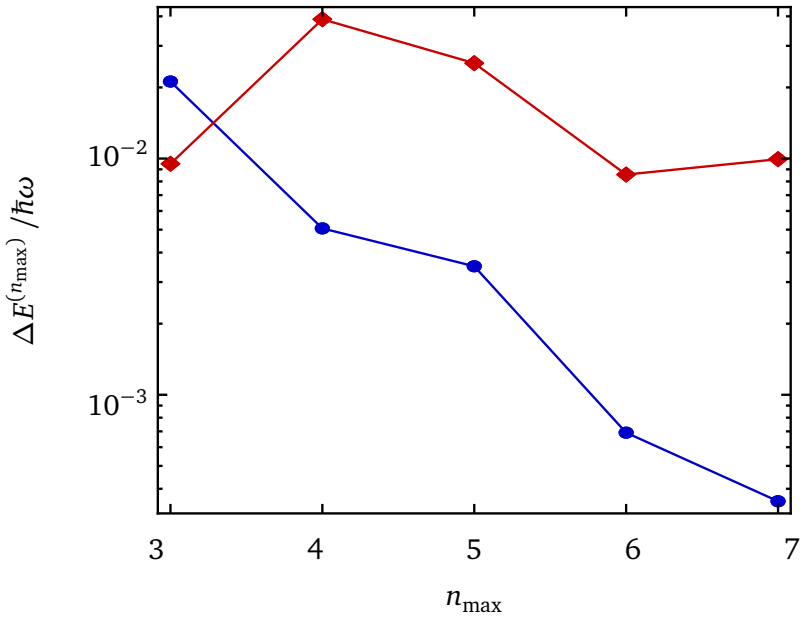

Figure 5.9.: The differences in the extrapolated energy of the ground state (●) and first exited state (◆) of a eight-particle fermionic system with $L^{\pi} = 0^{+}$ in the unitary limit as a function of $n_{\max}$. The calculations were performed using the NLO corrections to the EFT interaction.

errors of the $N_{\max}$ extrapolation. We estimate the error like for the $N_{\max}$ extrapolation by omitting the last point with largest $n_{\max}$. The extrapolated value is $(12.504 \pm 0.014)\hbar\omega$, in good agreement with the value of FN-DMC method $(12.58 \pm 0.03)\hbar\omega$ (see [12] or section 4.5). Since the ABF interaction converges slower than the EFT, still fewer data points are available to perform the extrapolation than in the case of the EFT. Consequently, we do not observe convergence for the ABF interaction.

In the available literature, an extrapolation to $n_{\max} \to \infty$ has only been performed by Alhassid, Bertsch and Fang [1] and by Gilbreth and Alhassid [33], and only for three or four particles in the unitary limit. They fitted a function of the form $\propto n_{\max}^{-\alpha}$ to $\log(\Delta E)$ with α between 0.5 and 1.5. Figure 5.10 was taken from [1]. Figure 5.10 (a) shows the ground-state energy of a three-particle fermionic system at unitarity as a function of the relative cutoff $q = n_{\max}$. Figure 5.10 (b) shows the error in the energy as a function of q in a logarithmic scale. Here, the renormalized contact interaction (open circles) and the ABF interaction (solid circles) were used. The energies are monotonically increasing and the ABF interaction shows fast convergence to the exact value.

As already mentioned we can remove the dependence of the calculated observables on $n_{\max}$ and hence the resulting errors by extrapolating to $n_{\max} \to \infty$. We have seen in this chapter that this works very well for small particle numbers. The ground-state energy for five particles in figure 5.7 shows convergence for both the EFT and ABF interactions. As expected the NLO corrections of the EFT interaction show better convergence than the LO of the EFT interaction alone. This behavior was already observed by other groups (such as Rotureau *et al.* [77]) for three particles. With increasing particle number, the error of the calculation increases, since we cannot calculate larger $N_{\max}$ because the dimension of the many-body space increases as well. Consequently, we have fewer values of $N_{\max}$ available which we can use for the extrapolation $N_{\max} \to \infty$ (see also section 5.3). These errors make the extrapolation to $n_{\max} \to \infty$ difficult, so we can see a good convergence behavior for five particles (figure 5.7) but not for eight (figure 5.8). These difficulties put the extrapolation of $n_{\max} \to \infty$ beyond our present capabilities. We hence have to choose a fixed $n_{\max}$ that is as large as possible but still computationally feasible. We discuss this in the next section.

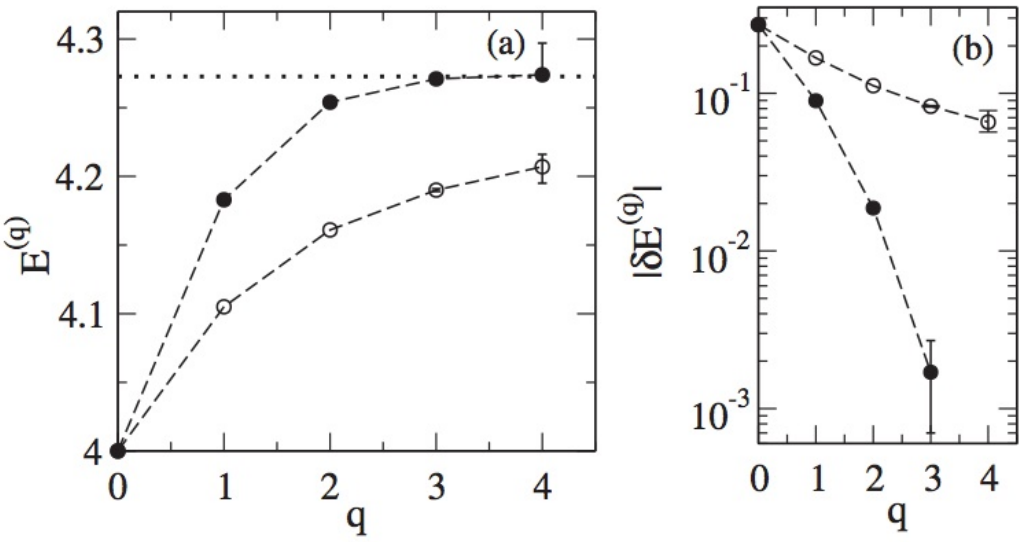

Figure 5.10.: Ground state energy of a three-particle fermionic system at unitarity with $L^\pi = 1^-$ as a function of the relative cutoff $q = n_{\max}$ (a). The dotted line is the exact energy, solid circles correspond to the ABF interaction and open circles to the renormalized contact interaction. Figure (b) shows the errors to the exact energy $|\delta E^{(q)}| = |E^{(q)} - E^{(\infty)}|$. The figure was taken from [1].

In this section we discuss the choice of the relative cutoff $n_{\max}$. To this end, we use the results of the calculation for 8 particles at unitarity (see section 5.3 and 5.5). For the energy of the first excited state using the ABF interaction, the relative cutoff $n_{\max} = 4$ is the last one with small error bars of the extrapolation to $N_{\max} \to \infty$ (see figure 5.8). If we consider the ground-state energy using the ABF interaction, the relative cutoff $n_{\max} = 5$ is the highest we can choose because the next one ($n_{\max} = 6$) does not converge up to $N_{\max} = 22$, the largest value of $N_{\max}$ used in the present thesis. The energy calculated using the EFT interaction converges for all calculated $n_{\max}$ (see figure 5.8), but $n_{\max} = 5$ is the last one with small error bars. With increasing $n_{\max}$ we need higher values of $N_{\max}$ to get near convergence, so for the ground-state energy calculated using the EFT interaction we are near convergence at $N_{\max} \approx 12$ for $n_{\max} = 2$ and for $n_{\max} = 4$ it is $N_{\max} \approx 16$ (see figure 5.8). Furthermore, for the extrapolation to $N_{\max} \to \infty$ we can only use $N_{\max} \geq 2n_{\max}$. Since we do not consider the convergence behavior for $n_{\max} \to \infty$, we have to choose one $n_{\max}$ to do the calculation for all considered particle numbers. The difference between the ground-state energies calculated using the NLO corrections of the EFT interaction for $n_{\max} = 4$ and 5 is only 0.6 percent. The deviation of the ground-state energy for $n_{\max} = 4$ calculated using the NLO corrections to the results calculated using the FN-DMC method is 2 percent. The additional computational effort required for $n_{\max} = 5$ compared to $n_{\max} = 4$ is not justified by a minor improvement of the results. Therefore, we use a relative cutoff of $n_{\max} = 4$ for the calculation presented in the remainder of this thesis.

5.6 Comparison between the IT-NCSM and the Full NCSM

In this section we compare the results of the importance-truncated calculation with the calculation in the full-space NCSM for four- and five-fermion two-component systems as a benchmark in order to demonstrate the robustness of the importance truncation scheme. For four-fermion systems, full NCSM calculations are possible up to very large $N_{\max}$ spaces, so that convergence can be achieved. We performed calculations for four- and five-fermion systems using both the ABF and the EFT interaction. For both the full NCSM and the IT-NCSM, we use only the leading order (LO, see section 3.6.1) and the

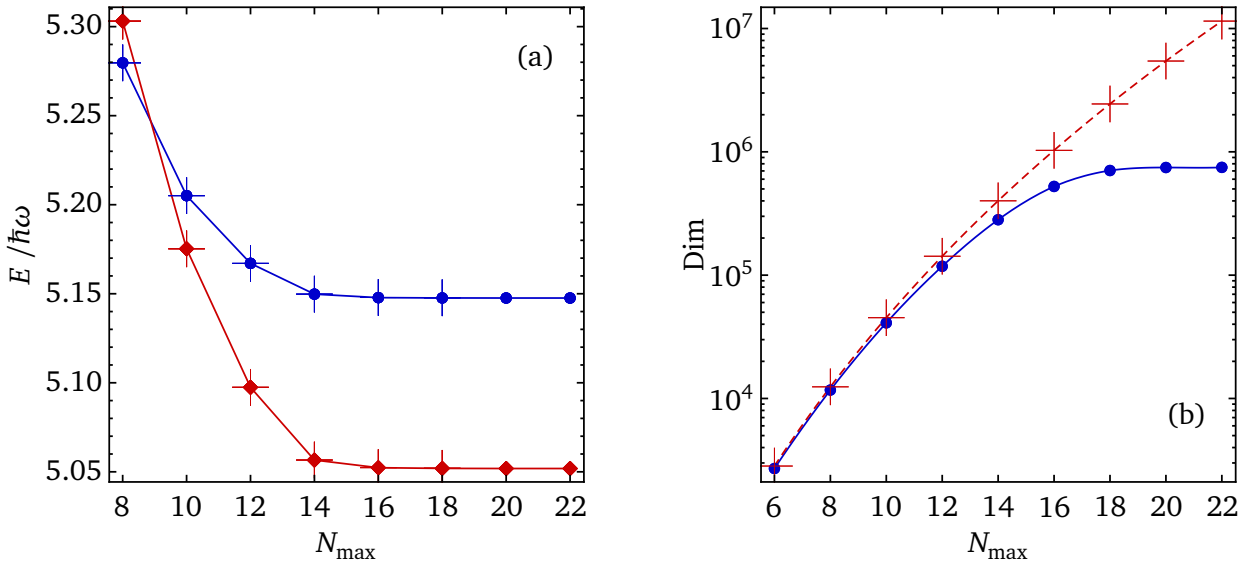

Figure 5.11.: The energy of the ground state with $L^\pi = 0^+$ of a $A = 4$ Fermi system in the unitary limit with increasing $N_{\max}$ (a) and the dimension of the model space (b). The calculation was done using the EFT interaction. We use $n_{\max} = 4$ as a two-body cutoff. The result of the IT-NCSM LO calculations are blue solid circles (●), NLO red solid diamonds (◆). The full NCSM results are shown as crosses at LO (+) and NLO (+).

next-to-leading order (NLO, see section 3.6.2) for calculating the matrix elements of the EFT interaction. The NLO terms are treated as first-order perturbations of the LO terms.

We use a cutoff of $n_{\max} = 4$ for the two-body system for both, the full and importance-truncated calculations of four- and five-fermion systems for the EFT interaction and a regularization parameter $n_{\max} = 4$ of the relative Hamiltonian for the ABF interaction. For four-particle fermionic systems, we use the reference threshold $C_{\min} = 1 \cdot 10^{-4}$ (see section 4.4) for each iteration step. For calculation of subsequent $N_{\max}$, we used a sequence of importance thresholds from $\kappa_{\min} = 10^{-5}$ to $\kappa_{\min} = 10^{-4}$ and extrapolated the results of the eigenvalue problem to the limit $\kappa_{\min} \to 0$ (see section 4.4). Calculations for five-particle systems were performed with a sequence of importance thresholds from $\kappa_{\min} = 3 \cdot 10^{-5}$ to $\kappa_{\min} = 1 \cdot 10^{-4}$ and we used the reference threshold $C_{\min} = 2 \cdot 10^{-4}$.

The extrapolation of the ground-state energy to $\kappa_{\min} \to 0$ is performed as explained in section 4.4.3 using the simpler estimation method, where we fit a p^{th}-order polynomial throughout the calculated energy for all $\kappa_{\min}$. We use here $p = 3$. For both particle numbers we use the empirical formula (5.5) for the extrapolation to $N_{\max} \to \infty$. We used only datapoints with $N_{\max} \geq 2n_{\max}$ for the extrapolation (see section 5.2).

Figure 5.11(a) shows the convergence of the ground-state energy for $A = 4$ fermions with respect to $N_{\max}$ for the EFT interaction up to NLO. With increasing $N_{\max}$ the energy decreases and converges for large $N_{\max}$. We increase $N_{\max}$ until convergence is achieved. In the case of four fermions with $n_{\max} = 4$ that is the case for $N_{\max} \approx 16$. The results of an importance-truncated NCSM calculations show perfect agreement with full NCSM calculations for each $N_{\max}$.

Figure 5.11(b) compares the dimensions of the full and the importance-truncated model spaces treated in the calculation for a four-particle Fermi system with EFT interaction. While the dimension of the model space grows exponentially for the full NCSM, the dimension of the importance truncated space saturates at approximately $N_{\max} = 16$ or 18. The saturation is not surprising because it is a sign of convergence. Once the state is converged there is nothing to add to the model space to improve the description of the state. The dimension of the model space for the full-NCSM calculations is one order of magnitude larger

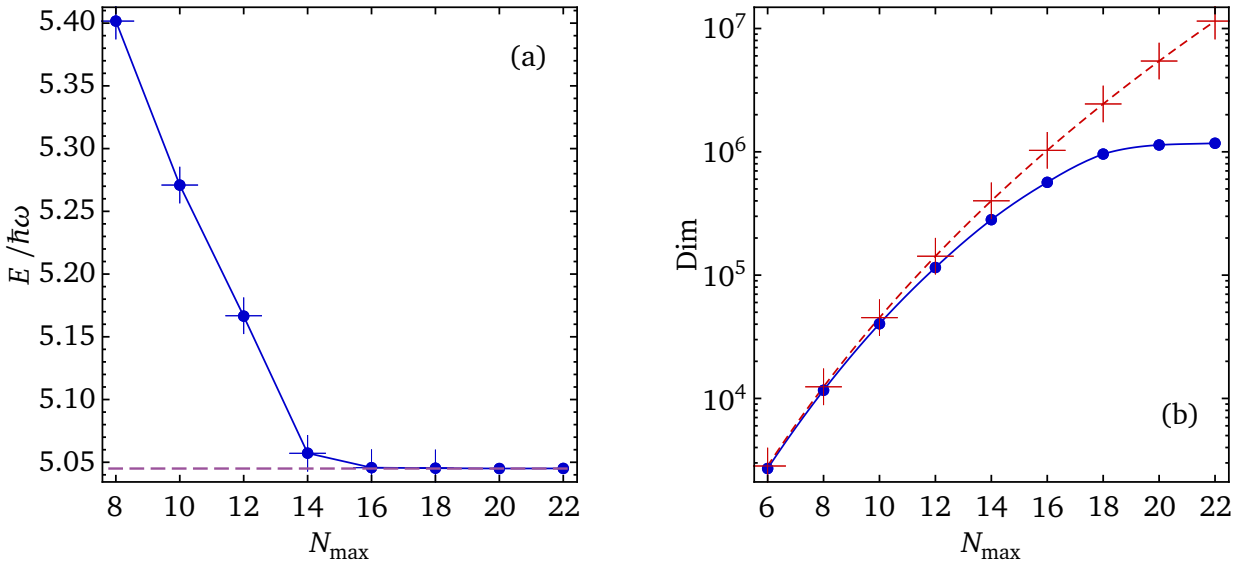

Figure 5.12.: Ground-state energy with $L^\pi = 0^+$ for $A = 4$ fermion system calculated using the ABF interaction (a) and the model space dimension with increasing $N_{\max}$ (b). The results of the full NCSM are shown as crosses (+) and the results of the importance-truncated calculation as solid circles (●). The dashed line is the approximated ground-state energy for $n_{\max} \to \infty$ [1].

than that of the IT-NCSM at the largest value of $N_{\max}$. The very good agreement of the energies calculated by the IT-NCSM with those calculated using other methods and the slowing growth of the dimension of the model space with increasing $N_{\max}$ shows the efficiency of the IT-NCSM. The converged result for the LO EFT interaction is $E = (5.148 \pm 0.001)\hbar\omega$, and for the NLO, $E = (5.052 \pm 0.001)\hbar\omega$, each with an error of $\pm 0.001\hbar\omega$ caused by the importance truncation. This is in excellent agreement with previous results, where the ground-state energy was found to be $E(n_{\max} = 5) = 5.02\hbar\omega$ [77], $(5.045 \pm 0.003)\hbar\omega$ [1], $(5.051 \pm 0.009)\hbar\omega$ (FN-DMC) and $5.028\hbar\omega$ (CG) [12].

Next, we consider the ABF interaction. For a four-fermion system, we perform full and importance-truncated NCSM calculations. In figure 5.12(a), the energy of the ground state for a four-particle system is shown. The converged result for $n_{\max} = 4$ is $E = (5.045 \pm 0.001)\hbar\omega$. The results calculated with the importance-truncated NCSM using the ABF interaction agree extremely well with full NCSM calculations for each $N_{\max}$. The result given by Alhassid *et al.* [1] for the energy of a four-particle fermionic system for infinite $n_{\max}$, $E = (5.045 \pm 0.003)\hbar\omega$ (dashed line in figure 5.12), also agrees very well with ours, as well as with the results of other groups (see above). The dimension of the importance-truncated space using the ABF interaction, shown in figure 5.12(b), is slightly larger than using the EFT interaction (see figure 5.11b). However, in both cases the dimension of the importance-truncated space is smaller by one order of magnitude than the full-NCSM space. This proves that the IT-NCSM is efficient.

The results for the ground-state energy of $A = 5$ fermions in the unitary limit for the EFT interaction with increasing $N_{\max}$ are shown in figure 5.13(a). Again, we considered only the LO and NLO terms of the EFT interaction. We performed the calculation both in the importance-truncated space and in the full-NCSM space. The $N_{\max} = 16$ space is intractable (in particular in terms of memory) using the full NCSM, but calculating the $N_{\max} = 22$ space using the IT-NCSM is feasible. Looking at the dimensions of the two model spaces, shown in figure 5.13(b), we can see that the dimension of the truncated $N_{\max} = 22$ space is of the order of 10^6, whereas the dimension of the highest calculated NCSM space ($N_{\max} = 18$) is of the order of 10^7 and the dimension of the NCSM space increases exponentially with increasing $N_{\max}$. Therefore, the dimension of the full NCSM space for $N_{\max} = 22$ should be two or three orders of

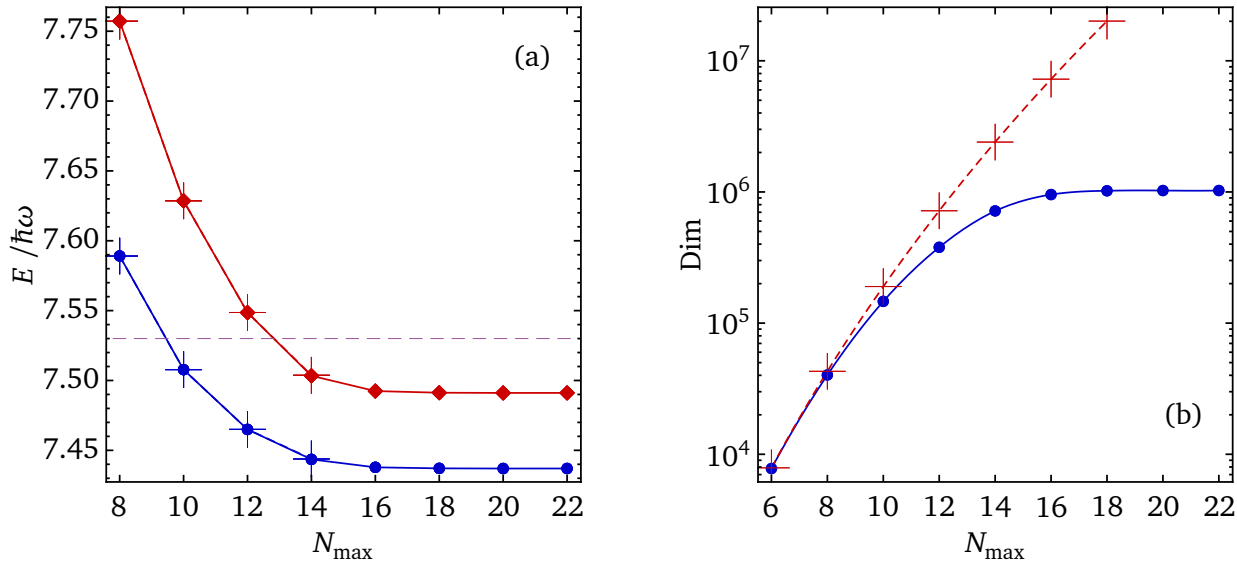

Figure 5.13.: Ground state energy with $L^\pi = 1^+$ of the $A = 5$ fermion system calculated using the LO and NLO EFT interaction (a) and the model-space dimension (b). Notation as in figure 5.11. The dashed line in (a) is the ground-state energy calculated using the CG approach [12].

magnitude larger than the dimension of the truncated $N_{\max} = 22$ space. The extrapolation of the energy for $N_{\max} \to \infty$ for IT-NCSM calculation is more precise, since we can take results for higher values of $N_{\max}$ into account. Again, the IT-NCSM proves to be more effective. For $n_{\max} = 4$ we get for the LO of the EFT interaction $E(N_{\max} \to \infty) = (7.4391 \pm 0.0007)\hbar\omega$ with an error of $\pm 0.0007\hbar\omega$ coming from the IT. Using the NLO correction, we obtain $E(N_{\max} \to \infty) = (7.487 \pm 0.001)\hbar\omega$ at NLO (see figure 5.13(a)), which agrees well with the results obtained by Blume *et al.*, $E = 7.61(1)\hbar\omega$, calculated using the FN-DMC method, see section 4.5, or $7.53\hbar\omega$ using CG [12], see section 4.6. The difference in NLO between the full and the truncated calculation for $N_{\max} = 16$ is $0.0002\hbar\omega$, which is still smaller than the difference at LO. For the NLO EFT we only calculate the NLO correction for the smallest value of $\kappa_{\min}$ used for the LO calculation (see also section 5.1). As already discussed in section 5.1 and as can be seen here, we can neglect the error by calculating the NLO correction only for the smallest value of $\kappa_{\min}$.

Figure 5.14(a) shows the ground-state energy for a five-fermion system calculated using the ABF interaction. Again the full NCSM and the IT-NCSM results show good agreement. The extrapolated ground-state energy of an IT-NCSM calculation is $(7.462 \pm 0.014)\hbar\omega$. We use here again the empirical formula (5.5) for the extrapolation. The uncertainty from the IT-NCSM extrapolation is of the order of 10^{-4} and, therefore, lower than the $N_{\max} \to \infty$ extrapolation. The dashed line shows the ground-state energy of the CG approach, $E = 7.53\hbar\omega$, the deviation is less than 1 percent.

Figure 5.14(b) shows the growth of the dimension with increasing $N_{\max}$ for a full NCSM calculation and an IT-NCSM calculation using the ABF interaction. The growth of the dimension of the NCSM space is nearly exponential while the growth of the truncated space slows down, so that the dimension of the full-NCSM space for $N_{\max} = 18$ is one order of magnitude larger than that of the truncated space for $N_{\max} = 20$. On the same computer, a full NCSM calculation at $N_{\max} = 14$ takes longer than an IT-NCSM calculation for the largest space ($N_{\max} = 20$ and using the ABF interaction).

As for the four-particle system, the dimension of the importance-truncated space using the EFT interaction at LO grows slower than with the ABF interaction, and hence the importance-truncated calculation using the ABF interaction takes longer than the importance-truncated calculation using the LO of the EFT interaction. We emphasize here again that we need higher order for the LO calculation, for example the NLO, to get the same results as using the ABF interaction.

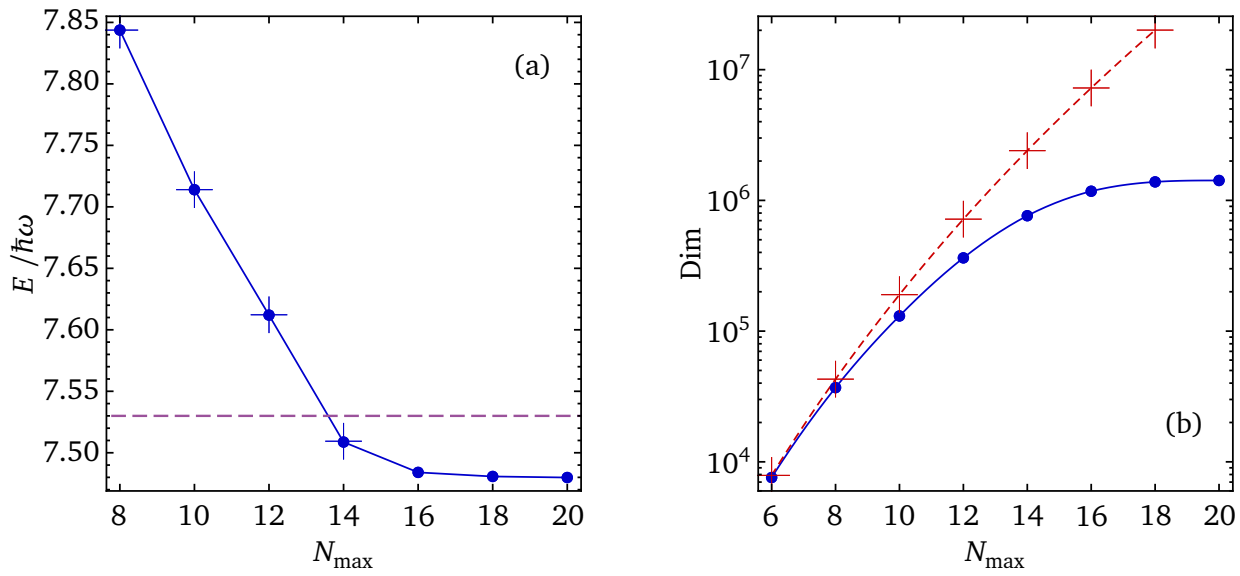

Figure 5.14.: Ground-state energy with $L^\pi = 1^-$ for $A = 5$ fermion system calculated using the ABF interaction (a) and the model space dimension with increasing N_{max} (b). Notation as in figure 5.11. The dashed line in (a) is the ground-state energy calculated using the CG approach [12]

5.7 $10 + 10$ Particles

We now consider a system of $10 + 10$ fermions at unitarity. Figure 5.15 shows the ground-state energy $L^\pi = 0^+$ as a function of the truncation parameter N_{max} of the many-body space. The calculation was done using only the EFT interaction, where we used $n_{max} = 2$ (a) and $n_{max} = 4$ (b) as the cutoff of the two-body space. We used the LO and NLO terms of the EFT interaction for both the calculation with $n_{max} = 2$ and $n_{max} = 4$. For the calculation with $10 + 10$, we set $C_{min} = 5{\cdot}10^{-4}$ and reduced κ_{min} from $5{\cdot}10^{-5}$ to $1.5{\cdot}10^{-4}$ successively, then extrapolated the result to $\kappa_{min} \to 0$ as described in section 4.4.3. As one can see in figure 5.15, the energy approaches asymptotically some value as N_{max} increases, but whereas we are in the vicinity of the convergence for $n_{max} = 2$, for $n_{max} = 4$ we are not. Looking at figure 5.4 (e) for eight fermions $(4 + 4)$ with $n_{max} = 4$ (see section 5.3) we cannot expect convergence for $N_{max} < 18$ for $n_{max} = 4$ for 20 fermions; it is likely that even higher values of N_{max} will be required because the energy of the two-body interaction can be distributed to more particles. Therefore we would need calculations for higher values of N_{max} in order to perform the extrapolation. However, this has not been possible in the context of the present thesis with the given computing resources. As already mentioned, in order to obtain meaningful results by extrapolation, only results for $N_{max} \geq 2n_{max}$ should be taken into account (see section 5.2).

The energy calculated by Blume *et al.* [12] for the ground state is $E = 41.30(8)\hbar\omega$. If we extrapolate the energy for the ground state for $n_{max} = 2$, we get a ground state energy of $E = 38.92 \pm 0.03$, where we used the empirical formula (see chapter 5.4). This corresponds to a difference of about 5.8% to the value calculated by Blume. To obtain a more precise result we have to perform calculations with higher two-body cutoffs n_{max}. Our result is below the value from [12] already at $N_{max} = 12$ for the LO part of the EFT and $n_{max} = 4$. The NLO corrects the result to a higher value ($(43.38 \pm 0.02)\hbar\omega$ for $n_{max} = 4$ and $N_{max} = 12$, see figure 5.15(b)). The NLO corrects the energy also to higher values — see, for example, $3 + 2$ and $4 + 4$ particles (figures 5.3, 5.4 and 5.5). Using higher values of n_{max} can also lead to higher energy values (see figures 5.7 and 5.8). This was also observed in [77] and in [1] for three particles (see

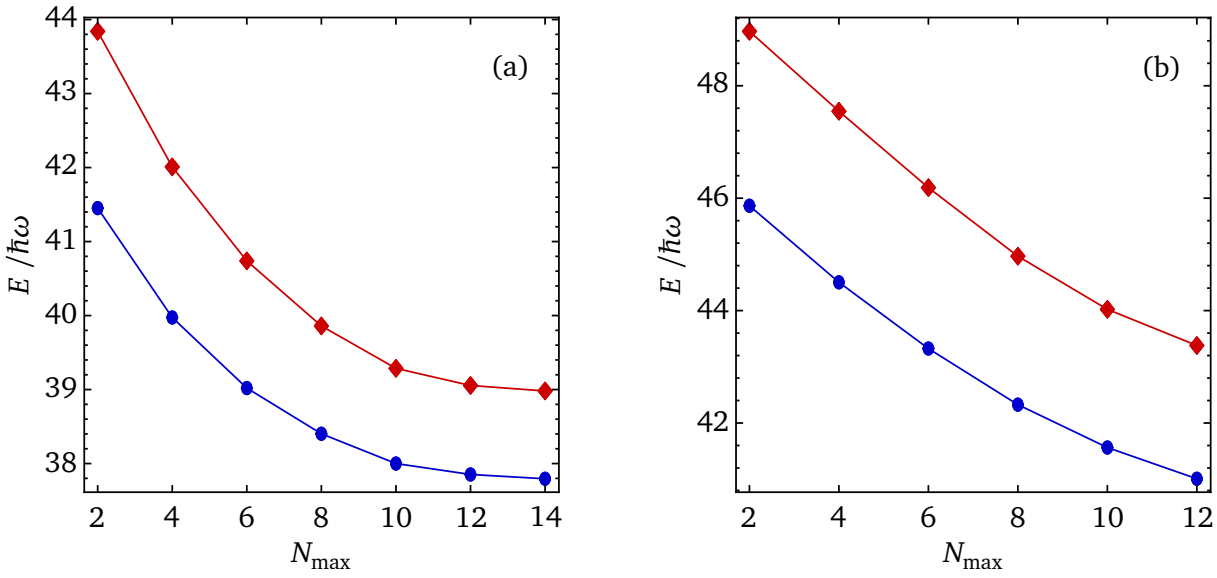

Figure 5.15.: Energy of the ground state with $L^\pi = 0^+$ of $10 + 10$ fermions calculated using the LO (●) and NLO (◆) EFT interaction as a function of $N_{\max}$. A two-body cutoff $n_{\max} = 2\ (a)$ and $n_{\max} = 4\ (b)$ was used.

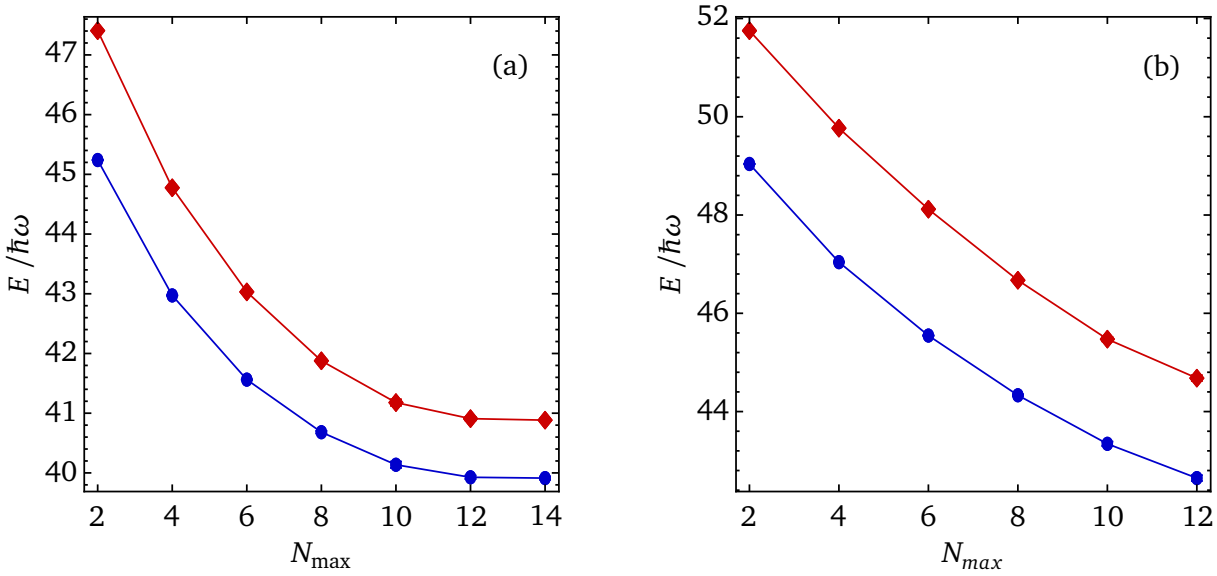

Figure 5.16.: Energy of the first excited state with $L^\pi = 0^+$ of $10 + 10$ fermions calculated using the LO (●) and NLO (◆) EFT interaction as a function of $N_{\max}$. A two-body cutoff $n_{\max} = 2\ (a)$ and $n_{\max} = 4\ (b)$ was used.

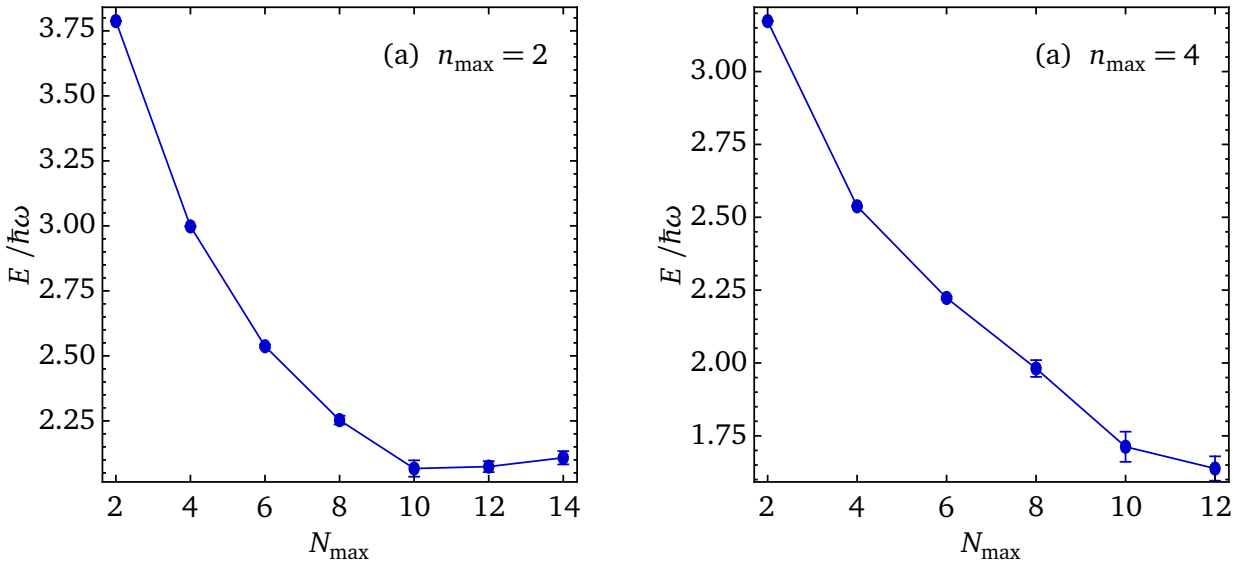

Figure 5.17.: Excitation energy of the first excited state with $L^\pi = 0^+$ of $10+10$ fermions calculated using the LO of the EFT as a function of $N_{\max}$. A two-body cutoff $n_{\max} = 2$ (a) and $n_{\max} = 4$ (b) was used.

figure 5.10) and the effect is visible for $10+10$ fermions in figure 5.15 as well. We expect our results for higher $n_{\max}$ and higher orders to be between our calculated value for $n_{\max} = 2$ and the value from [12].

As already mentioned we can get results for excited states at little additional cost, since the Lanczos algorithm takes more iterations to converge the additional states. Figure 5.16 shows the energy of the first excited state with $L^\pi = 0^+$ for a system with $A = 20$ fermions at unitarity for a two-body cutoff $n_{\max} = 2$ (a) and $n_{\max} = 4$ (b). As for the ground state we can perform calculations for $n_{\max} = 2$ using higher values of $N_{\max}$ than for $n_{\max} = 4$, hence the energy for $n_{\max} = 2$ is closer to convergence than that for $n_{\max} = 4$. We can extrapolate the energy of the first excited state for $n_{\max} = 2$ by using the empirical formula again, and we get $E(n_{\max} = 2) = (40.83 \pm 0.09)\,\hbar\omega$. This we consider as a lower bound for the energy of the first excited state, and again we have to go to higher two-body cutoffs $n_{\max}$ to obtain a more precise result.

We also plotted the excitation energy of the first 0^+ state (figure 5.17). One can see in the figure that the difference of the absolute energy of both states converges quickly with increasing $N_{\max}$. For $n_{\max} = 2$, the excitation energy converges already for $N_{\max} = 10$, and for $n_{\max} = 4$, it is almost converged for $N_{\max} = 12$. Therefore, like in nuclear physics [73], the threshold dependence of the absolute energy of both states is similar.

5.8 Benchmark Calculation for All Calculated Particle Numbers

Table 5.1 lists the ground-state energies and table 5.2 the first excited-state energies of two-component systems consisting of different numbers of fermions in units of $\hbar\omega$. Using the EFT interaction, we performed calculations for $A = 4$ through $A = 10$ as well as for $A = 20$ (see section 5.7). Using the ABF interaction [1], we only performed calculations for $A = 4$ through $A = 10$. We performed all calculations with a two-body cutoff $n_{\max} = 4$ (see section 5.5). For $A = 5$ through $A = 8$, we set $C_{\min} = 2{\cdot}10^{-4}$ and choose $3{\cdot}10^{-5} \leq \kappa_{\min} \leq 10^{-4}$; for $A = 9$ and $A = 10$, we set $C_{\min} = 5{\cdot}10^{-4}$ and choose $5{\cdot}10^{-5} \leq \kappa_{\min} \leq 1.5{\cdot}10^{-4}$.

Comparing our results with those obtained by Blume *et al.* [12], we see that the difference between their results and ours are small. The results of our calculations using the IT-NCSM agree well with those

Table 5.1.: Ground-state energy for ultra-cold two-component Fermi systems in a trap at unitarity in units of $\hbar\omega$ with $n_{\max} = 4$, extrapolated using the empirical formula (5.5).

	this work			Blume *et al.* [12]	
		EFT			
A	ABF	LO	NLO	CG	FN-DMC
3	4.273(1)	4.206(1)	4.269(1)	4.276	4.281(4)
4	5.05(1)	5.15(1)	5.06(1)	5.028	5.051(9)
5	7.46(1)	7.44(1)	7.49(1)	7.53	7.61(1)
6	8.44(4)	8.49(1)	8.46(1)	8.48	8.64(3)
7	11.08(1)	10.85(1)	11.09(1)		11.36(2)
8	12.20(3)	12.02(1)	12.32(1)		12.58(3)
9	15.27(5)	15.34(1)	15.51(1)		15.69(1)
10	16.6(2)	16.41(1)	16.71(1)		16.80(4)

Table 5.2.: First-excited-state energy for a ultra-cold two-component Fermi system in a trap at unitarity in units of $\hbar\omega$ with $n_{\max} = 4$, extrapolated using the empirical formula (5.5).

	this work			Blume *et al.* [12]
		EFT		
A	ABF	LO	NLO	CG
3	6.272(1)	6.190(1)	6.187(1)	6.276
4	7.05(1)	7.22(1)	7.08(1)	7.032
5	8.94(1)	9.05(1)	8.95(1)	8.83
6	10.26(4)	10.28(1)	10.24(1)	10.50
7	12.16(9)	12.26(2)	12.20(4)	
8	13.61(3)	13.34(1)	13.52(2)	
9	15.9(3)	15.80(1)	16.33(2)	
10	18.1(1)	17.25(1)	17.90(2)	

obtained from full-NCSM calculations (for small values of A) as well as from Monte-Carlo calculations. For instance, the differences between the ground-state energies calculated by us and those calculated using the CG method are less than 1% both for the ABF interaction and for the NLO of the EFT. This is a very good agreement considering that we used $n_{\max} = 4$ and included only the NLO corrections to the EFT, but no higher orders, meaning our results are afflicted with errors. For the first excited state, the differences are larger but still below 2.5%. Compared to the results for the ground-state energy obtained using the FN-DMC method, the differences are also larger but at most 2.4% for the NLO of the EFT and $4 + 4$; for $5 + 4$ and $5 + 5$, the differences are smaller than that. For the ground-state energy calculated using the ABF interaction, the differences in the energy compared to the results obtained by the FN-DMC method grow larger as the particle number increases; this can be caused by the slower convergence compared to the EFT interaction.

As already mentioned, the CG and FN-DMC methods are variational approaches and provide an upper bound for the energy, so it is reassuring that our energies are below the energies calculated using CG and FN-DMC methods. Furthermore, they use a Gaussian-shaped potential as interaction, instead of the EFT or ABF interactions used in this thesis. Trapped systems display universal properties as long as the HO length is large compared to the effective range of the interaction, hence the second constraint for the trapped systems at unitarity is $a_{\mathrm{HO}} \gg r_0$ [77, 91]. The EFT interaction uses the δ-function and their derivatives, and therefore it is zero everywhere but for $r = 0$. The ABF interaction is constructed like the

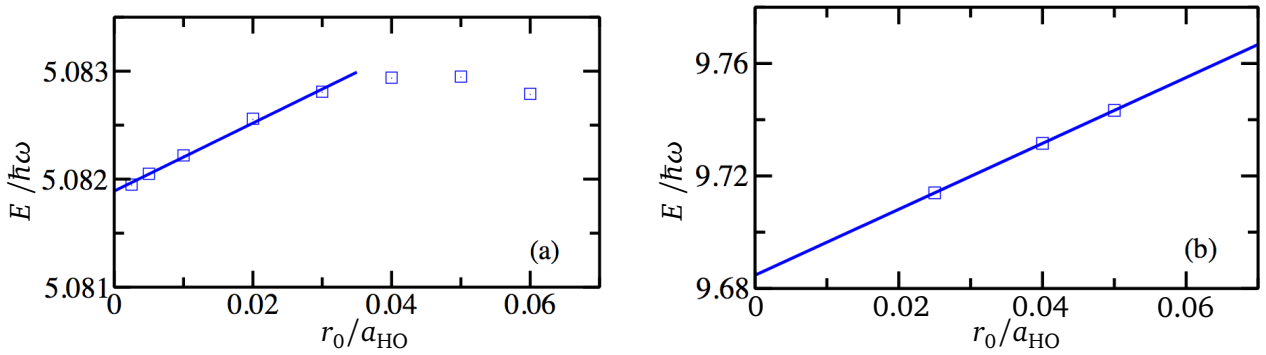

Figure 5.18.: Dependence of the ground-state (a) and excited-state (b) energy E on the range of the interaction r_0 of a four-body system at unitarity with $A_1 = 3$ and $A_2 = 1$. The energy was determined using the stochastic variational approach with CG basis set expansion. Figure taken from [65].

EFT interaction and is also only nonzero for $r = 0$. For calculations using Gaussian potentials, [65] used $r_0 \leq 0.01 a_{\mathrm{HO}}$ and extrapolated for the limit $r_0 \to 0$ (see, for example, figure 5.18). Therefore, the ABF and EFT interaction are more suitable for the unitary limit.

The CG method yields results for both the ground-state energy and the first excited-state energy, but only up to $A = 6$. The FN-DMC method, on the other hand, yields only the ground-state energy but at least up to $A = 30$ [12]. IT-NCSM calculations yield the energies of the first low-lying excited states at no additional cost. Using the IT-NCSM, the energies of systems with larger particle numbers A can be calculated for larger values of N_{max}. The range of values of N_{max} and A for which results can be obtained is primarily limited by the available computing power and not by the available memory [71].

We do not consider the convergence of the energy with n_{max} in this section (see section 5.5 for a discussion of that). The given errors contain only the errors from the importance truncation and the N_{max} extrapolation. Furthermore, we used only the LO and NLO orders of the EFT interaction. We can improve our results by considering the N^{2}LO of the EFT interaction and convergence with n_{max}.

5.9 Results for a Gaussian-shaped Potential

Up to this point, we used for our NCSM calculation the ABF and EFT interactions, which were also used by other groups using *ab initio* methods like CI or NCSM [1, 77]. As already mentioned, a Gaussian-shaped potential was used for calculation of energy spectra of fermionic systems at unitarity in the FN-DMC or CG methods. We also performed NCSM calculations at unitarity using a Gaussian-shaped potential of the form (3.85) in order to test the applicability of these potential for NCSM calculations, and present the results in this section. We did not conduct IT-NCSM calculations as we only used the Gaussian potential to calculate the energies of $A = 3$ two-component fermions. We determined V_0 for $a_0 \to \infty$ and different values of the range r_0 of the interaction in order to calculate the matrix elements in the relative coordinate frame. The range r_0 is chosen much smaller than the HO length a_{HO}. In determining V_0, we pretend the particles are in free space and not trapped in the HO potential.

We do not introduce any cutoff, in contrast to the other interactions studied in this work. Like for the other interactions, the matrix elements are calculated in the relative frame and are transformed into the laboratory frame using the Talmi-Moshinsky transformation explained in section 3.2.3.

For two-component fermion systems at unitarity, the Gaussian-shaped potential was used in [12, 65, 85, 88]. For the calculation, either one small value (e. g. $r_0 = 0.01 a_{\mathrm{HO}}$) was used or a number of values for the range r_0 of the interaction were considered with $r_0 \ll a_{\mathrm{HO}}$ (for example, $0.0025 a_{\mathrm{HO}} \leq r_0 \leq 0.08 a_{\mathrm{HO}}$ [65]) and the finite-range energies were extrapolated to $r_0 \to 0$. Figure 5.18 (taken from [65])

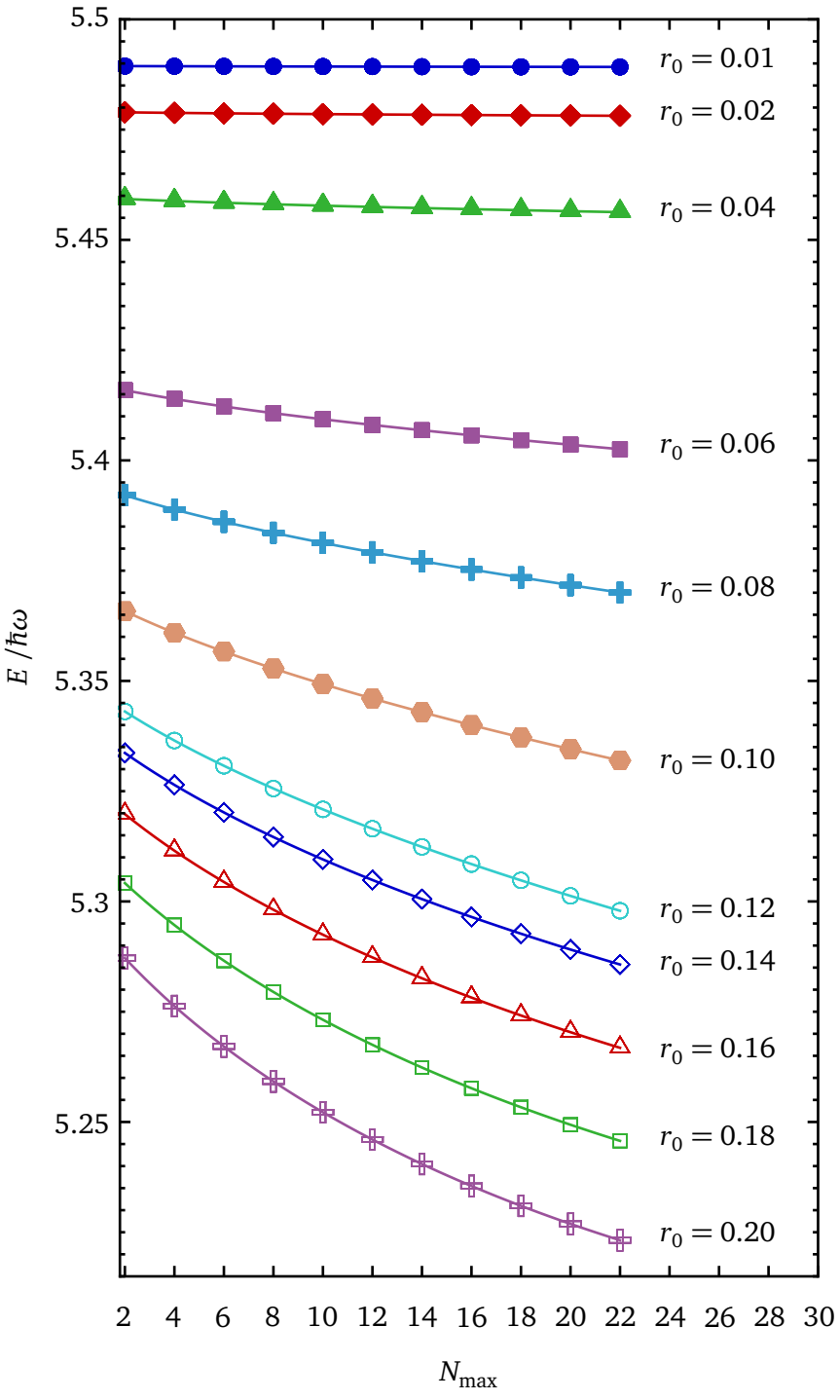

Figure 5.19.: Energy of the ground state with $L^\pi = 1^-$ of $A = 3$ fermions calculated using the Gaussian-shaped potential as a function of $N_{\max}$ for different r_0 (in units of a_{HO}).

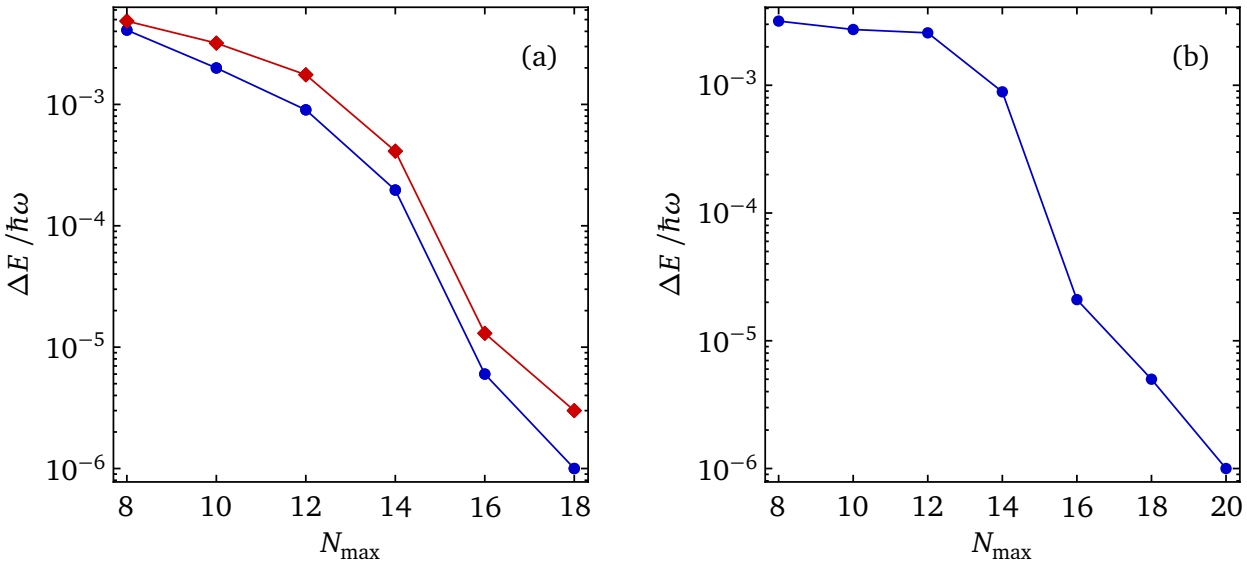

Figure 5.20.: Energy difference of the ground state with $L^\pi = 1^-$ of $A = 3$ fermions calculated using the EFT interaction (a) and according to Bertsch *et al.* (b) as a function of $N_{\max}$. We use here the two-body cutoff $n_{\max} = 4$. Logarithmic scale. The symbols of (a) corresponds the LO (●) and the NLO (◆) of the EFT interaction.

illustrates the energy dependence on r_0 and shows the ground-state energy and the energy of an excited state for different r_0 for a four-particle two-component Fermi system at unitarity. The calculation was done using the stochastic variational approach. The energies show a weak linear dependence with r_0 for sufficiently small r_0/a_{HO}. The results from other groups also show a linear dependence of the energy on r_0 [88].

We calculated the energy of a three-particle two-component fermionic system at unitarity with a range of the interaction of $r_0 = 0.01,\ 0.02,\ 0.04, \ldots, 0.2a_{\mathrm{HO}}$. We used the full NCSM method for those calculations. Figure 5.19 shows the calculated ground-state energies for $A = 3$ for increasing values of $N_{\max}$. The energies calculated using the stochastic variational approach, CG or FN-DMC converge to the exact value as $r_0 \to 0$; however, our results do not converge at all.

The exact ground-state energy for a three-particle fermionic system at unitarity is $4.2727243\hbar\omega$ [102] and the energy without the interaction is $5.5\hbar\omega$. In our calculations for small values of r_0, the energy is close to the noninteracting energy. The energy calculated for $r_0 = 0.01a_{\mathrm{HO}}$ and $N_{\max} = 22$ is $5.489\hbar\omega$ (see figure 5.19). As r_0 grows, the calculated energy decreases. However, even for $r_0 = 0.2a_{\mathrm{HO}}$ and $N_{\max} = 22$, the calculated energy is far above the exact energy.

The reason for the weak or non-existing convergence behavior is that the range of the potential is too small in comparison to the HO trap. In the unitary limit, we have $r_0 \ll a_{\mathrm{HO}}$. Other groups using the FN-DMC method or the CG approach chose e. g. $r_0 = 0.01a_{\mathrm{HO}}$, the largest value found in the available literature is $r_0 = 0.08a_{\mathrm{HO}}$ (see above). For larger r_0, the condition $r_0 \ll a_{\mathrm{HO}}$ is not fulfilled. In order to resolve the potential the eigenfunction of the HO potential should have at least the single-particle energy

$$e_i = \frac{a_{\mathrm{HO}}}{2r_0}. \tag{5.9}$$

Therefore, the eigenfunctions used for the calculation of our matrix elements cannot resolve the potential for $e_i < 50$ if we choose $r_0 = 0.01a_{\mathrm{HO}}$ as is often the case in the FN-DMC or CG method. For three fermions, we have $e_{\max} = N_{\max} + 1$. For the calculation with $r_0 = 0.08a_{\mathrm{HO}}$ at $N_{\max} = 6$, the eigenfunction

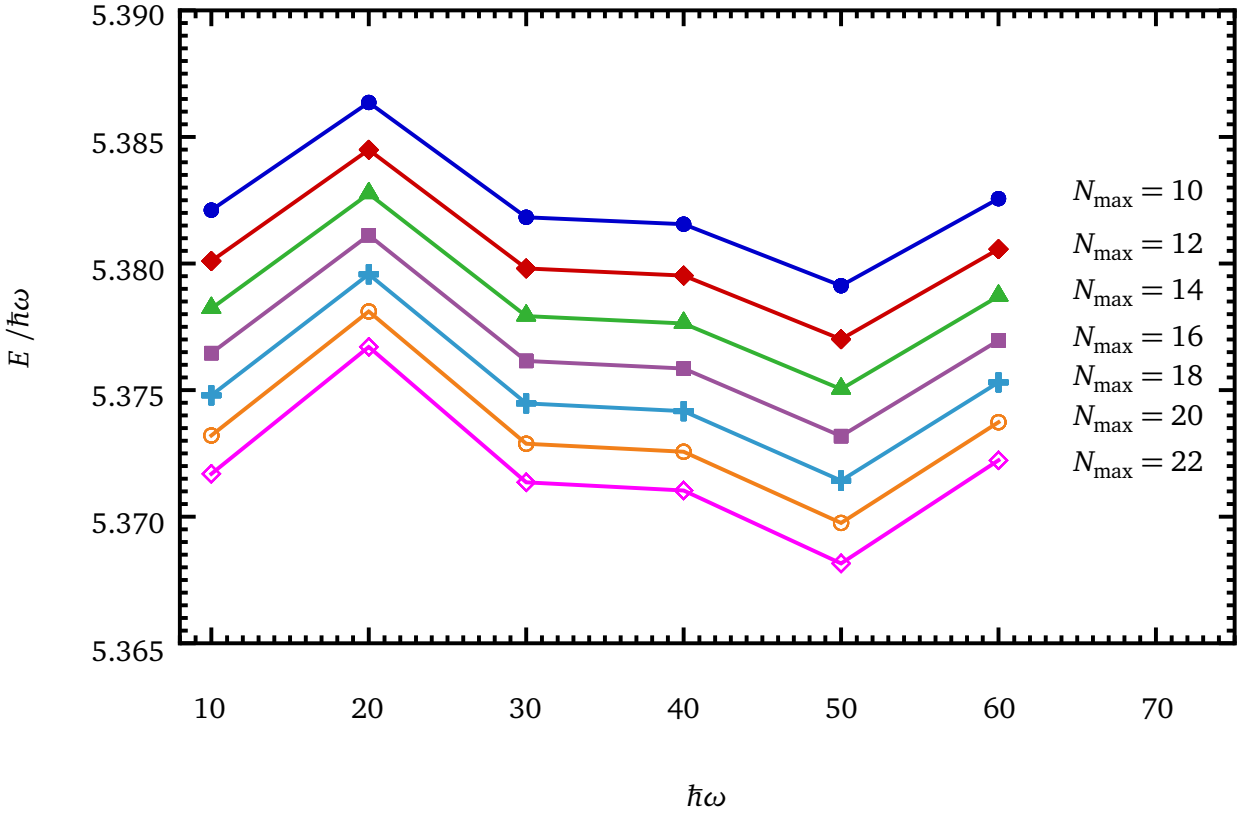

Figure 5.21.: Energy of the ground state with $L^\pi = 1^-$ of $A = 3$ fermions calculated using the Gaussian-shaped potential as a function of the HO energy $\hbar\omega$ for $r_0 = 0.1 a_{\text{HO}}$ for different $N_{\max}$. We used $N_{\max}$ from 10 to 22. The different symbols correspond to $N_{\max} = 10$ (●), 12 (◆), 14 (▲), 16 (■), 18 (✙), 20 (○), 22 (◇).

with $e_i = 6$ first appears which can "see" the potential. Since the influence of the eigenfunctions for larger values of e_i increases slowly, the calculated energy for $N_{\max} = 22$ is still in the vicinity of the non-interacting energy and no convergence appears. Using even smaller values of r_0 (in the aforementioned approaches, values down to $r_0 = 0.001 a_{\mathrm{HO}}$ have been used) makes little sense since the difference to the noninteracting energy would then be even smaller. At larger r_0 (for instance, $r_0 = 0.2 a_{\mathrm{HO}}$), the calculated energy for $N_{\max} = 22$ is closer to the exact energy but far away from convergence, and $r_0 = 0.2 a_{\mathrm{HO}}$ does not really satisfy the condition $r_0 \ll a_{\mathrm{HO}}$ anymore. Higher values of $N_{\max}$ would be needed in order to obtain converged results.

Furthermore, we analyzed the dependency of the calculated energies on the HO frequency ω when using the Gaussian interaction. The other two interactions used in the present thesis are independent of the HO frequency; the energy is always the same multiple of $\hbar\omega$ for any value of ω. Figure 5.21 shows the energy calculated using the Gaussian interaction for a fixed value of $r_0 = 0.1 a_{\mathrm{HO}}$ as a function of ω for $N_{\max} = 10, 12, 14, 16, 18, 20$. There is little to no dependency of the energy on the HO frequency. Here we won't discuss the errors introduced when determining V_0 numerically; the weak dependence of the energy on the HO frequency which can be seen in figure 5.21 could also be caused by those errors.

In summary, we can say that the Gaussian potential is not suited for the NCSM or the IT-NCSM because of the weak convergence in comparison to the other two interactions used in the present thesis. The ABF and EFT interaction used in the present thesis are renormalised, and hence deliver convergent results at low $N_{\max}\hbar\omega$. As a consequence of the renormalisation, calculations using either of the two interactions depend on the two-body cutoff, which is problematic because the convergence behavior with respect to that cutoff has not been systematically investigated yet and there is no consensus on which functions are physically justifiable for predicting the behavior as $n_{\max} \to \infty$. Using a Gaussian potential, which is not renormalised, does not require those extrapolations. However, for small values of r_0, the calculated energies are almost equal to the noninteracting energy and are far away from the exact value. Even for larger values of r_0, the calculated energies decrease, but even for the largest calculated $N_{\max}$ and r_0, the calculated energy is closer to the noninteracting energy than to the exact value, and the condition $r_0 \ll a_{\mathrm{HO}}$ is no longer fulfilled eventually. Convergence was not observed for any value of r_0, since in order to resolve the potential eigenvalues with higher single-particle energy are required. In order to improve the convergence behavior, much higher values of $N_{\max}$ and, consequently, larger model spaces would be needed, which would require a larger computational effort, also some sort of renormalisation for the Gauss potential would solve the convergence problem too. For this reason, we chose to not consider the Gaussian interaction in the remainder of this thesis.

In nuclear physics, unitary transformations, for example, the Similarity Renormalizaiton Group (SRG), are used to enhance the convergence behavior of many-body calculations [73]. The SRG transformation aims to decouple the low-momentum or low-energy states from high-lying stats leading to a universal Hamiltonian independent of the model-space and number of particles. The unitary transformation induces many-body contribution to the operators that go beyond the rank of the initial operator. Therefore, using the SRG we would have to handle three-body interactions. Because of the efforts required to develop the three-body interaction we did not use the SRG transformation for our calculations at unitarity. However, an SRG-type regularisation of the Gaussian interactions might have resolved the convergence issues we observed in the NCSM.

5.10 Conclusions

In this chapter, we discussed the results of our IT-NCSM calculations using both the EFT interaction and the ABF interaction and also the results of our NCSM calculation using the Gaussian-shaped potential. In section 5.1 we discussed the uncertainties of the NLO corrections to the EFT interaction, which we treat using perturbation theory. We have shown that we do not need to perform the calculations for all values of $\kappa_{\min}$; it is sufficient to add the NLO correction for the smallest value of $\kappa_{\min}$ to the LO result

calculated using the IT-NCSM. Another important result is that for the NLO calculations (as for the LO) it is possible to choose a value for the $C_{\min}$ threshold which is small enough not to influence the energies.

The uncertainties of the NCSM and also of the IT-NCSM can be quantified, which in turn allows us to quantify the uncertainties of the interaction itself. For both the EFT and the ABF interaction we introduce a relative cutoff (see section 3.5), hence the calculated energy depends on this arbitrarily chosen parameter. Furthermore the results depend also on the many-body truncation parameter $N_{\max}$.

The dependency on the trapping frequency ω_{HO} is explicit since it is physically motivated: The ultracold fermions are not a self-bound system but are trapped. The energy and other observables explicitly depend on the HO energy. Consequently, we cannot use theoretically motivated extrapolation functions for the IR cutoff, which have recently been introduced in nuclear physics (see section 5.4). The convergence behaviors of both the EFT and the ABF interaction are, by construction, independent of the HO frequency. For the Gaussian-shaped potential, our results (see section 5.9) suggest that the convergence of the calculated energy is too slow to allow for meaningful calculations.

Neither the NCSM nor the IT-NCSM can be used for calculations in an infinite HO model space; we truncate the HO space using an additional truncation parameter $N_{\max}$. The extrapolation to $N_{\max} \to \infty$ is a source of uncertainties. This extrapolation allows us to estimate the results for the energy and other observables for large model spaces, which we cannot calculate directly because of limits in the available computational resources. We discuss the dependency on the $N_{\max}$ for different values of $n_{\max}$. An important result is that there is no benefit in performing calculations $N_{\max} < 2n_{\max}$ for the extrapolation because the convergence behavior changes drastically beyond this point. With increasing $n_{\max}$, higher values of $N_{\max}$ are required to achieve convergence in IT-NCSM calculations. We discuss different possibilities to extrapolate the energy as $N_{\max} \to \infty$, and compare the results for the extrapolation using the empirical formula (5.5) and the formula introduced by Alhassid (5.8). Since neither of these formulae are physically motivated and the latter provides better results, we use the empirical formula for our calculations. Because the IT-NCSM method allows calculations for larger values of $N_{\max}$, simplifying the extrapolation to $N_{\max} \to \infty$, this simple extrapolation method is sufficient. It yields very robust results which agree well with those obtained by others using the CG and FN-DMC methods.

Furthermore, we analyzed the convergence behavior for $n_{\max} \to \infty$ for five- and eight-fermion systems at unitarity. Using the EFT interaction, we observed that the calculated energies asymptotically approach some value as $n_{\max}$ increases (convergent behavior). For five particles we see the convergence behavior; as expected both the NLO of the EFT interaction and the ABF interaction show improved convergence compared to the LO. For eight particles, our calculations did not extend to sufficiently large values of $n_{\max}$ to observe convergence. The convergence behavior is less pronounced for the ABF interaction. Since the errors introduced by the extrapolation to $N_{\max} \to \infty$ increase as $n_{\max}$ increases, we chose not to extrapolate the energies to $n_{\max} \to \infty$ for our other calculations. We chose $n_{\max} = 4$, which is the highest value for which we can converge our calculations with respect to $N_{\max} \to \infty$ for both interactions. The dependence on $n_{\max}$ can be reduced, for instance, by taking higher orders (such as $\mathrm{N^2LO}$) into account for the EFT.

Comparing the ABF interaction to the EFT interaction including the NLO corrections, we can see that the EFT shows a better convergence behavior; using the ABF interaction, the dimension of the importance truncated model space is larger and the results converge for larger values of $N_{\max}$ than they do using the EFT interaction. The calculations using the ABF interaction, therefore, require more time. The EFT interaction yields results that agree better with those published by other groups. The EFT interaction can, therefore, be considered superior; one downside is that we not only have to perform IT-NCSM calculations, but also calculate the NLO corrections using perturbation theory.

Our calculations with a Gaussian-shaped potential for three fermions did not converge to the results obtained with other interactions. The calculated values are nearer to the noninteracting energy than to the exact energy and do not show any convergence even for larger values of $N_{\max}$ or r_0. The reason is that in the unitary limit the condition $r_0 \ll a_{\mathrm{HO}}$ must hold, therefore only eigenfunctions of the HO

with high energy quantum number can resolve the Gaussian-shaped potential with such a small effective range and we need higher values of $N_{\max}$ in order to observe convergence.

We compared the results of calculations with the full NCSM (for four and five particles) and the IT-NCSM calculations. In summary, the results of full-NCSM calculations agree very well with those of the importance-truncated NCSM. The latter allows *ab initio* calculations for larger particle numbers and larger values of $N_{\max}$ and is, therefore, superior. Furthermore, we have done benchmark calculation for a system comprising $A = 20$ fermions at unitarity for $n_{\max} = 2$ and 4. Even the $A = 20$ system converges but for a cutoff $n_{\max} = 2$ in relative space. For up to 10 fermions at unitarity, we performed benchmark calculations using the IT-NCSM with $n_{\max} = 4$. We compared our results to those obtained by other groups using the CG basis set expansion method and the FN-DMC method and found good agreement. In summary, the IT-NCSM yields robust results and allows *ab initio* calculations for larger particle numbers and larger values of $N_{\max}$.

6 Conclusions and Outlook

Ultra-cold atomic Fermi gases have generated much interest in the past decade. *Ab initio* calculations for small ultra-cold systems have been performed using, for example, configuration interaction [1, 77] and correlated Gaussian methods [84]. These *ab initio* approaches are limited to small particle numbers, since the model space dimension increases rapidly as the particle number increases and more orbitals are included. Our goal was to extend the calculation of the energy spectra for ultra-cold atomic Fermi gases in the unitary limit to larger particle numbers and hence larger model spaces by applying the importance-truncation scheme to the NCSM. By introducing an *a priori* importance measure derived from multi-configurational perturbation theory we can estimate the relevance of individual basis states and hence reduce the basis dimension dramatically. The contribution of the neglected configurations can be estimated by using threshold-extrapolation techniques and perturbative estimates of the energy contribution of the neglected configurations. By using the IT-NCSM we solved the eigenvalue problem in this dramatically reduced model space and calculated the energy spectra for ultra-cold Fermi gases at unitarity of up to 20 particles.

We use a HO basis which depends on the HO frequency ω and the maximum basis excitation energy above the lowest allowed configuration $N_{\max}$ and hence the infrared and ultraviolet cutoffs. We introduced several extrapolation techniques in order to analyze these cutoffs. These extrapolation techniques allow us to estimate the corresponding energy (or other observables) for an infinite basis size. Unlike nuclei the ultra-cold quantum gases in a trap are not self-bound systems and hence the dependence on ω is explicit. Therefore, the only truncation affecting the calculated energy and other observables is the model space parameter $N_{\max}$. We extrapolate the energy for $N_{\max} \to \infty$ by using a simple exponential function.

Since we are in the unitary limit we can use a simple contact interaction to describe the interparticle interaction. However this interaction converges very slowly. In order to improve the convergence, two different approaches were introduced: the EFT approach, where the interaction is approximated by a δ-function and its derivatives, and the ABF interaction. The EFT interaction is a contact interaction and hence singular and has to be regularized. For this reason, a momentum cutoff in relative coordinates, which depends on $n_{\max}$, is introduced. The ABF interaction is not a contact interaction and has some connection with Suzuki's unitarity regularization. For the ABF interaction, a model space is constructed with the requirement that the model-space Hamiltonian converges for $2n_{\max} \to \infty$, where $n_{\max}$ is the regularization parameter. We considered the behavior for both interactions with increasing $n_{\max}$, but (other than [1, 33]) we do not extrapolate to infinite $n_{\max}$, since the errors become too large.

We performed IT-NCSM calculations using both interactions. These calculations show good agreement between the IT-NCSM energy spectra and the energy spectra calculated using the full NCSM for those particle numbers and $N_{\max}$ for which we were able to perform the full NCSM calculation. Furthermore, we have shown that the importance-truncation allows the calculation of the energy spectra for higher particle numbers and $N_{\max}$. We compare our results with results obtained using the CG method for the ground state and first excited state. Since the results for CG are only available for up to six particles, we also compared our results for the ground-state energy with results obtained using the FN-DMC method. The results for the first excited state are not available yet using other methods than the IT-NCSM. The IT-NCSM calculation is only limited by the time required to construct the importance-truncated many-body space, while the full NCSM that is limited by the available storage space. The IT-NCSM calculation can be parallelized very easily, achieving almost linear speed-up.

We also used a Gaussian-shaped potential like in the CG and FN-DMC method. Our results show very slow convergence with increasing $N_{\max}$; the HO basis is probably not the best choice for the Gaussian-shaped potential (see section 5.9).

The interactions used here are not restricted to the unitary limit. They can and have been used to describe few-body physics for finite scattering lengths [33, 77, 84]. At low momenta or if the range of the interaction is sufficiently short, then the dominant scattering processes occurs in the s-wave channel and the interaction can be characterized only by the s-wave scattering length. This is the case, for instance, in the BEC regime with finite positive scattering length a_0, where the Fermi gases form tightly bound dimers, and in the BCS regime with finite negative a_0, where they form Cooper pairs with superfluid behavior. The unitary limit is between both regimes in the BCS–BEC crossover with infinite scattering length. The crossover describes the transition between the two different statistical regimes, since the bosons and fermions are described by completely different statistical behavior. Each of these regimes is accessible experimentally as well as the BCS–BEC crossover.

The IT-NCSM can also be applied to multi-component Fermi gases. In comparison to two-component Fermi gases those systems are not necessarily stable against collapse [10]. Also dipolar systems can be investigated using the IT-NCSM. Such systems consisting of magnetic and electric dipoles can be trapped and cooled experimentally. In dipolar gases we have the short-range van-der-Waals interaction and long-range dipole-dipole interaction [6]. Furthermore Bose-Fermi mixtures and ultra-cold Fermi gases with different masses can also be investigated.

These *ab initio* IT-NCSM calculations for Bose-Fermi mixtures or dipolar systems are now enabled through the present work. For our calculation of energy-spectra in ultra-cold limit we had to perform calculations of the matrix elements of the different interactions and implement the importance-truncation scheme. Codes for these calculations previously existed only for nuclei; we have extended their applicability to two-component fermions, which have different quantum numbers and different interactions.

A The Perturbation Theory Approach

In this appendix we briefly describe the many-body perturbation theory used to calculate the correction to the leading order of the EFT interaction. Furthermore we perform the calculation of corrections to the energy and the basis state using multiconfigurational perturbation theory.

A.1 Many-Body Perturbation Theory

Problems which cannot be solved exactly are addressed by approximative methods, such as perturbation theory, a detailed description of which can be found in any textbook on quantum mechanics (for instance, [80, 82]). We want to solve the following eigenvalue problem:

$$\mathrm{H}\left|\psi\right\rangle = \left(H^{(0)} + W\right)\left|\psi\right\rangle = E\left|\psi\right\rangle, \tag{A.1}$$

where the Hamilton operator H is being decomposed into an unperturbed component $H^{(0)}$ and perturbation W. The eigenvalue problem of the unperturbed Hamiltonian

$$\mathrm{H}^{(0)}\left|\psi_n^{(0)}\right\rangle = E_n^{(0)}\left|\psi_n^{(0)}\right\rangle \tag{A.2}$$

with eigenvalues $E_n^{(0)}$ and eigenvectors $\left|\psi_n^{(0)}\right\rangle$ can be solved exactly and is known. In order to solve the problem, we introduce a formal parameter λ multiplying the perturbation component of the Hamilton operator:

$$H = H^{(0)} + \lambda W. \tag{A.3}$$

The eigenstates and eigenenergies can be written as a power series:

$$\left|\psi_n\right\rangle = \left|\psi_n^{(0)}\right\rangle + \lambda\left|\psi_n^{(1)}\right\rangle + \lambda^2\left|\psi_n^{(2)}\right\rangle + \cdots \tag{A.4}$$

$$E_n = E_n^{(0)} + \lambda E_n^{(1)} + \lambda^2 E_n^{(2)} + \cdots. \tag{A.5}$$

The unperturbed states are orthonormalized, that is, $\left\langle\psi_{n'}^{(0)}\middle|\psi_n^{(0)}\right\rangle = \delta_{n'n}$; the unperturbed states and their corrections are orthogonal to each other, that is, $\left\langle\psi_n^{(0)}\middle|\psi_n^{(k)}\right\rangle = \delta_{0,k}$. By inserting equations (A.4) and (A.5) into the Schrödinger equation, we obtain the following equations for the individual orders of λ:

$$\lambda^0 : \mathrm{H}^{(0)}\left|\psi_n^{(0)}\right\rangle = E_n^{(0)}\left|\psi_n^{(0)}\right\rangle \tag{A.6}$$

$$\lambda^1 : \mathrm{H}^{(0)}\left|\psi_n^{(1)}\right\rangle + \mathrm{W}\left|\psi_n^{(0)}\right\rangle = E_n^{(0)}\left|\psi_n^{(1)}\right\rangle + E_n^{(1)}\left|\psi_n^{(0)}\right\rangle \tag{A.7}$$

$$\lambda^2 : \mathrm{H}^{(0)}\left|\psi_n^{(2)}\right\rangle + \mathrm{W}\left|\psi_n^{(1)}\right\rangle = E_n^{(0)}\left|\psi_n^{(2)}\right\rangle + E_n^{(1)}\left|\psi_n^{(1)}\right\rangle + E_n^{(2)}\left|\psi_n^{(0)}\right\rangle \tag{A.8}$$

The correction to the zeroth order energy $E^{(0)}$ can be calculated by projecting equations (A.7) and (A.8) onto the $\left\langle\psi_n^{(0)}\right|$ and using the orthogonality relation $\left\langle\psi_{n'}^{(0)}\middle|\psi_n^{(0)}\right\rangle = \delta_{n'n}$. We perform schematically the calculations for the first- and second-order correction to the energy and for the first correction of the wave function $\left|\psi_n^{(0)}\right\rangle$ for the EFT interaction.

A.2 Perturbation Approach for Correction of an EFT

For the EFT interaction used in the present thesis, we also separate the perturbation into different orders, that is, $\mathrm{W} = \mathrm{V}^{(1)} + \mathrm{V}^{(2)} + \cdots$. The eigenstates and eigenenergies for the EFT interaction can be written as a power series, see eq. (A.4). We therefore obtain for the first- and second-order corrections:

$$\lambda^1 : \mathrm{H}^{(0)} \left|\psi_n^{(1)}\right\rangle + \mathrm{V}^{(1)} \left|\psi_n^{(0)}\right\rangle = E^{(0)} \left|\psi_n^{(1)}\right\rangle + E^{(1)} \left|\psi_n^{(0)}\right\rangle \tag{A.9}$$

$$\lambda^2 : \mathrm{H}^{(0)} \left|\psi_n^{(2)}\right\rangle + \mathrm{V}^{(1)} \left|\psi_n^{(1)}\right\rangle + \mathrm{V}^{(2)} \left|\psi_n^{(0)}\right\rangle = E^{(0)} \left|\psi_n^{(2)}\right\rangle + E^{(1)} \left|\psi_n^{(1)}\right\rangle + E^{(2)} \left|\psi_n^{(0)}\right\rangle \tag{A.10}$$

By projecting eq. (A.9) onto the unperturbed state $\left\langle \psi_n^{(0)}\right|$

$$\left\langle \psi_n^{(0)}\right| \left(H^{(0)} - E^{(0)}\right) \left|\psi_n^{(1)}\right\rangle = \left\langle \psi_n^{(0)}\right| \left(E^{(1)} - V^{(1)}\right) \left|\psi_n^{(0)}\right\rangle, \tag{A.11}$$

we obtain the first-order energy correction:

$$E^{(1)} = \left\langle \psi^{(0)}\right| V^{(1)} \left|\psi^{(0)}\right\rangle, \tag{A.12}$$

where we used that $\left|\psi^{(0)}\right\rangle$ and $\left|\psi^{(1)}\right\rangle$ are orthonormal, so that $\left\langle \psi^{(0)}\middle|\psi^{(1)}\right\rangle = 0$. The derivation for the first-order correction to the wavefunction can be found in [91].

In order to calculate the second-order energy correction, we multiply eq. (A.10) by the unperturbed state $\left\langle \psi^{(0)}\right|$:

$$E_n^{(2)} = \left\langle \psi_n^{(0)}\right| \mathrm{V}^{(1)} \left|\psi_n^{(1)}\right\rangle + \left\langle \psi_n^{(0)}\right| \mathrm{V}^{(2)} \left|\psi_n^{(0)}\right\rangle. \tag{A.13}$$

The second-order correction for EFT has not been used in the present thesis.

A.3 MCPT: Zeroth order and perturbation corrections

We calculate the zeroth-, first- and the second-order contributions to the energy in the frame of Perturbation Theory (see section 4.4.1). We start with the zeroth-order contribution to the energy:

$$\mathrm{H}_0 \left|\psi_{\mathrm{ref}}\right\rangle = \epsilon^{(0)} \left|\psi_{\mathrm{ref}}\right\rangle \tag{A.14}$$

with the unperturbed Hamiltonian H_0 defined in eq. (4.20). Multiplication of eq. (A.14) with $\left\langle \psi_{\mathrm{ref}}\right|$ yields:

$$\epsilon^{(0)} = \left\langle \psi_{\mathrm{ref}}\right| \mathrm{H}_0 \left|\psi_{\mathrm{ref}}\right\rangle = \epsilon_{\mathrm{ref}}. \tag{A.15}$$

For the first order correction we have to multiply

$$\mathrm{H}_0 \left|\psi^{(1)}\right\rangle + \mathrm{W} \left|\psi_{\mathrm{ref}}\right\rangle = \epsilon_{\mathrm{ref}} \left|\psi^{(1)}\right\rangle + E^1 \left|\psi_{\mathrm{ref}}\right\rangle \tag{A.16}$$

with the reference state $\left|\psi_{\mathrm{ref}}\right\rangle$ and obtain

$$\left\langle \psi_{\mathrm{ref}}\right| \mathrm{H}_0 \left|\psi^{(1)}\right\rangle + \left\langle \psi_{\mathrm{ref}}\right| \mathrm{W} \left|\psi_{\mathrm{ref}}\right\rangle = \epsilon_{\mathrm{ref}} \left\langle \psi_{\mathrm{ref}}\middle|\psi^{(1)}\right\rangle + E^1 \left\langle \psi_{\mathrm{ref}}\middle|\psi_{\mathrm{ref}}\right\rangle. \tag{A.17}$$

We can set $\left|\psi_n^{(1)}\right\rangle = \sum_{\mu \notin \mathscr{M}_{\mathrm{ref}}} c_\mu^{(1)} \left|\phi_\mu\right\rangle$ and calculate first

$$\left\langle \psi_{\mathrm{ref}}\middle|\psi^{(1)}\right\rangle = \sum_{\mu \notin \mathscr{M}_{\mathrm{ref}}} c_\mu^{(1)} \left\langle \psi_{\mathrm{ref}}\middle|\phi_\mu\right\rangle = \sum_{\nu \in \mathscr{M}_{\mathrm{ref}}} c_\nu^{(0)} \sum_{\mu \notin \mathscr{M}_{\mathrm{ref}}} c_\mu^{(1)} \left\langle \phi_\nu\middle|\phi_\mu\right\rangle = 0. \tag{A.18}$$

In the last step, we used that the states ϕ_μ outside $\mathscr{M}$ do not contribute to the reference state and hence ϕ_μ and $\langle \Psi_{\text{ref}}|$ are orthogonal.

For the matrix elements of H_0 between the basis states $\phi_\nu \notin \mathscr{M}_{\text{ref}}$ and ψ_{ref} we obtain

$$\langle \psi_{\text{ref}}| \mathrm{H}_0 |\psi^{(1)}\rangle = \langle \psi_{\text{ref}}| \epsilon_{\text{ref}} |\psi_{\text{ref}}\rangle \sum_{\nu\notin\mathscr{M}_{\text{ref}}} c_\nu \langle \psi_{\text{ref}}|\phi_\nu\rangle + \sum_{\nu\notin\mathscr{M}_{\text{ref}}} \epsilon_\nu \langle \psi_{\text{ref}}|\phi_\nu\rangle \langle \phi_\nu|\psi^{(1)}\rangle = 0. \quad \text{(A.19)}$$

Therefore,

$$\epsilon^{(1)} = \langle \psi_{\text{ref}}| \mathrm{W} |\psi_{\text{ref}}\rangle = \langle \psi_{\text{ref}}| \mathrm{H} |\psi_{\text{ref}}\rangle - \langle \psi_{\text{ref}}| \mathrm{H}_0 |\psi_{\text{ref}}\rangle = 0 \quad \text{(A.20)}$$

is the first-order contribution to the energy.

We get the first order correction to the many-body state by multiplying eq. (A.16) with the state $\langle \phi_\mu| \notin \mathscr{M}_{\text{ref}}$:

$$\langle \phi_\mu| \mathrm{H}_0 |\psi^{(1)}\rangle + \langle \phi_\mu| \mathrm{W} |\psi_{\text{ref}}\rangle = \langle \phi_\mu| \epsilon_{\text{ref}} |\psi^{(1)}\rangle + \langle \phi_\mu| \epsilon^{(1)} |\psi_{\text{ref}}\rangle \quad \text{(A.21)}$$

It holds that

$$\langle \phi_\mu|\psi^{(1)}\rangle = \sum_{\nu\notin\mathscr{M}_{\text{ref}}} c_\nu \langle \phi_\mu|\phi_\nu\rangle = c_\nu. \quad \text{(A.22)}$$

For the matrix elements of H_0 between the basis states ϕ_ν and $\psi^{(1)}$, we obtain:

$$\begin{aligned}\langle \phi_\mu| \mathrm{H}_0 |\psi^{(1)}\rangle &= \langle \phi_\mu| \left(\epsilon_{\text{ref}} |\psi_{\text{ref}}\rangle\langle \psi_{\text{ref}}| + \sum_{\nu\notin\mathscr{M}_{\text{ref}}} \epsilon_\nu |\phi_\nu\rangle\langle \phi_\nu| \right) |\psi^{(1)}\rangle \\ &= \sum_{\nu\notin\mathscr{M}_{\text{ref}}} \epsilon_\nu \langle \phi_\mu|\phi_\nu\rangle \sum_{\nu\notin\mathscr{M}_{\text{ref}}} c_{\nu'} \langle \phi_\nu|\phi_{\nu'}\rangle \\ &= \epsilon_\mu c_\mu \end{aligned} \quad \text{(A.23)}$$

We used here again that the reference state is orthogonal to the state outside of the reference space $\mathscr{M}_{\text{ref}}$. Hence we get

$$c_\mu \left(\epsilon_\mu - \epsilon_{\text{ref}}\right) = -\langle \phi_\mu| \mathrm{W} |\psi_{\text{ref}}\rangle \quad \text{(A.24)}$$

and consequently

$$|\psi_n^{(1)}\rangle = \sum_{\mu\notin\mathscr{M}_{\text{ref}}} c_\mu |\phi_\mu\rangle = -\sum_{\mu\notin\mathscr{M}_{\text{ref}}} \frac{\langle \phi_\mu| \mathrm{W} |\psi_{\text{ref}}\rangle}{\epsilon_\mu - \epsilon_{\text{ref}}} |\phi_\mu\rangle \quad \text{(A.25)}$$

as the first-order correction to the reference state.

For the second-order contribution to the energy, we get the equation

$$\mathrm{H}_0 |\phi^{(2)}\rangle + \mathrm{W} |\phi^{(1)}\rangle = \epsilon^{(0)} |\phi^{(2)}\rangle + \epsilon^{(1)} |\phi^{(1)}\rangle + \epsilon^{(2)} |\phi^{(0)}\rangle, \quad \text{(A.26)}$$

with the second-order correction to the eigenstate of the Hamiltonian being

$$\psi_n^{(2)} = \sum_{\mu\notin\mathscr{M}_{\text{ref}}} c_\mu |\phi_\mu\rangle . \quad \text{(A.27)}$$

Projecting eq. (A.26) onto the state $\langle \psi_{\text{ref}}|$ yields:

$$\epsilon^{(2)} = \langle \psi_{\text{ref}}| \mathrm{W} |\phi^{(1)}\rangle = -\sum_{\mu\notin\mathscr{M}_{\text{ref}}} \frac{\left|\langle \phi_\mu| \mathrm{W} |\psi_{\text{ref}}\rangle\right|^2}{\epsilon_\mu - \epsilon_{\text{ref}}} = -\sum_{\mu\notin\mathscr{M}_{\text{ref}}} \frac{\left|\langle \phi_\mu| \mathrm{H} |\psi_{\text{ref}}\rangle\right|^2}{\epsilon_\mu - \epsilon_{\text{ref}}} \quad \text{(A.28)}$$

We used here again that the states $|\phi_\nu\rangle$ outside of the reference space and the reference state $|\psi_{\text{ref}}\rangle$ are orthogonal and as well as for the first order the matrix elements of H_0 between the basis states $|\phi_\nu\rangle$ and $|\psi^{(2)}\rangle$ vanishes.

B EFT

In section 3.6 we introduced the interaction constructed using the effective field theory approach [91] we used for our IT-NCSM calculations. In this appendix we show in detail the derivation of some equations we need for the derivation of the matrix elements of the interaction.

B.1 EFT: Fourier Transformation

In the EFT approach, the interparticle short-range two-body interaction, eq. (3.46), can be expanded as a Taylor series in momentum space (see chapter 3.6). In this section, we perform the Fourier transformation of this potential, eq. (3.46), in momentum space into the coordinate space, eq. (3.47). We also show here the transformation of the potential in coordinate space from the eq. (3.47) to the eq. (3.48) by using the locality of the potential.

The potential in coordinate space is given by

$$V\left(\vec{r}',\vec{r}\right) = \left\langle \vec{r}' \middle| V \middle| \vec{r} \right\rangle = \iint d^3p' d^3p \left\langle \vec{r}' \middle| \vec{p}' \right\rangle \left\langle \vec{p}' \middle| V \middle| \vec{p} \right\rangle \left\langle \vec{p} \middle| \vec{r} \right\rangle \tag{B.1}$$

where we work in relative coordinates. We insert the momentum function in coordinate space [72, 82]:

$$\phi_{\vec{p}}(\vec{x}) = \left\langle \vec{x} \middle| \vec{p} \right\rangle = \frac{1}{(2\pi\hbar)^{3/2}} \exp\left(\frac{i}{\hbar}\vec{p}\cdot\vec{x}\right) \tag{B.2}$$

and get

$$V\left(\vec{r}',\vec{r}\right) = \frac{1}{(2\pi\hbar)^3} \iint d^3p' d^3p \exp\left(\frac{i}{\hbar}\vec{p}'\cdot\vec{x}'\right) \left(C_0 + C_2\left(\vec{p}'^2 + \vec{p}^2\right) + C_4\left(\vec{p}'^2 + \vec{p}^2\right)^2 + \ldots\right) \exp\left(\frac{i}{\hbar}\vec{p}\cdot\vec{x}\right). \tag{B.3}$$

We evaluate each order separately (LO and NLO). We start with the LO term:

$$\begin{aligned} V^{(0)}(\vec{r}',\vec{r}) &= \iint d^3p' d^3p \frac{1}{\left(2\pi\hbar^{3/2}\right)^2} \exp\left(-\frac{i}{\hbar}\vec{p}'\cdot\vec{r}'\right) C_0 \exp\left(\frac{i}{\hbar}\vec{p}\cdot\vec{r}\right) \\ &= \frac{C_0}{\left(2\pi\hbar^{3/2}\right)^2} \int d^3p' \exp\left(-\frac{i}{\hbar}\vec{p}'\cdot\vec{r}'\right) \int d^3p \exp\left(\frac{i}{\hbar}\vec{p}\cdot\vec{r}\right) \\ &= C_0\delta^3(\vec{r}')\delta^3(\vec{r}) \end{aligned} \tag{B.4}$$

where we used in last step

$$\int d^3p \exp\left\{\frac{i}{\hbar}(\vec{x}'-\vec{x})\cdot\vec{p}\right\} = (2\pi\hbar)^3\delta^3(\vec{x}'-\vec{x}). \tag{B.5}$$

In spherical coordinates, the δ-function takes the form

$$\begin{aligned} \delta\left(\vec{x}-\vec{x}'\right) &= \frac{1}{r^2 sin\theta}\delta\left(r-r'\right)\delta\left(\theta-\theta'\right)\delta\left(\phi-\phi'\right) \\ &= \frac{1}{r^2}\delta\left(r-r'\right)\delta\left(cos(\theta)-cos(\theta')\right)\delta\left(\phi-\phi'\right) \end{aligned} \tag{B.6}$$

Inserting the δ-function, we get for each integral of the LO part:

$$\begin{aligned}\int d^3r\,\delta(\vec{r})\phi(\vec{r}) &= \int_0^\infty\int_0^{2\pi}\int_0^\pi \frac{1}{r^2\sin\theta}\delta(r)\delta(\theta)\delta(\varphi)\phi(r,\theta,\varphi)2\pi r^2\sin(\theta)d\theta d\varphi dr\\ &= 2\pi\int_0^\infty\int_0^{2\pi}\int_0^\pi \delta(r)\delta(\cos(\theta))\delta(\varphi)\phi(r,\theta,\varphi)d\cos(\theta)d\varphi dr\\ &= \int_0^\infty \delta^3(r)\phi(r)dr\\ &= \phi(0)\end{aligned} \tag{B.7}$$

In the last step we used the rotational symmetry of the potential and integrated the δ-function. Hence we get for the LO part of the EFT potential:

$$V^{(0)}_{n,n'} = C_0\phi^*(0)\phi(0) \tag{B.8}$$

We continue with the NLO term:

$$\begin{aligned}V^{(1)}(\vec{r}',\vec{r}) &= \iint d^3p'd^3p\,\phi^*_{\vec{p}}(\vec{r}\,')C_2\left(\vec{p}\,'^2+\vec{p}^{\,2}\right)\phi_{\vec{p}}(\vec{r}) \qquad\text{(B.9)}\\ &= C_2\iint d^3p'd^3p\,\frac{1}{\left(2\pi\hbar^{3/2}\right)^2}\exp\left(-\frac{i}{\hbar}\vec{p}\,'\cdot\vec{r}'\right)\left(\vec{p}\,'^2+\vec{p}^{\,2}\right)\exp\left(\frac{i}{\hbar}\vec{p}\cdot\vec{r}\right)\end{aligned}$$

Using

$$-i\hbar\nabla\left\langle\vec{x}\middle|\vec{p}\right\rangle = \vec{p}\left\langle\vec{x}\middle|\vec{p}\right\rangle \tag{B.10}$$

yields the NLO part of the interparticle two-body potential in the coordinate space

$$\begin{aligned}V^{(1)}(\vec{r}',\vec{r}) &= \frac{C_2}{\left(2\pi\hbar^{3/2}\right)^2}\left(\frac{i}{\hbar}\right)^2\\ &\cdot\iint d^3p'd^3p\left\{\left[\nabla^2_{\vec{r}'}\exp\left(\frac{i}{\hbar}\vec{p}\,'\cdot\vec{r}'\right)\right]\exp\left(\frac{i}{\hbar}\vec{p}\cdot\vec{r}\right)+\exp\left(\frac{i}{\hbar}\vec{p}\,'\cdot\vec{r}'\right)\left[\nabla^2_{\vec{r}}\exp\left(\frac{i}{\hbar}\vec{p}\cdot\vec{r}\right)\right]\right\}\\ &= -C_2\frac{1}{\hbar^2}\left\{\left[\nabla^2\delta(\vec{r}')\right]\delta(\vec{r})+\delta(\vec{r}')\left[\nabla^2\delta(\vec{r})\right]\right\}.\end{aligned} \tag{B.11}$$

Higher orders can be transformed in the same way and we get eq. (3.48).

The interaction potential of the system is local and depend only on the momentum transfer $\tilde{\vec{p}} = \vec{p}-\vec{p}\,'$. Therefore we get for the LO term:

$$\begin{aligned}V^{(0)}(\vec{r}',\vec{r}) &= \iint d^3\tilde{p}d^3p\,\frac{1}{\left(2\pi\hbar^{3/2}\right)^2}\exp\left(-\frac{i}{\hbar}(\vec{p}-\tilde{\vec{p}})\cdot\vec{r}'\right)C_0\exp\left(\frac{i}{\hbar}\vec{p}\cdot\vec{r}\right)\\ &= C_0\iint d^3\tilde{p}d^3p\,\frac{1}{\left(2\pi\hbar^{3/2}\right)^2}\exp\left(\frac{i}{\hbar}\tilde{\vec{p}}\cdot\vec{r}'\right)\exp\left(\frac{i}{\hbar}\vec{p}\cdot(\vec{r}-\vec{r}')\right)\\ &= C_0\delta(\vec{r}')\delta(\vec{r}-\vec{r}')\end{aligned} \tag{B.12}$$

Furthermore, using the locality of the potential $V^{(0)}(\vec{r}',\vec{r}) = V^{(0)}(\vec{r})\delta(\vec{r}-\vec{r}')$ we can write

$$V^{(0)}(\vec{r}) = C_0\delta(\vec{r}) \tag{B.13}$$

Now we rewrite the NLO term of the potential

$$V^{(1)}(\vec{r}',\vec{r}) = \left\langle \vec{r}' \middle| V^{(1)} \middle| \vec{r} \right\rangle = \iint d^3p'\, d^3p \left\langle \vec{r}' \middle| \vec{p}' \right\rangle \left\langle \vec{p}' \middle| V^{(1)} \middle| \vec{p} \right\rangle \left\langle \vec{p} \middle| \vec{r} \right\rangle$$
$$= \iint d^3p'\, d^3p \left\langle \vec{r}' \middle| \vec{p}' \right\rangle C_2 \left(\vec{p}'^2 + \vec{p}^2\right) \left\langle \vec{p} \middle| \vec{r} \right\rangle \tag{B.14}$$

We use again that the local potential is only depends on the momentum transfer $\tilde{\vec{p}} = \vec{p}' - \vec{p}$

$$\begin{aligned} V^{(1)}(\vec{r}',\vec{r}) &= \frac{C_2}{\left(2\pi\hbar^{3/2}\right)^2} \iint d^3p' d^3p \, \exp\left(-\frac{i}{\hbar}\vec{p}'\cdot\vec{r}'\right)\left(\vec{p}'^2+\vec{p}^2\right)\exp\left(\frac{i}{\hbar}\vec{p}\cdot\vec{r}\right) \\ &= \frac{C_2}{\left(2\pi\hbar^{3/2}\right)^2} \iint d^3\tilde{p} d^3p \, \exp\left(\frac{i}{\hbar}\left(\tilde{\vec{p}}-\vec{p}\right)\cdot\vec{r}'\right)\left(\left(\tilde{\vec{p}}-\vec{p}\right)^2+\vec{p}^2\right)\exp\left(\frac{i}{\hbar}\vec{p}\cdot\vec{r}\right) \\ &= \frac{C_2}{\left(2\pi\hbar^{3/2}\right)^2} \iint d^3\tilde{p} d^3p \, \exp\left(\frac{i}{\hbar}\tilde{\vec{p}}\cdot\vec{r}'\right)\left(\tilde{\vec{p}}^2-2\tilde{\vec{p}}\vec{p}+2\vec{p}^2\right)\exp\left(\frac{i}{\hbar}\vec{p}\cdot\left(\vec{r}-\vec{r}'\right)\right) \\ &= \frac{C_2}{\left(2\pi\hbar^{3/2}\right)^2} \left\{\left[\nabla^2\delta(\vec{r}')\right]\delta\left(\vec{r}-\vec{r}'\right) - 2\left[\nabla\delta(\vec{r}')\right]\left[\nabla\delta\left(\vec{r}-\vec{r}'\right)\right] + \delta(\vec{r}')\left[\nabla^2\delta\left(\vec{r}-\vec{r}'\right)\right]\right\}. \end{aligned} \tag{B.15}$$

In the last step we used the definition (B.10). Now we can use integration by parts

$$\int d^3r \left[\nabla^n\delta(\vec{r})\right]\psi(\vec{r}) = (-1)^n \int d^3r \, \delta(\vec{r})\left[\nabla^n\psi(\vec{r})\right] \tag{B.16}$$

since the boundary term vanishes, hence symbolically

$$\left[\nabla^n\delta(\vec{r})\right]\psi(\vec{r}) = (-1)^n\delta(\vec{r})\left[\nabla^n\psi(\vec{r})\right]. \tag{B.17}$$

Therefore, for the NLO correction to the local potential and its rotational symmetry (see LO part) we get

$$V^{(1)}(\vec{r}',\vec{r}) = V^{(1)}(\vec{r})\delta\left(\vec{r}-\vec{r}'\right) = C_2\delta\left(\vec{r}-\vec{r}'\right)\left\{\left[\nabla^2\delta(\vec{r}')\right] + 2\left[\nabla\delta(\vec{r}')\right]\nabla + \delta(\vec{r}')\nabla^2\right\} \tag{B.18}$$

B.2 Calculation of the Leading Order Constant

For our calculation of the energy in LO we need to determine the coupling constant at LO $C_0^{(0)}$, which we do in section 3.6.1. In this section we show some intermediate steps of the calculation. We start with eq. (3.63) and set, in the following, $\epsilon = {}^{E^{(0)}}/_{(\hbar\omega)}$. Therefore, the denominator can be rewritten as

$$\begin{aligned} \frac{1}{\epsilon/2-(n+3/4)} &= \frac{n+1/2}{(n+1/2)(\epsilon/2-3/4-n)} \\ &= -\frac{n+1/2+1/4-\epsilon/2-1/4+\epsilon/2}{(n+1/2)(-\epsilon/2+3/4+n)} \\ &= -\frac{1}{n+1/2} + \frac{1/4-\epsilon/2}{(n+1/2)(a+n)}, \end{aligned} \tag{B.19}$$

where a has been set to $3/4-\epsilon/2$ in the last step. Therefore, the following equation holds for the coefficient C_0:

$$\frac{1}{C_0^{(0)}} = \frac{1}{2\pi^{3/2}a_{\mathrm{HO},\mu}^3\hbar\omega}\left[-\sum_{n=0}^{n_{\max}}\frac{L_n^{(1/2)}(0)}{n+1/2} + \frac{1-2\epsilon}{4}\sum_{n=0}^{n_{\max}}\frac{L_n^{(1/2)}(0)}{(n+1/2)(a+n)}\right] \tag{B.20}$$

Using the following identities for sums involving the generalized Laguerre polynomials at the origin:

$$\sum_{n=0}^{m}\frac{L_n^{(1/2)}(0)}{n+1/2} = \frac{4}{\sqrt{\pi}}\frac{\Gamma(m+3/2)}{\Gamma(m+1)} \tag{B.21}$$

and

$$\begin{aligned}\sum_{n=0}^{m}\frac{L_n^{(1/2)}(0)}{(n+1/2)(n+a)^2} = 2\sqrt{\pi}\Bigg[&\frac{\Gamma(a)}{\Gamma(a+1/2)} - \frac{\Gamma(n_{\max}+3/2)}{\Gamma(n_{\max}+2)} \\ &\cdot \frac{{}_3F_2(1, n_{\max}+3/2, a+n_{\max}+1; n_{\max}+2, a+n_{\max}+2; 1)}{\pi(a+n_{\max}+1)}\Bigg],\end{aligned} \tag{B.22}$$

where ${}_3F_2$ is the generalized hypergeometric function, eq. (B.20) becomes

$$\begin{aligned}\frac{1}{C_0^{(0)}} = -\frac{\mu}{2\hbar^3\pi^{3/2}a_{\mathrm{HO},\mu}}\Bigg\{&\frac{4}{\sqrt{\pi}}\frac{\Gamma(n_{\max}+3/2)}{\Gamma(n_{\max}+1)} - \frac{1-2\epsilon}{4}2\sqrt{\pi}\Bigg[\frac{\Gamma(a)}{\Gamma(a+1/2)} \\ &- \frac{\Gamma(n_{\max}+3/2)}{\Gamma(n_{\max}+2)}\frac{{}_3F_2(1, n_{\max}+3/2, a+n_{\max}+1; n_{\max}+2, a+n_{\max}+2; 1)}{\pi(a+n_{\max}+1)}\Bigg]\Bigg\}.\end{aligned} \tag{B.23}$$

By definition, $\Gamma(n+1) = n\Gamma(n)$, so that

$$\begin{aligned}\frac{1}{C_0^{(0)}} = -\frac{2}{\pi^2 a_{\mathrm{HO},\mu}^3\hbar\omega}\Bigg\{&\frac{\Gamma(n_{\max}+3/2)}{\Gamma(n_{\max}+1)} - \frac{1-2\epsilon}{8}\pi \\ &\cdot\left[\frac{\Gamma(a)}{(a-1/2)\Gamma(a-1/2)} - \frac{\Gamma(n_{\max}+3/2)}{(n_{\max}+1)\Gamma(n_{\max}+1)}\frac{{}_3F_2(\ldots)}{\pi(a+n_{\max}+1)}\right]\Bigg\}.\end{aligned} \tag{B.24}$$

Inserting $a = 3/4 - \epsilon/2$ yields, after several transformation steps,

$$\frac{1}{C_0^{(0)}} = -\frac{2}{\pi^2 a_{\mathrm{HO},\mu}^3\hbar\omega}\left\{\frac{\Gamma(n_{\max}+3/2)}{\Gamma(n_{\max}+1)}\left[1+R\left(n_{\max}, \epsilon/2\right)\right] - \frac{\pi}{2}\frac{\Gamma\left(3/4-\epsilon/2\right)}{\Gamma\left(1/4-\epsilon/2\right)}\right\} \tag{B.25}$$

with

$$R(m, \epsilon/2) = \frac{1-2\epsilon}{8(m+1)(m+7/4-\epsilon/2)}\,{}_3F_2\left(1, m+3/2, m+7/4-\epsilon/2; m+2, m+11/4-\epsilon/2; 1\right), \tag{B.26}$$

where ${}_3F_2$ is the generalized hypergeometric function. We use this equation to calculate the LO coefficient $C_0^{(0)}$.

B.3 NLO Contribution to the Energy

In oder to calculate the NLO coupling constants we need to derive the first-order energy correction $E^{(1)}$. In this section, we derive first the first-order correction (NLO) to the energy $E^{(1)}$, eq. (3.72), by using first-order perturbation theory. We start with the first-order correction equation (A.9)

$$\left(H^{(0)} - E^{(0)}\right)\psi_n^{(1)}(\vec{r}) = \left(E^{(1)} - V^{(1)}\right)\psi_n^{(0)}(\vec{r}) \tag{B.27}$$

in the appendix A.2. Projecting the first-order correction to the Schrödinger equation (A.9) on a state $\left\langle \psi^{(0)}\right|$ yields the NLO correction to the energy, eq. (B.33) (see appendix A.2 for more details): Inserting the NLO correction to the potential equation (3.57), we get:

$$\begin{aligned}\left\langle \psi^{(0)}\right| V^{(1)} \left|\psi^{(0)}\right\rangle &= \int d^3r \psi^{(0)*}(\vec{r}) V(\vec{r}) \psi^{(0)}(\vec{r}) \\ &= \int d^3r \psi^{(0)*}(\vec{r}) C_0^{(1)} \delta(\vec{r}) \psi^{(0)}(\vec{r}) \\ &\quad - C_2^{(1)} \int d^3r \psi^{(0)*}(\vec{r}) \left\{ [\nabla^2 \delta(\vec{r})] + 2[\vec{\nabla}\delta(\vec{r})]\vec{\nabla} + 2\delta(\vec{r})\nabla^2 \right\} \psi^{(0)}(\vec{r}).\end{aligned} \tag{B.28}$$

We calculate each term of eq. (B.28) separately and start with the term containing $C_0^{(1)}$:

$$\int d^3r \psi^{(0)*}(\vec{r}) C_0^{(1)} \delta(\vec{r}) \psi^{(0)}(\vec{r}) = C_0^{(1)} \int dr \psi^{(0)*}(r) \delta(r) \psi^{(0)}(r) = C_0^{(1)} \psi^{(0)*}(0) \psi^{(0)}(0), \tag{B.29}$$

again using the translational symmetry of the potential. We continue with the $C_2^{(1)}$ part of eq. (B.28) and also evaluate each part separately by using the translational symmetry of the potential and the integration by parts eq. (B.16) For the first term of the $C_2^{(1)}$ part of eq. (B.28), we get:

$$\begin{aligned}&\int d^3r \psi^{(0)*}(\vec{r}) [\nabla^2 \delta(\vec{r})] \psi^{(0)}(\vec{r}) \\ &\quad = \int dr \delta(r) \nabla^2 \left[\psi^{(0)*}(r) \psi^{(0)}(r) \right] \\ &\quad = \int dr \delta(r) \left[[\nabla^2 \psi^{(0)*}(r)] \psi^{(0)}(r) + 2[\nabla \psi^{(0)*}(r)][\nabla \psi^{(0)}(r)] + \psi^{(0)*}[\nabla^2 \psi^{(0)}(r)] \right] \\ &\quad = [\nabla^2 \psi^{(0)*}(r)]_{r=0} \psi^{(0)}(0) + 2[\nabla \psi^{(0)}(r)]_{r=0} [\nabla \psi^{(0)}(r)]_{r=0} + \psi^{(0)*}(0) [\nabla^2 \psi^{(0)}(r)]_{r=0}.\end{aligned} \tag{B.30}$$

For the second term of the $C_2^{(1)}$ part of eq. (B.28) we get:

$$\begin{aligned}&2 \int d^3r \psi^{(0)*}(\vec{r}) [\vec{\nabla}\delta(\vec{r})] \vec{\nabla} \psi^{(0)}(\vec{r}) \\ &\quad = -2 \int dr \delta(r) \nabla \left[\psi^{(0)*}(r) \nabla \psi^{(0)}(r) \right] \\ &\quad = -2 \int dr \delta(r) \left[[\nabla \psi^{(0)*}(r)][\nabla \psi^{(0)}(r)] + \psi^{(0)*}(r) [\nabla^2 \psi^{(0)}(r)] \right] \\ &\quad = -2 [\nabla \psi^{(0)*}(r)]_{r=0} [\nabla \psi^{(0)}(r)]_{r=0} - 2\psi^{(0)*}(0) [\nabla^2 \psi^{(0)}(r)]_{r=0},\end{aligned} \tag{B.31}$$

and for the last term of eq. (B.28), we get:

$$2\int d^3r\psi^{(0)*}(\vec{r})\delta(\vec{r})\left[\nabla^2\psi^{(0)}(\vec{r})\right] = 2\psi^{(0)*}(0)[\nabla^2\psi^{(0)}(r)]_{r=0} \tag{B.32}$$

All parts with $C_0^{(n)}$ and $C_2^{(n)}$ can be evaluated in a similar way, where n is the order. We summarize all terms with the coefficient $C_0^{(1)}$ and the three with the coefficient $C_2^{(1)}$ of eq. (B.28) and get as the NLO correction to the energy:

$$\begin{aligned} E^{(1)} &= \left\langle \psi^{(0)} \middle| V^{(1)} \middle| \psi^{(0)} \right\rangle \\ &= C_0^{(1)}\psi^{(0)2}(0) - C_2^{(1)}\left\{\left[\nabla^2\psi^{(0)}(r)\right]_{r=0}\psi^{(0)}(0) + \psi^{(0)}(0)\left[\nabla^2\psi^{(0)}(r)\right]_{r=0}\right\} \end{aligned} \tag{B.33}$$

If we apply the non-interacting Hamiltonian defined in eq. (3.26) to the wave function $\psi(\vec{r})$ we get

$$\frac{1}{2}\left[-\frac{\hbar^2}{\mu}\vec{\nabla}_r^2 + \mu\omega^2\vec{r}^2\right]\psi(\vec{r}) = H_0\sum_{n,l=0}^{e_{rel}\to\infty}\sum_{m=-l}^{l} c_{nlm}\phi_{nlm} = \sum_{n,l=0}^{e_{rel}\to\infty}\sum_{m=-l}^{l} c_{nlm}E_{nl}\phi_{nlm} \tag{B.34}$$

where we used equations (3.27) and (3.28). We are in the unitary limit with $l = 0$, hence for $r \to 0$ we arrive at

$$\hbar^2\left[\nabla^2\psi^{(0)}(r)\right]_{r=0} = -2\mu\sum_n c_n^{(0)}E_n\phi_n(0) = 2\mu\left[E^{(0)}\psi^{(0)}(0) + \kappa^{(0)}\sum_n\psi_n^2(0)\right]. \tag{B.35}$$

In the last step we use eq. (3.61) and $\psi_n(\vec{r}) = \sum_n c_n\phi_n(\vec{r})$. Inserting this into eq. (B.33), we get for the first-order correction to the energy:

$$\begin{aligned} E^{(1)} &= C_0^{(1)}\left(\psi^{(0)}(0)\right)^2 - \frac{4\mu C_2^{(1)}}{\hbar^2}\psi^{(0)}(0)\left[-E^{(0)}\psi^{(0)}(0) + \kappa^{(0)}\sum_n\phi_n^2(0)\right] \\ &= \frac{\left(\kappa^{(0)}\right)^2}{\left(C_0^{(0)}\right)^2}\left\{C_0^{(1)} + \frac{4\mu C_2^{(1)}}{\hbar^2}\left[E^{(0)} - \frac{C_0^{(0)}}{\pi^{3/2}a_{\mathrm{HO},\mu}^3}\sum_n L_n^{(1/2)}(0)\right]\right\}. \end{aligned} \tag{B.36}$$

Furthermore, we can use the identity [91]

$$\sum_{n=0}^{m} L_n^{(1/2)}(0) = \frac{4}{3\sqrt{\pi}}\frac{\Gamma(m+5/2)}{\Gamma(m+1)} \tag{B.37}$$

and get

$$E^{(1)} = \frac{\left(\kappa^{(0)}\right)^2}{\left(C_0^{(0)}\right)^2}\left\{C_0^{(1)} + \frac{4\mu C_2^{(1)}}{\hbar^2}\left[E^{(0)} - \frac{4C_0^{(0)}}{3\pi^2 a_{\mathrm{HO},\mu}^3}\frac{\Gamma\left(n_{\max}+5/2\right)}{\Gamma\left(n_{\max}+1\right)}\right]\right\} \tag{B.38}$$

as the first-order correction to the energy.

B.4 Calculation of the Next-to-Leading Order Constant

We calculate in this appendix the NLO coefficients $C_0^{(1)}$ and $C_2^{(1)}$ by inserting the first-order energy correction into eq. (3.71) [91]. Previously we show the derivation of the parameter $\kappa^{(0)}$ we need for the calculation of both parameters. Using the orthogonality of the wave function $\psi^{(0)}$ we get:

$$\left\langle \psi^{(0)} \middle| \psi^{(0)} \right\rangle = \sum_{n}^{n_{\max}} \sum_{n'}^{n'_{\max}} c_n c_{n'} \left\langle n \middle| n' \right\rangle = \sum_{n}^{n_{\max}} \sum_{n'}^{n'_{\max}} \left(\kappa^{(0)}\right)^2 \frac{\phi_n(0)}{E_i^{(0)} - E_n} \frac{\phi_{n'}(0)}{E_i^{(0)} - E_{n'}} \delta_{n,n'} = 1, \tag{B.39}$$

where we used for the wave function eq. (3.32) since the interaction acts only on the s-wave and the eq. (3.61) for the coefficients c_n and $c_{n'}$. Therefore, we can write for the parameter $\kappa^{(0)}\left(E_i^{(0)}\right)$

$$\left[\kappa^{(0)}\left(E_i^{(0)}\right)\right]^{-2} = \sum_{n}^{n_{\max}} \frac{\phi_n^2(0)}{(E_i^{(0)} - E_n)^2}, \tag{B.40}$$

where we use the notation $\kappa^{(0)}\left(E_i^{(0)}\right)$ since the parameter $\kappa^{(0)}$ depends on the Energy.

Now we use the eq. (3.72) in order to determine the both NLO constants. First we determine the coefficient $C_2^{(1)}$:

$$E_1^{(1)} / \left[\kappa^{(0)}\left(E_1^{(0)}\right)\right]^2 - E_0^{(1)} / \left[\kappa^{(0)}\left(E_0^{(0)}\right)\right]^2 = \frac{4\mu C_2^{(1)}}{\hbar^2 C_0^{(0)2}} \left(E_1^{(0)} - E_0^{(0)}\right) \tag{B.41}$$

Rearranging the formula yields [91]

$$\frac{4\mu C_2^{(1)}}{\hbar^2 C_0^{(0)2}} = \frac{E_1^{(1)} / \left[\kappa^{(0)}\left(E_1^{(0)}\right)\right]^2 - E_0^{(1)} / \left[\kappa^{(0)}\left(E_0^{(0)}\right)\right]^2}{E_1^{(0)} - E_0^{(0)}}. \tag{B.42}$$

Second, we determine the coefficient $C_0^{(1)}$ in a similar way:

$$\begin{aligned}
&E_0^{(0)} E_1^{(1)} / \left[\kappa^{(0)}\left(E_1^{(0)}\right)\right]^2 - E_1^{(0)} E_0^{(1)} / \left[\kappa^{(0)}\left(E_0^{(0)}\right)\right]^2 \\
&= \frac{C_0^{(1)}}{\left(C_0^{(0)}\right)^2} \left(E_0^{(0)} - E_1^{(0)}\right) \\
&+ \frac{4\mu C_2^{(1)}}{\left(C_0^{(0)}\right)^2 \hbar^2} \left[E_0^{(0)} E_1^{(0)} - E_1^{(0)} E_0^{(0)} - \frac{4C_0^{(0)}}{3\pi^2 a_{\mathrm{HO},\mu}^3} \frac{\Gamma\left(n_{\max} + 5/2\right)}{\Gamma\left(n_{\max} + 1\right)} \left(E_0^{(0)} - E_1^{(0)}\right)\right] \\
&= \frac{-\left(E_1^{(0)} - E_0^{(0)}\right)}{\left(C_0^{(0)}\right)^2} \left[C_0^{(1)} - \frac{4\mu C_2^{(1)}}{\hbar^2} \frac{4C_0^{(0)}}{3\pi^2 a_{\mathrm{HO},\mu}^3} \frac{\Gamma\left(n_{\max} + 5/2\right)}{\Gamma\left(n_{\max} + 1\right)}\right] \\
&= -\frac{E_1^{(1)} / \left[\kappa^{(0)}\left(E_1^{(0)}\right)\right]^2 - E_0^{(1)} / \left[\kappa^{(0)}\left(E_0^{(0)}\right)\right]^2}{4\mu \frac{C_2^{(1)}}{\hbar^2}} \left[C_0^{(1)} - \frac{4\mu C_2^{(1)}}{\hbar^2} \frac{4C_0^{(0)}}{3\pi^2 a_{\mathrm{HO},\mu}^3} \frac{\Gamma\left(n_{\max} + 5/2\right)}{\Gamma\left(n_{\max} + 1\right)}\right]
\end{aligned} \tag{B.43}$$

where we set in the last step the for the coefficient $C_2^{(1)}$ eq. (3.76). Rearranging the formula to solve for $C_0^{(1)} / 4\mu C_2^{(1)}$ yields

$$\frac{C_0^{(1)} \hbar^2}{4\mu C_2^{(1)}} = \frac{4C_0^{(0)}}{3\pi^2 a_{\mathrm{HO},\mu}^3} \frac{\Gamma\left(n_{\max} + 5/2\right)}{\Gamma\left(n_{\max} + 1\right)} - \frac{E_0^{(0)} E_1^{(1)} / \left[\kappa^{(0)}\left(E_1^{(0)}\right)\right]^2 - E_1^{(0)} E_0^{(1)} / \left[\kappa^{(0)}\left(E_0^{(0)}\right)\right]^2}{E_1^{(1)} / \left[\kappa^{(0)}\left(E_1^{(0)}\right)\right]^2 - E_0^{(1)} / \left[\kappa^{(0)}\left(E_0^{(0)}\right)\right]^2}. \tag{B.44}$$

Bibliography

[1] Y. Alhassid, G. F. Bertsch, and L. Fang, "New Effective Interaction for the Trapped Fermi Gas", in Physical Review Letters, vol. 100, pp. 230401/1–4, 2008

[2] J. O. Andersen, "Theory of the Weakly Interacting Bose Gas", in Review of Modern Physics, vol. 76, pp. 599–639, 2004

[3] J. B. Anderson, "Fixed-node quantum Monte Carlo", in International Reviews in Physical Chemistry, vol. 14, no. 1, pp. 85–112, 1995

[4] M. H. Anderson, J. R. Ensher, M. R. Matthews, C. E. Wieman, and E. A. Cornell, "Observation of Bose-Einstein Condensation in a Dilute Atomic Vapor", in Science, vol. 269, pp. 198–201, 1995

[5] G. E. Astrakharchik, J. Boronat, J. Casulleras, and S. Giorgini, "Equation of State of a Fermi Gas in the BEC-BCS Crossover: A Quantum Monte Carlo Study", in Physical Review Letters, vol. 93, no. 20, pp. 200404/1–4, 2004

[6] M. A. Baranov, "Theoretical Progress in Many-Body Physics with Ultracold Dipolar Gases", in Physics Reports 464, pp. 71–111, 2008

[7] J. Bardeeen, L. N. Cooper, and J. R. Schrieffer, "Theory of Superconductivity", in Physical Review, vol. 108, no. 5, pp. 1175–1204, 1957

[8] P. F. Bedaque and U. van Kolck, "Effective Field Theory for Few-Nucleon Systems", in Annual Review of Nuclear and Particle Science 52, pp. 339–396, 2002

[9] I. Bloch, "Ultracold quantum gases in optical lattices", in nature physics, vol. 1, pp. 23–30, 2005

[10] D. Blume, "Few-body physics with ultracold atomic and molecular systems in traps", in Reports on Progress in Physics 75, pp. 046401/1–37, 2012

[11] D. Blume and K. M. Daily, "Trapped two-component Fermi gases with up to six particles: Energetics, structural properties, and molecular condensate fraction", in Comptes Rendus Physique 12, pp. 86-109, 2011

[12] D. Blume, J. von Stecher, and C. H. Greene, "Universal Properties of a Trapped Two-Component Fermi Gas at Unitarity", in Physical Review Letters, vol. 99, pp. 233201/1–4, 2007

[13] S. N. Bose, "Plancks Gesetz und Lichtquantenhypothese" ("Plancks Law and Light Quantum Hypothesis"), in Zeitschrift für Physik 26, p. 178, 1924

[14] T. Bourdel, J. Cubizolles, L. Khaykovich, K. M. F. Magalhaes, S. J. J. M. F. Kokkelmans, G. V. Shlyapnikov, and C. Salomon, "Measurement of the Interaction Energy near a Feshbach Resonance in a ^{6}Li Fermi Gas", in Physical Review Letters, vol. 91, no. 2, pp. 020402/1–4, 2003

[15] E. Braaten and H.-W. Hammer, "Universality in few-body systems with large scattering length", in Physics Reports 428, pp. 259–390, 2006

[16] A. Bulgac, "Local-density-functional theory for superfluid fermonic systems: The unitary gas", in Physical Review *A*, vol. 76, pp. 040502/1–4, 2007

[17] T. Busch, B.-G. Englert, K. Rzażewski, and M. Wilkens, “Two Cold Atoms in a Harmonic Trap”, in Foundations of Physics, vol. 28, no. 4, pp. 549–559, 1998

[18] J. Carlson, S.-Y. Chang, V. R. Pandharipande, and K. E. Schmidt, “Superfluid Fermi Gases with Large Scattering Length”, in Physical Review Letters, vol. 91, no. 5, pp. 050401/1–4, 2003

[19] Y. Castin, “Basic theory tools for degenerate Fermi gases”, in Proceedings of the International School of Physics ‘Enrico Fermi’, p. 289–349, 2006

[20] E. Caurier, G. Martínez-Pinedo, F. Nowacki, A. Poves, and A. P. Zuker, “The shell model as a unified view of nuclear structure”, in Review of Modern Physics, vol. 77, pp. 427–488, 2005

[21] S. Y. Chang and G. F. Bertsch, “Unitary Fermi gas in a harmonic trap”, in Physical Review *A*, vol. 76, pp. 021603/1–4, 2007

[22] C. Chin, R. Grimm, P. Julienne, and E. Tiesinga, “Feshbach resonances in ultracold gases”, in Review of Modern Physics, vol. 82, p. 1225, 2010

[23] S. A. Coon, M. I. Avetian, M. K. G. Kruse, U. van Kolck, P. Maris, and J. P. Vary, “Convergence properties of *ab initio* calculations of light nuclei in a harmonic oscillator basis”, in Physical Review *C*, vol. 86, p. 054002, 2012

[24] P. Courteille, R. S. Freeland, D. J. Heinzen, F. A. van Abeelen, and B. J. Verhaar, “Observation of a Feshbach Resonance in Cold Atom Scattering”, in Physical Review Letters, vol. 81, no. 1, pp. 69–72, 1998

[25] K. M. Daily and D. Blume, “Energy spectrum of harmonically trapped two-component Fermi gases: Three- and four-particle problem”, in Physical Review *A*, vol. 81, pp. 053615/1–17, 2010

[26] F. Dalfovo, S. Giorgini, L. P. Pitaevskii, and S. Stringari, “Theory of Bose-Einstein condensation in trapped gases”, in Review of Modern Physics, vol. 71, no. 3, pp. 463–512, 1999

[27] J. Dalibard, “Collisional dynamics of ultra-cold atomic gases”, in Proceedings of the International School of Physics ‘Enrico Fermi’, p. 321, 1999

[28] K. B. Davis, M.-O. Mewes, M. R. Andrews, N. J. Druten, D. S. Drufee, D. M. Kurn, and W. Ketterle, “Bose-Einstein Condensation in a Gas of Sodium Atoms”, in Physical Review Letters, vol. 75, no. 22, pp. 3969–3974, 1995

[29] A. Einstein, “Quantentheorie des einatomigen idealen Gases”, in Sitzungsberichte der Preußischen Akademie der Wissenschaften, p. 261–267, 1924

[30] R. J. Furnstahl, G. Hagen, and T. Papenbrock, “Corrections to nuclear energies and radii in finite oscillator space”, in Physical Review *C*, vol. 86, pp. 031301/1–6, 2012

[31] R. J. Furnstahl, S. N. More, and T. Papenbrock, “Systematic expansion for infrared oscillator basis extrapolations”, in Physical Review *C*, vol. 89, p. 044301, 2014

[32] H. Georgi, “Effective field theory”, in Annual Review of Nuclear and Particle Science 43, pp. 209–252, 1993

[33] C. N. Gilbreth and Y. Alhassid, “A New Effective Interaction for the Two-Component Trapped Fermi Gas — the BEC to BCS Crossover”, in Physical Review *A*, vol. 85, p. 033621, 2012

[34] S. Giorgini, L. P. Pitaevskii, and S. Stringari, “Theory of ultracold atomic Fermi gases”, in Review of Modern Physics, vol. 80, pp. 1215–1274, 2008

[35] M. Greiner, C. A. Regal, and D. S. Jin, “Emergence of a molecular Bose-Einstein condensate from a Fermi gas”, in Nature, vol. 426, pp. 537–540, 2003

[36] R. Guardiola, “Monte Carlo Methods in Quantum Many-Body Theories”, in J. Navarro, A. Polls (eds.), Microscopic Quantum Many-Body Theories and Their Applications, pp. 269–336, Springer, 1997

[37] G. Hagen, T. Papenbrock, and D. J. Dean, “Solution of the Center-of-Mass Problem in Nuclear Structure Calculations”, in Physical Review Letters, vol. 103, p. 062503, 2009

[38] H. W. Hammer and R. J. Furnstahl, “Effective Field Theory for Dilute Fermi Systems”, in Nuclear Physics *A*, vol. 678, pp. 277–294, 2000

[39] K. M. O’Hara, S. L. Hemmer, M. E. Gehm, S. R. Grande, and J. E. Thomas, “Observation of a Strongly Interacting Degenerate Fermi Gas of Atoms”, in Science, vol. 298, pp. 2179–2182, 2002

[40] H. Hergert, S. Binder, A. Calci, J. Langhammer, and R. Roth, “Ab Initio Calculations of Even Oxygen Isotopes with Chiral Two- Plus Three-Nucleon Interactions”, in Physical Review Letters, vol. 110, p. 242501, 2013

[41] T. L. Ho, “Universal thermodynamics of degenerate quantum gases in the unitarity limit”, in Physical Review Letters, vol. 92, p. 090402, 2004

[42] E. Hylleraas, B. Undheim, “Numerische Berechnung der 2S-Terme von Ortho- und Par-Helium”, in Zeitschrift für Physik *A* 65, p. 759, 1930

[43] M. Inguscio, W. Ketterle, C. Salomon (eds.), Ultra-cold Fermi Gases. IOS Press, 2007

[44] S. Inouye, M. R. Andrews, J. Stenger, H.-J. Miesner, D. M. Stamper-Kurn, and W. Ketterle, “Observation of Feshbach resonances in a Bose-Einstein condensate”, in Nature, vol. 392, pp. 151–154, 1998

[45] D. S. Jin and C. A. Regal, “Fermi gas experiments”, in Proceedings of the International School of Physics ‘Enrico Fermi’, pp. 1–51, 2006

[46] P. Jönsson, A. Ynnermann, C. Froese-Fischer, M. R. Godefroid, and J. Olsen, “Large-scale MCHF and CI calculations of the transition probability and hyperfine structures in the sodium resonance transition”, in Physical Review *A*, vol. 53, p. 4021, 1996

[47] G. P. Kamuntavicius, R. K. Kalinauskas, B. R. Barrett, S. Mickevicius, and D. Germanas, “The general harmonic-oscillator brackets: compact expression, symmetries, sums and Fortran code”, in Nuclear Physics *A*, vol. 695, pp. 191–201, 2011

[48] P. R. Ch. Kent, Techniques and Applications of Quantum Monte Carlo, Dissertation, University of Cambridge (`http://web.ornl.gov/~pk7/thesis/Thesis.html`)

[49] W. Ketterle, D. S. Durfee and D. M. Stamper-Kurn, “Making, probing and understanding Bose-Einstein condensates” in Proceedings of the International School of Physics ‘Enrico Fermi’, p. 67, 1999

[50] W. Ketterle and M. W. Zwierlein, “Making, probing and understanding ultra cold Fermi gases”, in Proceedings of the International School of Physics ‘Enrico Fermi’, pp. 95–287, 2006

[51] M. Köhl, H. Moritz, T. Stöferle, K. Günter, and T. Esslinger, “”, in Physical Review Letters, vol. 94, pp. 080403/1–4, 2005

[52] U. van Kolck, “Effective field theory of short-range forces”, in Nuclear Physics *A*, vol. 645, pp. 273–302, 1999

[53] I. Kosztin, B. Faber, and K. Schulten, “Introduction to the Diffusion Monte Carlo Method”, in American Journal of Physics, vol. 64, p. 633, 1996

[54] R. V. Krems, Cold molecules: theory, experiment, applications. CRC Press, 2009

[55] M. K. G. Kruse, Importance-Truncation, Regulators and Reactions. Springer Theses, 2013

[56] R. B. Lehoucq, D. C. Sorensen, and C. Yang, ARPACK Users' Guide: Solution of Large Scale Eigenvalue Problems with Implicitly Restarted Arnoldi Methods, 1997. `http://www.caam.rice.edu/software/ARPACK/`

[57] R. Machleidt and D. R. Entem, “Chiral effective field theory and nuclear forces”, in Physics Reports 5003, pp. 1–75, 2011

[58] J. B. McGrory and B. H. Wildenthal, “Further Comment on Spurious Center-of-Mass Motion”, in Physics Letters, vol. 60, p. 1, 1975

[59] S. N. More, A. Ekström, R. J. Furnstahl, G. Hagen, and T. Papenbrock, “Universal properties of infrared oscillator basis extrapolations”, in Physical Review *C*, vol. 87, p. 044326, 2013

[60] M. Moshinsky, “Transformation brackets for harmonic oscillator functions” in Nuclear Physics, vol. 13, p. 104–116, 1959

[61] P. Navràtil, S. Quaglioni, I. Stetcu, and B. R. Barrett, “Recent developments in no-core shell-model calculations”, in Journal of Physics *G* 36, pp. 083101/1–54, 2009

[62] M. P. Nightingale and C. J. Umrigar, Quantum Monte Carlo methods in physics and chemistry. Kluwer, 1999

[63] D. R. Phillips, S. R. Beane, and T. D. Cohen, “Nonperturbative Regularization of Renormalization: Simple Examples form Nonrelativistic Quantum Mechanics”, in Annals of Physics, vol. 263, pp. 255–275, 1998

[64] A. Pich, “Effective field theory”, in Proceedings of the Les Houches Summer School 'Probing the Standard Model of particle interactions', 1999

[65] D. Rakshit, K. M. Daily, and D. Blume, “Natural and unnatural parity states of small trapped equal-mass two-component Fermi gases at unitarity and fourth-order virial coefficient”, in Physical Review *A*, vol. 85, p. 033634, 2012

[66] M. Randeria, “Pre-pairing for condensation”, in nature physics, vol. 6, pp. 561–562, 2010

[67] C. A. Regal, M. Greiner, and D. S. Jin, “Observation of Resonance Condensation of Fermionic Atom Pairs”, in Physical Review Letters, vol. 92, no. 4, pp. 040403/1–4, 2004

[68] P. J. Reynolds, D. M. Ceperley, B. J. Alder, and W. A. Lester Jr., “Fixed-node quantum Monte Carlo for molecules”, in Journal of Chemical Physics vol. 77, no. 11, pp. 5593–5603, 1982

[69] Z. Rolik, À. Szabados, and P. R. Surojàn, “On the perturbation of multiconfiguration wave function”, in Journal of Chemical Physics, vol. 119, no. 4, pp. 1922–1928, 2003

[70] R. Roth, Effektive Wechselwirkungen für Quantenflüssigkeiten und Quantengase. Dissertation, Technische Universität Darmstadt, 2000

[71] R. Roth, “Importance truncation for large-scale configuration interaction approaches”, in Physical Review *C*, vol. 79, pp. 064324/1–18, 2009

[72] R. Roth, Quantenmechanik. Lecture Script, Technische Universität Darmstadt, 2009

[73] R. Roth, A. Calci, J. Langhammer, and S. Binder, “Evolved Chiral NN + 3N Hamiltonians for Ab Initio Nuclear Structure Calculaltions”, in Physical Review *C*, vol. 90, p. 024325, 2013

[74] R. Roth, J. R. Gour, and P. Piecuch, “Center-of-mass problem in truncated configuration interaction and coupled-cluster calculations”, in Physics Letters *B*, vol. 679, p. 334, 2009

[75] R. Roth and P. Navrátil, “Ab Initio Study of ^{40}Ca with an Importance-Truncated No-Core Shell Model”, in Physical Review Letters, vol. 99, pp. 092501/1–4, 2007

[76] J. Rotureau, “Interaction for the trapped Fermi gas from a unitary transformation of the exact two-body spectrum”, in European Physical Journal *D* 67:153, 2013

[77] J. Rotureau, I. Stetcu, B. R. Barrett, M. C. Birse, and U. van Kolck, “Three and Four Harmonically Trapped Particles in an Effective Field Theory Framework”, in Physical Review *A*, vol. 82, p. 032711, 2010

[78] Y. Saad, Iterative Methods for Sparse Linear Systems, Second Edition. Society for Industrial and Applied Mathematics, 2003

[79] Y. Saad, Numerical Methods for Large Eigenvalue Problems, Second Edition. Society for Industrial and Applied Mathematics, 2011

[80] J. J. Sakuraj, Modern Quantum Mechanics. Addison-Wesley, 1994

[81] M. W. Schmidt and M. S. Gordon, “The construction and interpretation of MCSCF wavefunctions”, in Annual Review of Physical Chemistry 49, pp. 233–266, 1998

[82] F. Schwabl, Quantenmechanik I, 7. Auflage. Springer, 2007

[83] F. Serwane, G. Zürn, T. Lompe, T. B. Ottenstein, A. N. Wenz, and S. Jochim, “Deterministic Preparation of a Tunable Few-Fermion System”, in Science, vol. 332, pp. 336–338, 2011

[84] J. von Stecher, Trapped Ultracold Atoms with Tunable Interactions. PhD Thesis, University of Colorado, 2009

[85] J. von Stecher and C. H. Greene, “Spectrum and Dynamics of the BCS-BEC Crossover from a Few-Body Perspective”, in Physical Review Letters, vol. 99, pp. 090402/1–4, 2007

[86] J. von Stecher and C. H. Greene, “Correlated Gaussian hyper spherical method for few-body systems”, in Physical Review *A*, vol. 80, pp. 022504/1–12, 2009

[87] J. von Stecher, C. H. Greene, and D. Blume, “BEC–BCS crossover of a trapped two-component Fermi gas with unequal masses”, in Physical Review *A*, vol. 76, pp. 053613/1–10, 2007

[88] J. von Stecher, C. H. Greene, and D. Blume, “Energetics and structural properties of trapped two-component Fermi gases”, in Physical Review *A*, vol. 77, pp. 043619/1–20, 2008

[89] I. Stetcu, B. R. Barrett, U. van Kolck, and J. P. Vary, “Effective theory for trapped few-fermion systems”, in Physical Review *A*, vol. 76, pp. 063613/1–7, 2007

[90] I. Stetcu and J. Rotureau, “Effective interactions and operators in the no-core shell model”, in Progress in Particle and Nuclear Physics 69, pp. 182–224, 2013

[91] I. Stetcu, J. Rotureau, B. R. Barrett, and U. van Kolck, "An effective field theory approach to two trapped particles", in Annals of Physics, vol. 325, no. 8, pp. 1644–1666, 2010

[92] T. Stöferle, H. Moritz, K. Günter, M. Köhl, and T. Esslinger, "Molecules of Fermionic Atoms in an Optical Lattice", in Physical Review Letters, vol. 96, p. 030401, 2006

[93] H. T. C. Stoof, K. B. Gubels, and D. B. M. Dickerscheid, Ultracold quantum fields. Springer, 2009

[94] P.R. Surojàn, Z. Rolik, À. Szabados, and D. Köhalmi, "Partitioning in multiconfiguration perturbation theory", in Annals of Physics, vol. 13, no. 4, pp. 223–231, 2004

[95] Y. Suzuki, Stochastic variational approach to quantum mechanical few-body problems. Springer, 1998

[96] I. Talmi, "Nuclear spectroscopy with harmonic oscillator wave-functions", in Helvetica Chimica Acta 25, p. 185, 1952

[97] E. Timmermans, P. Tommasini, M. Hussein, A. Kerman, "Feshbach resonances in atomic Bose-Einstein condensates", in Physics Reports 315, 1999

[98] K. Varga and Y. Suzuki "Precise solution of few-body problems with the stochastic variational method on a correlated Gaussian basis", in Physical Review *C*, vol. 52, p. 2885, 1995

[99] K. Varga and Y. Suzuki "Solution of few-body problems with the stochastic variational method, I. Central forces with zero orbital momentum", in Computer Physics Communications 106, pp. 157–168, 1997

[100] C. M. Vincent, "Optimal Separation of Center-of-Mass Motions", in Physical Review *C*, vol. 8, no. 3, pp. 929–937, 1973

[101] S. Weinberg, "Nuclear forces from chiral Lagrangians", in Physics Letters *B*, vol. 251, no. 2, pp. 288–292, 1990

[102] F. Werner and Y. Castin, "Unitary Quantum Three-Body Problem in a Harmonic Trap", in Physical Review Letters, vol. 97, pp. 150401/1–4, 2006

[103] W. Zwerger, The BCS-BEC Crossover and the Unitary Fermi Gas. Springer, 2011

[104] M. W. Zwierlein, J. R. Abo-Shaeer, A. Schirotzek, C. H. Schunck, and W. Ketterle, "Vortices and superfluidity in a strongly interacting Fermi gas", in Nature, vol. 435, no. 23, pp. 1048–1051, 2005

[105] M. W. Zwierlein, C. A. Stan, C. H. Schunck, S. M. F. Raupach, A. J. Kerman, and W. Ketterle, "Condensation of Pairs of Fermionic Atoms near a Feshbach Resonance", in Physical Review Letters, vol. 92, no. 12, 2004

Danksagung

An dieser Stelle möchte ich allen Leuten danken, die mich bei meiner Doktorarbeit unterstützt haben und zum Gelingen dieser Arbeit beigetragen haben.

An erster Stelle möchte ich mich bei meinem Doktorvater, Professor Roth, für die Annahme als Doktorandin und die Gelegenheit, diese Arbeit zu verfassen, bedanken. Er ließ mir genügend Freiraum, um mich auf die Forschung zu konzentrieren, und stand stets als Ansprechpartner zur Verfügung.

Professor Jens Braun danke ich für die Übernahme des Zweitgutachtens.

Ich danke der TNP++-Arbeitsgruppe für die angenehme Arbeitsatmosphäre. Der Arbeitsgruppe und meinen Bürokollegen danke ich für die zahlreichen Gespräche über physikalische und nicht physikalischen Themen. Dabei möchte ich besonders Stefan Schulz, Roland Wirth und Eskendr Gebrerufael für das Durchlesen vorliegender Arbeit bedanken,

Ich möchte mich auch bei der Helmholtz-Graduiertenschule für Schwerionenforschung (*Helmholtz Graduate School for Heavy-Ion Research*, HGS-HIRe) dafür bedanken, dass sie die Anfertigung vorliegender Arbeit mit einem Promotionsstudium gefördert hat.

Meinen Eltern und Geschwistern danke ich dafür, dass sie mich nach Kräften unterstützt haben. Besonderer Dank geht an Christopher für seine anhaltende Unterstützung in den letzten Jahren und an Katharina und Elisabeth für ihre Geduld.

Curriculum Vitae

Zur Person

Name	Helena Spies, geb. Krutsch
Geburtsdatum	28. Juli 1979
Geburtsort	Frunse, Kirgisische SSR (heute Bischkek)

Ausbildung

09/1986–08/1993	Mittelschule Nr. 50, Frunse / Bischkek
09/1993–04/1995	Mittelschule Nr. 57, Bischkek
05/1995–06/1995	Georg-August-Zinn-Schule, Reichelsheim (Odenw.)
07/1995–07/1996	Schule am Sportpark, Erbach (Odenw.)
08/1996–07/1997	Berufliches Schulzentrum Odenwaldkreis, Michelstadt Hauptschulabschluss
08/1997–07/1999	Berufliches Schulzentrum Odenwaldkreis, Michelstadt Abschluss: mittlere Reife (Realschulabschluss)
08/1999–07/2002	Berufliches Schulzentrum Odenwaldkreis, Michelstadt Abschluss: allgemeine Hochschulreife (Abitur)
10/2002–03/2008	Diplom-Studium Physik, Fachbereich Physik, Technische Universität Darmstadt Abschluss: Diplom
04/2009–heute	Promotionsstudium Physik, Arbeitsgruppe Theoretical Nuclear Physics, Fachbereich Physik, Technische Universität Darmstadt

Relevante berufliche Tätigkeit

06/2008–02/2009	Wissenschaftliche Mitarbeiterin, Arbeitsgruppe Strahlen- und Kernphysik, Fachbereich Physik, Technische Universität Darmstadt